Protein-based seed germination: Conversion of proteins into carbohydrates, nitrogen compounds and energy during germination and seedling establishment of *Lupinus albus*

Doctoral thesis

for

the award of the doctoral degree

of the Faculty of Mathematics and Natural Sciences

of the University of Cologne

submitted by

Cecile Angermann

accepted in the year 2026

Abstract

The need for resource-efficient crops is increasing due to climate change, resource scarcity and the growing demand for plant-based protein sources. In this context, white lupin (*Lupinus albus*) is a particularly promising crop. Due to its high protein content and ability to thrive on nutrient-poor soils thanks to its specialised root structures and symbiosis with nitrogen-fixing bacteria, this legume represents a sustainable production system with great developmental potential. However, realising this potential fully requires a detailed understanding of the molecular mechanisms that govern early seed development and nutrient utilisation.

During germination, plant seeds are heterotrophic, relying mostly on their stored nutrients. *L. albus* is a protein crop, containing up to 40 % protein in its seeds, which act as the primary storage compound. The total seed proteome is made up of 85 % classical storage proteins, which act as reserves of carbon, nitrogen and sulfur. Our results indicated that these storage properties were maintained during germination, with the storage proteins remaining stable. Instead, lipids were used to fuel the germination. The protein fractions that were most mobilised during germination were those related to desiccation tolerance, such as LEA proteins, and storage lipids, such as oleosins. These were also highly abundant in seeds. Degradation of these proteins released large quantities of the amino acids alanine, glycine, and threonine. The catabolism of these amino acids provided the seed with pyruvate and glyoxylate. When combined with acetyl-CoA, a product of lipid β-oxidation, these intermediates were believed to fulfil a glyoxylate cycle bypass, providing the seed with the carbohydrates necessary for energy generation and biomass construction (see **Chapter 2: Manuscript 1**).

We found that the mitochondria in the seeds of *L. albus* were dynamic, pre-assembled systems that contained all of the necessary respiratory complexes. During imbibition, the activation of cofactor biosynthesis, transport, and redox homeostasis enabled the immediate provision of energy. We identified NAD-dependent formate dehydrogenase as the third most abundant seed mitochondrial protein. The high abundance of this protein, in combination with those of other dehydrogenases involved in mitochondrial amino acid catabolism, suggests that seeds have specialised mitochondrial metabolism, providing energy and carbohydrate precursors while carrying out detoxification. Furthermore, our study revealed that a significant proportion of the

mitochondrial proteins found in *L. albus* seeds were uncharacterised, with no close homologues identified in *Arabidopsis*. This suggests the existence of legume-specific mitochondrial adaptations (see **Chapter 4: Manuscript 3**).

During the epigeal growth phase after germination, the cotyledons of *L. albus* were exposed to light and turned green. At this time, the degradation of storage proteins was intensified, leading in an increased concentration of free amino acids, particularly asparagine (see **Chapter 2: Manuscript 1**). The synthesis of the proteins necessary for photosynthesis was also induced, resulting in these proteins becoming the most abundant in the cotyledon proteome. Photosynthesis of the cotyledon enabled the production of light-based energy and carbohydrates, but it was less efficient than that of true leaves. Therefore, before the first true leaves have fully developed, the seedling relies on stored reserves, especially in nutrient-limiting conditions. Premature cotyledon loss triggered drastic nitrogen-saving strategies, including a reduction in protein levels, particularly those related to photosynthesis and metabolism, and a significant decrease in biomass. Once there were enough true leaves for autotrophy, the cotyledons began to senesce and the metabolism shifted to recycling and export processes (see **Chapter 3: Manuscript 2**).

This thesis provides valuable insights into the molecular biology of protein-rich seeds. It demonstrates that the germination and seedling establishment of *L. albus* are characterised by the precise interplay of energy metabolism, reserve mobilisation, organ transformation, and organelle reactivation. These processes rely on the seeds stored resources.

Zusammenfassung

Der Bedarf an ressourceneffizienten Nutzpflanzen steigt aufgrund des Klimawandels, der globalen Ressourcenknappheit und der wachsenden Nachfrage nach pflanzlichen Proteinquellen, immer weiter. In diesem Zusammenhang ist die weiße Lupine (*Lupinus albus*) eine besonders vielversprechende Pflanzenart. Als Leguminose mit hohem Proteingehalt gedeiht sie aufgrund ihrer besonderen Wurzelmodifikationen und der Etablierung einer Symbiose mit stickstofffixierenden Bakterien auch auf nährstoffarmen Böden. Somit stellt sie ein nachhaltiges Produktionssystem mit großem Entwicklungspotenzial dar. Um dieses Potenzial jedoch voll auszuschöpfen, ist ein detailliertes Verständnis der molekularen Mechanismen erforderlich, die die frühe Pflanzenentwicklung und Speicherstoffverwertung steuern.

Während der Keimung sind Pflanzensamen heterotroph und nutzen hauptsächlich ihren eingelagerten Reserven als Nährstoffe. *L. albus* ist eine proteinakkumulierende Nutzpflanze, deren Samen bis zu 40 % Protein enthalten. Das Samenproteom besteht zu 85 % aus klassischen Speicherproteinen, die als Reserve für Kohlenstoff, Stickstoff und Schwefel dienen. Unsere Ergebnisse zeigen, dass diese Speichereigenschaften über die Keimung hinaus erhalten blieben. Stattdessen werden während der Keimung Lipide als Energie- und Kohlenhydratquelle genutzt. Währenddessen wurden vor allem Proteingruppen mobilisiert, die an der Trockenheitstoleranz von Samen beteiligt sind, darunter LEA-Proteine und Oleosine, die mit Speicherlipiden interagieren. Beide waren in den Samen von *L. albus* hochabundant und ihr Abbau setzte große Mengen der Aminosäuren Alanin, Glycin und Threonin frei. Der Katabolismus dieser Aminosäuren generierte Pyruvat und Glyoxylat. Wir vermuten, dass diese Stoffwechselintermediate, in Kombination mit Acetyl-CoA, einem Produkt der Lipid-β-Oxidation, einen Glyoxylatzyklus-Bypass bilden, der den Samen mit den für die Energieerzeugung und den Aufbau von Biomasse erforderlichen Kohlenhydraten versorgt (siehe **Kapitel 2: Manuskript 1**).

Bei der Untersuchung von Mitochondrien aus *L. albus*-Samen stellten wir fest, dass diese trotz der besonderen Bedingungen im Pflanzensamen als dynamische und reaktionsbereite Organellen vorlagen und alle erforderlichen Atmungskettenkomplexe enthielten. Während der Imbibition ermöglichte die Aktivierung der Cofaktor-Biosynthese, des Transports und der Redox-Homöostase eine sofortige Energiebereitstellung. Wir identifizierten die NAD-abhängige Formiatdehydrogenase

als dritthäufigstes mitochondriales Protein in Lupinensamen. Dehydrogenasen, die am mitochondrialen Aminosäurekatabolismus beteiligt sind, waren ebenfalls hochabundant vorhanden. Dies lässt vermuten, dass die Samen von *L. albus* über einen spezialisierten mitochondrialen Stoffwechsel verfügen. Dieser liefert Energie und Kohlenhydratvorläufer und führt gleichzeitig Entgiftungsprozesse durch. Darüber hinaus zeigte unsere Studie, dass ein erheblicher Teil des mitochondrialen Proteoms von *L. albus*-Samen nicht charakterisierte Proteine aufwies, für die keine Homologie zu *Arabidopsis* Proteinen festgestellt werden konnte. Dies deutet auf leguminosenspezifische mitochondriale Anpassungen hin (siehe **Kapitel 4: Manuskript 3**).

Nach der Keimung zeigte *L. albus* epigäisches Wachstum. Die Keimblätter wurden über das Substrat angehoben, dem Licht ausgesetzt und ergrünten. Wir konnten feststellen, dass zu diesem Zeitpunkt eine Intensivierung des Speicherproteinabbaus stattfand, was zu einem Anstieg der freien Aminosäuren, insbesondere Asparagin, führte (siehe **Kapitel 2: Manuskript 1**). Ebenso wurde die Synthese von Proteinen, die an der Photosynthese beteiligt sind, induziert, sodass diese zur häufigsten Proteinfraktion im Keimblatt-Proteom anstiegen. Die Photosynthese der Keimblätter ermöglichte die Produktion von lichtbasierter Energie und Kohlenhydraten, war jedoch weniger effizient als die der echten Blätter. Dies lässt vermuten, dass der Keimling bis zur Etablierung der ersten echten Blätter weiterhin auf gespeicherte Reservestoffe aus den Keimblättern angewiesen ist, insbesondere unter nährstoffarmen Bedingungen. Ein vorzeitiger Verlust der Keimblätter führte zu drastischen Stickstoffeinsparstrategien. Dazu zählten eine Verringerung des Proteingehalts, hauptsächlich von Proteinen, die mit der Photosynthese und dem Proteinstoffwechsel in Verbindung stehen. Außerdem wurde die Biomasse erheblich reduziert. Sobald ausreichend echte Blätter etabliert wurden und die Pflanze somit autotroph war, begann die Seneszenz der Keimblätter und ihr Stoffwechsel verlagerte sich auf Recycling- und Exportprozesse (siehe **Kapitel 3: Manuskript 2**).

Diese Arbeit liefert wichtige Erkenntnisse zur Molekularbiologie proteinreicher Samen. Es wird gezeigt, dass die Keimung und die frühe Entwicklung von *L. albus* durch das präzise Zusammenspiel von Energiestoffwechsel, Mobilisierung von Reservestoffen, Organumwandlung und Reaktivierung von Organellen gekennzeichnet sind. Dafür sind die in den Samen eingelagerten Reserven unerlässlich.

Contributing publications

The following publications and manuscripts contributed to this thesis:

1. **Cecile Angermann***, Björn Heinemann*, Jule Hansen, Nadine Töpfer, Hans-Peter Braun, Tatjana M. Hildebrandt (2024) Proteome reorganization and amino acid metabolism during germination and seedling establishment in *Lupinus albus*, *Journal of Experimental Botany*, Volume 75, Issue 16, Pages 4891-4903 https://doi.org/10.1093/jxb/erae197
   * Equally contributing first authors

2. **Cecile Angermann**, Björn Heinemann, Bianca Bueno Nogueira, Hans-Jörg Mai, Petra Bauer, Tatjana M. Hildebrandt (2025) Balancing nutrient remobilization and photosynthesis: proteomic insights into the dual role of lupin cotyledons after germination, *the plant journal*, Volume 123, Issue 2, e70357 http://doi.org/10.1111/tpj.70357

3. **Cecile Angermann**, Hans-Peter Braun, Tatjana M. Hildebrandt (2025) The seed mitochondrial proteome of *Lupinus albus* provides insight into energy metabolism during germination, *bioRxiv* https://doi.org/10.1101/2025.09.19.677279 [Preprint]

Abbreviations

Table 1: Explanation of relevant terms and acronyms used in this dissertation.

Abbreviation	Explanation
2D	Two-dimensional
2OB	2-oxobutyrate
2OG	2-oxoglutarate
2OGDH	2-oxoglutarate dehydrogenase complex
3D	Three-dimensional
3PG	3-phosphoglycerate
A. thaliana	*Arabidopsis thaliana*
AA	Amino acid
ACO	Aconitase
ACoA	Acetyl-CoA
ADH	Alcohol dehydrogenase
AdoMet	S-adenosylmethionine
ADP	Adenosine diphosphate
Ala	Alanine
AlaAT	Alanine aminotransferase
altDH	Alternative NADH dehydrogenases
altNDH	Alternative NADH dehydrogenase
ANT	ADP/ATP carrier
Arg	Arginine
Asn	Asparagine
Asp	Aspartate / aspartic acid
ATP	Adenosine triphosphate
BCAA	Branched chain amino acid
BN	Blue native
BN/SDS-PAGE	Blue native / sodium dodecyl sulfate-polyacrylamide gel electrophoresis
C1	One-carbon-metabolism
Chl	Chlorophyll
CI	Chapter 2: Manuscript 1: citrate Chapter 4: Manuscript 3: respiratory chain complex 1
CII	Respiratory chain complex 2

Abbreviation	Explanation
CIII	Respiratory chain complex 3
CIV	Respiratory chain complex 4
CM	Chorismate
CoA	Coenzyme A
CoM	Coenzyme metabolism
Cot	Cotyledons
CSY	Citrate synthase
CV	Respiratory chain complex 5
Cw	Cell wall
cy	Cytosolic
Cys	Cysteine
Cyt C	Cytochrome C
D2HGDH	D-2-hydroxyglutarate dehydrogenase
DAMP	Damage-associated molecular pattern
DDA	Data-dependent acquisition
DDA-PASEF	Data-dependent acquisition parallel accumulation–serial fragmentation
DFG	Deutsche Forschungsgemeinschaft
DH	Dehydrogenase
DHAP	Dihydroxyacetone phosphate
DHO	Dihydroorotate
DHODH	Dihydroorotate dehydrogenase
DNA	Deoxyribonucleic acid
DTT	Dithiothreitol
DW	Dry weight
EDTA	Ethylenediaminetetraacetic acid
EGTA	Ethylene glycol-bis(β-aminoethyl ether)-N,N,N′,N′-tetra acetic acid
Eno	Enolase
ET	Ethylene
ETFQO	Electron-transfer flavoprotein
$FADH_2$	Flavin adenine dinucleotide (reduced form)
FC	Fold change

Abbreviation	Explanation
FDH	Formate dehydrogenase
FeS	Iron–sulfur cluster
FMOC	Fluorenyl methoxycarbonyl
FU	Fumarate
G3P	Glycerol-3-phosphate
GABA	γ-aminobutyric acid
GCS	Glycine cleavage system
GDH	Glutamate dehydrogenase
Glce	Glycerate
Glco	Glycolate
GLDH	L-galactono-1,4-lactone dehydrogenase
Gln	Glutamine
Glu	Glutamate / glutamic acid
Gly	Glycine
GPD	Glycerol-3-phosphate dehydrogenase
GX	Glyoxylate
GXAT	Glyoxylate aminotransferase
HEPES	4-(2-Hydroxyethyl)-1-piperazineethanesulfonic acid
HPLC	High-performance liquid chromatography
Hpyr	Hydroxy pyruvate
HSD	Honest significant difference
Hyp	Hypocotyl
IAM	Iodoacetamide
iBAQ	Intensity-based absolute quantification values
ICL	Isocitrate lyase
ICP-MS	Inductively coupled plasma mass spectrometry
IDH	Isocitrate dehydrogenase
Ile	Isoleucine
IMS-MS/MS	Ion mobility mass spectrometry
KEGG	Kyoto encyclopaedia of genes and genomes
L. albus	*Lupinus albus*
Lb	Lipid body
LC3	Light curve protocol #3

Abbreviation	Explanation
LC-MS/MS	Liquid chromatography–tandem mass spectrometry
LEA	Late embryogenesis abundant protein
Leu	Leucine
LFQ	Label-free quantification values
L-Gal	L-galactono-1,4-lactone
LM	Lipid metabolism
Lys	Lysine
MA	Malate
MapMan	Mapping and visualization of omics data onto diagrams of metabolic pathways and biological processes
MDH	Malate dehydrogenase
ME	Malic enzyme
Met	Methionine
metab.	Metabolism
Mg	Magnesium
misc.	Miscellaneous
MoCo	Molybdenum cofactor
mod.	Modification
MOPS	3-(N-morpholino)-propane sulfonic acid
MRC	Mitochondrial respiratory chain
mRNA	Messenger ribonucleic acid
MS	Related to pathways: malate synthase Otherwise: mass spectrometry
mt	Mitochondrial
N	Introduction, Fig. 8: nucleus
n.d.	Not detected
NAD	Nicotinamide adenine dinucleotide
NADH	Nicotinamide adenine dinucleotide (reduced form)
NM	Nucleotide metabolism
NPQ2	Non-photochemical quenching protocol #2
OA	Oxaloacetate / oxaloacetic acid
OG	Oxoglutarate
OLE	Oleosin

Abbreviation	Explanation
OPA	Ophthaldialdehyde
OXPHOS	Oxidative phosphorylation
P5CDH	Delta-1-pyrroline-5-carboxylate dehydrogenase
PAGE	Polyacrylamide gel electrophoresis
PASEF	Parallel accumulation–serial fragmentation
Pb	Protein body
PDC	Pyruvate dehydrogenase complex
PDH	Pyruvate dehydrogenase
PEP	Phosphoenolpyruvate
PEPCK	Phosphoenolpyruvate carboxykinase
Phe	Phenylalanine
Pip	Pipecolic acid
PK	Pyruvate kinase
pl	Plastidic
PMSF	Phenylmethylsulfonyl fluoride
PPDK	Pyruvate phosphate dikinase
PPi	Inorganic pyrophosphate
PR	Photorespiration
Pro	Proline
PS	Photosynthesis
px	Peroxisomal
Pyr	Pyruvate
R5P	Ribose-5-phosphate
RFO	Raffinose family oligosaccharides
RT	Room temperature
S	Introduction, Fig. 8: starch
SC	Succinate
SD	Standard deviation
SDH	Succinate dehydrogenase (respiratory chain complex 2)
SDP1	Sugar-dependent lipase 1
SDS	Sodium dodecyl sulfate
SDS-PAGE	Sodium dodecyl sulfate-polyacrylamide gel electrophoresis

Abbreviation	Explanation
SDT	Sodium dodecyl sulfate, dithiothreitol, tris(hydroxymethyl) aminomethane
Ser	Serine
SP	Storage protein
SP3	Single-pot solid-phase-enhanced sample preparations
SP4	Solvent precipitation, single-pot, solid-phase-enhanced sample preparation
SSA	Succinic semialdehyde
SSADH	Succinic semialdehyde dehydrogenase
SUBA	The subcellular localization database for *Arabidopsis thaliana*
SucCoA	Succinyl-CoA
TAG	Triacylglycerol
TAIR10	The *Arabidopsis* information resource, genome version 10
TCA	Tricarboxylic acid
TES	N-tris [hydroxymethyl]-methyl-2-aminoethanesulphonic acid
Thr	Threonine
ThrAld	L-threonine aldolase
Tris	Tris(hydroxymethyl)aminomethane
Trp	Tryptophan
Tyr	Tyrosine
UDP	Uridine diphosphate
UHPLC	Ultra-high-performance liquid chromatography
UTP	Uridine triphosphate
Val	Valine
VDAC	Voltage-dependent anion channel

Figures

Introduction

Chapter 2: Manuscript 1

Chapter 3: Manuscript 2

Chapter 4: Manuscript 3

Content

1 Introduction

In the context of climate change, mineral resource depletion and rising global demand for plant-based food, agricultural production systems are facing profound challenges. In order to ensure a secure supply of high-quality food and feed in conditions of nutrient deficiency or drought, robust, efficient and adaptable crops are required. Improving plant resource efficiency, the ability to produce high levels of biomass or protein with minimal inputs of nutrients or water, is therefore central. Understanding the molecular mechanisms underlying resource uptake, allocation and utilisation is essential for increasing crop productivity and enhancing adaptability to nutrient-poor and water-limited soils (FAO, 2017).

Legumes play a pivotal role in this context. Through their symbiotic relationship with rhizobia, they can fix atmospheric nitrogen. This substantially reduces the demand for energy-intensive nitrogen fertilisers, thereby significantly reducing greenhouse gas emissions. Legumes are also a sustainable source of plant-based protein whose production requires considerably less land, water and energy than producing animal protein. They also promote biodiversity, enrich the soil microbiome, and stabilise agroecosystems in diverse crop rotations (Ferreira et al., 2021; Yanni et al., 2023). To gain a better understanding of these benefits at a molecular level, research is increasingly focusing on model legumes that combine good agricultural performance with high nutritional value.

The world's leading cultivated legume crop is the soybean (*Glycine max*). The high protein content (40 %) of its seeds, combined with large amounts of lipids (up to 24 %), makes them a perfect plant-based protein source (Medic et al., 2014). Unfortunately, soybean production in Europe is difficult, resource-intensive, and limited due to its strict growing requirements (Rotundo et al., 2024). Nevertheless, Europe has become heavily dependent on soybeans and, consequently, on importing them (Fig. 1A). South America is the main producer and large areas of rainforest are being cleared there to increase soybean production (Villoria et al., 2022). Importing them to Europe leads to large amounts of greenhouse gas emissions and is bad for the global climate (Lucić et al., 2025). Therefore, an ideal solution would be an alternative that combines a high protein content with growth conditions adapted to the European climate.

Such an alternative is the white lupin (*Lupinus albus*). Its seed protein content is comparable to that of soybean, but it originates from the Mediterranean area and

therefore is adapted to the local climate conditions (LUCAS ET AL., 2015). In 2023 Europe represents 26.8 % of global lupin production (Fig. 1B) (FAO, 2025).

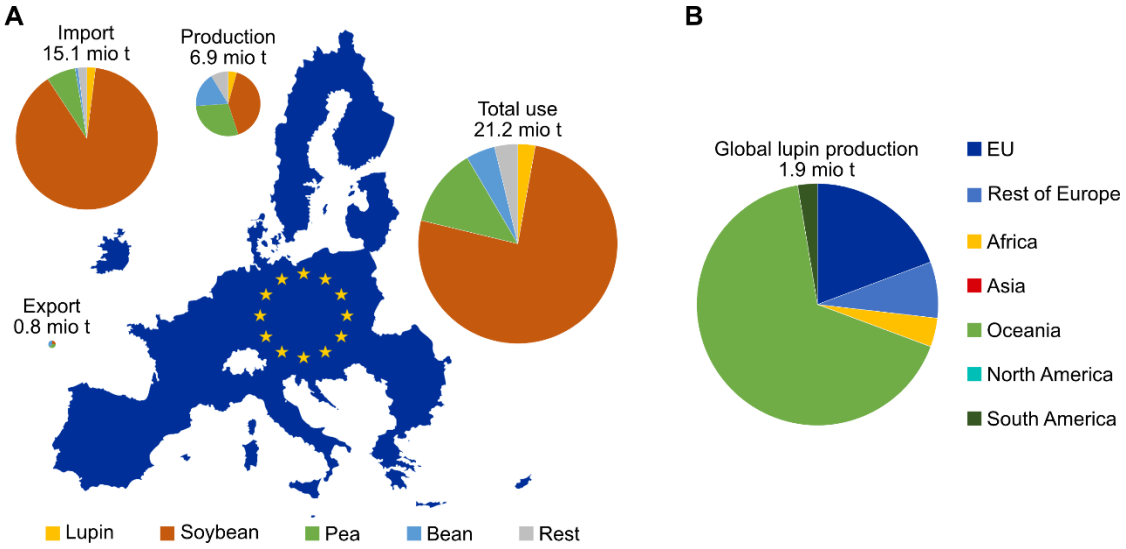

Fig. 1: The lupin market in 2023. (**A**) Production, imports, exports and demand for protein crops in the EU. Demand is much higher than production, so large quantities must be imported. (**B**) Global lupin production. The main producer is Oceania with a 66.7 % share, followed by Europe (adapted from FAO, 2025. Map from DRRANDOMFACTOR, 2023).

1.1 Taxonomy, morphology, and adaptive traits of *Lupinus albus*

Lupinus albus belongs to the family of Fabaceae, also known as legumes. The genus *Lupinus* contains more than 200 species, most native in North and South America, some originate from Europe and North Africa (DRUMMOND ET AL., 2012). Today, four species are from agricultural and nutritional importance: *Lupinus mutabilis* (andean lupin) is characterised by its exceptionally high protein (up to 45 %) and fat content (up to 20 %). It has long been cultivated in its origin area South America as a traditional food crop (CARVAJAL-LARENAS ET AL., 2016). In Europe the three-remaining species, *Lupinus angustifolius* (blue or narrow-leaf lupin), *Lupinus luteus* (yellow lupin), and *Lupinus albus* (white lupin), which originate from the Mediterranean region, are agriculturally relevant. While all three are used in food and feed production, they differ in seed size, protein content, environmental requirements, and alkaloid contend (VALENTE ET AL., 2023).

L. albus is an annual, herbaceous plant (Fig. 2). It reaches heights of 50 to 150 cm, its leaves are palmate, comprising five to nine leaflets (Fig. 2G). The flowers conform to the typical papilionaceous type, are white to bluish (Fig. 2E) and are organised in an

upstanding, multifloral raceme (Fig. 2D). Both, branched and terminal varieties exist. Seeds are about 1 cm in size, white to cream in colour (Fig. 2H) and mature within pods (Fig. 2F) (GEORGIEVA ET AL., 2018). *L. albus* develops a taproot with numerous lateral roots, often forming specialised structures known as cluster roots (Fig. 2B). These consist of root zones with a dense aggregation of short root hairs, markedly increasing root surface area. Cluster roots exude organic acids and enzymes into the rhizosphere, thereby mobilising poorly soluble nutrients, especially phosphate compounds, and making them available to the plant (CHENG ET AL., 2011). This strategy enables *L. albus* to thrive even in phosphorus-deficient soils.

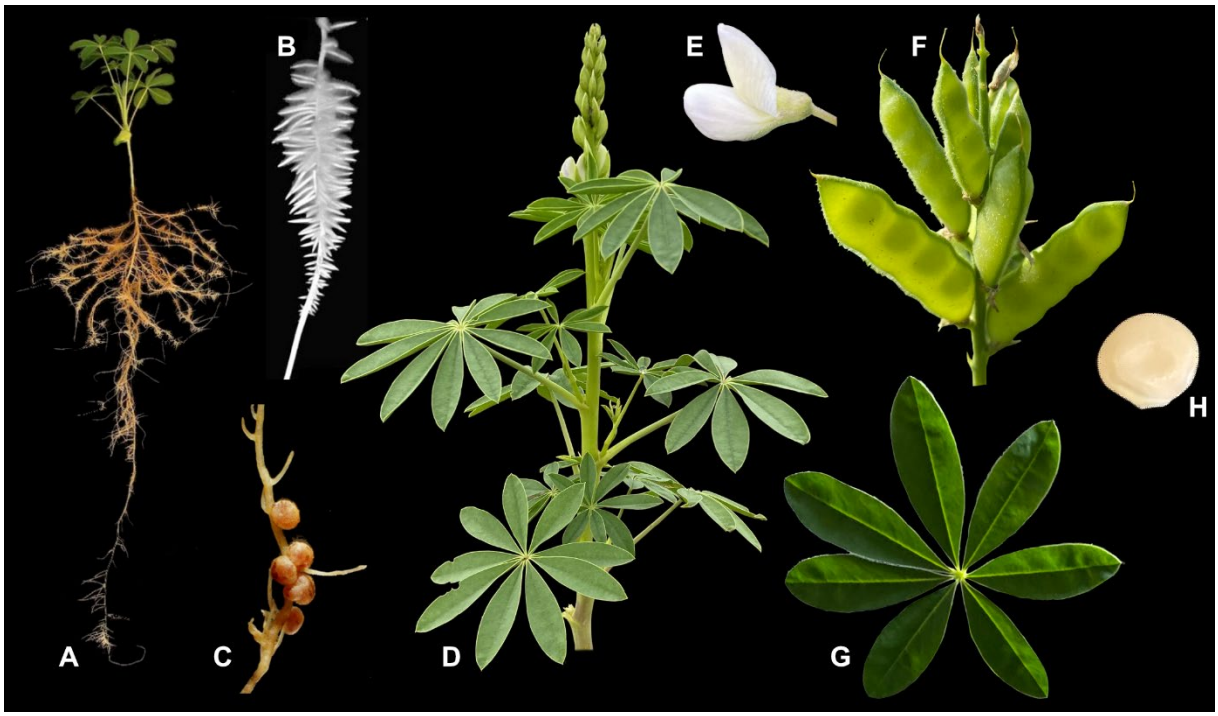

Fig. 2: Morphology of *Lupinus albus*. (**A**) Overall view of a *L. albus* plant showing root system and shoot (adapted from PERET LAB, 2019). (**B**) Cluster roots (adapted from SHANE ET AL., 2003). (**C**) Root nodules (adapted from MARQUÈS ET AL., 2024). (**D**) Shoot with leaves and emerging inflorescence. (**E**) Single flower. (**F**) Pods. (**G**) Leaf. (**H**) Seed. Unless otherwise indicated, photographs are the authors own. Illustrations are not to scale and are intended to provide an impression of morphology rather than size comparison.

Additionally, lupin roots can form symbiotic relationships with nitrogen-fixing *Bradyrhizobium* bacteria, including the formation of root nodules (Fig. 2C). Within these nodules, the bacteria differentiate into bacteroids that are capable of nitrogen fixation (BREWIN, 1991). A specialised haem protein called leghemoglobin ensures the low-oxygen environment required for nitrogen fixation in the nodules (OTT ET AL., 2005). Using the enzyme nitrogenase, bacteroids convert atmospheric nitrogen, which is otherwise unavailable to plants, into ammonium. The ammonium is transferred to the

plant, where it is incorporated into amino acids and proteins. In return, the bacteria receive photosynthetically derived carbohydrates from the host plant (Downie, 2014). *L. albus* is well adapted to the European climate. It thrives on sandy, nitrogen-poor soils but is sensitive to soil compaction, waterlogging, and calcareous conditions (Lucas et al., 2015).

However, its cultivation has declined markedly worldwide in recent decades as a result of anthracnose, a fungal disease that severely impacts yields (Talhinhas et al., 2016). Anthracnose is caused by fungal pathogens belonging to the *Colletotrichum* genus. The first signs of infection are dark lesions on all parts of the plant and twisted sprouts. Afflicted plants wither and die. Seeds grown in infected pods carry latent spores, posing a substantial risk of further spread. The infection can spread rapidly throughout the plant and across the crop, leading to total crop failure and yield losses (Falconí and Yánez-Mendizábal, 2022). Consequently, lupin cultivation in Germany and other European countries declined sharply in the early 1990s (Jacob et al., 2017). Currently there is no effective pesticide available. However, the establishment of tolerant species has laid the foundation for sustainable and economically viable lupin cultivation in regional farming systems (Schwertfirm et al., 2024).

All experiments of this thesis were performed with the sweet *Lupinus albus* cultivar 'Nelly'.

1.1.1 *Lupinus albus* as a model for protein-rich seed metabolism

Lupinus albus occupies a particularly prominent position among legumes. It combines agronomical, nutritional and ecological advantages in a unique way. As well as having a high protein content (Prusinski, 2017), it is characterised by its adaptability to diverse environments, sustainable cultivation traits and its versatility (Gresta et al., 2023; Valente et al., 2024). Consequently, *L. albus* is a promising model organism to investigate the molecular processes of protein-rich seed metabolism, and to develop strategies for breeding future-proof crops.

To explore this potential, the present thesis employs proteomic approaches to analyse and comprehend the metabolic mechanisms that occur during the germination and establishment of *L. albus* seedlings. This establishes a link between genetic information and observed physiology. Therefore, a detailed, well-annotated reference proteome database was lacking. Although there were two genomes of *L. albus* (Hufnagel et al., 2020; Xu et al., 2020) containing approximately 46 500 protein-

coding genes, only 5 % of these proteins were functionally annotated in the reference database available on uniprot.org. In order to bridge the gap between genome data and experimental proteomics, and to enable functional analysis to observe protein plasticity and investigate metabolic changes, we curated the *L. albus* proteome annotation database (see **Chapter 2: Manuscript 1**). Based on BLASTp comparisons with the legumes *Lupinus angustifolius* and *Medicago truncatula* as well as the model organism *Arabidopsis thaliana*, up to 71 % of the *L. albus* proteins could be annotated. Due to the correlation with *A. thaliana* homologues, the use of bioinformatic tools such as SUBA, KEGG, and MapMan was enabled, allowing prediction of subcellular localisation and functional annotation. Nevertheless, 20 140 proteins remain uncharacterised and are thought to be specific to lupins without an *Arabidopsis* homologue.

1.2 Anatomy and functional organisation of the *Lupinus albus* seed

Seeds play a key role in the plant life cycle by enabling generative reproduction. They are the defining feature of seed plants (Spermatophyta), which are classified as either gymnosperms (0.4 %) or angiosperms (99.6 %) (Ran et al., 2018). Depending on the plant species and environmental factors, seeds can be highly specialised and variable, but three structural elements are highly conserved across all species: testa, embryo and endosperm (Fig. 3).

The testa is the coat of the seed and provides the necessary mechanical defence and impermeability for dormancy. During seed development, the testa plays an important role in providing and transporting nutrients. Later, during seed maturation and desiccation, programmed cell death occurs, resulting in cell shrinking and death (Smýkal et al., 2014).

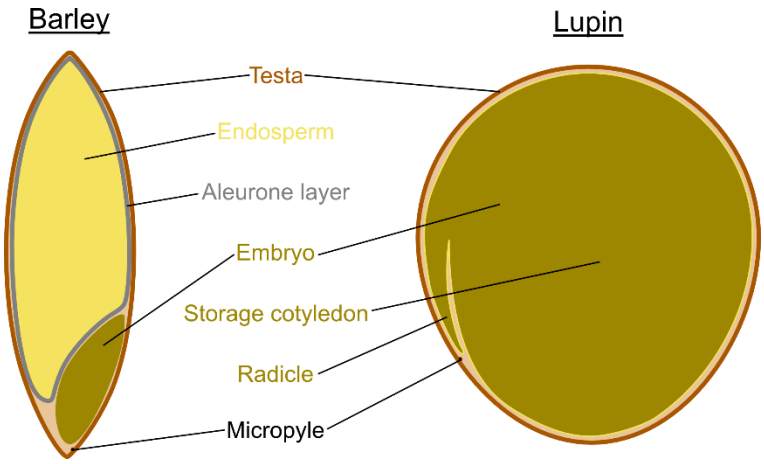

Fig. 3: Schematic cross-sections showing the structure of a plant seed. While the external morphology of seeds is highly species-specific and diverse, they share a conserved basic organisation consisting of the testa, embryo, and storage tissue. Left: Barley as an example of a monocot starch-storing seed. The embryo is comparatively small, whereas the endosperm is well developed, specialised in carbohydrate storage and enclosed by the aleurone layer (adapted from GORZOLKA ET AL., 2016). Right: Lupin as an example of a dicot seed with nutrient-storing cotyledons. The embryo is particularly pronounced, specially its cotyledons. The endosperm is greatly reduced or entirely absent, and nutrients are mainly accumulated in the large cotyledons (adapted from ROBLES-DÍAZ ET AL., 2016).

The testa of *Lupinus albus* compromises three layers: the macrosclereid, the osteosclereid and the parenchyma (MARZOUK, 2018) (Fig. 4). The macrosclereid cells, the outermost layer, are elongated and show extensive asymmetric secondary cell wall formation. Cutin and suberin can be integrated to provide impermeability and mechanical defence. A surrounding layer of cutin and waxes, the cuticle, provides an additional barrier for water and gas exchange (SMÝKAL ET AL., 2014). In *L. albus* the macrosclereid is formed by two cell layers and is 0.118 mm thick (MARZOUK, 2018). The middle layer, the osteosclereid, is sclerified and lignified, containing large air-filled intercellular spaces that form a barrier against pathogens and physical damage (SMÝKAL ET AL., 2014). The innermost layer of the testa consists of parenchyma cells that are in direct contact with the inner seed structures. In *L. albus,* 60 % of the testa is made of parenchyma cells (MARZOUK, 2018). These cells can accumulate various protective compounds such as pigments, antioxidants, phenols and flavonoids to protect the seed against herbivores, oxidative stress and regulate temperature (RADCHUK AND BORISJUK, 2014). The structure of the testa can also be influenced by environmental conditions (HYVÄRINEN ET AL., 2025).

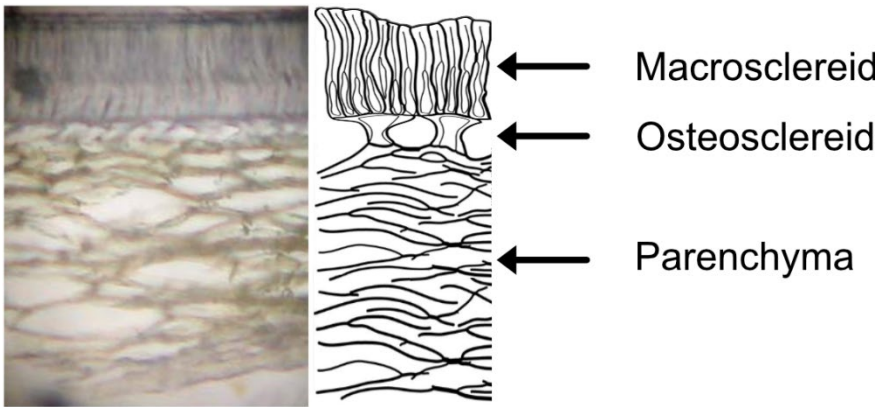

Fig. 4: Arrangement of the testa of *Lupinus albus*. Left: transverse section, right: schematic drawing. The outermost part is the macrosclereid, which has elongated cells with thickened cell walls. The central part of the testa differentiates into an osteosclereid with large apoplastic areas. The innermost layers, the parenchyma cells, are in direct contact with the inner seed structures (adapted from MARZOUK, 2018 and SMÝKAL ET AL., 2014).

The Endosperm and the embryo are located within and protected by the testa. The endosperm is a specialised seed storage tissue that accumulates and stores reserves, which it later provides to the embryo. The composition, the size and the persistence of the endosperm vary by species. In species that store the endosperm, such as many cereals, it constitutes a highly specialised organ that occupies nearly the entire interior of the seed (Fig. 3, left) (SHEWRY ET AL., 2023). In contrast, in embryo-storing species such as legumes and brassicas, the endosperm is greatly reduced or absent in the mature seed, with reserves accumulating directly in the embryo (Fig. 3, right) (YAN ET AL., 2014).

The embryo is the central unit of the seed, representing the future plant in an undifferentiated stage of development. It already shows a subdivision into the rudimentary primary organs: the radicle (embryonic root), the plumule (embryonic shoot), and the cotyledons (embryonic leaves) (BEWLEY AND BLACK, 1994).

Unlike many other species, the mature seeds of *L. albus* contain no endosperm, as this is consumed by the embryo during seed development and maturation. Instead, it is the embryo, particularly the cotyledons, that occupies almost the entire interior of the seed, serving as the main storage organ (Fig. 3, right) (ESCUDERO-FELIU ET AL., 2023; WINNICKI ET AL., 2019).

1.2.1 Seed storage compounds and strategies

Plant seeds are heterotrophic, relying mostly on their stored reserves during germination and early seedling establishment. Therefore, efficient storage of these

reserves is essential for successful plant reproduction. Storage compounds can be classified into three main categories of macromolecular reserves: carbohydrates, lipids, and proteins. Each class has unique chemical properties that make them ideally suited to long-term, compact storage and subsequent rapid remobilisation (SREENIVASULU, 2017). Different plant species use different storage strategies: cereals, such as wheat, rice, and corn, are plants that store carbohydrates. Their endosperm is specially adapted to store large quantities of carbohydrates, mainly starch, and is surrounded by the aleurone layer. This is a specific type of cell that plays a crucial role in starch mobilisation during germination (Fig. 3, left) (OLSEN, 2007). Oilseed crops, such as rapeseed and sunflowers, store lipids, primarily in form of triacylglycerols (TAGs), as highly reduced carbon compounds (VER SAGUN ET AL., 2023). Legumes, such as *L. albus*, predominantly store proteins. These storage proteins not only function as carbon reserves but also contain significant amounts of nitrogen and sulfur (GALLARDO ET AL., 2008).

1.2.2 Composition and nutritional characteristics

In line with these general seed storage strategies, the composition of *Lupinus albus* seeds reflect their protein-based reserve metabolism. They are characterised by their exceptionally high nutritional value (Fig. 5). Compared with many other plant species, they have much higher protein content, typically ranging from 30 to 40 % of dry weight (DW) (PRUSINSKI, 2017). They also contain a considerable lipid fraction (5 - 15 %) (RYBIŃSKI ET AL., 2018) and carbohydrates. Unlike many plants and also legumes, *L. albus* seeds contain almost no starch. Their main carbohydrates are oligosaccharides and non-starch polysaccharides, which are primarily derived from the cell wall and are therefore metabolically unavailable for the seed (MALEKIPOOR ET AL., 2022; PEREIRA ET AL., 2022).

We analysed proteins, which were the most abundant storage compound found in *L. albus* seeds, accounting for 34 % DW (see **Chapter 2: Manuscript 1**). Free amino acids represented 1.5 % of DW. Total lipid content was quantified at 10.7 % DW. Total carbohydrates accounted for 29.8 % DW. These results are consistent with previous studies and exemplify the classification of *L. albus* as a protein-storing plant. The high protein content reflects the ability to accumulate nitrogen through symbiosis with nitrogen-fixing bacteria, enabling the storage of ’expensive’ nitrogen sources during seed development. The carbohydrate content mainly includes oligosaccharides from

the raffinose family, which can be used as a resource during germination, as well as cell wall oligosaccharides that are not metabolically available to the seed. Lipids act as a compact energy source with a high carbon content, albeit in smaller amounts than the other two storage compounds. This finding led to the hypothesis that *L. albus* relies on its most abundant storage compound, protein, for the process of germination.

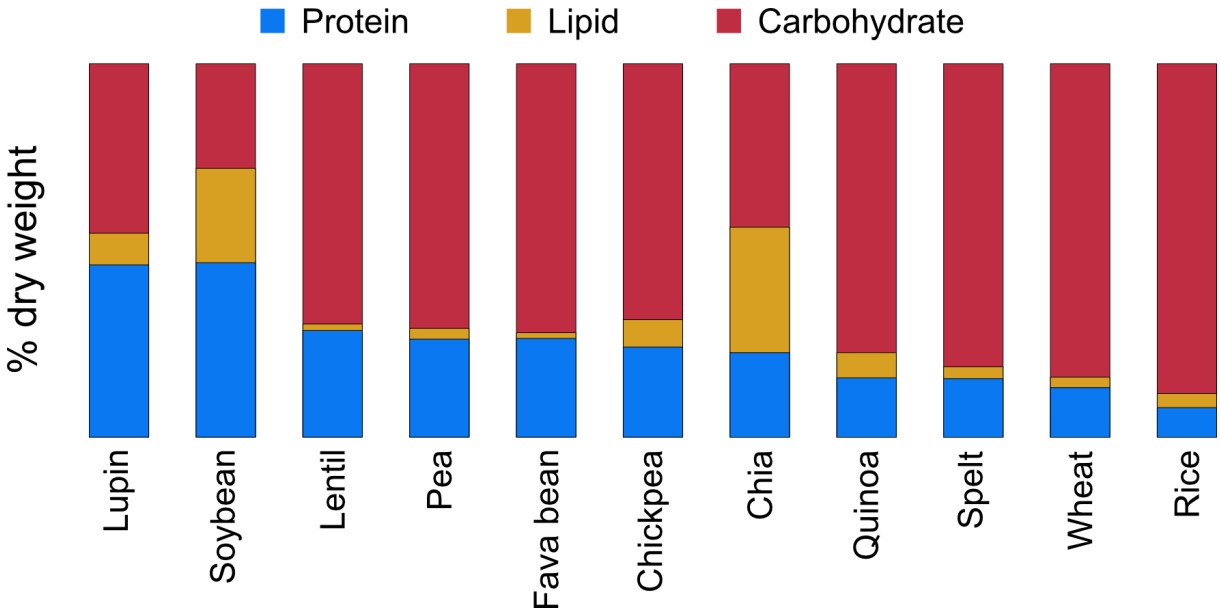

Fig. 5: Macronutrient composition of seed storage compounds in different crops. Legumes such as lupin, soybean, lentil, pea, fava bean and chickpea are characterised by their high protein content. Lupin and soybeans have exceptionally high protein content, making them an excellent source of plant-based protein. Spelt, wheat and rice are cereals characterised by their monocotyledonous nature and high carbohydrate content, primarily in the form of starch. Chia and quinoa are pseudocereals. Although they are dicotyledons, they are commercially used like cereals. Both chia and soybeans contain large amounts of lipids, making them valuable oil crops (adapted from KOURIS-BLAZOS AND BELSKI, 2016).

L. albus seeds are also a valuable source of micronutrients and minerals, including calcium, phosphorus, magnesium, potassium, sodium, and manganese. Additionally, they contain vitamins such as thiamine (B1), niacin (B3), riboflavin (B2), tocopherols (vitamin E), and carotenoids (PEREIRA ET AL., 2022). Furthermore, lupins accumulate significant levels of phytochemicals, including polyphenols (flavones, phenolic acids, isoflavones), phytosterols (β-sitosterol, stigmasterol), and triterpenes (squalene, ursolic acid) (KHAN ET AL., 2015).

As with all lupin species, wild forms of *L. albus* produce quinolizidine alkaloids. These bitter-tasting secondary metabolites protect the plant against herbivory. They are found in high concentrations in the seeds and leaves of the plant, and can be neurotoxic to humans in large quantities. Wild type varieties may contain up to 11 % alkaloids and

are therefore unsuitable for use as food or animal feed. However, through targeted breeding, 'sweet' cultivars with drastically reduced alkaloid content (typically below 0.02 %) have been developed, rendering them safe for consumption (Osorio and Till, 2022).

1.2.3 Carbohydrate composition and functional significance

The seeds of *Lupinus albus* have a distinctive carbohydrate profile, setting them apart from other grain legumes. Unlike beans and peas, which are recognised for their substantial starch content, *L. albus* contain negligible amounts of starch (Mohamed and Rayas-Duarte, 1995). The carbohydrate content accounts for 30 to 40 % of the seed DW. It is mainly divided into cell wall polysaccharides, such as cellulose, hemicellulose, arabinogalactan, and pectin, as well as into raffinose family oligosaccharides (RFOs), which include stachyose, raffinose, and verbascose (Mohamed and Rayas-Duarte, 1995; Pereira et al., 2022). Small amounts of sucrose and glucose complete the carbohydrate profile (Martínez-Villaluenga et al., 2005; Mohamed and Rayas-Duarte, 1995). In combination with late embryogenesis abundant (LEA) proteins, RFOs are essential for seed desiccation tolerance. They form the viscous vitreous matrix that preserves the integrity of membranes, organelles, and enzymes until rehydration (Buitink and Leprince, 2008).

1.2.4 Lipid content and fatty acid composition

Depending on the cultivar, location, and environmental conditions, *Lupinus albus* seeds contain, a total lipid content ranging from 7 to 14 % of DW (Borek et al., 2015). They mainly occur in the form of TAGs and serve as a highly concentrated energy source (Ver Sagun et al., 2023). Storage lipids are packaged in lipid droplets, called oleosomes, which are surrounded by a phospholipid monolayer and stabilised by proteins, called oleosins (Borek et al., 2009). The fatty acid profile of *L. albus* is primary composed of unsaturated fatty acids, which make up 70 to 80 % of the total lipid content. Oleic acid accounts for about 50 % of the total fatty acid pool, whereas linoleic acid constitutes around 35 %. Saturated fatty acids are found in relatively low levels (10 - 15 %), primary consisting of palmitic and stearic acid. This composition provides both oxidative stability, which is attributed to the high level of oleic acid, as well as improved nutritional value compared to soybean oil (Al-Amrousi et al., 2022; Rybiński et al., 2018).

1.2.5 Composition and functional characterisation of the proteome

Our results indicated that the proteome of *Lupinus albus* seeds was dominated by proteins involved in nutrient storage, desiccation tolerance, and stabilising lipid bodies. This suggests that the seeds employ adaptive strategies to ensure successful germination and survival under variable environmental conditions (see **Chapter 2: Manuscript 1**).

The most dominant protein group that we identified in *L. albus* seeds was the storage proteins (see **Chapter 2: Manuscript 1**). They are mainly organised into protein bodies and protein storage vacuoles (Ibl and Stoger, 2012). Inside these storage organelles, proteins aggregate to form dense structures that protect them against premature degradation and enable controlled release during mobilisation (Antonets et al., 2020). Some storage proteins have dual functions, acting as both nutrient reserves and functional enzymes or antioxidant agents, further highlighting evolutionary efficiency (Bojórquez-Velázquez et al., 2019; Cândido et al., 2011; Escudero-Feliu et al., 2023).

L. albus storage proteins make up around 85 % of seed protein. According to Osborne's classification, they belong to albumins and globulins in a ratio of one to nine (Balrove and Gillespie, 1975). Albumins are functional proteins that exhibit metabolic, inhibitory and lectin activities (Casey, 1999; Domoney, 1999; dos Ramos et al., 1997). Globulins are typical seed proteins with storage function. The main protein families in *L. albus* are conserved, but there is heterogeneity according to variety and environmental impact (Duranti et al., 2008). They are traditionally referred as conglutin and classified into four families: α-, β-, γ-, and δ-conglutin, based on their electrophoretic properties (Duranti et al., 2008; Foley et al., 2011).

Structurally, *L. albus* α-conglutin belongs to the 11S globulins (legumin-like) and accounts for up to 35 % of the total storage protein content (Duranti et al., 1984). It is synthesised as a trimeric pro-peptide that undergoes proteolytic cleavage during maturation (Adachi et al., 2003). The mature subunits exist in a concentration and pH-dependent equilibrium, forming either hexamers of 300 to 400 kDa or corresponding trimeric structures (Duranti et al. 1988). The monomers of α-conglutin consist of acidic and basic polypeptide chains, linked by disulphide bonds (Devkota et al., 2023; Foley et al., 2015). They exhibit a heterogeneous pattern in SDS-PAGE separation, indicating a multigenic origin and post-translational modifications, as

observed in homologous proteins in other species (Duranti et al. 2008). Some subunits have been shown to undergo glycosylation (Duranti et al., 1988; Duranti et al., 1992). 3D structure analyses of α-conglutin have shown that the basic subunits are located in the protein core, making them more resistant to proteolysis during germination (Adachi et al., 2003). Similar properties have been observed *in vitro* where the acidic subunit degrades faster (Duranti and Giani, 1989).

The most abundant storage protein in *L. albus* is β-conglutin, accounting for up to 45 % of the total storage protein content (Duranti et al., 1981). It is a 7S globulin (vicilin-like) that assembles as a heterogeneous trimer with a molecular weight of 150 to 210 kDa (Blagrove and Gillespie, 1975). The pro-peptide exhibits various proteolytic sites, resulting in over 40 distinct monomers ranging from 16 to 70 kDa (Duranti et al. 2008; Magni et al., 2007). β-conglutin shows no disulphide bonds, but several glycosylation sites (Duranti et al. 2008). It is postulated to be a storage protein (Duranti et al., 1984), but dos Ramos et al. (1997) also demonstrated the lectin-like activity of a β-conglutin monomer, suggesting additional biological functions.

γ-conglutin is a 7S glycoprotein that is classified as a globulin (Duranti et al. 2008). It accounts for around 5 % of *L. albus* total storage protein (Duranti et al. 1981). It assembles into tetramers or higher oligomers with a molecular weight of 200 kDa (Duranti et al. 2008). At low pH, the oligomers decompose into monomers (Duranti et al., 1986). Each monomer comprises two subunits, one of them is glycosylated (Eaton-Mordas and Moore, 1978). The mature protein is stabilised by various disulphide bonds (Restani et al., 1981). γ-conglutin exhibits several characteristics that distinguish it from typical storage proteins. As well as being found in protein bodies, it has also been found in the apoplast of germinating lupin cotyledons (Duranti et al., 1994). Its stability against proteolytic degradation is notable and unusual for a storage protein (Duranti et al., 1995). Furthermore, γ-conglutin is able to bind divalent metal ions. This suggests that, in addition to its storage function, γ-conglutin has bioactive properties (Duranti et al. 2008).

δ-conglutin belongs to the group of 2S albumins and makes up around 5 % of the total storage protein in *L. albus* seeds (Sironi et al., 2005). It is notably rich in sulfur, and its subunits are linked by disulphide bonds (Salmanowich and Weder, 1997). Its cellular localisation and biological function remain unknown. However, findings in homologous proteins in other legumes suggest localisation in protein storage vacuoles,

with an inhibitory activity that leads to defence functions (Duranti et al. 2008; Gayler et al., 1989).

We found other abundant seed-related protein groups in *L. albus* that do not fall directly into the category of storage proteins. These included LEA proteins and oleosins (see **Chapter 2: Manuscript 1**). LEA proteins are small, hydrophilic proteins that accumulate in large quantities in seeds (Banerjee and Roychoudhury, 2016). They are intrinsically disordered when hydrated but adopt stable conformations under water-limiting conditions (Leprince et al., 2017). During desiccation in maturating seeds LEA proteins replace water molecules in membranes and proteins. This stabilises hydration shells, preventing denaturation and aggregation, which would otherwise cause irreversible damage (Chakrabortee et al., 2007; Hong-Bo et al., 2005). In combination with sugars such as RFOs, LEA proteins form a viscous vitreous matrix that immobilises biomolecules, suppressing unwanted chemical reactions and interactions (Ballesteros and Walters, 2011). This preserves the integrity of membranes, organelles, and enzymes in seeds until rehydration (Buitink and Leprince, 2008).

Oleosins are structural proteins responsible for stabilising oleosomes in *L. albus* seeds. They consist of two amphipathic (C- and N-terminal) and a central hydrophobic domain (Tzen et al., 2003). The highly conserved hydrophobic centre acts as an anchor and is incorporated into the oleosome. The terminal domains associate with the surrounding monolayer (Tzen, 2012). Oleosins play a key role in stabilising oleosomes, preventing aggregation through electronegative repulsion and steric hindrance (Tzen et al., 1992). Some oleosins are thought to contain enzymatic activities related to lipid degradation during germination, but this needs to be investigated further (Parthibane et al., 2012).

1.3 Seed dormancy and germination control in *Lupinus albus*

Having examined the structural and biochemical composition of *Lupinus albus* seeds, it is equally important to understand the physiological mechanisms that control their dormancy and germination.

The basis of a new plant is established once seed development, maturation, and desiccation are complete. However, the transition to germination is controlled by environmental cues and intricate internal mechanisms and does not happen instantly.

Dormancy, which varies in form and intensity between species and plays a key role in determining the timing and spatial pattern of germination, lies at the heart of this regulation. Baskin and Baskin (2004) distinguish three main categories: morphological, physiological and physical dormancy.

Due to their hard, impermeable testa, *L. albus* exhibits physical dormancy (Wen et al., 2024). By limiting germination to circumstances conducive to the successful establishment of seedlings, this approach ensures the survival of populations in a variety of habitats (Paulsen et al., 2013). This is considered one of the most important adaptations for persistence in ecosystems that are prone to aridity or flooding (Moreira and Pausas, 2012; Rosbakh et al., 2023). In natural settings, the testa experiences mechanical stresses and microcracks due to temperature variations and frost-thaw cycles, which aid in the release of dormancy. Additionally, the testa may be locally weakened by fungi and microorganisms (Jones et al., 2016; Nautiyal et al., 2023).

Dormancy is artificially broken in agriculture. The testa is damaged by abrasion during mechanical scarification, which increases its water permeability. To make the testa brittle, thermal techniques such as hot-water treatment are also employed. Furthermore, breeding has significantly reduced dormancy in cultivated varieties of *L. albus* by softening of the testa (Smýkal et al., 2014; Tiryaki and Topu, 2014).

1.4 Phases and molecular mechanisms of germination

Seed germination begins as soon as dormancy is broken and favourable environmental conditions are met. It can be divided into three distinct phases: imbibition, plateau phase and testa rupture (Fig. 6) (Bewley, 1997). These closely synchronised processes are controlled by the interaction of water uptake, hormonal signalling, reserve mobilisation and metabolic activation.

1.4.1 Phase I: Imbibition – initiation of metabolic reactivation

Imbibition is defined as the passive absorption of water by the seed and is the first step in the germination process (Moret-Fernández et al., 2024; Vertucci, 1989). The water potential of dry seeds is significantly negative due to their low water content (5 - 15 %) (Finch-Savage and Footitt, 2017). This draws water from the surrounding environment, with the micropyle, a less lignified and more permeable part of the testa, usually serving as the first entry point (Jaganathan et al., 2019). The seed volume

rapidly increases due to the absorbed water (swelling). The testa is subject to mechanical tension as a result of the stretched cell walls and increase in internal pressure. Hydrophilic structures within the seed, such as polysaccharides and storage proteins, bind water and become hydrated (Grandis et al., 2024; Plenzler et al., 2002; Xu et al., 2017). The internal repair mechanisms of the seed are triggered during this process. Membrane lipids relocalise to restore membrane continuity and regain fluidity through rehydration. Mitochondrial respiration begins (Nietzel et al., 2020). Such restructuring signifies the pivotal change from a dormant seed to metabolically active tissue (Pompelli et al., 2023).

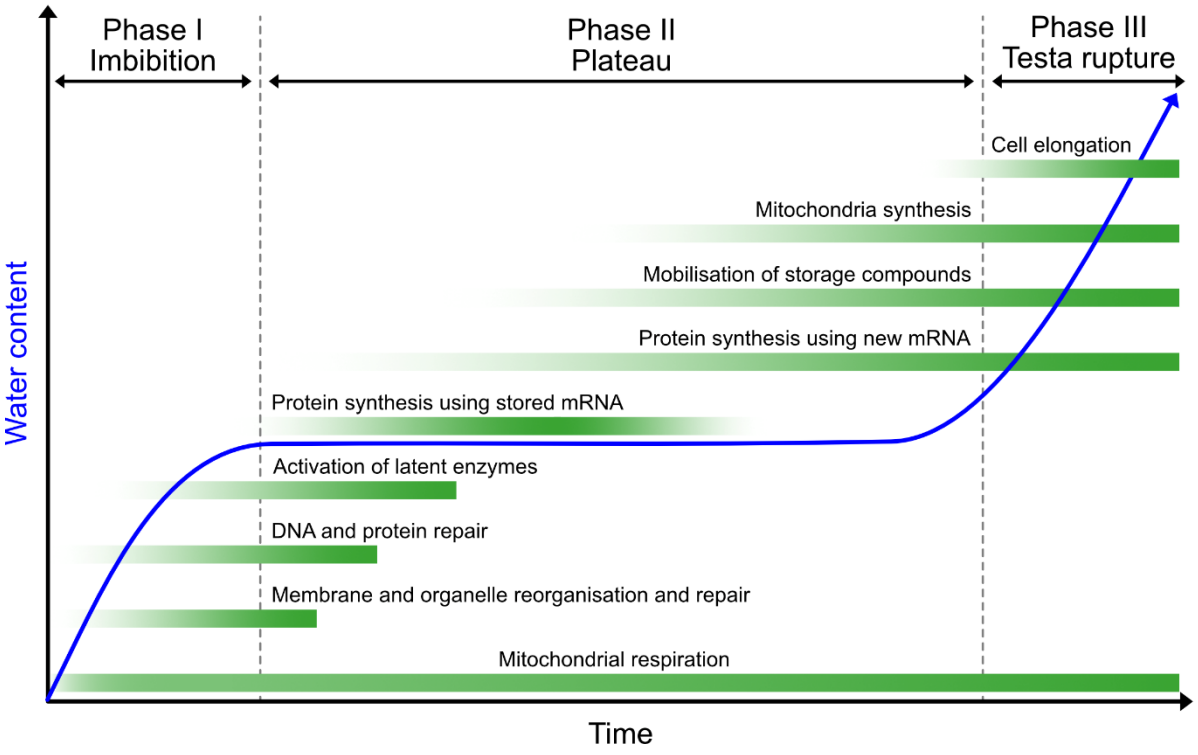

Fig. 6: Seed hydration curve and phases of germination in seed plants. Water uptake plays a key role in germination. During imbibition, passive water absorption hydrated the seed hydration and reorganises its cellular components, activating initial metabolic processes. This is followed by a plateau phase in water uptake, during which metabolic activity increases markedly, storage reserves are mobilised, and cell division processes are initiated. Germination is complete when the radicle emerges through the testa. The time required for these events can range from several hours to many weeks, depending on the plant species and germination conditions (adapted from Bewley, 1997).

1.4.2 Phase II: Plateau phase – cellular repair and metabolic activation

The plateau phase begins when the seed water content stabilises after imbibition. This phase is characterised by intense reorganization and metabolic activation, even in the absence of additional water uptake (Weitbrecht et al., 2011). The seed now absorbs more gases from the environment (Wiraguna, 2022). Latently stored enzymes are activated, including those involved in DNA and protein repair mechanisms, such as methionine sulfoxide reductases and apurinic/apyrimidinic endonucleases (El-Maarouf-Bouteau et al., 2013; Kiran et al., 2020), as well as antioxidant enzymes, including catalase, superoxide dismutase and peroxiredoxins (Gidrol et al., 1994). Apart from enzymes, the seed also contains stored mRNA that is ready for translation as soon as imbibition occurs. Despite transcription being severely limited during the early stages of germination due to condensed chromatin and the transient absence of transcriptional machinery, this enables the rapid synthesis of essential proteins (Sano et al., 2020). So, the proteins required for metabolic activation, such as chaperones, membrane and signalling proteins, and enzymes involved in energy and nutrient metabolism, are latently stored in seeds or are primarily encoded by these stored mRNA (Bai et al., 2019). Cellular organelles are restored and activated as membrane and protein repair progresses. ATP synthesis improves with increased aerobic respiration in the mitochondria (Nietzel et al., 2020). As transcription resumes, proteins essential for the respiratory chain, lipid biosynthesis, repair processes, regulatory roles and mitochondrial import machinery are synthesised (Silva et al., 2017; Wang et al., 2014). Complete reactivation of mitochondrial metabolism, including the TCA cycle, cellular respiration and oxidative phosphorylation, in combination with the glyoxylate cycle, meets the high demand for ATP and reducing equivalents (NADH and $FADH_2$) (Zafari et al., 2020). DNA replication and protein biosynthesis for cytoskeletal and cell wall components are first steps in meristematic preparation for cell division (Waterworth et al., 2022). The production of biomass and respiratory substrates is facilitated by the hydrolysis of nutrient reserves (Joshi, 2018). Their breakdown alters the osmotic potential, allowing aquaporins to permit water to enter the embryos cells due to their low water potential (Vander Willigen et al., 2006).

1.4.3 Phase III: Radicle emergence – completion of germination

Water uptake into the seed resumes at the end of the plateau phase. The expansion of embryonic cells caused by the inflow of water results in a steady rise in turgor pressure, particularly in the radicle. At the same time, enzymatic attacks weaken the testa, which eventually breaks. Seed germination is concluded by the mechanical rupture of the testa and the emergence of the radicle. The seedling then enters the post-germination phase (BEWLEY ET AL., 2013).

1.4.4 Kinetics of water uptake and germination progress in *Lupinus albus*

In *Lupinus albus* we observed the typical three-phase separation of germination. Seed swelling, as evidenced by an increase in fresh weight and radicle length, occurred immediately and persisted for 18 hours, after which a period of rest associated with increased respiration ensured. Thirty hours after imbibition, the testa ruptured and germination was complete, after which post-germination growth commenced (see **Chapter 2: Manuscript 1**).

Similar observations were made by GARNCZARSKA ET AL. (2007), who investigated the water-related germination processes in lupins using magnetic resonance imaging and gravimetric analysis (Fig. 7). They observed that a seed water content of less than 10 % leads to a metabolic resting state. Water uptake begins at the micropyle, first hydrating the embryonic axis and then the cotyledons from the outside in. During the initial stages of hydration, water primarily binds to cell walls and proteins, forming hydration shells and stabilising membranes. Later, the amount of free water increases. Imbibition, which was observed as exponential water uptake, took place over five hours. The water content increased 18-fold, reaching 1.8 g H_2O per g DW. During the plateau phase, the water level remained stable, but reallocation continued until the entire seed was fully saturated. This took 18 hours from the start of imbibition.

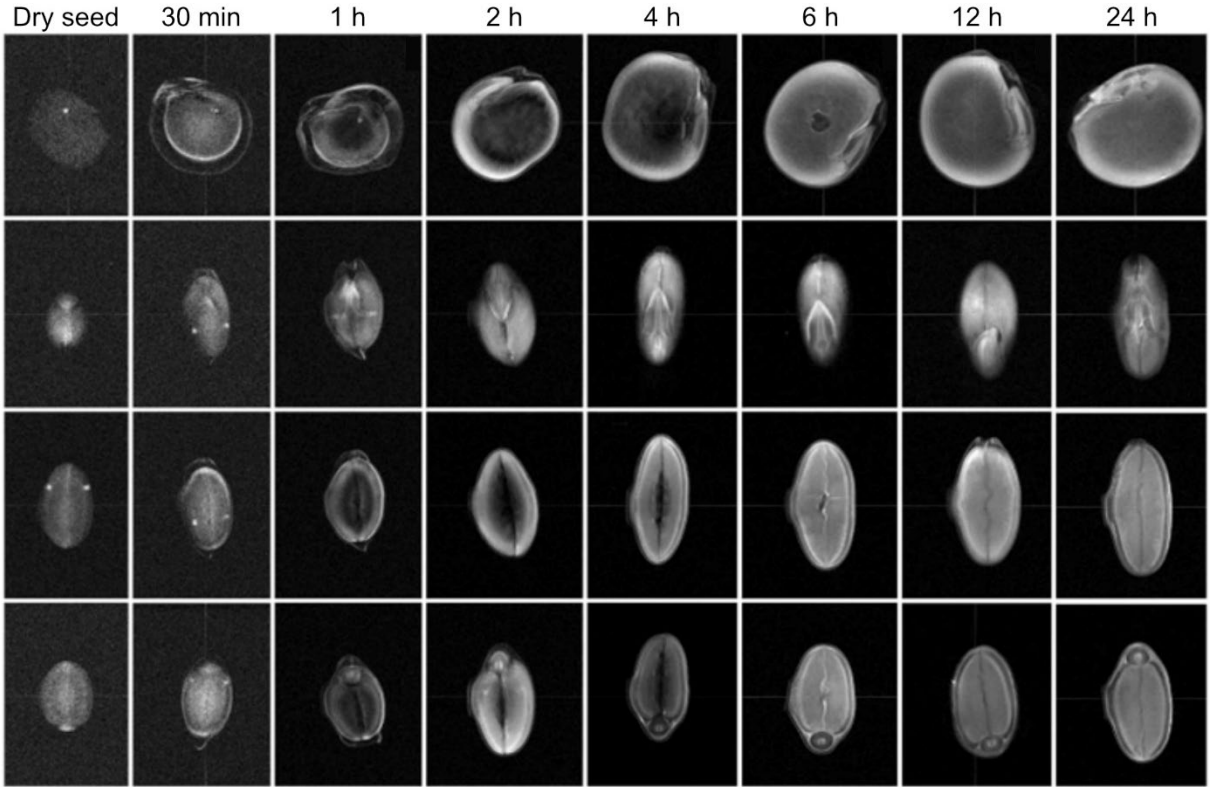

Fig. 7: Magnetic resonance imaging of germinating lupin seeds. The signal is caused by differences in the mobility of hydrogen protons, local proton density, and transverse relaxation times. Bright signals indicate high intensity and therefore high-water content. Dark areas show low intensity and the absence of water. Storage compounds have low transverse relaxation times, so the signals primarily represent the spatial distribution of free water. Hydration times: 0 min, 30 min, 1 h, 2 h, 6 h, 12 h and 24 h. Sagittal plane (first row), coronal plane (superficial slice (second row) and near-median slice (third row)) and axial plane (fourth row) (from GARNCZARSKA ET AL., 2007).

1.5 Enzymatic mobilisation of storage reserves during germination of *Lupinus albus*

During germination seeds are heterotrophic, relying mostly on their stored reserves. Therefore, efficient storage and controlled release of these reserves is essential for successful seedling establishment. Resource mobilisation is conducted by enzymatic degradation by hydrolases (Fig. 8).

The hydrolysis of the RFOs is carried out by α-galactosidase, which cleaves the galactosyl residues from the RFOs, generating sucrose and galactose. Sucrose can be further degraded into glucose and fructose by invertase, or metabolised by sucrose synthase to yield UDP-glucose and fructose. Galactose is then phosphorylated into galactose-1-phosphate by an ATP-dependent galactokinase. Further digestion can occur via pyrophosphorylase, which converts galactose-1-phosphate and UTP to UDP-galactose and PPi. UDP-galactose is then converted into UDP-glucose by the NAD-

dependent UDP-galactose-4-epimerase. These monosaccharides can be used in glycolysis or the TCA cycle for energy production and as precursors for carbohydrate metabolism (SALVI ET AL., 2022).

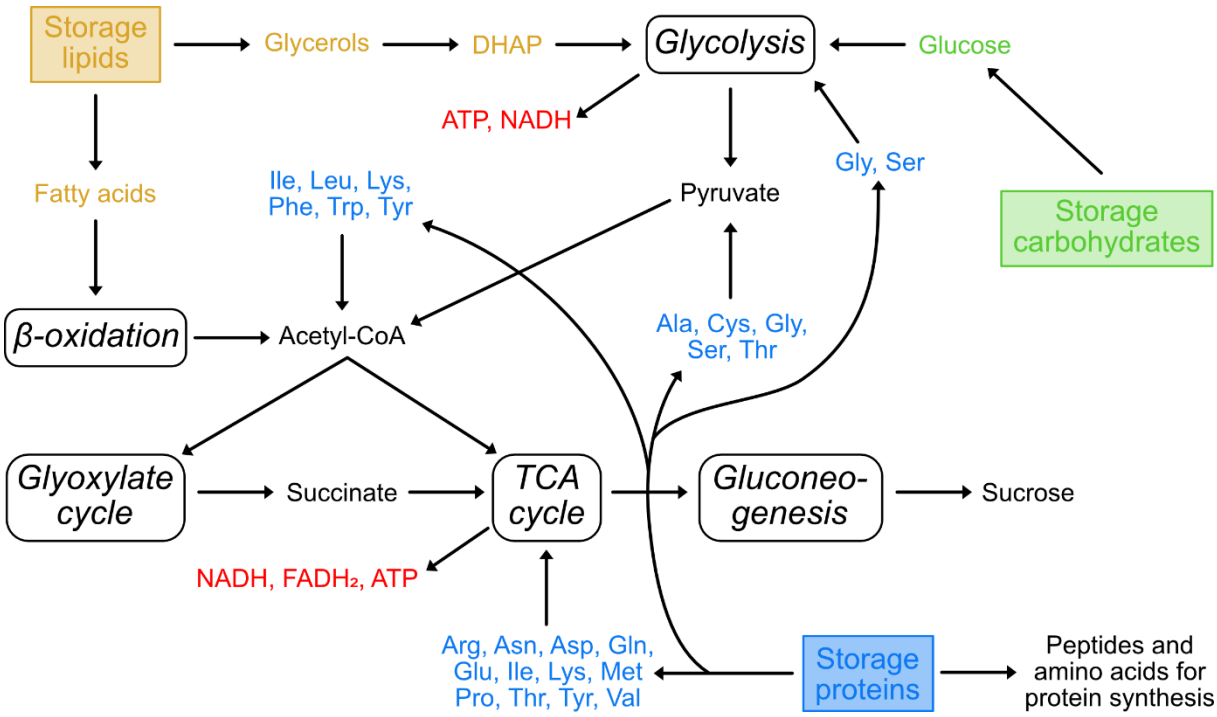

Fig. 8: Potential integration of storage compound remobilisation pathways during *Lupinus albus* germination. Lipid degradation produces glycerol and fatty acids. Glycerol is catabolised to dihydroxyacetone phosphate (DHAP), which enters glycolysis. Fatty acid β-oxidation generates acetyl-CoA. Carbohydrates, mainly RFOs, are enzymatically hydrolysed to glucose and enter glycolysis. Pyruvate, the end product of glycolysis, can also be converted into acetyl-CoA. Acetyl-CoA feeds into either the glyoxylate cycle or the tricarboxylic acid (TCA) cycle. Intermediates of the glyoxylate cycle can enter the TCA cycle, while TCA cycle intermediates can serve as substrates for sucrose synthesis via gluconeogenesis. Glycolysis and the TCA cycle generate ATP and other energy equivalents. Proteins are degraded into peptides and amino acids, which can serve as precursors for protein synthesis or be channelled into lipid or carbohydrate degradation pathways to contribute to energy and carbohydrate production (adapted from HILDEBRANDT ET AL., 2015; KAUR ET AL., 2021).

In order for lipid hydrolysis to occur, the protective structure of the oleosomes must be made accessible to hydrolytic enzymes. Although the exact identity of the enzymes involved is still up for debate, evidence points a ubiquitination signal to break down the stabilising oleosins. Once transferred to a conjugation enzyme and activated in an ATP-dependent reaction, a ubiquitin ligase attaches ubiquitin to oleosins. The end product of repeated cycles is polyubiquitinated oleosins (DERUYFFELAERE ET AL., 2015). Segregases, which extract oleosins from the oleosome, recognise and bind to polyubiquitinated oleosins. The oleosins are then unfolded and delivered to the

proteasome for breakdown. This destabilises the oleosome surface, and allowing access for lipolytic enzymes such as lipases (Deruyffelaere et al., 2018).

The most notable lipase found in plant seeds is the sugar-dependent lipase 1 (SDP1), which is located in the peroxisomal membrane. While germination, peroxisomes create membrane protrusions that facilitate communication between SDP1 and oleosomes (Thazar-Poulot et al., 2015). Lipase breaks the ester bond between the fatty acid and the glycerol (Wilson and Knoll, 2018). Because glycerol is water-soluble, it diffuses into the cytosol, where it is phosphorylated by glycerol kinase. The resulting glycerol-3-phosphate is then oxidised by glycerol-3-phosphate dehydrogenase to produce dihydroxyacetone phosphate (DHAP). DHAP is a by-product of glycolysis and gluconeogenesis that can be used for sucrose biosynthesis or energy production (Eastmond, 2004).

Free fatty acids have to be metabolised quickly as they are lipophilic and potentially harmful. Coenzyme A (CoA) and ATP activate them to produce acyl-CoA, with AMP and PPi as by-products (Fulda et al., 2002). ABC transporters then carry the acyl-CoA into the peroxisome where it undergoes β-oxidation (Kunz et al., 2009). This pathway produces hydrogen peroxide, which is detoxified by catalase through the oxidation of acyl-CoA to trans-Δ^2-enoyl-CoA. Following hydration to form 3-hydroxyacyl-CoA, enoyl-CoA undergoes oxidation to produce 3-ketoacyl-CoA. The thiolase enzyme then breaks down this intermediate, releasing acetyl-CoA and shortening the fatty acid chain in the process. The resulting acyl-CoA then re-joins the cycle (Pan et al., 2019). Once the acetyl-CoA enters the glyoxylate cycle, its intermediates can be directed towards gluconeogenesis to synthesise sucrose (Eastmond et al., 2000; Walker et al., 2021). In the germination of *L. albus*, sucrose serves as both a structural precursor and an energy source. A fraction if it is transiently polymerised into starch in amyloplasts for short-term storage (Eastmond and Rawsthorne, 1998).

Storage proteins are degraded by proteolysis, primarily by cysteine proteases. These enzymes are synthesised during seed development and stored in seed vacuoles. They remain latent during dormancy due to a N-terminal pro-peptide (Tsuji et al., 2013). Acidification during germination leads to the autocatalytic cleavage of the pro-peptide and the activation of the cysteine protease (Kuroyanagi et al., 2002). The degradation of storage proteins is initiated by the deprotonation of a catalytic cysteine residue in the active site of the enzyme, catalysed by histidine. This produces a highly

reactive thiolate anion, which creates a tetrahedral intermediate by attacking the carbonyl carbon of a peptide bond in the storage protein. When this intermediate collapses, the peptide bond is cleaved and the amino terminus is released. The carbonyl end remains covalently attached to the protease cysteine residue in the form of a thioester. A hydroxide ion targets this thioester, breaking the bond between the peptide fragment and the enzyme and releasing a second peptide fragment with a terminal carboxyl group, thus regenerating the protease (ELSÄSSER AND GOETTIG, 2021). Afterwards, exopeptidases hydrolyse the resulting oligopeptides to produce free amino acids (TAN-WILSON AND WILSON, 2012). Specialized transporters, such as amino acid permeases, actively export these amino acids from storage organelles, making them available to the developing seedling as alternative respiration substrates for energy production, intermediates in other metabolic pathways, or precursors for the synthesis of enzymes and structural proteins (HILDEBRANDT ET AL., 2015; TEGEDER, 2012).

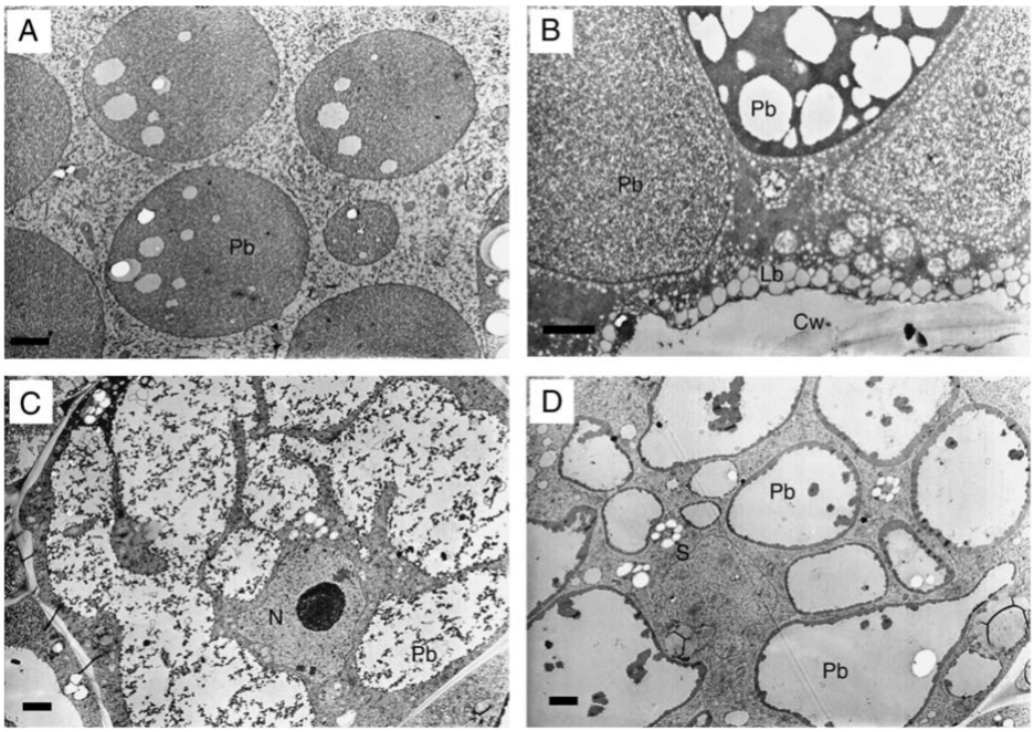

Fig. 9: Transmission electron micrograph showing cotyledon parenchyma cells of lupin seeds. Dry seed (**A**) and seeds germinating for 2h (**B**), 12 h (**C**) and 24 h (**D**). In dry seeds, protein bodies occupy the largest proportion of the cell volume. During germination, the uptake of water leads to swelling of the protein bodies, which is followed by their dissolution. Lipid bodies could also be observed, but they remained stable. The bars represent 1 µm. Cw, cell wall; Lb, lipid body; N, nucleus; Pb, protein body; S, starch (from GARNCZARSKA ET AL., 2007).

GARNCZARSKA ET AL. (2007) documented the transition of storage organelles during lupin germination. Using transmission electron microscopy, they demonstrateed the stepwise changes of protein bodies. During imbibition, the seed swells and the protein density decrease, while the lipid droplets change less significantly (Fig. 9). This suggests that imbibition leads to a transition from storage to metabolically active tissue. The hydration and hydrolysis of storage proteins are initiated rapidly, while the mobilisation of lipids is initiated later.

1.6 Post-germinative development and metabolic transition in *Lupinus albus*

The metabolic activation that occurs during germination paves the way for the subsequent post-germinative development and establishment of the seedling. Post-germinative growth of *Lupinus albus* is of the epigeal type. The radicle anchors the seed in the soil and forms the first root hairs (BEWLEY ET AL., 2013). The hypocotyl experiences strong elongation growth, curves upwards and form a hook (SÁNCHEZ-BRAVO ET AL., 2008).

We observed a consistent biomass content throughout the first four days of *L. albus* seedling growth. At the same time, the distribution of storage compounds changed. The amount of carbohydrates decreased slightly, while the amount of lipids decreased by more than 50 %. Interestingly, the protein content remained constant, while the overall amino acid content (free and protein-bound) increased slightly. Combining this with the measured oxygen consumption of the seedling during this period made it possible to calculate the substrates required for respiration and energy production. Our results indicated that the energy required for *L. albus* germination was predominantly supplied by lipid degradation with limited, with only limited contributions from the oxidation of proteins or carbohydrates. In line with these findings, levels of enzymes involved in β-oxidation, the glyoxylate cycle, and gluconeogenesis increased significantly, indicating lipid degradation as well (see **Chapter 2: Manuscript 1**).

While the protein content remained stable during the first four days of seedling establishment, the amino acid composition of the *L. albus* proteome changed. In particular, the storage protein content remained steady, while a notable decrease in oleosins and LEA proteins were observed. These contained high levels of alanine, glycine and threonine. The degradation of fatty acids produced acetyl-CoA. The degradation of alanine, glycine, and threonine released glyoxylate and pyruvate.

Therefore, we hypothesised the integration of fatty acid and amino acid degradation during the germination of *L. albus* (Fig. 10). We suggest that the products of these two degradation pathways could be incorporated together into a glyoxylate cycle bypass to fulfil the conversion into carbohydrates via gluconeogenesis (see **Chapter 2: Manuscript 1**).

Additionally, we observed an increase in free amino acids, particularly asparagine (see **Chapter 2: Manuscript 1**). Asparagine is a non-essential amino acid that plays a key role in plant nitrogen metabolism. Chemically, it is the amide of aspartic acid, containing two nitrogen atoms per molecule. This gives asparagine a favourable C/N ratio, enabling the storage of large amounts of nitrogen with comparatively little carbon (LEA AND AZEVEDO, 2007). In an ATP-dependent process, asparagine synthetase converts aspartate to glutamine or free ammonium to produce asparagine. Stressors such as carbon starvation, darkness and nitrogen excess, increase its synthesis. Accordingly, asparagine serves as a buffer for excess or hazardous ammonium, as well as being an effective nitrogen store and transport mechanism (GAUFICHON ET AL., 2016).

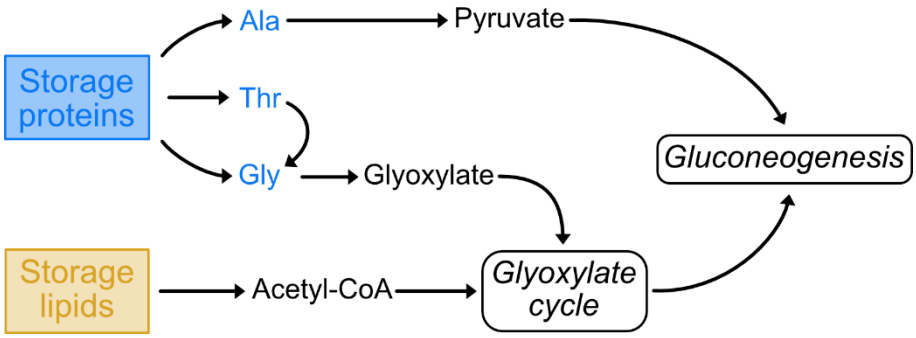

Fig. 10: Potential integration of fatty acid and amino acid metabolism during germination and seedling establishment of *Lupinus albus*. During the germination and seedling establishment of *L. albus*, we observed an increase in enzymes involved in lipid β-oxidation and parts of the glyoxylate cycle. Simultaneously, protein degradation led to changes in the pool of protein-bound amino acids, notably a reduction in alanine, glycine and threonine. The degradation of these amino acids fulfils the pathway from fatty acid degradation to gluconeogenesis, which leads us to hypothesise that these two metabolic pathways are integrated to create a glyoxylate cycle bypass (see **Chapter 2: Manuscript 1**).

During epigeal growth the cotyledons are raised above the ground when the straightened hypocotyl breaks through the soil surface. This mechanism guards against mechanical damage to the fragile shoot apical meristem during soil penetration. The testa is shed as the hypocotyl grows, revealing the cotyledons. Photosynthesis is initiated when the cotyledons enlarge and turn green in response to the light (GATAULINA ET AL., 2021). The shoot apical meristem, which emerges between

the cotyledons, gives rise to the shoot axis and the first true leaves, which grow within a few days. At this stage, cotyledon senescence begins and the lupin becomes completely photoautotrophic (BROWN AND HUDSON, 2015).

We noticed the cotyledons emerging from the soil five days after imbibition (Fig. 11). They turned green the following day. By day seven, the first true leaves had appeared and the lateral roots had grown. By day eight, the cotyledons had spread, and by day ten, the first true leaves had expanded and the next set of leaves had started to grow. On day 12, the growth of the first cluster roots could be observed (see **Chapter 2: Manuscript 1**).

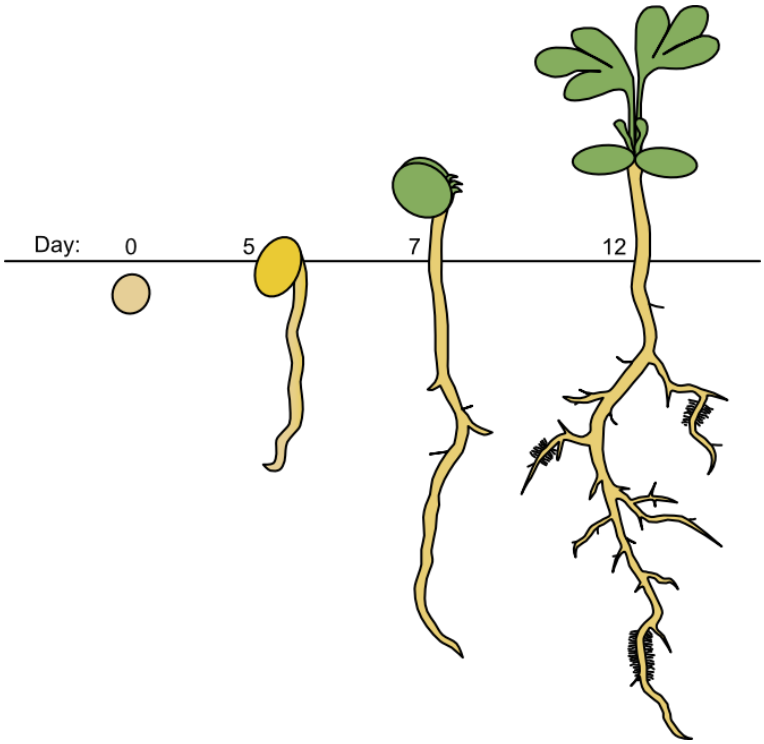

Fig. 11: Schematic overview of germination and seedling establishment in *Lupinus albus*. The dry seed is buried in soil. During germination, the seed swells and increases in size. Thirty hours after imbibition, germination is concluded with the rupture of the testa. The radicle grows into the soil and the hypocotyl pushes the cotyledons above the surface, where they turn green and become photosynthetically active. Within the first week of seedling establishment, the first true leaves are established, and within two weeks, the first specialised root structures (cluster roots) are initiated (see **Chapter 2: Manuscript 1**).

Despite the extent of the phenotypic change, we did not observe any changes in biomass content during the first twelve days of seedling establishment. During this period, the decrease in carbohydrate content continued, with the amount of lipids reaching a minimum on day eight and remaining stable thereafter. Once the cotyledons emerged from the soil at day eight, the storage proteins were degraded and the proteome was reorganised more quickly. Storage protein degradation led to stronger

accumulation of free amino acids than before, interestingly, the total amount of amino acids (free and protein-bound) remained steady for 12 days, but their allocation changed. Asparagine acted as the primary nitrogen store and its level at day twelve increased by a factor of nearly 200 compared to the seed. Enzymes involved in the synthesis of sulfur amino acids were strongly induced, which was important for redox protection. A phytochrome peak occurred on day four, alongside a continued increase in rubisco and the photosynthesic complexes. This marked the onset of photomorphogenesis and the transition to autotrophy (see **Chapter 2: Manuscript 1**). An increase in photosynthetic proteins was observed in the cotyledons of *L. albus* until day 16. Afterwards, stabilisation took place. The cotyledons exhibited photosynthetic efficiency similar to that of true leaves, but only 10 % of their net photosynthetic performance. Therefore, while cotyledonary photosynthesis did support energy and carbon provision during seedling establishment, it was insufficient to feed the whole seedling (see **Chapter 3: Manuscript 2**).

Until day 12 premature cotyledon loss resulted in significant growth inhibition in adult *L. albus* plants. This simulated nutrient starvation and wounding stress and plants responded by reducing metabolic processes and prioritising survival and defence at the expense of growth. The expression of proteins related to catabolism, transport and the stress response increased, while the expression of proteins related to photosynthesis decreased (see **Chapter 3: Manuscript 2**).

1.7 Mitochondrial energy metabolism and functional transitions during *Lupinus albus* germination

Metabolic adjustments are closely linked to mitochondrial function, as mitochondria play a vital part in the energy and metabolic pathways of plants during germination and seedling establishment. They are the site of oxidative phosphorylation, where electrons from the catabolism of organic compounds are transferred via the mitochondrial electron transport chain to oxygen. Simultaneously, a proton gradient is established across the inner mitochondrial membrane, driving the mitochondrial ATP synthase (Braun, 2020). Besides, mitochondria are involved in the catabolic degradation of carbohydrates, amino acids, and lipids. Pyruvate from glycolysis is oxidised in the TCA cycle and amino acids are trans- and deaminated, with the resulting carbon intermediates feeding into the TCA cycle. Furthermore, mitochondria play a key role in maintaining redox homeostasis by regulating electron fluxes and controlling reactive

oxygen species (MØLLER ET AL., 2021). Mitochondria are dynamic structures that move along the cytoskeleton and undergo constant fusion and fission events. They modify their shape and activity in response to the developmental stage and environmental conditions (LOGAN, 2010).

1.7.1 Mitochondrial organisation and function in dry seeds

Desiccation during seed development creates an extremely challenging environment for mitochondria. A high level of desiccation tolerance is necessary to support longevity by controlling water loss. Matrix condensation, which is caused by water loss, increases the local concentrations of ions, metabolites, and free radicals. This can hinder enzyme activity and, worse still, cause oxidative damage. Protective molecules such as antioxidants, as well as specialised protective proteins such as LEA and heat shock proteins, bind directly to mitochondrial structures. This stabilises membranes and enzymes, thereby preventing oxidative damage during desiccation (SANO ET AL., 2016; TOLLETER ET AL., 2007). During seed maturation and desiccation, respiration decreases drastically and becomes barely detectable, suggesting that mitochondrial activity remains in a ‘frozen’ state (IVANOVA ET AL., 2022).

Despite their crucial role in plant metabolism, the organisation of the mitochondria in dry seeds is still up for debate and the subject of ongoing research. According to early ultrastructural research, dry seeds contain ‘pro-mitochondria’, which are highly undifferentiated organelles devoid of cristae and fully assembled respiratory complexes (ATTUCCI ET AL., 1991; LOGAN ET AL., 2001). This model proposes that transcription, translation and complex assembly only resume after imbibition, marking the start of functional maturation (LAW ET AL., 2012; PASZKIEWICZ ET AL., 2017). However, more recent proteomic and functional analyses, especially in A*rabidopsis thaliana,* call this opinion into question. Research suggests that dry seeds may already contain mitochondria with pre-assembled respiratory complexes. Rehydrating them restores activity. This suggestion is supported by the fact that mitochondrial energy metabolism is activated almost instantly in germinating seeds. This is evidenced by the rapid formation of a membrane potential, as well as strong increases in ATP synthase activity and oxygen consumption (CZARNA ET AL., 2016; DITZ ET AL., 2025; NIETZEL ET AL., 2020). Furthermore, certain protein modifications that enhance mitochondrial resilience to desiccation stress have been identified recently (DITZ ET AL., 2025; NIETZEL ET AL., 2020).

We observed fully assembled mitochondrial OXPHOS systems in cold-stratified and dry seeds of *Lupinus albus*. Around 40 % of the mitochondrial proteins were found to be related to respiratory chain complexes and ATP synthase. This suggests that seed mitochondria are not fragmented or incomplete, but rather structurally and functionally complete and pre-assembled (see **Chapter 4: Manuscript 3**).

1.7.2 Mitochondrial activation and biogenesis during germination

Regardless of the ongoing controversy surrounding the condition of the mitochondria in dry seeds, it is clear that mitochondrial function is essential for successful germination. Mitochondria provide the majority of the necessary ATP, mobilising stored reserves very early after imbibition. Reduced seed viability and vigour, along with poor germination, are consistently the outcomes of mitochondrial dysfunction (Ferguson et al., 1990; Kühn et al., 2015; Racca et al., 2022). As a result of imbibition, the seed swells and the mitochondria inside it hydrate and expand. To maximise overall organellar efficiency, two or more mitochondria fuse and mix their matrices. This enables intact mitochondria to share proteins, lipids, and mitochondrial genomes with their impaired partner (Gao and Hu, 2021). The fission of mitochondria begins once the water content has been stabilised, and repair procedures continue. Mitochondrial protein synthesis is initiated. Nuclear-encoded mitochondrial proteins are synthesised in the cytosol and imported (Law et al., 2014). Ongoing mitochondrial fission and biogenesis provides enough energy for cell division, nutrient transport, and other essential functions (Logan et al., 2001). Remobilisation of storage reserves provides the necessary substrates.

Our results indicated that the mitochondria in the seeds of *Lupinus albus* were fully functional and contain the complete respiratory machinery. During imbibition, the hydration of the mitochondria was sufficient to activate mitochondrial metabolism. Consequently, ATP production and redox homeostasis were rapidly established. Proteome comparisons revealed that *L. albus* seed mitochondria were optimised for catabolism and energy production from storage reserves, while leaf mitochondria focused on photorespiration. Compared to leaf mitochondria, seed mitochondria contained significantly higher amounts of alternative dehydrogenases, which were used for producing NADH. The NAD-dependent formate dehydrogenase was especially abundant in *L. albus* seed mitochondria. This suggests a combination of detoxification and energy generation during germination. The high abundance of other

dehydrogenases involved in mitochondrial amino acid catabolism also indicated specialised mitochondrial metabolism in seeds to provide energy and carbohydrate precursors. Our study also revealed a large proportion of uncharacterised *L. albus* seed mitochondrial proteins that lack close homologues in *Arabidopsis.* This suggests the possibility of legume-specific mitochondrial adaptations (see **Chapter 4: Manuscript 3**).

1.8 Conclusions: Integrative insights into protein-based germination in *Lupinus albus*

Lupinus albus is a promising model organism for investigating the molecular basis of protein-rich seed metabolism and for developing strategies to breed resilient crops. This thesis provides a comprehensive molecular and physiological framework for understanding the early developmental stages of *L. albus*. By integrating proteomics, metabolomics and physiological data, it establishes *L. albus* as a model species for protein-rich seeds. The studies highlight the metabolic and organellar adaptations that enable efficient germination and seedling establishment in environments with limited nutrients by utilising stored reserves.

As a first step and prerequisite for functional proteome studies, curation of a detailed *L. albus* proteome annotation database enabled subcellular localisation prediction and functional annotation. This allowed the identification of previously unannotated proteins and their functional assignment, providing insight into biological coherences. Therefore, the interpretation of proteomic changes and the analysis of storage protein conversion were enabled, providing a better understanding of metabolic processes.

Improvements in the isolation of intact *L. albus* mitochondria from dry and germinating seeds allowed their comparison from different seed conditions, while minimising fixation- and rehydration-induced artefacts. This enabled reliable assessment of structural and functional integrity. The purity of the mitochondrial fractions obtained from imbibed seeds enabled them to be characterised in detail.

Integration of proteomics, metabolomics, and physiology enabled the combination of molecular, metabolic and functional levels. This approach empowered the prediction of holistic, coherent overall models, facilitating the establishment of reasonable relations and reducing misinterpretation.

Building on the methodological achievements, this thesis provides new molecular insights into the germination and seedling establishment of *L. albus* and facilitated a

better understanding of metabolic processes relying on proteins as primary storage compound (Fig. 12).

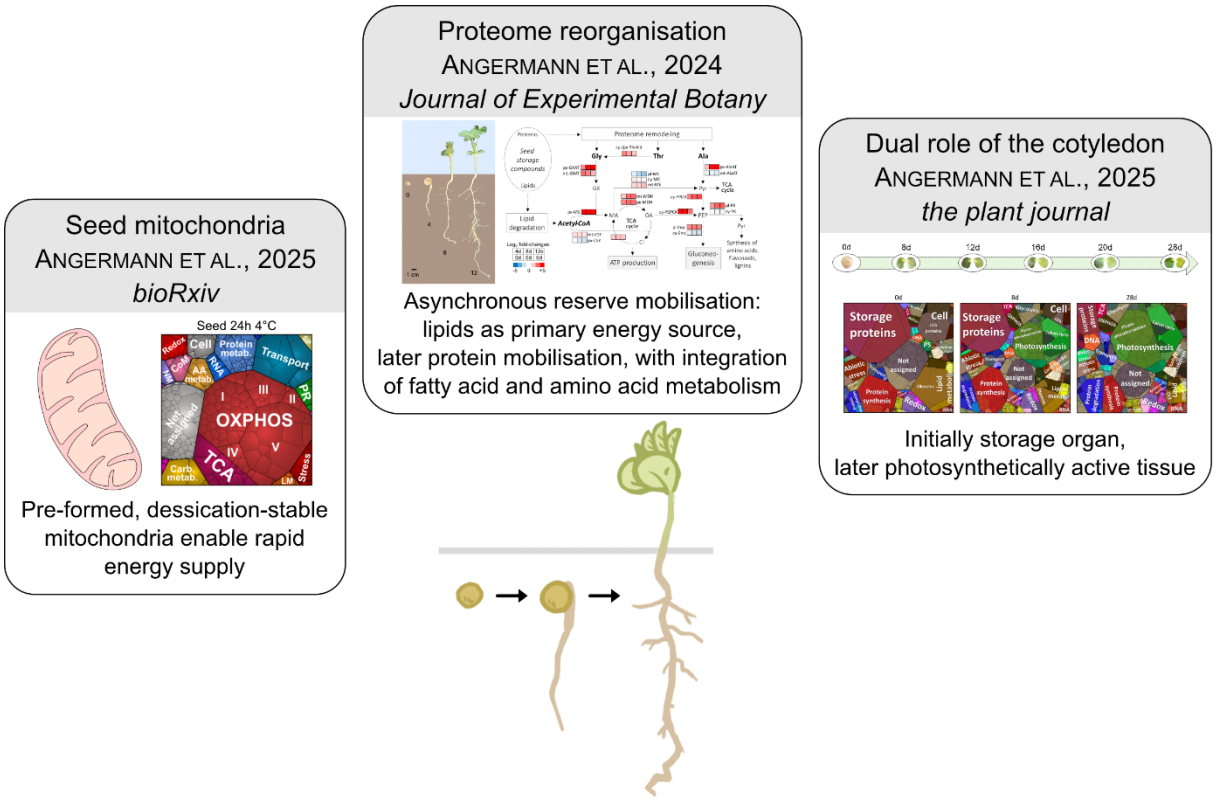

Fig. 12: The transition from seed to seedling in *Lupinus albus* is enabled by coordinated metabolic and organelle functions. This thesis presents three studies that reveal the processes involved in the transition from seed to plant in *L. albus*. Germination and seedling establishment are complex, pre-programmed processes that involve coordinating energy balance, nutrient distribution and organelle function. The studies demonstrate that *L. albus* has evolved a resource-efficient strategy for germination and seedling establishment, adapted to nutrient-poor environments. The presence of preformed, functional mitochondria enabled the seed to provide energy immediately after water uptake (see **Chapter 4, Manuscript 3**). In *L. albus*, this rapid activation relied on alternative respiratory substrates, such as fatty acids, rather than carbohydrates. The preference for lipids as an energy source, alongside the maintenance of storage proteins as a nitrogen reserve, revealed targeted metabolic prioritisation, coupled with rapid growth and efficient nutrient utilisation (see **Chapter 2, Manuscript 1**). Finally, the dual function of the cotyledons as storage and temporarily photosynthetic organs demonstrated the integration of heterotrophic and autotrophic processes. This ensured growth in the early stages, even under nutrient-limited conditions (see **Chapter 3, Manuscript 2**). Together, these studies move beyond analysing individual pathways to emphasise that germination and seedling establishment in *L. albus* are coordinated processes involving tightly interconnected metabolic activation, energy provision and physiological adjustments. This systemic understanding provides a framework for exploring how protein-rich legumes optimise their early growth in the absence of external nutrients. This process is also central to improving seedling survival and nutrient efficiency.

Our proteomic, metabolomic and physiological analyses revealed the close relationship between fatty acid and amino acid metabolism during the germination of

L. albus. We propose that these combined pathways fulfil a glyoxylate cycle bypass, generating carbohydrates for biomass and energy production (see **Chapter 2: Manuscript 1**).

We discovered that the mitochondria in *L. albus* seeds were dynamic, pre-assembled systems that contained all the necessary respiratory complexes and became instantly activated upon imbibition. It appears that they have adapted their metabolism to combine detoxification pathways with energy and carbohydrate production, increasing the levels of dehydrogenases in the seed mitochondria (see **Chapter 4: Manuscript 3**).

Our results indicated that the cotyledons of *L. albus* initially functioned as storage tissues. During epigeal post-germinative growth, they emerged from the soil and photomorphogenesis occurred. Storage protein degradation then increased the accumulation of free amino acids, providing nitrogen for the synthesis of photosynthetic proteins. Premature cotyledon loss reduced the protein content and biomass of adult plants, demonstrating the importance of cotyledons in early plant development as a tissue that continues to provide resources even after photosynthesis becomes active (see **Chapter 3: Manuscript 2**).

In summary, this thesis clarifies the pivotal role of proteins as multifunctional storage compounds that promote germination and seedling establishment in *L. albus*. The results illuminate the mechanisms by which seed proteins serve as nutrient stores, as well as and their role in metabolic reprogramming during the transition from heterotrophic to autotrophic growth. This enhances our understanding of nitrogen use efficiency and energy provision in legume crops, paving the way for breeding strategies that boost metabolic resilience under nutrient-limited environments.

1.9 Future perspectives

Based on these findings, the next section sets out experimental strategies for testing the proposed metabolic mechanisms and exploring their functional significance during germination and early seedling establishment in *Lupinus albus*. As genetic modification in *L. albus* has not yet been established, the predicted mechanisms must be validated using non-transgenic experimental approaches.

This thesis comprises three studies that generated a large amount of proteomic, metabolomic and physiological data. Integrating this data into a mathematical model could help to better understand the interactions of the individual metabolites and

processes, and their metabolomic correlation. This allows nutrient and energy fluxes to be simulated and anticipated under varying physiological or environmental conditions.

Our results indicated immediate activation of mitochondrial metabolism at imbibition, alongside strong reorganisation of storage compounds during the first four days of germination and seedling establishment. Therefore, it would be interesting to analyse these processes over a shorter, more detailed time period. This could provide further information about metabolic timing.

This thesis had a clear focus on proteomics. Metabolic pathways were hypothesised based on the abundance of the relevant enzymes. However, the presence of an enzyme does not necessarily indicate that it is active. Therefore, transcriptome analyses could help clarify the genomic regulation of germination and seedling establishment, as well as determining whether proteomic changes are reflected at the transcriptional level.

Further experiments focusing on metabolic processes, building on the observed patterns of nutrient distribution in *L. albus*, would provide important insights into the mechanisms that control these dynamics. Understanding how nutrients are mobilised, transported and recycled within the plant is essential for deciphering the physiological strategies that enable lupins to thrive in nutrient-poor conditions. Targeted approaches, such as enzyme activity assays, isotope labelling, feeding experiments and inhibitor studies, could elucidate the biochemical pathways responsible for nutrient remobilisation and reveal how these processes are regulated at different developmental stages or in response to environmental stress.

The cotyledons constitute the largest part of the lupin seed, and our research has demonstrated their pivotal role in ensuring optimal plant development and growth. Understanding how storage organs transition into active photosynthetic tissue and estimating the role of cotyledonary photosynthesis could help to understand how young seedlings establish their autotrophic capacity, and how they manage their internal energy and carbon balance. One way to achieve this would be to analyse the peroxisomal proteome in order to determine whether β-oxidation or photorespiration predominates at different developmental stages. Furthermore, the functional relevance of cotyledon photosynthesis could be assessed using inhibitor or shading treatments to quantify its contribution to seedling growth and nutrient remobilisation.

The mitochondrial status of dry seeds has been investigated for decades, but is still not fully understood. To examine the mitochondrial structure in seeds of *L. albus*, cryo-electron microscopy could be used to reveal ultrastructural adaptations associated with activation. We observed a high abundance of proteins related to cofactor biosynthesis in the mitochondrial proteome of *L. albus* seeds. In order to investigate the role of coordinated cofactor supply in mitochondrial activation, time-resolved quantification of cofactor pools and respiration could be performed to provide insight into the temporal regulation of metabolic fluxes. Furthermore, acute depletion rescue assays in seeds and isolated mitochondria could be used to investigate the influence of cofactor availability on mitochondrial activation.

The proposed strategies combine high-resolution structural, biochemical and physiological approaches, which will enable the validation of hypothetical metabolic pathways and clarify the functional significance of the proteins and processes identified in this thesis. Ultimately, these investigations will bridge the gap between descriptive omics data and functional insights, enhancing our comprehension of how *L. albus* achieves efficient and resilient germination and seedling development, even in nutrient-poor environments, by relying mostly on stored reserves within the seed.

1.10 References

Adachi, M., Kanamori, J., Masuda, T., Yagasaki, K., Kitamura, K., Mikami, B. and Utsumi, S. (2003) Crystal structure of soybean 11S globulin: glycinin A3B4 homohexamer. *Proc. Natl. Acad. Sci. U.S.A.*, 100, 7395–7400.

Al-Amrousi, E.F., Badr, A.N., Abdel-Razek, A.G., Gromadzka, K., Drzewiecka, K. and Hassanein, M.M.M. (2022) A Comprehensive Study of Lupin Seed Oils and the Roasting Effect on Their Chemical and Biological Activity. *Plants*, 11, 2301.

Angermann, C., Braun, H.-P. and Hildebrandt, T.M. (2025) The seed mitochondrial proteome of *Lupinus albus* provides insight into energy metabolism during germination. *bioRxiv*.

Angermann, C., Heinemann, B., Hansen, J., Töpfer, N., Braun, H.-P. and Hildebrandt, T.M. (2024) Proteome reorganization and amino acid metabolism during germination and seedling establishment in *Lupinus albus*. *J. Exp. Bot.*, 75, 4891–4903.

Angermann, C., Heinemann, B., Nogueira, B.B., Mai, H.-J., Bauer, P. and Hildebrandt, T.M. (2025) Balancing nutrient remobilization and photosynthesis: proteomic insights into the dual role of lupin cotyledons after germination. *Plant J.*, 123, e70357.

Antonets, K.S., Belousov, M.V., Sulatskaya, A.I., Belousova, M.E., Kosolapova, A.O., Sulatsky, M.I., Andreeva, E.A., Zykin, P.A., Malovichko, Y.V., Shtark, O.Y., Lykholay, A.N., Volkov, K.V., Kuznetsova, I.M., Turoverov, K.K., Kochetkova, E.Y., Bobylev, A.G., Usachev, K.S., Demidov, O.N., Tikhonovich, I.A. and Nizhnikov, A.A. (2020) Accumulation of storage proteins in plant seeds is mediated by amyloid formation. *PLoS Biol.*, 18, e3000564.

Attucci, S., Carde, J.P., Raymond, P., Saint-Gès, V., Spiteri, A. and Pradet, A. (1991) Oxidative phosphorylation by mitochondria extracted from dry sunflower seeds. *Plant Physiol.*, 95, 390–398.

Bai, B., van der Horst, S., Cordewener, J.H.G., America, T.A.H.P., Hanson, J. and Bentsink, L. (2020) Seed-Stored mRNAs that Are Specifically Associated to Monosomes Are Translationally Regulated during Germination. *Plant Physiol.*, 182, 378–392.

Ballesteros, D. and Walters, C. (2011) Detailed characterization of mechanical properties and molecular mobility within dry seed glasses: relevance to the physiology of dry biological systems. *Plant J.*, 68, 607–619.

Banerjee, A. and Roychoudhury, A. (2016) Group II late embryogenesis abundant (LEA) proteins: structural and functional aspects in plant abiotic stress. *Plant Growth Regul.*, 79, 1–17.

Baskin, J.M. and Baskin, C.C. (2004) A classification system for seed dormancy. *Seed Sci. Res.*, 14, 1–16.

Berger, F., Fitz Gerald, J.N. and Ingouff, M. (2007) *Arabidopsis* as a Model for Understanding the Basics of Endosperm Development. In *Endosperm. Developmental and Molecular Biology (*Olsen, O.-A., ed). Berlin, Heidelberg: Springer, pp. 91–110.

Bewley, J.D. (1997) Seed Germination and Dormancy. *Plant Cell*, 9, 1055–1066.

Bewley, J.D. and Black, M. (1994) Seeds. In *Seeds. Physiology of Development and Germination.* 2nd edn. (Bewley, J.D., ed). New York, NY: Springer, pp. 1–33.

Bewley, J.D., Bradford, K., Hilhorst, H. and Nonogaki, H. (2013) *Seeds. Physiology of development, germination and dormancy.* 3rd edn. New York, Heidelberg: Springer.

Bewley, J.D. (1994) *Seeds. Physiology of Development and Germination.* 2nd edn. New York, NY: Springer.

Blagrove, R.J. and Gillespie, J.M. (1975) Isolation, Purification and Characterization of the Seed Globulins of *Lupinus angustifolius*. *Funct. Plant Biol.*, 2, 13.

Bojórquez-Velázquez, E., Barrera-Pacheco, A., Espitia-Rangel, E., Herrera-Estrella, A. and La Barba de Rosa, A.P. (2019) Protein analysis reveals differential accumulation of late embryogenesis abundant and storage proteins in seeds of wild and cultivated amaranth species. *BMC Plant Biol.*, 19, 59.

Borek, S., Pukacka, S., Michalski, K. and Ratajczak, L. (2009) Lipid and protein accumulation in developing seeds of three lupine species: *Lupinus luteus* L., *Lupinus albus* L., and *Lupinus mutabilis* Sweet. *J. Exp. Bot.*, 60, 3453–3466.

Borek, S., Ratajczak, W. and Ratajczak, L. (2015) Regulation of storage lipid metabolism in developing and germinating lupin (*Lupinus* spp.) seeds. *Acta Physiol. Plant.*, 37, 1–11.

Braun, H.-P. (2020) The Oxidative Phosphorylation system of the mitochondria in plants. *Mitochondrion*, 53, 66–75.

Brewin, N.J. (1991) Development of the legume root nodule. *Annu. Rev. Cell Biol.*, 7, 191–226.

Brown, A.V. and Hudson, K.A. (2015) Developmental profiling of gene expression in soybean trifoliate leaves and cotyledons. *BMC Plant Biol.*, 15, 169.

Buitink, J. and Leprince, O. (2008) Intracellular glasses and seed survival in the dry state. *C. R. Biol.*, 331, 788–795.

Cândido, E.d.S., Pinto, M.F.S., Pelegrini, P.B., Lima, T.B., Silva, O.N., Pogue, R., Grossi-de-Sá, M.F. and Franco, O.L. (2011) Plant storage proteins with antimicrobial activity: novel insights into plant defense mechanisms. *FASEB J.*, 25, 3290–3305.

Carvajal-Larenas, F.E., Linnemann, A.R., Nout, M.J.R., Koziol, M. and van Boekel, M.A.J.S. (2016) *Lupinus mutabilis*: Composition, Uses, Toxicology, and Debittering. *Crit. Rev. Food Sci. Nutr.*, 56, 1454–1487.

Casey, R. (1999) Distribution and Some Properties of Seed Globulins. In *Seed Proteins (*Shewry, P.R., ed). Dordrecht: Springer Netherlands, pp. 159–169.

Chakrabortee, S., Boschetti, C., Walton, L.J., Sarkar, S., Rubinsztein, D.C. and Tunnacliffe, A. (2007) Hydrophilic protein associated with desiccation tolerance exhibits broad protein stabilization function. *Proc. Natl. Acad. Sci. U.S.A.*, 104, 18073–18078.

Cheng, L., Bucciarelli, B., Shen, J., Allan, D. and Vance, C.P. (2011) Update on lupin cluster roots. Update on white lupin cluster root acclimation to phosphorus deficiency. *Plant Physiol.*, 156, 1025–1032.

Czarna, M., Kolodziejczak, M. and Janska, H. (2016) Mitochondrial Proteome Studies in Seeds during Germination. *Proteomes*, 4, 19.

Dadlani, M. and Yadava, D.K., eds. (2023) *Seed Science and Technology. Biology, Production, Quality.* 1st edn. Singapore: Springer Nature Singapore; Imprint Springer.

Deruyffelaere, C., Bouchez, I., Morin, H., Guillot, A., Miquel, M., Froissard, M., Chardot, T. and D'Andrea, S. (2015) Ubiquitin-Mediated Proteasomal Degradation of Oleosins is Involved in Oil Body Mobilization During Post-Germinative Seedling Growth in *Arabidopsis*. *Plant Cell Physiol.*, 56, 1374–1387.

Deruyffelaere, C., Purkrtova, Z., Bouchez, I., Collet, B., Cacas, J.-L., Chardot, T., Gallois, J.-L. and D'Andrea, S. (2018) PUX10 Is a CDC48A Adaptor Protein That Regulates the Extraction of Ubiquitinated Oleosins from Seed Lipid Droplets in *Arabidopsis*. *Plant Cell*, 30, 2116–2136.

Devkota, L., Kyriakopoulou, K., Bergia, R. and Dhital, S. (2023) Structural and Thermal Characterization of Protein Isolates from Australian Lupin Varieties as Affected by Processing Conditions. *Foods*, 12, 908.

Ditz, N., Gasper, M., Brandt, D., Röhricht, H., Wallbott, A., Eirich, J., Rugen, N., Hegermann, J., Niehaus, M., Del Martinez, M.P., Heinemann, B., Kühn, K., Maurino, V., Müller-Schüssele, S., Hildebrandt, T., Schwarzländer, M., Braun, H.-P., Meyer, E., Herde, M., Eubel, H. and Finkemeier, I. (2025) Seed Mitochondria are Equipped with Cristae and a Full Proteome to Kickstart Germination. *Curr. Biol. [preprint]*.

Domoney, C. (1999) Inhibitors of Legume Seeds. In *Seed Proteins (*Shewry, P.R., ed). Dordrecht: Springer Netherlands, pp. 635–655.

dos Ramos, P.C., Ferreira, R.M., Franco, E. and Teixeira, A.R. (1997) Accumulation of a lectin-like breakdown product of beta-conglutin catabolism in cotyledons of germinating *Lupinus albus* L. seeds. *Planta*, 203, 26–34.

Downie, J.A. (2014) Legume nodulation. *Curr. Biol.*, 24, R184-90.

DrRandomFactor (2023) A flag map of the European Union with the Stars inside, rather than outside. CC BY-SA 3.0. *https://creativecommons.org/licenses/by-sa/3.0 via Wikimedia Commons.*, 23.10.2025.

Drummond, C.S., Eastwood, R.J., Miotto, S.T.S. and Hughes, C.E. (2012) Multiple continental radiations and correlates of diversification in *Lupinus* (Leguminosae): testing for key innovation with incomplete taxon sampling. *Syst. Biol.*, 61, 443–460.

Duranti, M. (1986) Enzymatic subunit splitting of lupine storage proteins. *Food / Nahrung*, 30, 271–274.

Duranti, M. and Giani, D. (1989) Proteolytic events in legume storage proteins. *Acta Aliment.*, 18, 89–96.

Duranti, M., Guerrieri, N., Cerletti, P. and Vecchio, G. (1992) The legumin precursor from white lupin seed. Identity of the subunits, assembly and proteolysis. *Eur. J. Biochem.*, 206, 941–947.

Duranti, M., Consonni, A., Magni, C., Sessa, F. and Scarafoni, A. (2008) The major proteins of lupin seed: Characterisation and molecular properties for use as functional and nutraceutical ingredients. *Trends Food Sci. Technol.*, 19, 624–633.

Duranti, M., Cucchetti, E. and Cerletti, P. (1984) Changes in composition and subunits in the storage proteins of germinating lupine seeds. *J. Agric. Food Chem.*, 32, 490–493.

Duranti, M., Faoro, F. and Harris, N. (1994) The Unusual Extracellular Localization of Conglutin γ in Germinating *Lupinus albus* Seeds Rules out its Role as a Storage Protein. *J. Plant Physiol.*, 143, 711–716.

Duranti, M., Gius, C., Sessa, F. and Vecchio, G. (1995) The Saccharide Chain of Lupin Seed Conglutin γ is not Responsible for the Protection of the Native Protein from Degradation by Trypsin, but Facilitates the Refolding of the Acid-Treated Protein to the Resistant Conformation. *Eur. J. Biochem.*, 230, 886–891.

Duranti, M., Guerrieri, N., Takahashi, T. and Cerletti, P. (1988) The legumin-like storage protein of *Lupinus albus* seeds. *Phytochemistry*, 27, 15–23.

Duranti, M., Restani, P., Poniatowska, M. and Cerletti, P. (1981) The seed globulins of *Lupinus albus*. *Phytochemistry*, 20, 2071–2075.

Eastmond, P.J., Germain, V., Lange, P.R., Bryce, J.H., Smith, S.M. and Graham, I.A. (2000) Postgerminative growth and lipid catabolism in oilseeds lacking the glyoxylate cycle. *Proc. Natl. Acad. Sci. U.S.A.*, 97, 5669–5674.

Eastmond, P.J. and Rawsthorne, S. (1998) Comparison of the metabolic properties of plastids isolated from developing leaves or embryos of *Brassica napus* L. *J. Exp. Bot.*, 49, 1105–1111.

Eastmond, P.J. (2004) Glycerol-insensitive *Arabidopsis* mutants: gli1 seedlings lack glycerol kinase, accumulate glycerol and are more resistant to abiotic stress. *Plant J.*, 37, 617–625.

Eaton-Mordas, C.A. and Moore, K.G. (1978) Seed glycoproteins of *Lupinus angustifolius*. *Phytochemistry*, 17, 619–621.

El-Maarouf-Bouteau, H., Meimoun, P., Job, C., Job, D. and Bailly, C. (2013) Role of protein and mRNA oxidation in seed dormancy and germination. *Front. Plant Sci.*, 4, 77.

Elsässer, B. and Goettig, P. (2021) Mechanisms of Proteolytic Enzymes and Their Inhibition in QM/MM Studies. *Int. J. Mol. Sci.*, 22, 3232.

Escudero-Feliu, J., Lima-Cabello, E., Rodríguez de Haro, E., Morales-Santana, S. and Jimenez-Lopez, J.C. (2023) Functional Association between Storage Protein Mobilization and Redox Signaling in Narrow-Leafed Lupin (*Lupinus angustifolius* L.) Seed Germination and Seedling Development. *Genes*, 14, 1889.

Falconí, C.E. and Yánez-Mendizábal, V. (2022) Available Strategies for the Management of Andean Lupin Anthracnose. *Plants*, 11, 654.

FAO – Food and Agriculture Organization of the United Nations (2017) *The future of food and agriculture. Trends and challenges.* 1st edn. Rome, Italy: Food and Agriculture Organization of the United Nations.

FAO – Food and Agriculture Organization of the United Nations (2025) FAOSTAT – Crops and livestock products*. https://www.fao.org/faostat/en/#data/QCL,* 23.10.2025.

Ferguson, J.M., TeKrony, D.M. and Egli, D.B. (1990) Changes During Early Soybean Seed and Axes Deterioration: I. Seed Quality and Mitochondrial Respiration. *Crop Sci.*, 30, 175–179.

Ferreira, H., Pinto, E. and Vasconcelos, M.W. (2021) Legumes as a Cornerstone of the Transition Toward More Sustainable Agri-Food Systems and Diets in Europe. *Front. Sustain. Food Syst.*, 5, 694121.

Finch-Savage, W.E. and Footitt, S. (2017) Seed dormancy cycling and the regulation of dormancy mechanisms to time germination in variable field environments. *J. Exp. Bot.*, 68, 843–856.

Foley, R.C., Gao, L.-L., Spriggs, A., Soo, L.Y.C., Goggin, D.E., Smith, P.M.C., Atkins, C.A. and Singh, K.B. (2011) Identification and characterisation of seed storage protein transcripts from *Lupinus angustifolius*. *BMC Plant Biol.*, 11, 59.

Foley, R.C., Jimenez-Lopez, J.C., Kamphuis, L.G., Hane, J.K., Melser, S. and Singh, K.B. (2015) Analysis of conglutin seed storage proteins across lupin species using transcriptomic, protein and comparative genomic approaches. *BMC Plant Biol.*, 15, 106.

Fulda, M., Shockey, J., Werber, M., Wolter, F.P. and Heinz, E. (2002) Two long-chain acyl-CoA synthetases from *Arabidopsis thaliana* involved in peroxisomal fatty acid beta-oxidation. *Plant J.*, 32, 93–103.

Gallardo, K., Thompson, R. and Burstin, J. (2008) Reserve accumulation in legume seeds. *C. R. Biol.*, 331, 755–762.

Gao, S. and Hu, J. (2021) Mitochondrial Fusion: The Machineries In and Out. *Trends Cell Biol.*, 31, 62–74.

Garnczarska, M., Zalewski, T. and Kempka, M. (2007) Water uptake and distribution in germinating lupine seeds studied by magnetic resonance imaging and NMR spectroscopy. *Physiol. Plant.*, 130, 23–32.

Gataulina, G.G., Medvedeva, N.V., Pilipenko, S.E. and Shitikova, A.V. (2021) Formation of seedlings of white lupin, *Lupinus albus* L. and blue lupin, *Lupinus angustifolius* L. in laboratory and field experiments. *Casp. J. Environ. Sci.*, 19, 771–776.

Gaufichon, L., Rothstein, S.J. and Suzuki, A. (2016) Asparagine Metabolic Pathways in *Arabidopsis*. *Plant Cell Physiol.*, 57, 675–689.

Gayler, K.R., Wachsmann, F., Kolivas, S., Nott, R. and Johnson, E.D. (1989) Isolation and Characterization of Protein Bodies in *Lupinus angustifolius*. *Plant Physiol.*, 91, 1425–1431.

Georgieva, N.A., Kosev, V.I., Genov, N.G. and Butnariu, M. (2018) Morphological and Biological Characteristics of White Lupine Cultivars (*Lupinus albus* L.). *Rom. Agric. Res.*, 35, 109–119.

Gidrol, X., Lin, W.S., Dégousée, N., Yip, S.F. and Kush, A. (1994) Accumulation of reactive oxygen species and oxidation of cytokinin in germinating soybean seeds. *Eur. J. Biochem.*, 224, 21–28.

Gorzolka, K., Kölling, J., Nattkemper, T.W. and Niehaus, K. (2016) Spatio-Temporal Metabolite Profiling of the Barley Germination Process by MALDI MS Imaging. *PLoS One*, 11, e0150208.

Grandis, A., Santos, H.P., Tonini, P.P., Salles, I.S., Peres, A.S.C., Carpita, N.C. and Buckeridge, M.S. (2024) Role of cell wall polysaccharides in water distribution during seed imbibition of *Hymenaea courbaril* L. *Plant Biol.*, 26, 955–967.

Gresta, F., Oteri, M., Scordia, D., Costale, A., Armone, R., Meineri, G. and Chiofalo, B. (2023) White Lupin (*Lupinus albus* L.), an Alternative Legume for Animal Feeding in the Mediterranean Area. *Agriculture*, 13, 434.

Hemantaranjan, A. (2003) *Advances In Plant Physiology (Vol. 6):* Scientific Publishers.

Hildebrandt, T.M., Nunes Nesi, A., Araújo, W.L. and Braun, H.-P. (2015) Amino Acid Catabolism in Plants. *Mol. Plant*, 8, 1563–1579.

Hong-Bo, S., Zong-Suo, L. and Ming-An, S. (2005) LEA proteins in higher plants: structure, function, gene expression and regulation. *Colloids Surf. B Biointerfaces*, 45, 131–135.

Hufnagel, B., Marques, A., Soriano, A., Marquès, L., Divol, F., Doumas, P., Sallet, E., Mancinotti, D., Carrere, S., Marande, W., Arribat, S., Keller, J., Huneau, C., Blein, T., Aimé, D., Laguerre, M., Taylor, J., Schubert, V., Nelson, M., Geu-Flores, F., Crespi, M., Gallardo, K., Delaux, P.-M., Salse, J., Bergès, H., Guyot, R., Gouzy, J. and Péret, B. (2020) High-quality genome sequence of white lupin provides insight into soil exploration and seed quality. *Nat. Commun.*, 11, 492.

Hyvärinen, L., Fuchs, C., Utz-Pugin, A., Gully, K., Megies, C., Holbein, J., Iwasaki, M., Demonsais, L., Capitão, M.B., Barberon, M., Franke, R.B., Nawrath, C., Loubéry, S. and Lopez-Molina, L. (2025) Temperature-dependent polar lignification of a seed coat suberin layer promoting dormancy in *Arabidopsis thaliana*. *Proc. Natl. Acad. Sci. U.S.A.*, 122, e2413627122.

Ibl, V. and Stoger, E. (2012) The formation, function and fate of protein storage compartments in seeds. *Protoplasma*, 249, 379–392.

Ivanova, A., O Leary, B., Signorelli, S., Falconet, D., Moyankova, D., Whelan, J., Djilianov, D. and Murcha, M.W. (2022) Mitochondrial activity and biogenesis during resurrection of *Haberlea rhodopensis*. *New Phytol.*, 236, 943–957.

Jacob, I., Feuerstein, U., Heinz, M., Schott, M. and Urbatzka, P. (2017) Evaluation of new breeding lines of white lupin with improved resistance to anthracnose. *Euphytica, 213(10), 236.*

Jaganathan, G.K., Li, J., Biddick, M., Han, K., Song, D., Yang, Y., Han, Y. and Liu, B. (2019) Mechanisms underpinning the onset of seed coat impermeability and dormancy-break in *Astragalus adsurgens*. *Sci. Rep.*, 9, 9695.

Jones, T.A., Johnson, D.A., Bushman, B.S., Connors, K.J. and Smith, R.C. (2016) Seed Dormancy Mechanisms in Basalt Milkvetch and Western Prairie Clover. *Rangel. Ecol. Manag.*, 69, 117–122.

Joshi, R. (2018) Role of enzymes in seed germination. *Int. J. Creat. Res. Thoughts*, 6, 1481–1485.

Kaur, M., Tak, Y., Bhatia, S., Asthir, B., Lorenzo, J.M. and Amarowicz, R. (2021) Crosstalk during the Carbon-Nitrogen Cycle That Interlinks the Biosynthesis, Mobilization and Accumulation of Seed Storage Reserves. *Int. J. Mol. Sci.*, 22, 12032.

Khan, M.K., Karnpanit, W., Nasar-Abbas, S.M., Huma, Z.- and Jayasena, V. (2015) Phytochemical composition and bioactivities of lupin: a review. *Int. J. Food Sci. Technol.*, 50, 2004–2012.

Kiran, K.R., Deepika, V.B., Swathy, P.S., Prasad, K., Kabekkodu, S.P., Murali, T.S., Satyamoorthy, K. and Muthusamy, A. (2020) ROS-dependent DNA damage and repair during germination of NaCl primed seeds. *J. Photochem. Photobiol. B*, 213, 112050.

Kouris-Blazos, A. and Belski, R. (2016) Health benefits of legumes and pulses with a focus on Australian sweet lupins. *Asia Pac. J. Clin. Nutr.*, 25, 1–17.

Kühn, K., Obata, T., Feher, K., Bock, R., Fernie, A.R. and Meyer, E.H. (2015) Complete Mitochondrial Complex I Deficiency Induces an Up-Regulation of Respiratory Fluxes That Is Abolished by Traces of Functional Complex I. *Plant Physiol.*, 168, 1537–1549.

Kunz, H.-H., Scharnewski, M., Berlepsch, S. von, **Shahi, S., Fulda, M., Flügge, U.-I. and Gierth, M.** (2010) Nocturnal energy demand in plants: insights from studying mutants impaired in β-oxidation. *Plant Signal. Behav.*, 5, 842–844.

Kuroyanagi, M., Nishimura, M. and Hara-Nishimura, I. (2002) Activation of *Arabidopsis* vacuolar processing enzyme by self-catalytic removal of an auto-inhibitory domain of the C-terminal propeptide. *Plant Cell Physiol.*, 43, 143–151.

Law, S.R., Narsai, R., Taylor, N.L., Delannoy, E., Carrie, C., Giraud, E., Millar, A.H., Small, I. and Whelan, J. (2012) Nucleotide and RNA metabolism prime translational initiation in the earliest events of mitochondrial biogenesis during *Arabidopsis* germination. *Plant Physiol.*, 158, 1610–1627.

Law, S.R., Narsai, R. and Whelan, J. (2014) Mitochondrial biogenesis in plants during seed germination. *Mitochondrion*, 19 Pt B, 214–221.

Lea, P.J. and Azevedo, R.A. (2007) Nitrogen use efficiency. 2. Amino acid metabolism. *Ann. Appl. Biol.*, 151, 269–275.

Leprince, O., Pellizzaro, A., Berriri, S. and Buitink, J. (2017) Late seed maturation: drying without dying. *J. Exp. Bot.*, 68, 827–841.

Logan, D.C., Millar, A.H., Sweetlove, L.J., Hill, S.A. and Leaver, C.J. (2001) Mitochondrial biogenesis during germination in maize embryos. *Plant Physiol.*, 125, 662–672.

Logan, D.C. (2010) Mitochondrial fusion, division and positioning in plants. *Biochem. Soc. Trans.*, 38, 789–795.

Lucas, M.M., Stoddard, F.L., Annicchiarico, P., Frías, J., Martínez-Villaluenga, C., Sussmann, D., Duranti, M., Seger, A., Zander, P.M. and Pueyo, J.J. (2015) The future of lupin as a protein crop in Europe. *Front. Plant Sci.*, 6, 705.

Lucić, R., Raposo, M., Chervinska, A., Domingos, T. and Teixeira, R.F.M. (2025) Global Greenhouse Gas Emissions and Land Use Impacts of Soybean Production: Systematic Review and Analysis. *Sustainability*, 17, 3396.

Magni, C., Scarafoni, A., Herndl, A., Sessa, F., Prinsi, B., Espen, L. and Duranti, M. (2007) Combined 2D electrophoretic approaches for the study of white lupin mature seed storage proteome. *Phytochemistry*, 68, 997–1007.

Malekipoor, R., Johnson, S.K. and Bhattarai, R.R. (2022) Lupin Kernel Fibre: Nutritional Composition, Processing Methods, Physicochemical Properties, Consumer Acceptability and Health Effects of Its Enriched Products. *Nutrients*, 14, 2845.

Marquès, L., Divol, F., Boultif, A., Garcia, F., Soriano, A., Maurines-Carboneill, C., Fernandez, V., Verstraeten, I., Pidon, H., Izquierdo, E., Hufnagel, B. and Péret, B. (2024) Autoregulation of cluster root and nodule development by white lupin CCR1 receptor-like kinase. *bioRxiv*, 2024.07.04.602037.

Martínez-Villaluenga, C., Frías, J. and Vidal-Valverde, C. (2005) Raffinose family oligosaccharides and sucrose contents in 13 Spanish lupin cultivars. *Food Chem.*, 91, 645–649.

Marzouk, R. (2018) Taxonomic consequences of seed morphology and anatomy in three *Lupinus* species (Fabaceae-Genisteae). *Catrina: Int. J. Environ. Sci.*, 1, 1–8.

Medic, J., Atkinson, C. and Hurburgh, C.R. (2014) Current Knowledge in Soybean Composition. *J. Am. Oil Chem. Soc.*, 91, 363-384.

Mohamed, A.A. and Rayas-Duarte, P. (1995) Composition of *Lupinus albus*. *Cereal Chem.*, 72, 643–647.

Mohamed, A.A. and Rayas-Duarte, P. (1995) Nonstarchy polysaccharide analysis of cotyledon and hull of *Lupinus albus*. *Cereal Chem.*, 72, 648–651.

Møller, I.M., Rasmusson, A.G. and van Aken, O. (2021) Plant mitochondria - past, present and future. *Plant J.*, 108, 912–959.

Moreira, B. and Pausas, J.G. (2012) Tanned or burned: the role of fire in shaping physical seed dormancy. *PLoS One*, 7, e51523.

Moret-Fernández, D., Tormo, J. and Latorre, B. (2024) A new methodology to characterize the kinetics of a seed during the imbibition process. *Plant Soil*, 498, 181–197.

Nautiyal, P.C., Sivasubramaniam, K. and Dadlani, M. (2023) Seed Dormancy and Regulation of Germination. In *Seed Science and Technology. Biology, Production, Quality.* 1st edn. (Dadlani, M. and Yadava, D.K., eds). Singapore: Springer Nature Singapore; Imprint Springer, pp. 39–66.

Nietzel, T., Mostertz, J., Ruberti, C., Née, G., Fuchs, P., Wagner, S., Moseler, A., Müller-Schüssele, S.J., Benamar, A., Poschet, G., Büttner, M., Møller, I.M., Lillig, C.H., Macherel, D., Wirtz, M., Hell, R., Finkemeier, I., Meyer, A.J., Hochgräfe, F. and Schwarzländer, M. (2020) Redox-mediated kick-start of mitochondrial energy metabolism drives resource-efficient seed germination. *Proc. Natl. Acad. Sci. U.S.A.*, 117, 741–751.

Olsen, O.-A. (2007) *Endosperm. Developmental and Molecular Biology.* Berlin, Heidelberg: Springer.

Osorio, C.E. and Till, B.J. (2021) A Bitter-Sweet Story: Unraveling the Genes Involved in Quinolizidine Alkaloid Synthesis in *Lupinus albus*. *Front. Plant Sci.*, 12, 795091.

Ott, T., van Dongen, J.T., Günther, C., Krusell, L., Desbrosses, G., Vigeolas, H., Bock, V., Czechowski, T., Geigenberger, P. and Udvardi, M.K. (2005) Symbiotic leghemoglobins are crucial for nitrogen fixation in legume root nodules but not for general plant growth and development. *Curr. Biol.*, 15, 531–535.

Pan, R., Liu, J. and Hu, J. (2019) Peroxisomes in plant reproduction and seed-related development. *J. Integr. Plant Biol.*, 61, 784–802.

Parthibane, V., Rajakumari, S., Venkateshwari, V., Iyappan, R. and Rajasekharan, R. (2012) Oleosin is bifunctional enzyme that has both monoacylglycerol acyltransferase and phospholipase activities. *J. Biol. Chem.*, 287, 1946–1954.

Paszkiewicz, G., Gualberto, J.M., Benamar, A., Macherel, D. and Logan, D.C. (2017) *Arabidopsis* Seed Mitochondria Are Bioenergetically Active Immediately upon Imbibition and Specialize via Biogenesis in Preparation for Autotrophic Growth. *Plant Cell*, 29, 109–128.

Paulsen, T.R., Colville, L., Kranner, I., Daws, M.I., Högstedt, G., Vandvik, V. and Thompson, K. (2013) Physical dormancy in seeds: a game of hide and seek? *New Phytol.*, 198, 496–503.

Pereira, A., Ramos, F. and Sanches Silva, A. (2022) Lupin (*Lupinus albus* L.) Seeds: Balancing the Good and the Bad and Addressing Future Challenges. *Molecules*, 27, 8557.

Peret Lab White Lupin Genome *[Webseite]; https://www.whitelupin.fr/;* 2. October 2025.

Plenzler, G.B., Napierała, D.M. and Baranowska, H.M. (2002) Hydration of starch and protein seeds in early phase of germination. In *ŻYWNOŚĆ.* 9th edn. (Sikora, T., ed): PTTŻ Scientific Publishing House, p. 24.

Pompelli, M.F., Jarma-Orozco, A. and Rodriguez-Páez, L.A. (2023) Imbibition and Germination of Seeds with Economic and Ecological Interest: Physical and Biochemical Factors Involved. *Sustainability*, 15, 5394.

Prusinski, J. (2017) White lupin (*Lupinus albus* L.) - nutritional and health values in human nutrition - a review. *Czech J. Food Sci.*, 35, 95–105.

Racca, S., Gras, D.E., Canal, M.V., Ferrero, L.V., Rojas, B.E., Figueroa, C.M., Ariel, F.D., Welchen, E. and Gonzalez, D.H. (2022) Cytochrome c and the transcription factor ABI4 establish a molecular link between mitochondria and ABA-dependent seed germination. *New Phytol.*, 235, 1780–1795.

Radchuk, V. and Borisjuk, L. (2014) Physical, metabolic and developmental functions of the seed coat. *Front. Plant Sci.*, 5, 510.

Ran, J.-H., Shen, T.-T., Wang, M.-M. and Wang, X.-Q. (2018) Phylogenomics resolves the deep phylogeny of seed plants and indicates partial convergent or homoplastic evolution between Gnetales and angiosperms. *Proc. R. Soc. B Biol. Sci.*, 285.

Restani, P., Duranti, M., Cerletti, P. and Simonetti, P. (1981) Subunit composition of the seed globulins of *Lupinus albus*. *Phytochemistry*, 20, 2077–2083.

Robles-Díaz, E., Flores, J. and Yáñez-Espinosa, L. (2016) Paths of water entry and structures involved in the breaking of seed dormancy of *Lupinus*. *Plant Physiol.*, 192, 75–80.

Rosbakh, S., Carta, A., Fernández-Pascual, E., Phartyal, S.S., Dayrell, R.L.C., Mattana, E., Saatkamp, A., Vandelook, F., Baskin, J. and Baskin, C. (2023) Global seed dormancy patterns are driven by macroclimate but not fire regime. *New Phytol.*, 240, 555–564.

Rotundo, J.L., Marshall, R. and McCormick, R. (2024) European soybean to benefit people and the environment. *Sci. Rep.*, 14, 7612.

Rybiński, W., Święcicki, W., Bocianowski, J., Börner, A., Starzycka-Korbas, E. and Starzycki, M. (2018) Variability of fat content and fatty acids profiles in seeds of a Polish white lupin (*Lupinus albus* L.) collection. *Genet. Resour. Crop Evol.*, 65, 417–431.

Salmanowicz, B.P. and Weder, J.K.P. (1997) Primary structure of 2S albumin from seeds of *Lupinus albus*. *Z. Lebensm. Unters. Forsch. A*, 204, 129–135.

Salvi, P., Varshney, V. and Majee, M. (2022) Raffinose family oligosaccharides (RFOs): role in seed vigor and longevity. *Biosci. Rep.*, 42.

Sánchez-Bravo, J., Oliveros-Valenzuela, M.R., Nicolás, C. and Acosta, M. (2008) Growing in darkness: The etiolated lupin hypocotyls. *Plant Signal. Behav.*, 3, 406–408.

Sano, N., Rajjou, L. and North, H.M. (2020) Lost in Translation: Physiological Roles of Stored mRNAs in Seed Germination. *Plants*, 9, 347.

Sano, N., Rajjou, L., North, H.M., Debeaujon, I., Marion-Poll, A. and Seo, M. (2016) Staying Alive: Molecular Aspects of Seed Longevity. *Plant Cell Physiol.*, 57, 660–674.

Schwertfirm, G., Schneider, M., Haase, F., Riedel, C., Lazzaro, M., Ruge-Wehling, B. and Schweizer, G. (2024) Genome-wide association study revealed significant SNPs for anthracnose resistance, seed alkaloids and protein content in white lupin. *Theor. Appl. Genet.*, 137, 155.

Shane, M.W., Vos, M. de, **Roock, S.** de and **Lambers, H.** (2003) Shoot P status regulates cluster-root growth and citrate exudation in *Lupinus albus* grown with a divided root system. *Plant Cell Environ.*, 26, 265–273.

Shewry, P.R. (1999) *Seed Proteins.* Dordrecht: Springer Netherlands.

Shewry, P.R. (2023) *ICC Handbook of 21st Century Cereal Science and Technology.* San Diego: Elsevier Science & Technology.

Shewry, P.R., Mantila, U.H. and Serna-Saldivar, S.O. (2023) Structure and development of cereal grains. In *ICC Handbook of 21st Century Cereal Science and Technology (*Shewry, P.R., ed). San Diego: Elsevier Science & Technology, pp. 17–30.

Sikora, T. (2002) *ŻYWNOŚĆ.* 9th edn.: PTTŻ Scientific Publishing House.

Silva, A.T., Ligterink, W. and Hilhorst, H.W.M. (2017) Metabolite profiling and associated gene expression reveal two metabolic shifts during the seed-to-seedling transition in *Arabidopsis thaliana*. *Plant Mol. Biol.*, 95, 481–496.

Sironi, E., Sessa, F. and Duranti, M. (2005) A simple procedure of lupin seed protein fractionation for selective food applications. *Eur. Food Res. Technol.*, 221, 145–150.

Smýkal, P., Vernoud, V., Blair, M.W., Soukup, A. and Thompson, R.D. (2014) The role of the testa during development and in establishment of dormancy of the legume seed. *Front. Plant Sci.*, 5, 351.

Sreenivasulu, N. (2017) Systems biology of seeds: deciphering the molecular mechanisms of seed storage, dormancy and onset of germination. *Plant Cell Rep.*, 36, 633–635.

Stanwood, P.C., McDonald, M.B. and McDonald, M.B., eds. (1989) *Seed moisture. Proceedings of a symposium.* Madison, Wis., USA: CSSA.

Talhinhas, P., Baroncelli, R., Le Floch, G. (2016) Anthracnose of Lupins caused by *Colletotrichum lupini*: A recent disease and a successful worldwide pathogen. *J. Plant Pathol*. 98, 5–14.

Tan-Wilson, A.L. and Wilson, K.A. (2012) Mobilization of seed protein reserves. *Physiol. Plant.*, 145, 140–153.

Tegeder, M. (2012) Transporters for amino acids in plant cells: some functions and many unknowns. *Curr. Opin. Plant Biol.*, 15, 315–321.

Thazar-Poulot, N., Miquel, M., Fobis-Loisy, I. and Gaude, T. (2015) Peroxisome extensions deliver the *Arabidopsis* SDP1 lipase to oil bodies. *Proc. Natl. Acad. Sci. U.S.A.*, 112, 4158–4163.

Tiryaki, I. and Topu, M. (2014) A Novel Method to Overcome Coat-Imposed Seed Dormancy in *Lupinus albus* L. and *Trifolium pratense* L. *J. Bot.*, 2014, 1–6.

Tolleter, D., Jaquinod, M., Mangavel, C., Passirani, C., Saulnier, P., Manon, S., Teyssier, E., Payet, N., Avelange-Macherel, M.-H. and Macherel, D. (2007) Structure and function of a mitochondrial late embryogenesis abundant protein are revealed by desiccation. *Plant Cell*, 19, 1580–1589.

Tsuji, A., Tsukamoto, K., Iwamoto, K., Ito, Y. and Yuasa, K. (2013) Enzymatic characterization of germination-specific cysteine protease-1 expressed transiently in cotyledons during the early phase of germination. *J. Biochem.*, 153, 73–83.

Tzen, J.T., Lie, G.C. and Huang, A.H. (1992) Characterization of the charged components and their topology on the surface of plant seed oil bodies. *J. Biol. Chem.*, 267, 15626–15634.

Tzen, J.T.C., Wang, M.M.C., Tai, S.S.K., Lee, T.T.T. and Peng, C.C. (2003) The abundant proteins in sesame seed: storage proteins in protein bodies and oleosins in oil bodies. In *Advances In Plant Physiology (Vol. 6) (*Hemantaranjan, A., ed): Scientific Publishers, pp. 93–104.

Tzen, J.T.C. (2012) Integral Proteins in Plant Oil Bodies. *ISRN Bot.*, 2012, 1–16.

Valente, I.M., Monteiro, A., Sousa, C., Miranda, C., Maia, M.R.G., Castro, C., Cabrita, A.R.J., Trindade, H. and Fonseca, A.J.M. (2024) Agronomic, Nutritional Traits, and Alkaloids of *Lupinus albus*, *Lupinus angustifolius* and *Lupinus luteus* Genotypes: Effect of Sowing Dates and Locations. *ACS Agric. Sci. Technol.*, 4, 450–462.

Valente, I.M., Sousa, C., Almeida, M., Miranda, C., Pinheiro, V., Garcia-Santos, S., Ferreira, L.M.M., Guedes, C.M., Maia, M.R.G., Cabrita, A.R.J., Fonseca, A.J.M. and Trindade, H. (2023) Insights from the yield, protein production, and detailed alkaloid composition of white (*Lupinus albus*), narrow-leafed (*Lupinus angustifolius*), and yellow (*Lupinus luteus*) lupin cultivars in the Mediterranean region. *Front. Plant Sci.*, 14, 1231777.

Vander Willigen, C., Postaire, O., Tournaire-Roux, C., Boursiac, Y. and Maurel, C. (2006) Expression and inhibition of aquaporins in germinating *Arabidopsis* seeds. *Plant Cell Physiol.*, 47, 1241–1250.

Ver Sagun, J., Yadav, U.P. and Alonso, A.P. (2023) Progress in understanding and improving oil content and quality in seeds. *Front. Plant Sci.*, 14, 1116894.

Vertucci, C.W. (1989) The Kinetics of Seed Imbibition: Controlling Factors and Relevance to Seedling Vigor. In *Seed moisture. Proceedings of a symposium (*Stanwood, P.C., McDonald, M.B. and McDonald, M.B., eds). Madison, Wis., USA: CSSA, pp. 93–115.

Villoria, N., Garrett, R., Gollnow, F. and Carlson, K. (2022) Leakage does not fully offset soy supply-chain efforts to reduce deforestation in Brazil. *Nat. Commun.*, 13, 5476.

Walker, R.P., Chen, Z.-H. and Famiani, F. (2021) Gluconeogenesis in Plants: A Key Interface between Organic Acid/Amino Acid/Lipid and Sugar Metabolism. *Molecules*, 26, 5129.

Wang, Y., Law, S.R., Ivanova, A., van Aken, O., Kubiszewski-Jakubiak, S., Uggalla, V., van der Merwe, M., Duncan, O., Narsai, R., Whelan, J. and Murcha, M.W. (2014) The mitochondrial protein import component, TRANSLOCASE OF THE INNER MEMBRANE17-1, plays a role in defining the timing of germination in *Arabidopsis*. *Plant Physiol.*, 166, 1420–1435.

Waterworth, W.M., Latham, R., Wang, D., Alsharif, M. and West, C.E. (2022) Seed DNA damage responses promote germination and growth in *Arabidopsis thaliana*. *Proc. Natl. Acad. Sci. U.S.A.*, 119, e2202172119.

Weitbrecht, K., Müller, K. and Leubner-Metzger, G. (2011) First off the mark: early seed germination. *J. Exp. Bot.*, 62, 3289–3309.

Wen, Z., Lu, X., Wen, J., Wang, Z. and Chai, M. (2024) Physical Seed Dormancy in Legumes: Molecular Advances and Perspectives. *Plants*, 13.

Wilson, S.K. and Knoll, L.J. (2018) Patatin-like phospholipases in microbial infections with emerging roles in fatty acid metabolism and immune regulation by Apicomplexa. *Mol. Microbiol.*, 107, 34–46.

Winnicki, K., Ciereszko, I., Leśniewska, J., Dubis, A.T., Basa, A., Żabka, A., Hołota, M., Sobiech, Ł., Faligowska, A., Skrzypczak, G., Maszewski, J. and Polit, J.T. (2019) Irrigation affects characteristics of narrow-leaved lupin (*Lupinus angustifolius* L.) seeds. *Planta*, 249, 1731–1746.

Wiraguna, E. (2022) Adaptation of Legume Seeds to Waterlogging at Germination. *Crops*, 2, 111–119.

Xu, E., Chen, M., He, H., Zhan, C., Cheng, Y., Zhang, H. and Wang, Z. (2016) Proteomic Analysis Reveals Proteins Involved in Seed Imbibition under Salt Stress in Rice. *Front. Plant Sci.*, 7, 2006.

Xu, W., Zhang, Q., Yuan, W., Xu, F., Muhammad Aslam, M., Miao, R., Li, Y., Wang, Q., Li, X., Zhang, X., Zhang, K., Xia, T. and Cheng, F. (2020) The genome evolution and low-phosphorus adaptation in white lupin. *Nat. Commun.*, 11, 1069.

Yan, D., Duermeyer, L., Leoveanu, C. and Nambara, E. (2014) The functions of the endosperm during seed germination. *Plant Cell Physiol.*, 55, 1521–1533.

Yanni, A.E., Iakovidi, S., Vasilikopoulou, E. and Karathanos, V.T. (2023) Legumes: A Vehicle for Transition to Sustainability. *Nutrients*, 16, 98.

Zafari, S., Hebelstrup, K.H. and Igamberdiev, A.U. (2020) Transcriptional and Metabolic Changes Associated with Phytoglobin Expression during Germination of Barley Seeds. *Int. J. Mol. Sci.*, 21, 2796.

2 Manuscript 1: Proteome reorganization and amino acid metabolism during germination and seedling establishment in *Lupinus albus*

Cecile Angermann*[1], Björn Heinemann*[1], Jule Hansen[2], Nadine Töpfer[3], Hans-Peter Braun[2], Tatjana M. Hildebrandt[1]

Journal of Experimental Botany, Volume 75, Issue 16, 28 August 2024, Pages 4891-4903, https://doi.org/10.1093/jxb/erae197

[1]Institute for Plant Sciences, Cluster of Excellence on Plant Sciences (CEPLAS), University of Cologne, Zülpicher Straße 47a, 50674 Cologne, Germany

[2]Institute of Plant Genetics, Leibniz Universität Hannover, Herrenhäuser Str. 2, 30419 Hannover, Germany.

[3]Institute for Plant Sciences, Cluster of Excellence on Plant Sciences (CEPLAS), University of Cologne, Luxemburger Str. 90, 50939 Cologne, Germany

* Equally contributing first authors

Type of authorship:	Shared first author
Type of article:	Research article, peer reviewed
Contribution to the publication:	I participated in designing the project. I prepared all the sample material and performed all the experiments, except for the SDS-PAGE preparation and shotgun proteomics, for which I provided support. I analysed the data from my experiments, with the support of TMH and BH. I contributed to constructing figures and writing the manuscript.
Journal:	Journal of Experimental Botany
Impact factor:	5.7 (2024)
Date of publication:	28. August 2024
DOI:	10.1093/jxb/erae197

2.1 Abstract

During germination plants rely entirely on their seed storage compounds to provide energy and precursors for the synthesis of macromolecular structures until the seedling has emerged from the soil and photosynthesis can be established. Lupin seeds use proteins as their major storage compounds, accounting for up to 40 % of the seed dry weight. Lupins are therefore a valuable complement to soy as a source of plant protein for human and animal nutrition. The aim of this study was to elucidate how storage protein metabolism is coordinated with other metabolic processes to meet the requirements of the growing seedling. In a quantitative approach, we analysed seedling growth, as well as alterations in biomass composition, the proteome, and metabolite profiles during germination and seedling establishment in *Lupinus albus*. The reallocation of nitrogen resources from seed storage proteins to functional seed proteins was mapped based on a manually curated functional protein annotation database. Although classified as a protein crop, *Lupinus albus* does not use amino acids as a primary substrate for energy metabolism during germination. However, fatty acid and amino acid metabolism may be integrated at the level of malate synthase to combine stored carbon from lipids and proteins into gluconeogenesis.

2.2 Introduction

The genus *Lupinus* is part of the *Fabaceae* family and includes the annual herbaceous species *L. albus*, *L. angustifolius*, *L. luteus*, and *L. mutabilis* cultivated as crops (Lucas et al., 2015). The white lupin (*Lupinus albus*) originated in the Mediterranean region and produces large, vigorous seeds facilitating rapid growth and completion of the lifecycle before summer drought (Berger et al., 2017). Due to their high protein content of 30 – 40 % and an adequate balance of essential amino acids, *L. albus* seeds are an excellent protein source for a plant-based diet (Sujak et al., 2006). A low oil and high dietary fibre content in combination with high levels of tocopherols and a low glycemic index add to the positive seed qualities (Boschin et al., 2008; Boschin and Arnoldi, 2011; Fontanari et al., 2012). Lupin cultivation does not require nitrogen or phosphate fertilization due to rhizobial symbiosis and specialized cluster root structures. It can therefore be categorized as particularly environmentally friendly (Lucas et al., 2015; Xu et al., 2020; Pueyo et al., 2021). However, *L. albus* wild varieties and landraces accumulate high concentrations of toxic quinolizidine alkaloids (≤ 11 %) in their seeds (Rybiński et al., 2018). These specialized metabolites derived

from the amino acid lysine protect the plant from pathogen attack but cause symptoms of poisoning in humans, affecting the nervous, circulatory, and digestive systems (Boschin and Resta, 2013). Mutations at the pauper locus decrease the seed alkaloid levels below 0.02 % in the cultivated sweet *L. albus* varieties making them suitable for human consumption and animal feed (Osorio and Till, 2021).

From the plant perspective, the seed storage compounds provide energy and precursors for the synthesis of macromolecular structures until the seedling has emerged from the soil and photosynthesis has been established. In some species including lupins the cotyledons are not shed but converted to photosynthetically active leaves after germination and thus can serve as a storage tissue for a prolonged time. About 35 – 40 % of the dry weight of *L. albus* seeds consists of carbohydrates, mostly cellulose and oligosaccharides of the raffinose family, which are non-digestible in humans and other monogastric animals (Gdala and Buraczewska, 1996; Sanyal et al., 2023). Plants activate α-galactosidases during germination to hydrolyse raffinose to sucrose and galactose, which can then serve as a source of energy and as a precursor for cellulose synthesis (Elango et al., 2022, Sanyal et al., 2023). *Lupinus albus* seeds also store lipids in oil bodies (7 – 14 %; Borek et al., 2012). During germination the triacylglycerols are hydrolysed by lipases and the free fatty acids are further metabolized to acetyl-CoA and NADH via β-oxidation in the peroxisomes (Baker et al., 2006; Graham, 2008). The glyoxylate cycle, including peroxisomal steps catalysed by isocitrate lyase, citrate synthase and malate synthase as well as cytosolic steps catalysed by aconitase and malate dehydrogenase, converts acetyl-CoA to succinate for the synthesis of carbohydrates during gluconeogenesis (Baker et al., 2006; Pracharoenwattana and Smith, 2008). For fatty acid respiration citrate is exported from the peroxisomes into the mitochondria and feeds into the TCA cycle to produce ATP (Pracharoenwattana et al., 2005). Storage lipid metabolism has been extensively studied in lupins (Borek et al., 2012, 2013, 2015). In addition to their role in gluconeogenesis and ATP production, it has been demonstrated that lipid-derived carbon skeletons are converted to amino acids (Borek et al., 2003; Borek and Ratajczak, 2010), which is astonishing given the fact that lupin seeds contain 30 – 40 % protein consisting predominantly of storage proteins from the globulin class (Duranti et al., 2008). Thus, the demand for free amino acids during germination should be covered by storage protein breakdown. Surprisingly little research has systematically focused on amino acid metabolism in germinating lupin seeds.

Asparagine, which is the major transport form of nitrogen in many plant species including lupins, strongly accumulates during seedling establishment (LEA ET AL., 2007). Asparagine synthesis assimilates free ammonium via the combined activities of glutamine synthetase and asparagine synthetase (LEA AND FOWDEN, 1975). The most obvious source of ammonium in germinating seeds without external nitrogen supply would be its release during amino acid catabolism. It has been postulated that the oxidation of amino acids provides alternative substrates for mitochondrial respiration in germinating lupins (BOREK ET AL., 2017). Amino acid oxidation pathways are strongly induced during energy deficiency responses in *Arabidopsis* (HEINEMANN AND HILDEBRANDT, 2021) and have been suggested to be relevant during seed development (GALILI ET AL., 2014). It has also been shown that excised pea embryo axes and isolated mitochondria are able to use externally supplied glutamate as a respiratory substrate (MORKUNAS ET AL., 2000). However, to our knowledge the postulated role of amino acids derived from storage protein degradation as substrates for mitochondrial respiration in germinating lupins has not been demonstrated yet.

The release of high-quality genome data for *L. albus* by two different groups in 2020 (HUFNAGEL ET AL., 2020; XU ET AL., 2020) recently opened up the possibility to comprehensively address quantitative changes in the proteome of germinating lupin seeds by proteomics approaches. The genome assembly presented by HUFNAGEL ET AL. (2020) covers 451 Mb; 38 258 protein coding genes were predicted based on RNAseq data from 10 different tissue types in combination with the proteome of *Medicago truncatula*. The assembly by XU ET AL. (2020) is larger (559 Mb) and includes 46 596 coding sequences predicted using protein coding sequences of *Arabidopsis* and several legume species as well as RNAseq data from root, leaf and stem tissue. However, functional annotation of the proteins in the reference database available on uniport.org and gene ontology classifications are still fragmented, which limits the interpretation of proteomics and transcriptomics datasets. We therefore created a manually curated protein annotation database for *L. albus* including functional categorization according to a modified version of the MapMan annotation system (THIMM ET AL., 2004). In this study we combine proteomics based on the new annotation database with metabolite and physiological data to investigate nitrogen resource allocation and utilization of seed storage proteins during germination and seedling development in *L. albus*. Our results provide new insight into the specific

challenges and chances associated with the use of proteins as major seed storage compounds.

2.3 Results

2.3.1 The *Lupinus albus* proteome

The genome of *L. albus* contains approximately 46 500 protein coding genes (HUFNAGEL ET AL., 2020; XU ET AL., 2020). However, only 5 % of the proteins have been functionally annotated so far in the reference database available on uniprot.org (UP000464885, UP000447434). The annotation tool Mercator (https://www.plabipd.de/mercator_main.html; SCHWACKE ET AL., 2019; BOLGER ET AL., 2021) offers a fast and convenient way to greatly improve the coverage of the proteome. However, a curated mapping file specific for *Lupinus albus* is not available yet, leading to gaps in the classification of characteristic lupin proteins such as seed storage proteins. We therefore created an extended annotation database based on sequence alignments (BLASTp) of *L. albus* proteins against the proteomes of *Lupinus angustifolius* (UP000188354), *Medicago truncatula* (UP000002051) and *Arabidopsis* (TAIR10). We used the larger genome assembly (XU ET AL., 2020) for initial sequence alignments and subsequently assigned the genes detected by HUFNAGEL ET AL. (2020) via blast. This allowed us to name 71 % of the proteins in the *Lupinus albus* proteome (M1-Fig. 1; Supp. Dataset S1). Linking each lupin protein to the closest homologue in *Arabidopsis* makes it possible to apply bioinformatic tools and resources available for the model plant *Arabidopsis* to *L. albus* datasets. For functional annotation we divided the *L. albus* proteome into 20 major categories with two levels of sub-categories based on a modified version of the MapMan annotation system (THIMM ET AL., 2004; Supp. Dataset S1). Fifty-four percent of the proteome could confidently be assigned to a functional category (blast bitscore > 200) and an additional 3 % was tentatively assigned (bitscore < 200) (M1-Fig. 1B; Supp. Dataset S1). The remaining 20 140 proteins are homologues of previously uncharacterized proteins or of proteins lacking a functional annotation in *Arabidopsis* and therefore remain in the category ‘not assigned’.

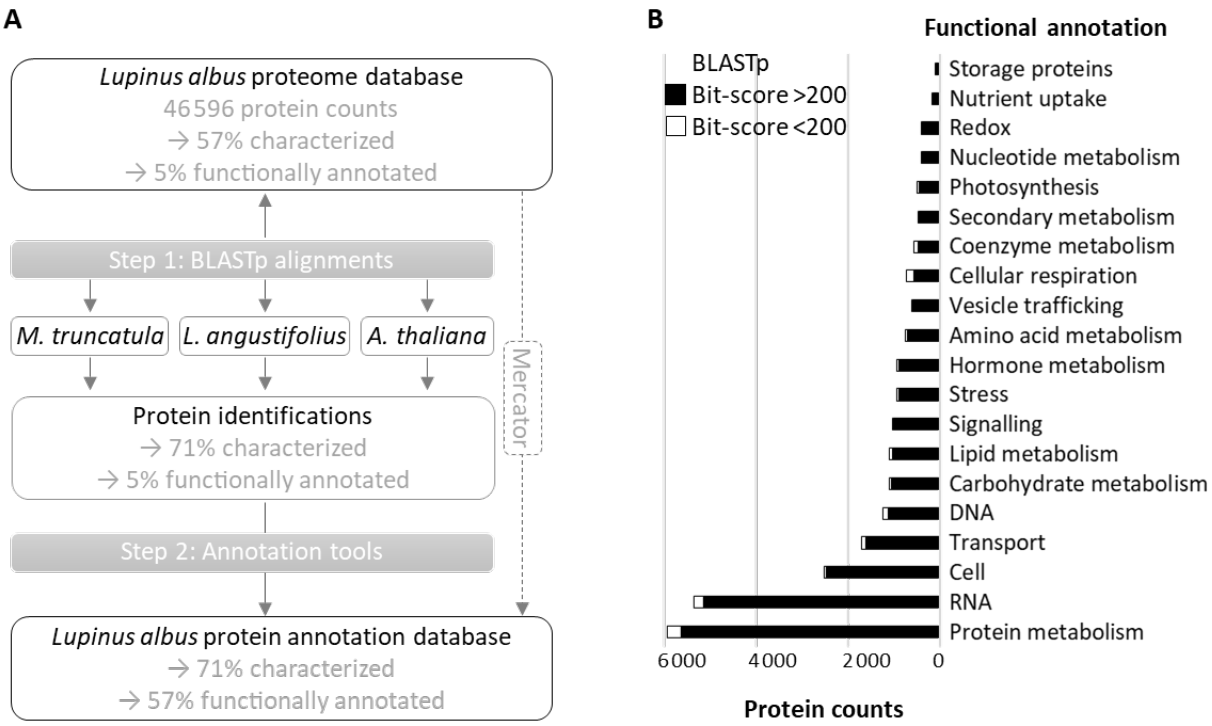

M1-Fig. 1: *Lupinus albus* proteome annotation. (**A**) Schematic presentation of the workflow used for curating the *L. albus* proteome annotation database. Proteins were identified based on sequence alignments and subsequently assigned to functional categories according to a modified version of the MapMan annotation system (THIMM ET AL., 2004). (**B**) Number of proteins assigned to the 20 major functional categories of the annotation system. The category 'not assigned' containing 20 140 proteins is not shown.

2.3.2 Energy requirements and changes in biomass composition during germination and seedling establishment

In order to monitor the specific metabolic adaptations required for using protein as a major seed storage compound we cultivated *L. albus* seedlings for 12 d and harvested the plant material at four different time points (0, 4, 8, 12 d after sowing; M1-Fig. 2A). The first two samples represent early seedling development in the dark whereas in the later stages photosynthesis was already active. The total biomass (dry weight) of the plants remained constant over the first 12 d, but its composition changed drastically (M1-Fig. 2B; Supp. Dataset S2). In the dark phase during the first 4 d there was no significant change in protein content but a decrease in lipid content by 50 % from 25.6 ± 2.5 to 12.4 ± 1.3 mg plant^{-1}. We measured the respiration rate of the seedlings to estimate the total energy demand for early seedling establishment up to the onset of photosynthesis, which has to be covered exclusively by storage compound metabolism (M1-Fig. 2C). An average individual seedling consumed a total amount of ~224 µmol O_2 during the first 4 d, which would correspond to the complete oxidation

of 2.5 mg oleic acid (the most abundant fatty acid in *L. albus* seeds; GDALA AND BURACZEWSKA, 1996) or 6.7 mg glucose (Supp. Dataset S2). Thus, the energy required for seedling establishment can easily be provided by lipid and/or carbohydrate degradation. A decrease in total protein content could only be detected at later developmental stages (8 – 12 d), and at the same time free amino acids strongly accumulated. By far the largest fraction of nitrogen (≥ 80 %) was included in proteins and free amino acids, and the nitrogen demand for chlorophyll synthesis was comparatively low in the developing seedling (M1-Fig. 2B). C/N analysis indicated that the sum of all nitrogen-containing compounds quantified individually (proteins, free amino acids, chlorophyll, ammonium, nitrate) corresponded very well to the total nitrogen content of the plant at the later developmental stages (8 – 12 d), but a fraction of 20 % and 11 % was not yet covered in the dry seed and the 4-day-old seedling, respectively (M1-Fig. 2B; Supp. Dataset S2).

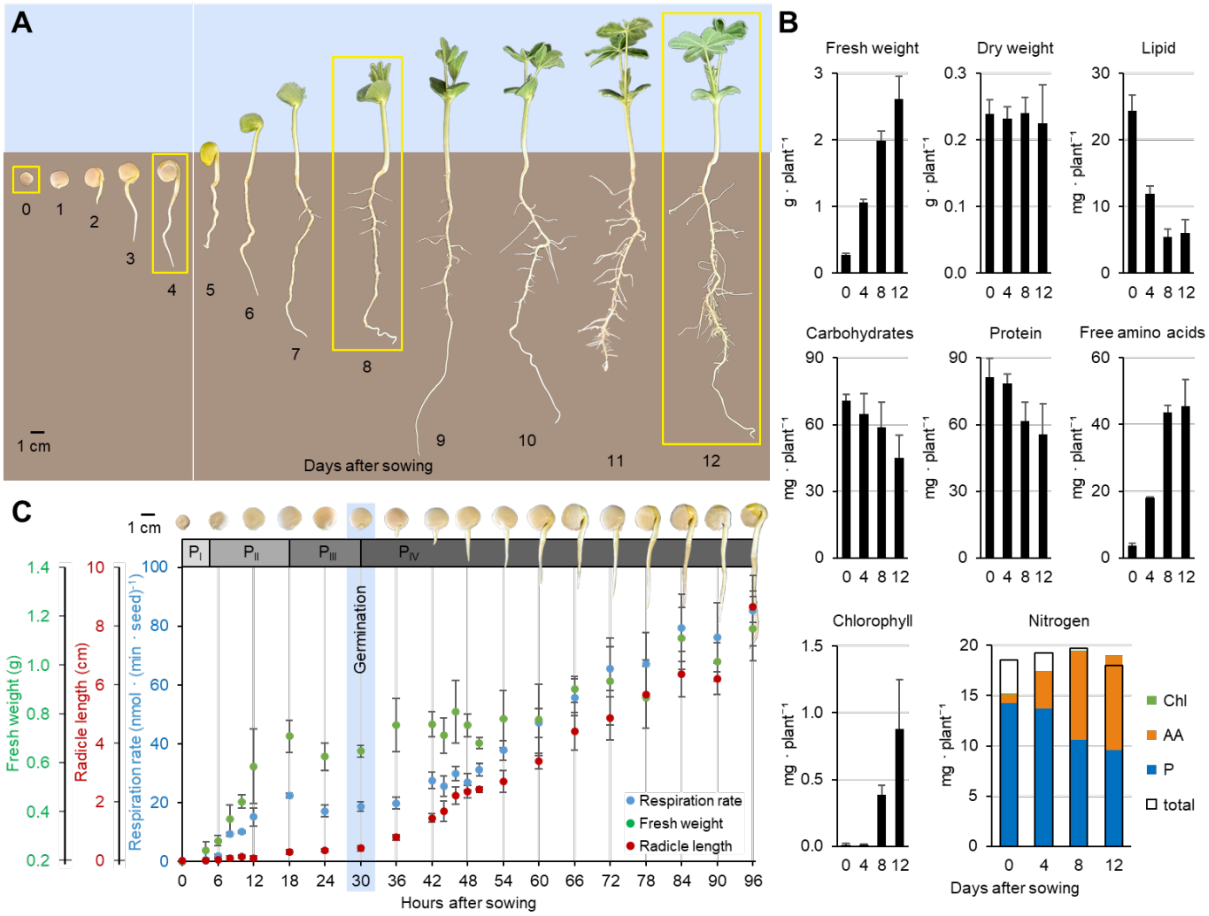

M1-Fig. 2: Germination and seedling establishment in *Lupinus albus*. (**A**) Phenotype of representative plants during the first 12 d of growth. Yellow boxes mark sample groups. (**B**) Biomass and composition of the seeds/seedlings at 0, 4, 8, and 12 d after sowing. The total nitrogen content was analysed using a C/N-analyser and compared with the sum of calculated nitrogen contents of proteins, free amino acids (AA), and chlorophyll (Chl). Data presented are means ± SD (n = 5). (**C**) Respiration rate of *Lupinus albus* during four phases (PI – IV) of

germination and seedling development in the first 4 d after sowing. PI, initial onset of oxygen consumption at low rates; PII, seed swelling and preparation for germination; PIII, completion of germination (blue box; germination = testa rupture); PIV, early seedling establishment. Data presented are means ± SD (n = 4).

2.3.3 Proteome remodelling from seed to seedling

In order to gain a more precise insight into the metabolic transformations during seedling development we analysed the quantitative composition of the *L. albus* proteome (M1-Fig. 3; Supp. Dataset S3). On the basis of our manually curated annotation table, we were able to assign 87 % of the seed protein content to functional categories including the large fractions of storage proteins, late embryogenesis abundant (LEA) proteins, and structural proteins of the storage oil bodies (oleosins) (M1-Fig. 3; Supp. M1-Fig. S1). Twelve days after imbibition the proteome of the seedling was more diverse and Rubisco subunits had become the proteins with the highest abundance (M1-Fig. 3B, C). During germination and initial seedling establishment in the dark, LEA proteins rapidly decreased by 88 % (M1-Fig. 3D). Asparagine synthetase as well as the enzymes involved in the glyoxylate cycle and gluconeogenesis showed the highest relative increase in protein content (log_2 fold change: 5.6 – 6.2; Supp. Dataset S3). A distinct peak in phytochrome A protein abundance was visible at day 4 shortly before emergence of the cotyledons from the soil (M1-Fig. 3D). The most pronounced proteome remodelling occurred during development of the first true leaves (day 4 – 8) including massive degradation of storage proteins and synthesis of the photosynthetic apparatus (M1-Fig. 3; Supp. M1-Fig. S1). Oleosins were completely degraded at this stage.

2.3.4 Amino acid metabolism during germination and seedling establishment

A large fraction of the amino acids released by proteolysis is stored in the free amino acid pool leading to a shift between the free and protein-bound amino acid pools (M1-Fig. 4A; Supp. Dataset S4). Asparagine strongly accumulated in the free pool (from 6 ± 2 to 1198 ± 150 µmol g^{-1} dry weight) and most of the other amino acids also significantly increased (2.3 – 134-fold) with the exception of glutamate and arginine, which decreased during development (M1-Fig. 4B; Supp. Dataset S4). Most of the enzymes involved in amino acid metabolism increased in their abundance during germination and seedling establishment (Figs 3D, 4C; Supp. Dataset S4). The most pronounced induction could be detected in the pathway required for nitrogen

(re)assimilation into asparagine, in photorespiration, and in sulfur amino acid metabolism. Some pathways contain isoenzymes localizing to different subcellular compartments. Since to our knowledge localization studies have not been performed for enzymes involved in *L. albus* amino acid metabolism so far, assignments of subcellular compartments are based on sequence homologies to *Arabidopsis* (Supp. M1-Fig. S2).

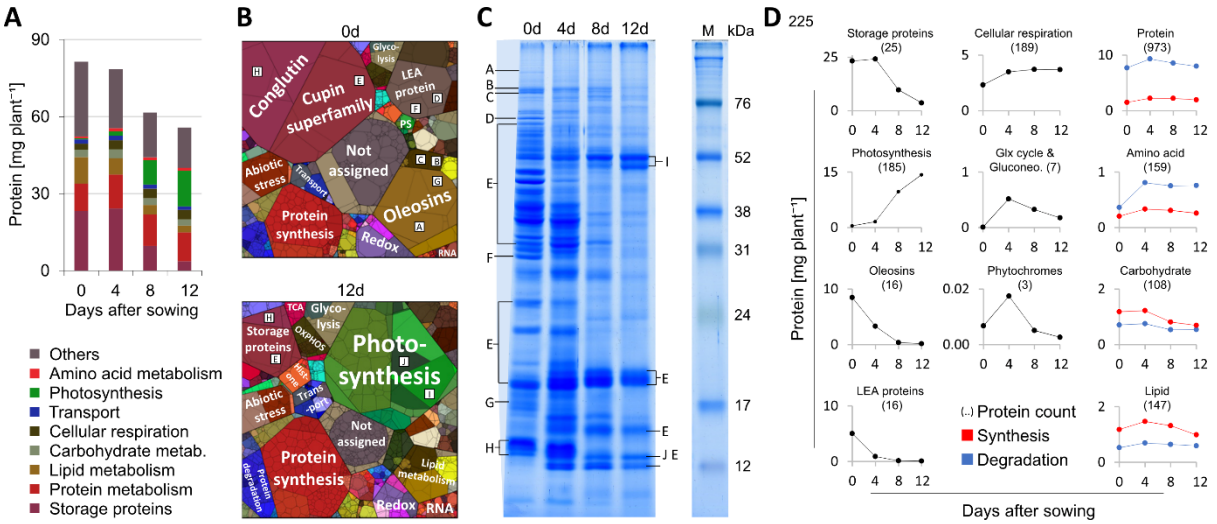

M1-Fig. 3: Quantitative composition of the *Lupinus albus* proteome during germination and seedling establishment. (**A**) Total protein content and mass fractions covered by the major functional categories at day 0, 4, 8, and 12 after sowing. Mass fractions [protein abundances obtained by MS (intensity-based absolute quantification), multiplied by protein molecular mass] for all individual proteins are provided in Supp. Dataset S3. (**B**) Proteomap illustrating the quantitative composition of the *L. albus* proteome at day 0 and 12 after sowing. Proteins are shown as polygons whose sizes represent their mass fractions; see (A). Proteins involved in similar cellular functions are arranged in adjacent locations and visualized by colours. Letters correspond to the major proteins detected in the most prominent bands after SDS-PAGE. (**C**) Glycine-SDS-PAGE of proteins extracted from 5 mg lyophilized lupin sample stained with colloidal Coomassie blue. The most prominent bands (marked by letters) were analysed by MS (Supp. Dataset S3). Major proteins: A, G: oleosin; B, C: lipoxygenase; D, F: late embryogenesis abundant protein; E: cupin; H: conglutin; I: ribulose bisphosphate carboxylase large chain; J: ribulose bisphosphate carboxylase small chain. (**D**) Protein abundance profiles of selected functional categories at day 0, 4, 8, and 12 after sowing. Numbers in parentheses indicate the number of different proteins detected in the respective category; LEA, late embryogenesis abundant. Abundance profiles for additional functional categories as well as information on the calculation method are provided in Supp. Dataset S3.

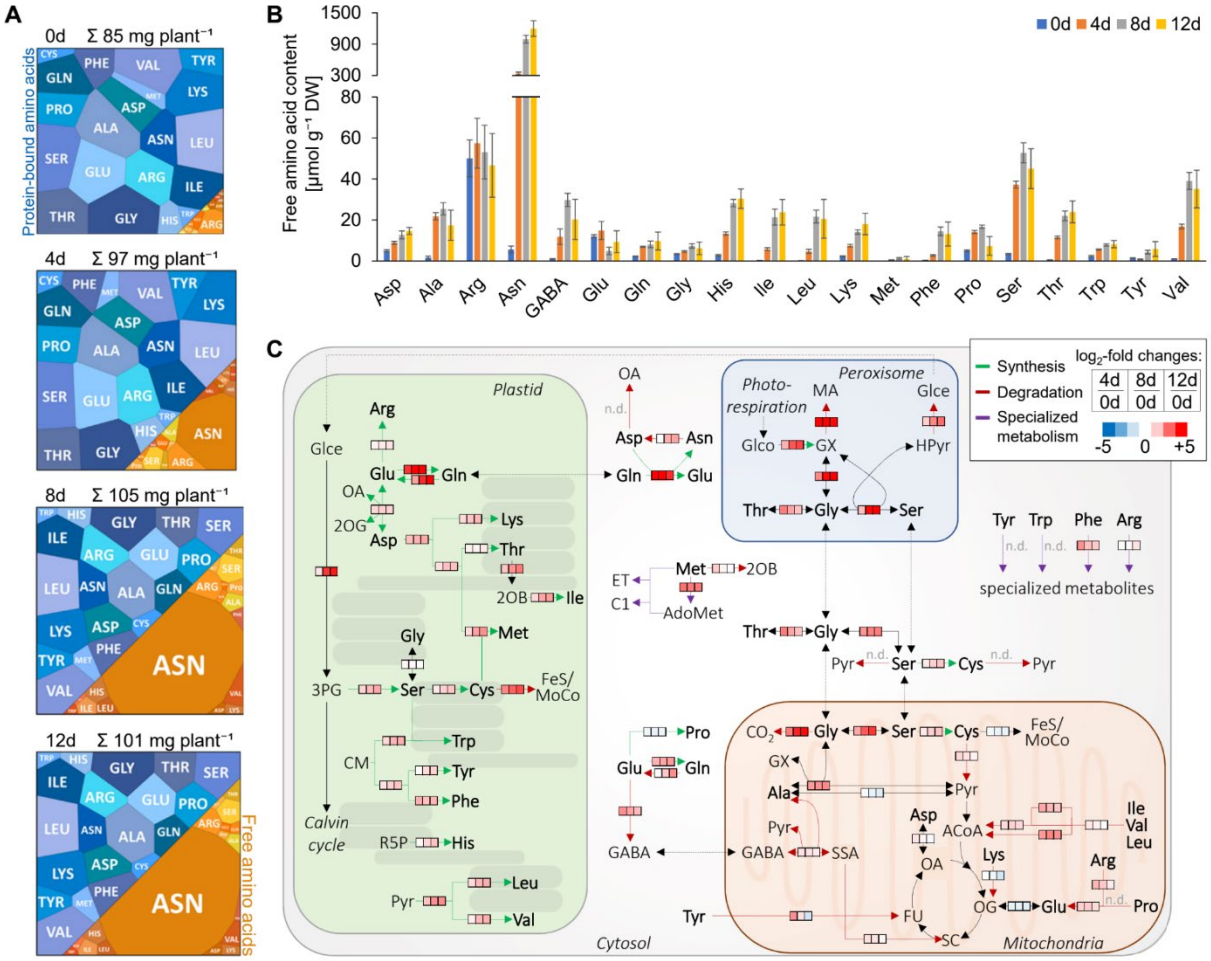

M1-Fig. 4: Amino acid metabolism in *Lupinus albus* during germination and seedling establishment. (**A**) Quantitative composition of the free (orange) and protein-bound (blue) amino acid pools at day 0, 4, 8, and 12 after sowing. Amino acids are shown as polygons whose sizes represent the molar fractions. Free amino acid contents were quantified by HPLC, and the quantitative amino acid composition of the proteome was calculated on the basis of molar composition of the proteome (see Supp. Dataset S4). (**B**) Free amino acid contents of the seeds/seedlings at day 0, 4, 8, and 12 after sowing. Data presented are means ± SD (n = 5). (**C**) Relative protein abundance of amino acid metabolic pathways during germination and seedling establishment. The coloured squares represent the means of all log_2 fold changes in the abundance of enzymes involved in the respective branch of the pathway at day 4, 8, and 12 compared with day 0. The full table of amino acid metabolism is provided in Supp. Dataset S4 and Supp. M1-Fig. S3. 2OB, 2-oxobutyrate; 2OG, 2-oxoglutarate; 3PG, 3-phosphoglycerate; ACoA, Acetyl-CoA; AdoMet, S-adenosylmethionine; C1, C1-metabolism; CM, chorismate; ET, ethylene; FeS, iron–sulfur cluster; FU, fumarate; GABA, γ-aminobutyric acid; Glce, glycolate; GX, glyoxylate; Hpyr, hydroxypyruvate; MA, malate; MoCo, molybdenum cofactor; n.d., not detected; OA, oxaloacetic acid; OG, oxoglutarate; Pyr, pyruvate; R5P, ribose-5-phosphate; SC, succinate; SSA, succinic semialdehyde.

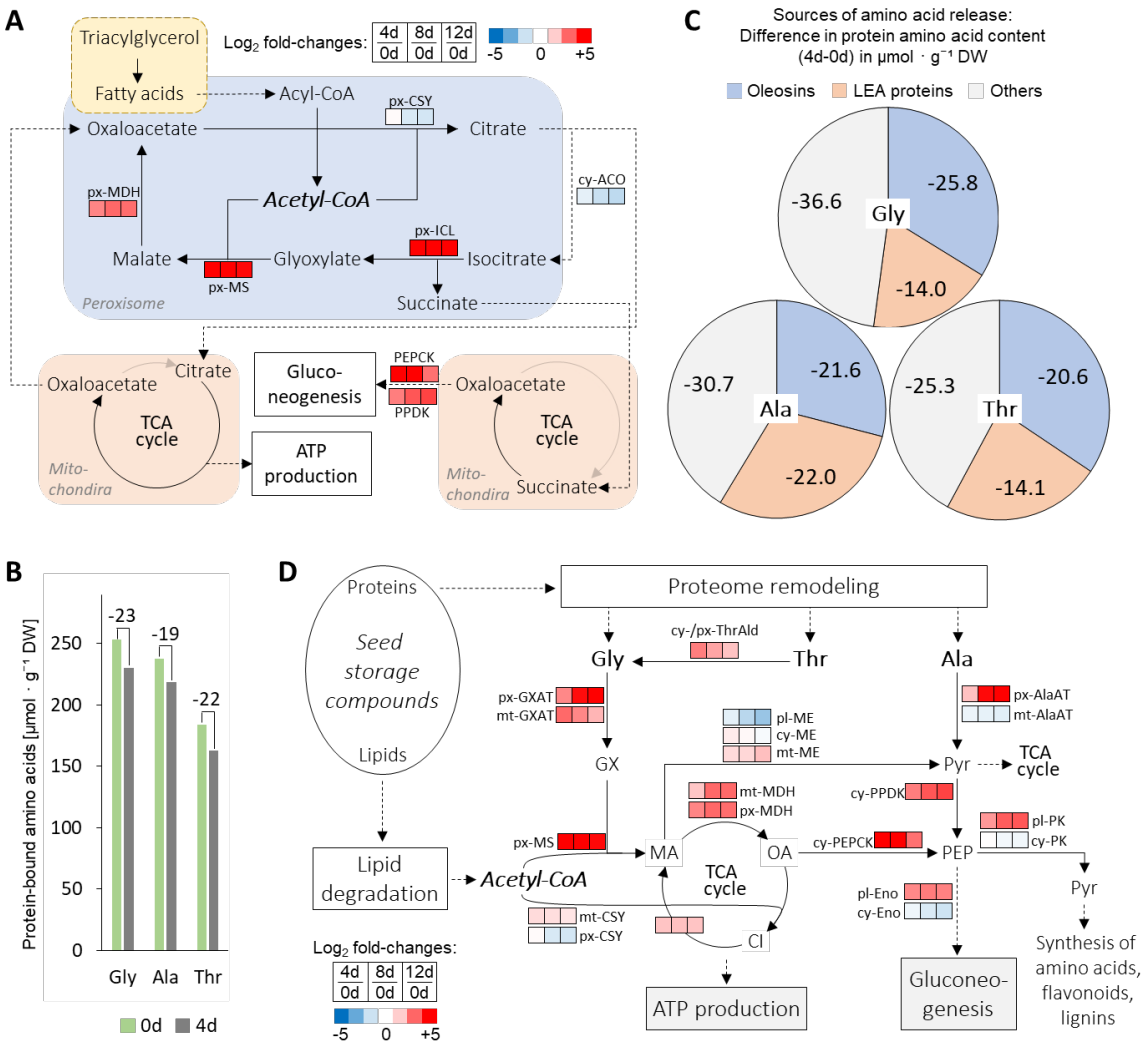

M1-Fig. 5: Potential integration of fatty acid and amino acid metabolism during germination and seedling establishment. (**A**) Relative protein abundance of glyoxylate cycle enzymes. The coloured squares represent the means of $\log_2$ fold changes in the abundance of tissue specific isoforms at day 4, 8, and 12 compared with day 0. The full dataset is provided in Supp. Dataset S5. (**B**) Protein-bound contents of glycine, alanine, and threonine [µmol g^{-1} dry weight (DW)] in seeds and 4-day-old seedlings. A complete list of free and protein-bound amino acid contents at all time points is provided in Supp. Dataset S4. (**C**) Total amount of glycine, alanine, and threonine released by protein degradation within 4 d after germination. The two major categories (late embryogenesis abundant proteins and oleosins) are shown individually whereas all other categories have been combined. (**D**) Relative protein abundance of enzymes required for a combined metabolism of amino acids and fatty acids to carbohydrates. The coloured squares represent the means of $\log_2$ fold changes in the abundance of tissue specific isoforms at day 4, 8, and 12 compared with day 0. The full dataset is provided in Supp. Dataset S5. Assignments of subcellular compartments are based on sequence homologies to *Arabidopsis* (Supp. M1-Fig. S4). ACO, aconitase; AlaAT, alanine aminotransferase; CI, citrate; CSY, citrate synthase; cy, cytosolic; Eno, enolase; GX, glyoxylate; GXAT, glyoxylate aminotransferase; ICL, isocitrate lyase; MA, malate; MDH, malate dehydrogenase; ME, malic enzyme; MS, malate synthase; mt, mitochondrial; OA, oxaloacetate; PEP, phosphoenolpyruvate; PEPCK, phosphoenolpyruvate carboxykinase; PK, pyruvate kinase; pl, plastidic; PPDK, pyruvate; phosphate dikinase; px, peroxisomal; Pyr, pyruvate; ThrAld, l-threonine aldolase.

2.3.5 Integration of fatty acid and amino acid metabolism

Storage lipids can either be converted to carbohydrates via the glyoxylate cycle and gluconeogenesis or serve as a substrate for mitochondrial ATP production (M1-Fig. 5A). In both cases metabolites have to be cycled back to the peroxisomes to supply acceptor molecules for the acetyl groups from fatty acid β-oxidation. The enzymes involved in lipid breakdown and fatty acid β-oxidation as well as three steps of the glyoxylate cycle (isocitrate lyase, malate synthase, malate dehydrogenase) strongly increased in the developing *L. albus* seedlings. The abundance of phosphoenolpyruvate carboxykinase required for gluconeogenesis from fatty acid catabolism peaked at day 4 after sowing. However, the isoforms of citrate synthase and aconitase required for completing the glyoxylate cycle were decreased in their abundance whereas isoforms in other subcellular compartments were moderately induced (M1-Fig. 5A; Supp. Dataset S5). Since lupin seeds use proteins as a major storage compound we reinvestigated a potential contribution of amino acids to seedling carbohydrate and energy metabolism. A moderate but continuous increase in relative protein abundance over the entire 12-day period studied was detectable for pyruvate orthophosphate dikinase (PPDK), an enzyme required for recovering carbon from pyruvate produced by amino acid catabolism (M1-Fig. 5D; EASTMOND ET AL., 2015). The total protein content of the seedlings did not change significantly during the initial phase of development prior to emergence from the soil (M1-Fig. 2B), but interestingly there were clear differences in the quantitative amino acid composition of the proteome. The protein set-up of the seedling at day 4 had a lower content of glycine, alanine, and threonine than that of the dry seed while the fractions of the other 17 amino acids in the proteome remained fairly constant (M1-Fig. 5B; Supp. Dataset S5). By far the major source of glycine, alanine, and threonine release were two categories of seed proteins, LEA proteins and oleosins (M1-Fig. 5C). These proteins are of high abundance (6 – 10 %) in the dry seed, they were degraded early during germination and seedling establishment, and they are specifically rich in glycine, threonine, and alanine (M1-Fig. 3; Supp. Datasets S3, S5). Strikingly, transamination of glycine provides glyoxylate, and threonine can directly be converted to glycine via aldol cleavage (HILDEBRANDT ET AL., 2015). Thus, the unusual amino acid composition of specific seed proteins might provide an additional source of glyoxylate to support fatty acid metabolism during germination (M1-Fig. 5D). The enzymes required for the production of glyoxylate from glycine and the conversion of threonine to glycine were

strongly induced in the developing lupin seedlings. The same trend was visible for subsequent reaction steps metabolizing glyoxylate and acetyl-CoA to phosphoenolpyruvate as a substrate for gluconeogenesis (malate synthase, malate dehydrogenase, phosphoenolpyruvate carboxykinase). Transamination of alanine produces pyruvate, which can either be phosphorylated to phosphoenolpyruvate by PPDK for gluconeogenesis or serve as an amino group acceptor during transamination of glycine to glyoxylate. Via glutamate and glutamine, the ammonium can then be transferred to asparagine for storage and transport. Our datasets so far do not distinguish between the different tissues of the developing seedling. In order to test, whether the enzymes required for a combined metabolism of amino acids and fatty acids to carbohydrates were induced in the same tissue, we analysed the proteome of the cotyledons and the hypocotyl of 4-day-old seedlings separately (Supp. Dataset S6; Supp. M1-Fig. S5). All the enzymes involved in this postulated combined pathway increased in abundance in both tissues compared with the dry seed with a more pronounced induction in the cotyledons. In contrast, the amino acid synthesis pathways increased more strongly in the growing hypocotyl (Supp. Dataset S6; Supp. M1-Fig. S5).

2.4 Discussion

2.4.1 Energy and carbohydrate metabolism of *Lupinus albus* during germination

During germination seeds exclusively rely on their storage compounds to supply substrates for ATP production as well as precursors for the synthesis of structural elements and cellular components. At this stage their energy metabolism is chemotrophic in contrast to the characteristic photoautotrophic strategy of plants at later developmental stages. The obvious idea for seeds that use proteins as major storage compounds such as legumes would be to oxidize amino acids as alternative respiratory substrates and to convert them into carbohydrates via the glyoxylate cycle and gluconeogenesis. Both pathways are present in plants and have been shown to be relevant for seedling establishment in *Arabidopsis* (EASTMOND ET AL., 2015; HENNINGER ET AL., 2022). However, our quantitative data indicate that in *Lupinus albus* there is no net decrease in total protein content up to a stage when the seedling emerges from the soil and develops first true leaves (M1-Fig. 2). Nevertheless, the

composition of the proteome clearly changes within the first 4 d of germination and seedling development with a strong decrease in oleosins and LEA proteins and an induction of metabolic enzymes (M1-Fig. 3). We detected only a moderate increase in the pathways characteristic for an energy deficiency response such as lysine, tyrosine, and branched-chain amino acid degradation as well as PPDK, required for efficient recovery of carbon from storage proteins (Eastmond et al., 2015; Pedrotti et al., 2018). In contrast, the total lipid content dropped by more than 50 % during the initial phase of seedling establishment and the pathways catalysing fatty acid catabolism and gluconeogenesis were strongly induced. These results agree with previous findings on storage lipid metabolism in *L. albus* that already demonstrated a pivotal function during germination (Borek et al., 2015). Electron micrographs of white lupin cotyledons show a strong decrease in the number of oil bodies and more but smaller protein storage vesicles after 4 d of *in vitro* cultivation (Borek et al., 2011). Our estimation based on seedling respiration rates indicates that the lower limit for covering the ATP demand until the onset of photosynthesis would be ~10.5 mg lipid g^{-1} dry weight (2.5 mg per seed). Thus, in order to secure vigorous seedling establishment, breeding strategies should not aim at low fat varieties with a lipid content below 1.5 – 2 %. Surprisingly, no increase in peroxisomal citrate synthase or cytosolic aconitase was detectable. Citrate synthase is essential for fatty acid respiration when citrate is used as the carbon transport form from the peroxisomes to the mitochondria, which has been postulated for the oilseeds *Arabidopsis* and *Helianthus annuus* (Raymond et al., 1992; Pracharoenwattana et al., 2005). Both, citrate synthase and aconitase are required for regeneration of the initial acetyl acceptor in the glyoxylate cycle (Baker et al., 2006; Pracharoenwattana and Smith, 2008). Citrate synthase activity can be modified by redox regulation and allosteric effectors (Schmidtmann et al., 2014; Nishio and Mizushima, 2020). Thus, an increase in enzyme activity could be achieved without a concomitant increase in protein abundance via post-translational mechanisms. However, our results indicate that in germinating seeds of *L. albus*, the amino acids glycine and threonine, which are strikingly enriched in two classes of seed specific proteins (oleosins and LEA proteins), might provide an alternative source of glyoxylate (M1-Fig. 5). Oleosins are the predominant lipid droplet coat proteins and their degradation is coordinated with triacylglycerol mobilization (Traver and Bartel, 2023). Thus, according to our hypothesis, fatty acids would be delivered together with the suitable amino acids for their efficient utilization during germination. This integration

of fatty acid and amino acid metabolism would utilize a linear flux mode through parts of the glyoxylate cycle to combine stored carbon from lipids and proteins into gluconeogenesis. A potential next step involves conducting computational analysis of a network representation of *L. albus* primary metabolism by means of flux-balance techniques. This approach would allow the making of quantitative predictions of metabolic flux modes during the different stages of early seedling establishment. Since photosynthesis has not yet been established during these developmental phases, the system operates in a chemotroph mode. As such, all metabolic processes are driven by internal energy and matter conversions, which will enable us to confidentially constrain the model based on experimental measurements. Such a model has the potential to elucidate the combined roles of fatty acid degradation and amino acid metabolism to support fluxes into gluconeogenesis and to highlight constraints and capacities associated with the use of proteins as major seed storage compounds. Since we detected no decrease in net protein content during early seedling development, at least part of the carbohydrates produced in the cotyledons is most likely used for amino acid synthesis and the production of a functional protein set-up in the growing seedling.

2.4.2 Nitrogen resource allocation in the *Lupinus albus* seedling

Amino acids and proteins contain by far the largest fraction of nitrogen in white lupin seeds and seedlings (≥ 80 %). Additional nitrogen containing compounds such as chlorophyll and nucleotides quantitatively require no major input of nitrogen resources. However, about 20 % of the seed nitrogen content could not be assigned to a substance class by our approach. This most likely includes non-protein amino acids and polyamines, which are present in dry lupin seeds and might have a protective function against abiotic stress (ANISZEWSKI ET AL., 2001; BANO ET AL., 2020). Asparagine strongly accumulated in the lupin seedlings with a peak after the onset of photosynthesis (M1-Fig. 4). Asparagine is a suitable storage and transport form of reduced nitrogen within the plant since it has a favourable C/N ratio, little net charge, and low reactivity under physiological conditions (LEA ET AL., 2007). It also serves as the major end product of nitrogen fixation in lupins and accounts for 60 – 80 % of the total amino acids in nodulated roots, leaves, and developing seeds of nitrogen-fixing *L. albus* (PATE ET AL., 1981). During early seedling establishment, the induction of asparagine synthesis preceded a net decrease in total protein content indicating an

incorporation of nitrogen from alternative sources such as degradation of specialized defence compounds in the seeds. The carbon skeletons for early asparagine synthesis might be at least partially provided by storage lipid catabolism, which would explain the observed carbon flux from lipids to amino acids (BOREK ET AL., 2003; BOREK AND RATAJCZAK, 2010). Asparagine accumulation continued and even accelerated at later developmental stages (8 to 12 d after sowing) when the seedling had already emerged from the soil and photosynthesis was active, but at this stage was clearly connected to proteolysis and a massive shift of amino acids from the protein bound to the soluble pool. A major function of this shift is most likely remobilization and transport of nitrogen to the growing tissues (LEA ET AL., 2007). Since the free amino acid concentration in the seedlings reached almost 200 mM, this process might in addition be relevant for osmoregulation. In nitrogen-poor soils the lupin seedlings rely on the nitrogen stored in amino acids until the symbiosis with N_2-fixing rhizobia has been established, which is usually achieved within 2 – 3 weeks after germination. Our results indicate that supply of nitrogen derived from storage proteins from the cotyledons to the growing seedling peaks during the second week of development, which would suggest a pivotal role of the cotyledons not only for successful germination but also for subsequent establishment on nitrogen-poor soil. Successfully populating these habitats requires the large internal nitrogen store provided by storage proteins in lupins and other legume plants to meet the demands of the growing seedling up to the point when rhizobial symbiosis is fully functional.

2.5 Conclusions

Although classified as a protein crop, *Lupinus albus* does not use amino acids as a primary resource during germination and early seedling establishment. The total protein content decreases substantially only after emergence of the seedling from the soil. The major advantage of storing large quantities of protein in the seeds would therefore be to provide the nitrogen resources required for successfully populating nitrogen deprived habitats for a prolonged period (2 – 3 weeks) after germination until the symbiosis with N_2-fixing rhizobia has been established. However, our results also point to the metabolic potential of integrating fatty acid and amino acid catabolism at the level of malate synthase during germination. Conversion of glycine to glyoxylate would allow the integration of acetyl-CoA from fatty acid β-oxidation into oxaloacetate

for gluconeogenesis without the full glyoxylate cycle. The physiological relevance of this combined pathway during germination will have to be elucidated.

2.6 Materials and methods

2.6.1 Plant material

White lupin (*Lupinus albus* cv. 'Nelly') seeds were stored in the dark at 4 °C until use. Before cultivation, the seeds were soaked in demineralized water at 20 °C for 16 h and then transferred to water-saturated expanded clay substrate (LamstedtDan, 4 – 8 mm, Fibo ExClay Deutschland GmbH, Lamstedt, Germany). Plants were cultivated in a phytochamber (22 – 24 °C, 16 h light, 8 h dark, 110 µmol m^{-2} s^{-1} light). At harvest, the seed coats were removed and the remaining plant organs were deep-frozen in liquid nitrogen. The plant material was lyophilized in an Alpha 1-2 LD+ freeze dryer (Christ, Osterode, Germany). The dried material was then ground into powder and used for the investigations. For dry seeds and young seedlings several plants were pooled (10 seeds, five seedlings at day 4, two seedlings at day 8), and five different plants or pools were analysed at each time point as biological replicates. The time points for harvesting were selected based on preliminary experiments to cover germination as well as the subsequent seedling developmental stages characterized by massive degradation of seed storage proteins.

2.6.2 Quantification of total carbon and nitrogen

The total carbon and nitrogen content of the samples was measured according to ANDRINO ET AL. (2019), using an Elementar vario MICRO cube C/N analyser (Elementar GmbH, Hanau, Germany).

2.6.3 Quantification of total lipids

The total lipid content was determined using the sulfo-phospho-vanillin method described in PARK ET AL. (2016). Commercial lupin oil was used as a standard.

2.6.4 Quantification of total carbohydrates

The total carbohydrate content was determined using the phenol–sulfuric acid method described by TAMBOLI ET AL. (2020). Five milligrams of lyophilized plant powder were dissolved in 1 ml of 2.5 M HCl and incubated for 3 h at 95 °C, shaking. The extracts were diluted (1:50) with demineralized water and 10 µl phenol and 1 ml concentrated

sulfuric acid were added. After incubation (10 min, 95 °C, shaking) the absorbance was measured at 490 nm with a plate reader (Multiskan Sky, Thermo Fisher Scientific, Dreieich, Germany).

2.6.5 Quantification of cellulose

The cellulose content was determined using a modification of the method originally described by UPDEGRAFF (1969). Five milligrams of lyophilized plant powder were dissolved in 1 ml acetic acid–demineralized water–nitric acid (8/2/1, v/v/v) and incubated shaking for 30 min at 100 °C. After a centrifugation step, the supernatant was evaporated in a vacuum concentrator, and the pellets were washed with demineralized water and then dissolved in 1 ml sulfuric acid (72 %). The samples were further diluted to 5 ml with demineralized water. Fifty microliters of the extract were mixed with 150 µl of demineralized water and 500 µl of anthrone solution (0.3 % anthrone in concentrated sulfuric acid) and incubated shaking at 100 °C for 20 min. The absorbance at 620 nm was measured and quantified against a cellulose standard.

2.6.6 Quantification of chlorophyll

The quantification of chlorophyll was carried out according to a modified version of the method described by LICHTENTHALER (1987). Five milligrams of plant powder were dissolved in 700 ml methanol (100 %) and incubated for 20 min at 80 °C with shaking. After centrifugation (10 min, 4 °C, 18 800 ×g), the chlorophyll content of the supernatant was quantified with a plate reader (wavelengths: 470, 653, and 666 nm).

2.6.7 Quantification of proteins

The protein extraction protocol for quantification of the total seed/seedling protein content was rigorously tested and optimized for quantitative recovery of all proteins. Four milligrams of lyophilized plant powder were dissolved in 1 ml methanol (100 %) and incubated for 20 min at −20 °C. After centrifugation (14 200 ×g, 5 min, 4 °C) the pellet was dissolved in 1.4 ml of 0.1 M NaOH containing 2 % SDS (v/w) and incubated for 1 h at 60 °C, shaking. After centrifugation (7000 ×g, 10 min, room temperature), the supernatant was diluted with demineralized water (1:10). The Pierce BCA Protein Assay Kit (Thermo Fisher Scientific, Rockford, IL, USA) was used for protein quantification with globulin as a standard. This protein extraction protocol was clearly superior to phenol and trichloroacetic acid precipitation in terms of protein recovery

from *Lupinus albus* seeds. Defatting of the plant material did not further increase protein recovery.

2.6.8 Quantification of free amino acids

Free amino acids were quantified according to BATISTA-SILVA ET AL. (2019). The pre-column derivatization with ophthaldialdehyde (OPA) and fluorenylmethoxycarbonyl (FMOC) was based on the Agilent application note 'Automated amino acids analysis using an Agilent Poroshell HPH-C18 Column'. Samples were injected onto a 100 mm, 3 mm InfinityLab Poroshell HPH-C18 column (2.7 mm) using an Ultimate 3000 HPLC system (Thermo Fisher Scientific, Germering, Germany).

2.6.9 Respiration measurements

Respiration rates of seeds and seedlings were measured at 20 °C in demineralized water using an Oxygraph-2k respirometer (Oroboros Instruments Corp., Innsbruck, Austria).

2.6.10 SDS-PAGE

Proteins were separated by glycine SDS-PAGE according to a modified protocol of LAEMMLI (1970). Exactly 5 mg of plant powder was dissolved in 1 ml methanol (100 %) and incubated for 20 min at −20 °C. After centrifugation (10 min, 4 °C, 18 800 ×g) the pellet was air dried. Then 200 µl of sample buffer (125 mM Tris–HCl, pH: 6.8, 4 % SDS, 20 % glycerol) was added and incubated for 1 h at 95 °C, shaking. The samples were cooled on ice and centrifuged (5 min, 18 800 ×g, 4 °C). The supernatant was used for glycine-SDS-PAGE. Separation gels contained 4.5 % polyacrylamide. Amersham ECL Rainbow Marker—Full Range (High Range, Cytiva RPN756E, Sigma-Aldrich, St Louis, MO, USA) was used as size standard. The same volume of protein extract was used per sample. Gels were stained with colloidal Coomassie Blue. Selected protein bands were cut and digested with trypsin as described in KLODMANN ET AL. (2010), desalted using homemade C18-StageTips (KULAK ET AL., 2014), and identified by mass spectrometry as detailed in the section entitled 'Quantitative proteomics by shotgun mass spectrometry'.

2.6.11 Protein extraction and purification for proteome analysis via mass spectrometry

For protein extraction, clean-up, and digestion, we used an adapted 'single-pot solid-phase-enhanced sample preparations (SP3)' protocol from HUGHES ET AL. (2019) and MIKULÁŠEK ET AL. (2021). The mechanism relies on hydrophilic interactions between proteins and paramagnetic beads, which can be accumulated on a magnetic rack for fast washing steps and buffer exchanges. The approach is known for its efficient, unbiased, and robust processing of protein samples for proteomic analysis. In brief, 5 mg of lyophilized plant powder (~500 µg plant protein) was dissolved in 250 µl of 2×SDT buffer (8 % SDS, 0.2 M dithiothreitol, 0.2 M Tris pH: 7.6) and incubated at 60 °C for 30 min to extract, denature, and reduce the proteins. Samples were then sonicated for 10 min and centrifuged at 20 000 ×g for 10 min. Thirty microliters (~30 µg protein) of the supernatant was transferred to new tubes and mixed with 7.5 µl iodoacetamide (0.1 M) in order to alkylate the reduced disulfide bridges. The samples were incubated for 30 min in the dark. Then 2 µl dithiothreitol (0.1 M) was added to each sample to neutralize excess amounts of iodoacetamide. Preparation of the magnetic beads (Sera-Mag carboxylate-modified beads, hydrophobic solids no. 441521050250, hydrophilic solids no. 241521050250, GE Healthcare Life Sciences), protein binding and washing steps were performed on a magnetic rack as described in MIKULÁŠEK ET AL. (2021). We used a bead to protein ratio of 20:1 (w/w; 600 µg beads). The bound and purified proteins were digested overnight at 37 °C with 0.5 µg trypsin (mass spectrometry grade, Promega) per sample. The peptide-containing supernatants were collected in tubes with low peptide binding. The magnetic beads were rinsed in 60 µl ammonium bicarbonate (50 mM) to recover the remaining peptides. Both eluates were combined and acidified with formic acid. The peptides were desalted with 50 mg Sep-Pak tC18 columns (WAT054960, Waters, Milford, Massachusetts, USA) and quantified using the Pierce Quantitative Colorimetric Peptide Assay Kit (Thermo Fisher Scientific, Rockford, IL, USA). The samples were finally diluted to a target concentration of 200 ng μl^{-1} in 0.1 % formic acid.

2.6.12 Quantitative proteomics by shotgun mass spectrometry

Four hundred nanograms of peptides was injected via a nanoElute UHPLC (Bruker Daltonics, Bremen, Germany) and separated on an analytical reversed-phase C18 column (Aurora Ultimate 25 cm × 75 µm, 1.6 µm, 120 Å; IonOpticks). Using a

multistage linear gradient (eluent A: MS grade water containing 0.1 % formic acid, eluent B: acetonitrile containing 0.1 % formic acid, gradient: 0 min, 2 %; 54 min, 25 %; 60 min, 37 %; 62 min, 95 %; 70 min, 95 % eluent B), peptides were eluted and ionized by electrospray ionization using a captive spray source with a flow of 300 nl min^{-1}. A standard application method [data-dependent acquisition parallel accumulation–serial fragmentation (DDA-PASEF) cycle time 1.1 s] was used for data collection without further modification. Ion mobility spectrometry–MS/MS spectra were analysed using MaxQuant (version 2.0.3.0, COX AND MANN, 2008). Protein identification was based on the proteome of *Lupinus albus* published on uniport.org by XU ET AL. (2020) (UP000464885). The search parameters of the software were set as follows: carbamidomethylation (C) as fixed modification, oxidation (M) and acetylation (protein N-term) as variable modifications. The specific digestion mode was set to trypsin (P), with a maximum of two missing cleavage sites allowed. A positive peptide identification had to contain at least seven amino acids. Mass tolerance for fragment ions was set at 40 ppm. The false discovery rate at the protein and peptide spectrum match level was set at 1 %. The minimum number of unique peptides per protein group was 1. Both label-free quantification (LFQ) values and intensity-based absolute quantification (iBAQ) values were calculated for the identified proteins.

2.6.13 Data processing and functional annotation

Intensities of unique and razor peptides were used for protein quantification. Further analysis and statistical evaluation based on iBAQ values and LFQ values generated by MaxQuant was performed using Perseus (version 1.6.1.1) (TYANOVA ET AL., 2016). Fold changes of individual proteins can be estimated using LFQ values (COX ET AL., 2014). This approach is suitable for identifying proteins that are induced and could therefore be particularly relevant under the conditions tested. However, changes in the absolute amounts of individual proteins can be estimated by iBAQ values. The MaxQuant output table was filtered to remove non-plant contaminants, reversed sequences, and proteins identified only on the basis of modified peptides. Proteins were excluded from further analysis if they were not detected in at least four out of five biological replicates in at least one of the sample groups. Subsequently, the missing protein intensities were considered too low for proper quantification and were randomly replaced with low values of a normal distribution. Significant changes were calculated from the LFQ values using Student's t-test ($p = 0.05$). A functional annotation database

(Supp. Dataset S1) was built by sequence alignments (BLASTp) of the proteome of *Lupinus albus* (UP000464885) against proteomes of *Lupinus angustifolius* (UP000188354), *Medicago truncatula* (UP000002051) and *Arabidopsis* (TAIR10). Candidate consensus was achieved by highest bit score and/or manual curation. We then used common bioinformatics tools of the model plant *Arabidopsis* to obtain further information on the subcellular localization (SUBA.live) and metabolic pathway involvement (mapman.gabipd.org) of all individual proteins.

2.7 Data availability

The mass spectrometry proteomics data have been deposited to the ProteomeXchange Consortium (http://proteomecentral.proteomexchange.org) via the PRIDE partner repository (Perez-Riverol et al., 2022) with the dataset identifier PXD046789.

2.8 Funding

Research in TMH's lab and NT's group is funded by the Deutsche Forschungsgemeinschaft (DFG, German Research Foundation) under Germany's Excellence Strategy—EXC-2048/1—project ID 390686111.

2.9 Author contributions

TMH and HPB initiated the project; TMH, CA, and BH designed the research; BH and TMH developed the *Lupinus albus* protein annotation database; BH performed and evaluated the shotgun proteomics experiments; JH performed the experiments for individual analysis of cotyledons and hypocotyl; CA performed all the other experiments; TMH, CA, and BH analysed the data; NT contributed to pathway evaluations; TMH wrote the paper with support from CA, BH, NT, and HPB. TMH agrees to serve as the author responsible for contact and ensures communication.

2.10 Acknowledgements

We thank Hashani Amarasinghe for preliminary work on this project and Dagmar Lewejohann for skilful technical assistance. Constructive discussions with Marco Herde and Holger Eubel are highly appreciated. We also thank Alberto Andrino de la Fuente for support during C/N analysis.

2.11 Supplemental data

The following supplemental data are available at JXB online.

Supp. Dataset S1: Manually curated *Lupinus albus* protein annotation database.

Supp. Dataset S2: Composition and respiration rate of *Lupinus albus* seeds and seedlings (dataset corresponding to M1-Fig. 2).

Supp. Dataset S3: Proteome of *Lupinus albus* seeds and seedlings (dataset corresponding to M1-Fig. 3).

Supp. Dataset S4: Amino acid metabolism in *Lupinus albus* seeds and seedlings (dataset corresponding to M1-Fig. 4).

Supp. Dataset S5: Potential integration of fatty acid and amino acid metabolism during germination and seedling establishment (dataset corresponding to M1-Fig. 5).

Supp. Dataset S6: Proteome of *Lupinus albus* cotyledons and hypocotyl 4 d after imbibition.

2.12 Supplemental figures

A

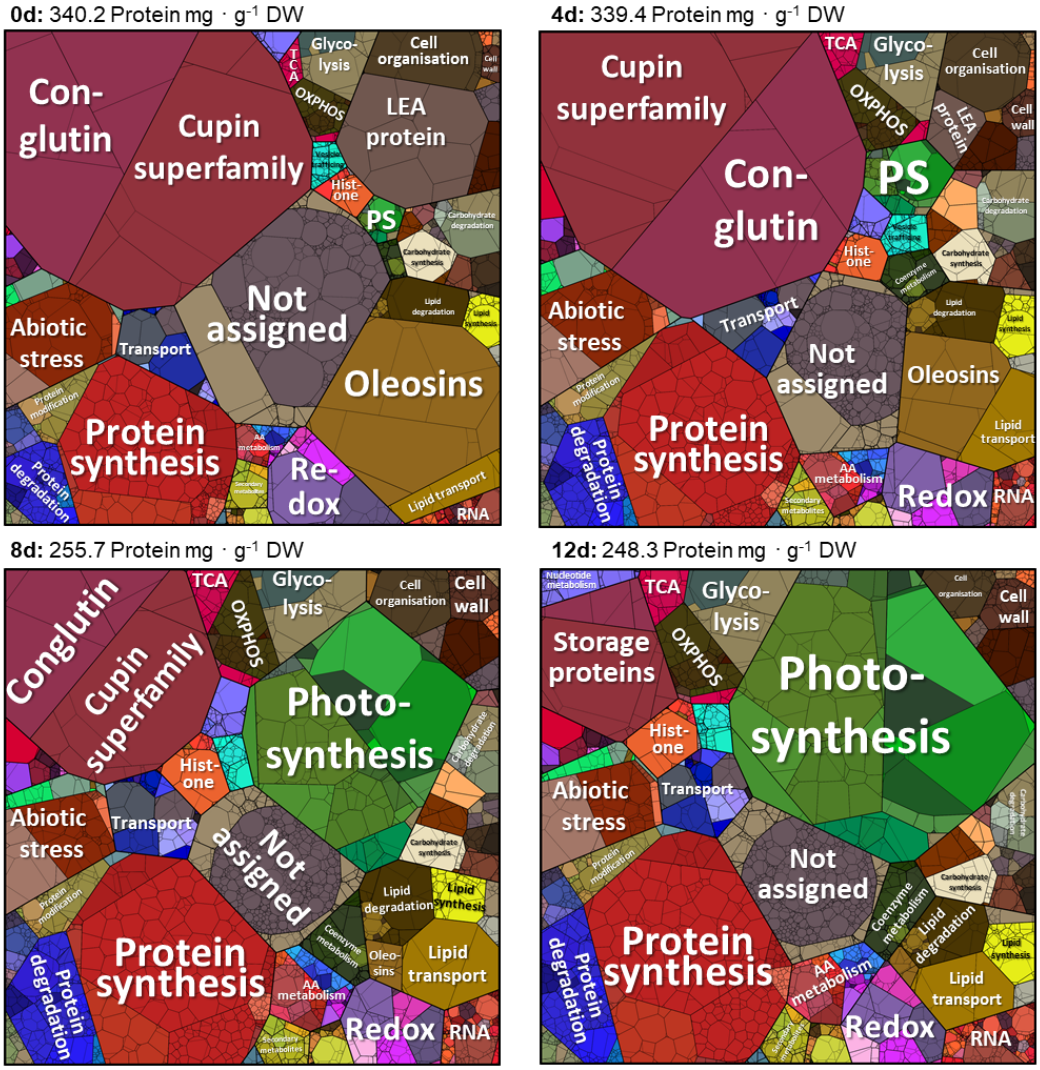

B

	iBAQ%				Protein in mg · g^{-1} (DW)				Protein in mg · plant^{-1}				log2 fold-changes			Significant proteins		
Categories (protein count)	0d	4d	8d	12d	0d	4d	8d	12d	0d	4d	8d	12d	4d_0d	8d_0d	12d_0d	4d_0d	8d_0d	12d_0d
Storage proteins (25)	28.6	30.8	15.8	6.6	97.3	104.5	40.3	16.3	23.3	24.2	9.7	3.7	0.4	0.5	-0.7	17	23	23
Lipid metabolism (219)	14.0	9.5	7.4	5.9	47.5	32.3	18.8	14.5	11.4	7.5	4.5	3.3	0.7	1.1	1.0	135	167	180
Protein metabolism (973)	13.1	16.9	19.9	20.2	44.7	57.3	50.8	50.2	10.7	13.3	12.2	11.3	0.4	0.6	0.7	564	735	788
Not assigned (878)	12.7	7.9	6.9	6.8	43.3	26.9	17.5	16.8	10.4	6.2	4.2	3.8	0.4	0.7	0.8	445	671	735
Cell (353)	9.9	5.5	4.3	3.8	33.7	18.7	11.0	9.4	8.1	4.3	2.7	2.1	0.5	0.9	0.9	187	265	284
Stress (165)	4.5	5.0	4.5	4.4	15.2	17.0	11.4	10.8	3.6	3.9	2.8	2.4	0.8	0.8	0.9	110	132	140
Carbohydrate metabolism (260)	3.5	4.4	4.3	4.4	12.0	14.8	11.0	10.9	2.9	3.4	2.6	2.4	0.7	0.9	0.9	185	217	228
Redox (117)	3.3	3.1	2.8	2.9	11.2	10.4	7.2	7.3	2.7	2.4	1.7	1.6	0.7	1.0	1.1	71	97	99
Cellular respiration (189)	2.9	4.4	6.0	6.6	9.7	15.1	15.4	16.5	2.3	3.5	3.7	3.7	0.5	0.8	0.8	109	130	142
Transport (134)	2.1	2.3	2.6	2.4	7.2	7.9	6.6	6.1	1.7	1.8	1.6	1.4	0.9	1.5	1.8	80	109	121
RNA (305)	0.8	1.1	1.5	1.8	2.7	3.7	3.8	4.4	0.6	0.9	0.9	1.0	0.4	0.7	1.0	135	196	229
Amino acid metabolism (181)	0.8	1.7	2.0	2.1	2.6	5.6	5.1	5.3	0.6	1.3	1.2	1.2	0.9	1.3	1.3	126	151	151
Secondary metabolism (112)	0.7	0.9	0.8	0.9	2.4	3.0	2.1	2.1	0.6	0.7	0.5	0.5	0.9	1.1	1.3	64	93	94
DNA (63)	0.6	0.9	1.4	1.4	2.1	2.9	3.5	3.5	0.5	0.7	0.8	0.8	0.4	0.8	0.9	27	47	49
Photosynthesis (181)	0.6	2.0	15.3	24.8	2.0	6.8	39.2	61.7	0.5	1.6	9.4	13.8	1.1	4.1	4.9	82	162	174
Vesicle trafficking (121)	0.5	0.7	0.6	0.7	1.6	2.2	1.6	1.6	0.4	0.5	0.4	0.4	0.2	0.0	0.1	68	77	92
Hormone metabolism (63)	0.5	0.9	1.0	1.0	1.6	3.0	2.6	2.6	0.4	0.7	0.6	0.6	0.7	0.6	0.8	40	47	58
Nucleotide metabolism (69)	0.3	0.5	0.8	0.9	1.1	1.8	2.1	2.2	0.3	0.4	0.5	0.5	0.7	1.2	1.3	43	55	51
Signalling (79)	0.3	0.5	0.6	0.6	1.0	1.7	1.5	1.6	0.3	0.4	0.4	0.4	0.5	0.6	0.8	38	49	59
Coenzyme metabolism (110)	0.3	1.0	1.4	1.6	1.0	3.4	3.7	4.1	0.2	0.8	0.9	0.9	1.4	2.0	2.1	69	95	94
Nutrient uptake (14)	0.1	0.1	0.1	0.1	0.2	0.3	0.2	0.2	0.0	0.1	0.1	0.1	0.5	0.8	1.1	6	9	9
Total (4611)	100.0	100.0	100.0	100.0	340.2	339.4	255.7	248.3	81.4	78.6	61.6	55.7	0.6	1.0	1.1	2601	3527	3800

M1-Fig. S1: Quantitative composition of the *Lupinus albus* proteome during germination and seedling establishment. (**A**) Proteomaps depicting the quantitative composition of *the L. albus* proteome at day 0, 4, 8, and 12 after sowing. Proteins are represented as polygons, with their sizes reflecting their mass fractions. Proteins with similar cellular functions are grouped together and indicated by distinct colours. (**B**) Protein abundance, fold-changes, and the number of significantly altered proteins within the main functional categories (Level 1).

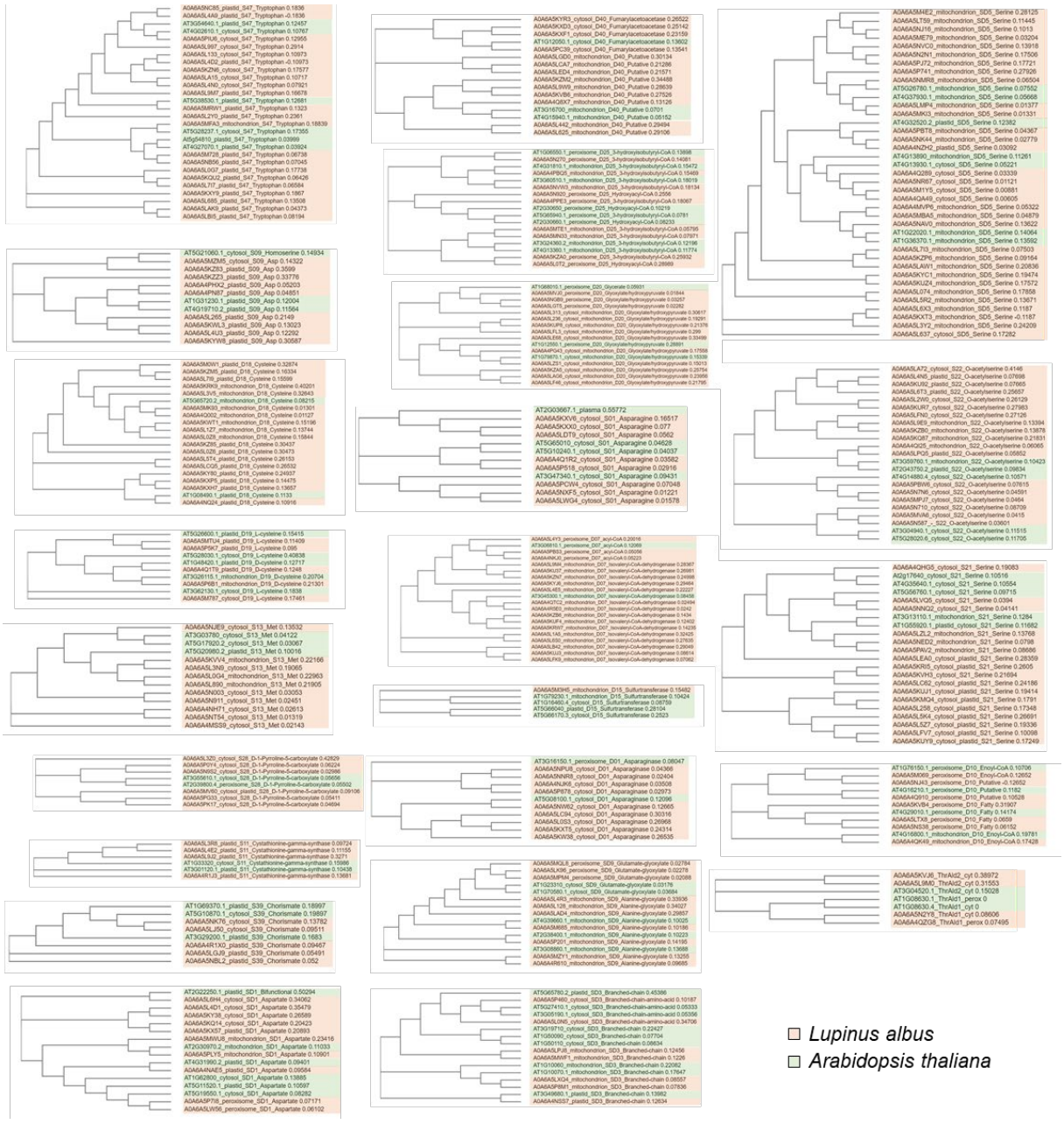

M1-Fig. S2: Multiple sequence alignments of *Arabidopsis thaliana* and *Lupinus albus* isoenzymes of amino acid metabolic pathways localized to different subcellular compartments. Phylogenetic trees were constructed using the Clustal Omega tool (https://www.ebi.ac.uk/Tools/msa/clustalo/).

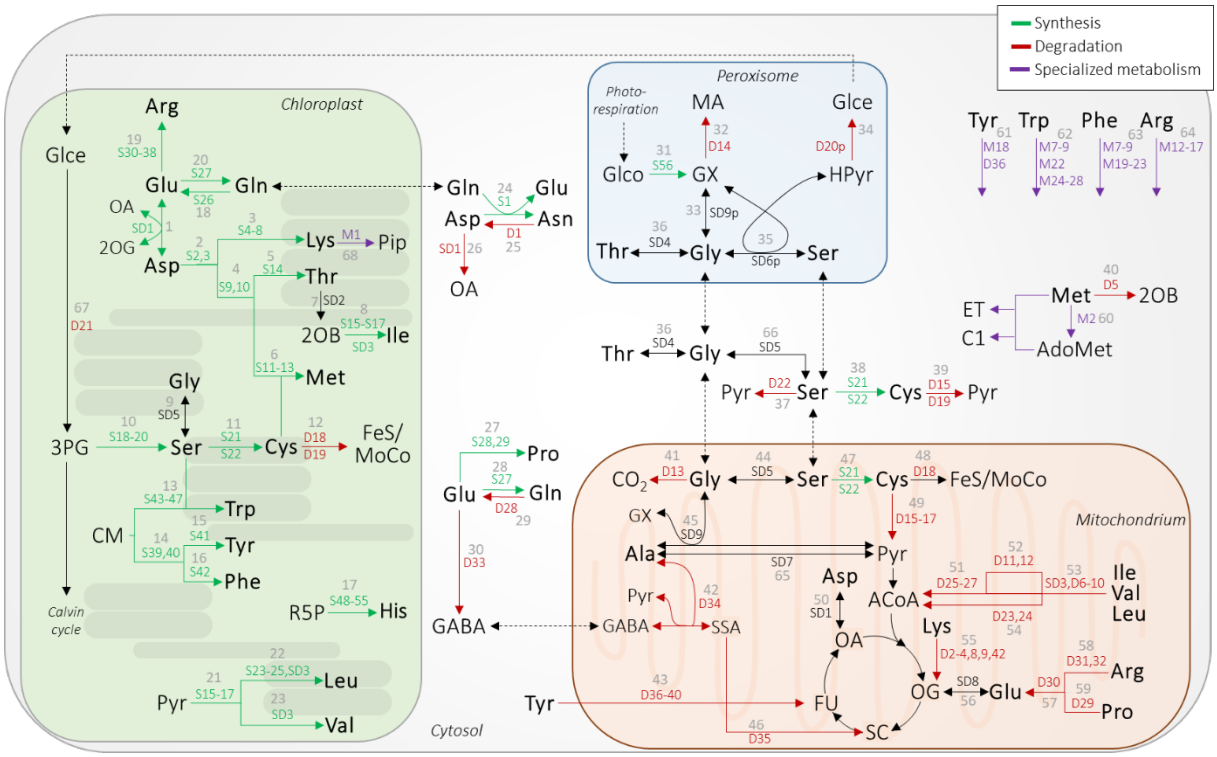

M1-Fig. S3: Amino acid metabolism in *Lupinus albus*. Pathways involved in amino acid metabolism, including the enzymes known to be involved in amino acid synthesis, degradation, and their connections to specialized metabolism. Enzyme abundance data can be obtained from proteomics datasets using the corresponding arrow numbers. For example, arrow 19, which represents the anabolic pathway of Arginine, corresponds to enzymes S30 - S38. Detailed enzyme nomenclature is available in Supp. Dataset S1.

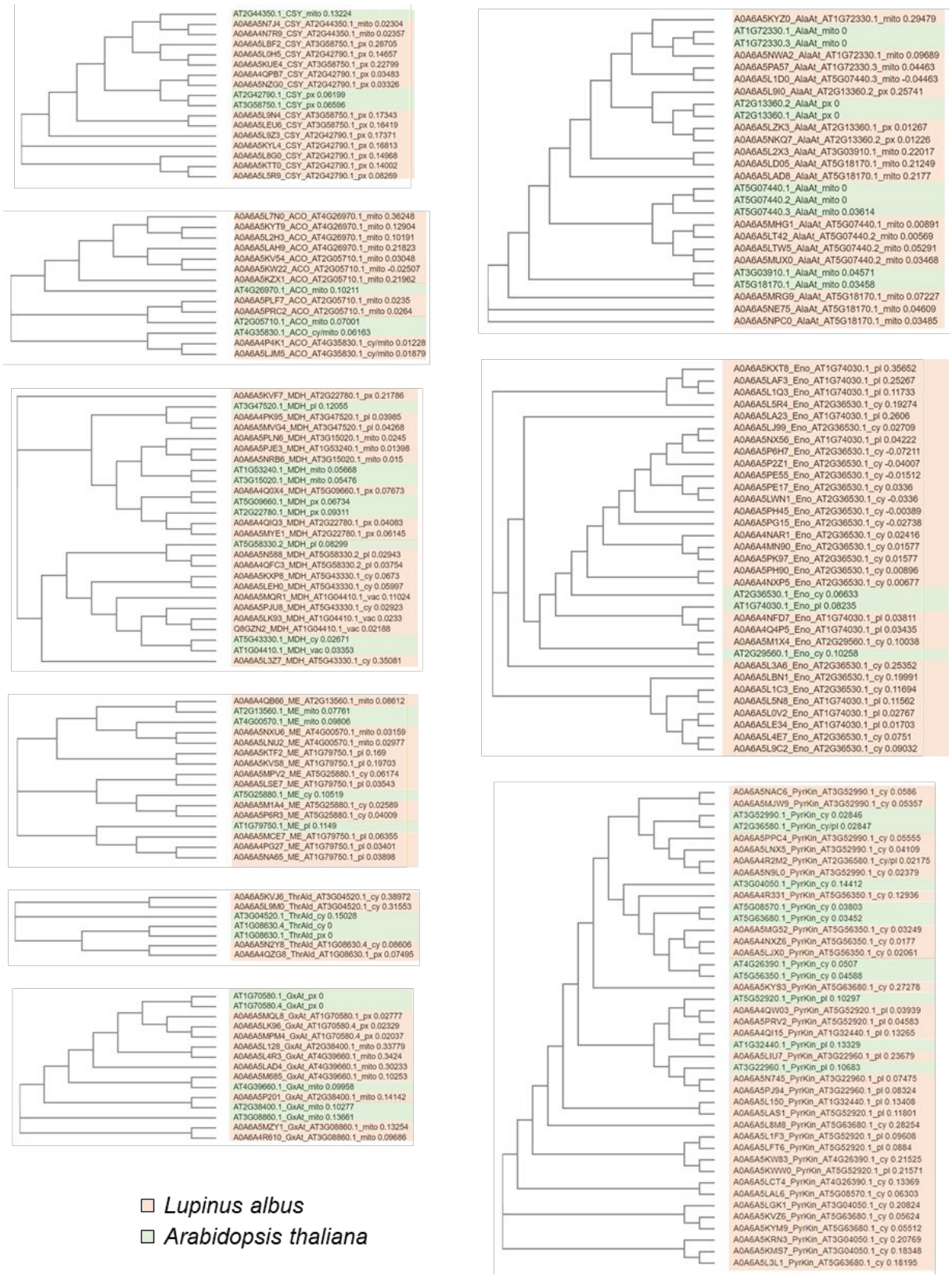

M1-Fig. S4: Multiple sequence alignments of *Arabidopsis thaliana* and *Lupinus albus* isoenzymes in the glyoxylate cycle localized to different subcellular compartments. Phylogenetic trees were constructed using the Clustal Omega tool. (https://www.ebi.ac.uk/Tools/msa/clustalo/)

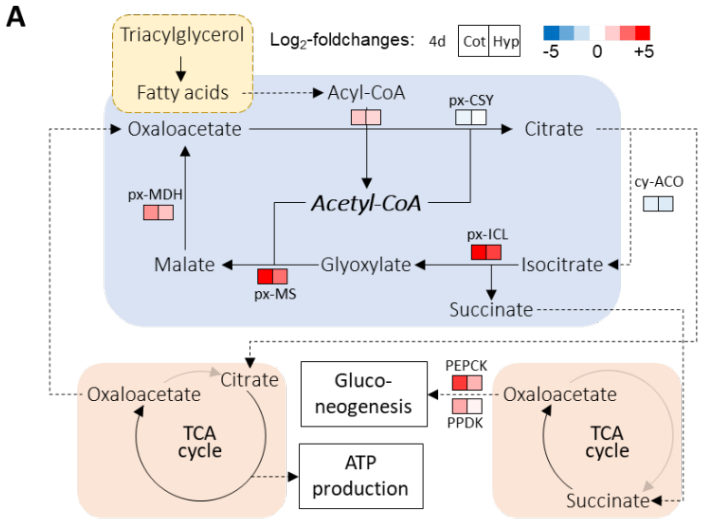
A
Triacylglycerol
Fatty acids
Log2-foldchanges: 4d Cot Hyp
-5 0 +5
Acyl-CoA
px-CSY
Oxaloacetate
Citrate
cy-ACO
px-MDH
Acetyl-CoA
px-ICL
Malate
Glyoxylate
Isocitrate
px-MS
Succinate
Citrate
Oxaloacetate
TCA cycle
Gluco-neogenesis
PEPCK
PPDK
Oxaloacetate
TCA cycle
Succinate
ATP production

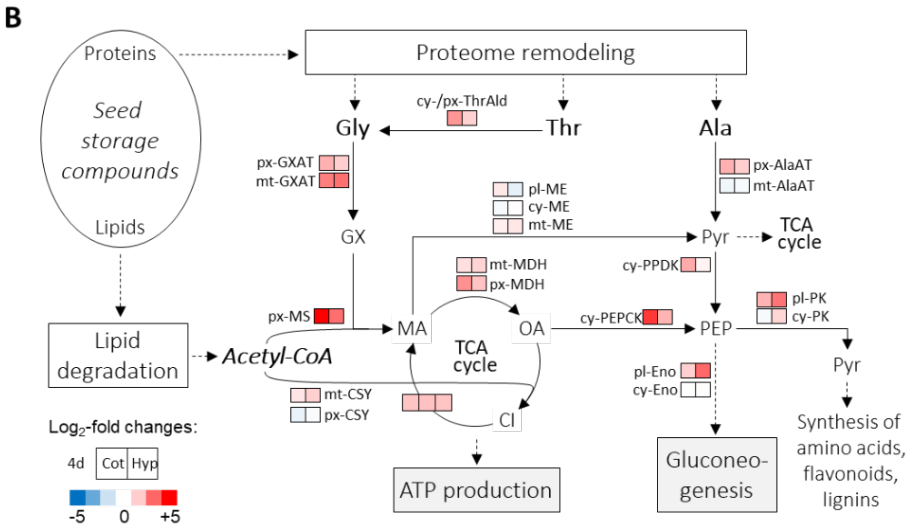
B
Proteins
Seed storage compounds
Lipids
Proteome remodeling
cy-/px-ThrAld
Gly
Thr
Ala
px-GXAT
mt-GXAT
px-AlaAT
mt-AlaAT
pl-ME
cy-ME
mt-ME
GX
Pyr
TCA cycle
mt-MDH
px-MDH
cy-PPDK
pl-PK
cy-PK
px-MS
MA
OA
cy-PEPCK
PEP
Lipid degradation
Acetyl-CoA
TCA cycle
pl-Eno
cy-Eno
Pyr
mt-CSY
px-CSY
CI
Synthesis of amino acids, flavonoids, lignins
Log2-fold changes:
4d Cot Hyp
-5 0 +5
ATP production
Gluconeo-genesis

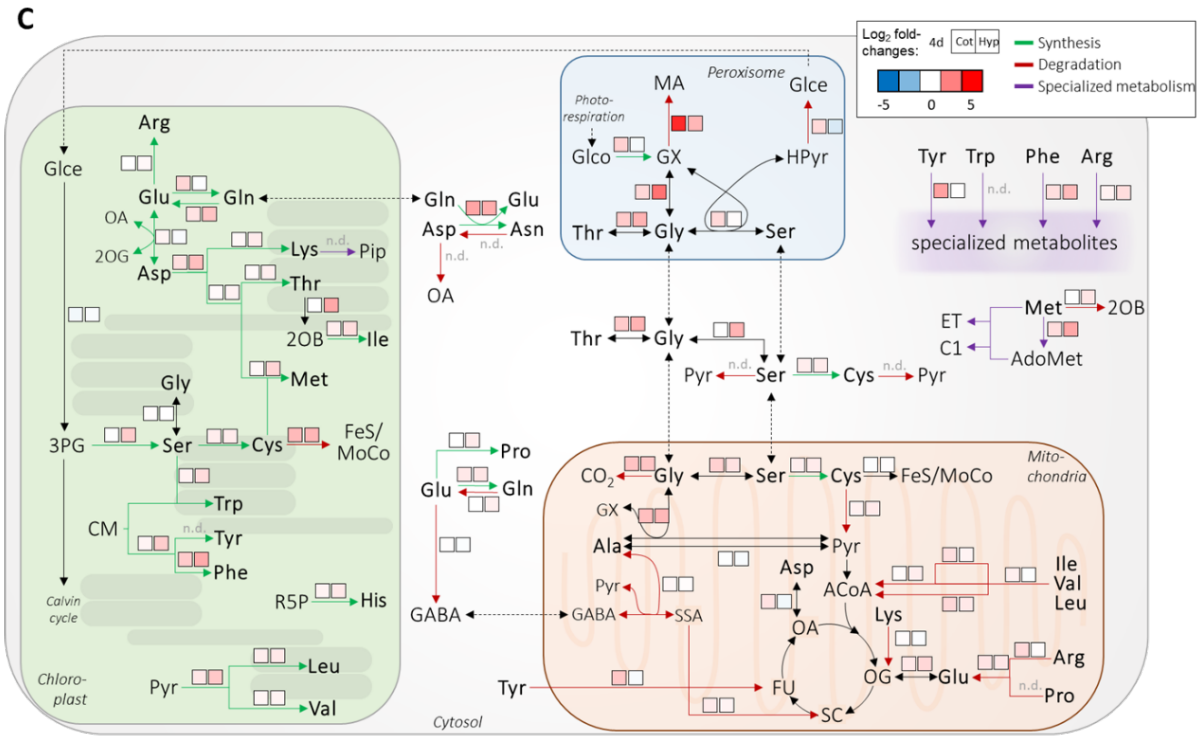
C
Log2 fold-changes: 4d Cot Hyp
-5 0 5
Synthesis
Degradation
Specialized metabolism
Peroxisome
Photo-respiration
MA
Glce
Glco
GX
HPyr
Thr
Gly
Ser
Tyr Trp Phe Arg
n.d.
specialized metabolites
Arg
Glce
Glu
Gln
OA
2OG
Asp
Lys
n.d.
Pip
Thr
2OB
Ile
Met
Gly
3PG
Ser
Cys
FeS/ MoCo
Trp
CM
Tyr
Phe
Calvin cycle
R5P
His
Chloro-plast
Pyr
Leu
Val
Gln
Glu
Asp
Asn
n.d.
OA
Thr
Gly
Ser
Met
2OB
ET
C1
AdoMet
Pyr
Ser
Cys
Pyr
Pro
Glu
Gln
GABA
CO2
Gly
Ser
Cys
FeS/MoCo
Mito-chondria
GX
Ala
Pyr
Asp
ACoA
Ile
Val
Leu
Pyr
GABA
SSA
OA
Lys
Arg
Tyr
FU
OG
Glu
n.d.
Pro
SC
Cytosol

M1-Fig. S5: Potential integration of fatty acid and amino acid metabolism in *Lupinus albus* cotyledons and hypocotyl during seedling establishment. (**A**) Relative protein abundance of glyoxylate cycle enzymes. The coloured squares indicate the mean log_2-fold changes in the abundance of tissue-specific isoforms at day 4 compared to day 0. The complete dataset is available in Supp. Dataset S6. (**B**) Relative protein abundance of enzymes required for the combined metabolism of amino acids and fatty acids into carbohydrates. The coloured squares represent the mean log_2-fold changes in the abundance of tissue-specific isoforms at day 4 compared to day 0. The full dataset can be found in Supp. Dataset S6. Assignments of subcellular compartments are based on sequence homologies to *A. thaliana* (Supp. M1-Fig. 4). (**C**) Relative protein abundance of amino acid metabolic pathways during germination and seedling establishment. The coloured squares show the mean log_2-fold changes in the abundance of enzymes involved in the respective branch of the pathway at day 4 in the cotyledons and the hypocotyl compared to day 0. The complete table of amino acid metabolism is provided in Supp. Dataset S6. Abbreviations A+B: ACO: Aconitase, AlaAT: Alanine aminotransferase, CI: Citrate, Cot: Cotyledons, CSY: Citrate synthase, cy: cytosolic, Eno: Enolase, GX: Glyoxylate, GXAT: Glyoxylate aminotransferase, Hyp: Hypocotyl, ICL: Isocitrate lyase, MA: Malate, MDH: Malate dehydrogenase, ME: Malic enzyme, MS: Malate synthase, mt: mitochondrial, OA: Oxaloacetate, PEP: Phosphoenolpyruvate, PEPCK: Phosphoenolpyruvate carboxykinase, PK: Pyruvate kinase, pl: plastidic, PPDK: Pyruvate, phosphate dikinase, px: peroxisomal, Pyr: Pyruvate, ThrAld: L-threonine aldolase. Abbreviations C: 2OB: 2-oxobutyrate, 2OG: 2-oxoglutarate, 3PG: 3-phosphoglycerate, ACoA: Acetyl-CoA, AdoMet: S-adenosylmethionine, C1: C1-metabolism, CM: chorismate, ET: ethylene, FeS: iron-sulfur cluster, FU: fumarate, GABA: γ-aminobutyric acid, Glce: glycerate, Glco: glycolate, GX: glyoxylate, Hpyr: Hydroxypyruvate, MA: malate, MoCo: molybdenum cofactor, n.d., OA: oxaloacetic acid, Pyr: pyruvate, Pip: pipecolic acid, R5P: ribose-5-phosphate, SC: succinate, SSA: succinic semialdehyde.

2.13 References

Andrino, A., Boy, J., Mikutta, R., Sauheitl, L. and Guggenberger, G. (2019) Carbon Investment Required for the Mobilization of Inorganic and Organic Phosphorus Bound to Goethite by an Arbuscular Mycorrhiza (*Solanum lycopersicum* x *Rhizophagus irregularis*). *Front. Environ. Sci.*, 7.

Aniszewski, T., Ciesiołka, D. and Gulewicz, K. (2001) Equilibrium between basic nitrogen compounds in lupin seeds with differentiated alkaloid content. *Phytochemistry*, 57, 43–50.

Baena-González, E., Rolland, F., Thevelein, J.M. and Sheen, J. (2007) A central integrator of transcription networks in plant stress and energy signalling. *Nature*, 448, 938–942.

Baker, A., Graham, I.A., Holdsworth, M., Smith, S.M. and Theodoulou, F.L. (2006) Chewing the fat: beta-oxidation in signalling and development. *Trends Plant Sci.*, 11, 124–132.

Bano, C., Amist, N. and Singh, N.B. (2020) Role of polyamines in plants abiotic stress tolerance: Advances and future prospects. *Plant Life Under Changing Environment*, 481–496.

Batista-Silva, W., Heinemann, B., Rugen, N., Nunes-Nesi, A., Araújo, W.L., Braun, H.-P. and Hildebrandt, T.M. (2019) The role of amino acid metabolism during abiotic stress release. *Plant Cell Environ.*, 42, 1630–1644.

Berger, J.D., Shrestha, D. and Ludwig, C. (2017) Reproductive Strategies in Mediterranean Legumes: Trade-Offs between Phenology, Seed Size and Vigor within and between Wild and Domesticated *Lupinus* Species Collected along Aridity Gradients. *Front. Plant Sci.*, 8, 548.

Bolger, M., Schwacke, R. and Usadel, B. (2021) MapMan Visualization of RNA-Seq Data Using Mercator4 Functional Annotations. *Methods Mol. Biol.* (Clifton, N.J.), 2354, 195–212.

Borek, S., Kubala, S. and Kubala, S. (2013) Diverse regulation by sucrose of enzymes involved in storage lipid breakdown in germinating lupin seeds. *Acta Physiol. Plant.*, 35, 2147–2156.

Borek, S., Kubala, S., Kubala, S. and Ratajczak, L. (2011) Comparative study of storage compound breakdown in germinating seeds of three lupine species. *Acta Physiol. Plant.*, 33, 1953–1968.

Borek, S., Paluch-Lubawa, E., Pukacka, S., Pietrowska-Borek, M. and Ratajczak, L. (2017) Asparagine slows down the breakdown of storage lipid and degradation of autophagic bodies in sugar-starved embryo axes of germinating lupin seeds. *J. Plant Physiol.*, 209, 51–67.

Borek, S., Pukacka, S. and Michalski, K. (2012) Regulation by sucrose of storage compounds breakdown in germinating seeds of yellow lupine (*Lupinus luteus* L.), white lupine (*Lupinus albus* L.) and Andean lupine (*Lupinus mutabilis* Sweet). II. Mobilization of storage lipid. *Acta Physiol. Plant.*, 34, 1199–1206.

Borek, S. and Ratajczak, L. (2010) Storage lipids as a source of carbon skeletons for asparagine synthesis in germinating seeds of yellow lupine (*Lupinus luteus* L.). *J. Plant Physiol.*, 167, 717–724.

Borek, S., Ratajczak, W. and Ratajczak, L. (2003) A transfer of carbon atoms from fatty acids to sugars and amino acids in yellow lupine (*Lupinus luteus* L.) seedlings. *J. Plant Physiol.*, 160, 539–545.

Borek, S., Ratajczak, W. and Ratajczak, L. (2015) Regulation of storage lipid metabolism in developing and germinating lupin (*Lupinus* spp.) seeds. *Acta Physiol. Plant.*, 37.

Boschin, G. and Arnoldi, A. (2011) Legumes are valuable sources of tocopherols. *Food Chemistry*, 127, 1199–1203.

Boschin, G., D'Agostina, A., Annicchiarico, P. and Arnoldi, A. (2008) Effect of genotype and environment on fatty acid composition of *Lupinus albus* L. seed. *Food Chem.*, 108, 600–606.

Boschin, G. and Resta, D. (2013). Alkaloids derived from lysine: quinolizidine (a focus on lupin alkaloids). In *Natural products*, 381-403. Springer, Berlin, Heidelberg.

Cox, J., Hein, M.Y., Luber, C.A., Paron, I., Nagaraj, N. and Mann, M. (2014) Accurate proteome-wide label-free quantification by delayed normalization and maximal peptide ratio extraction, termed MaxLFQ. *Mol. Cell. Proteomics*, 13, 2513–2526.

Cox, J. and Mann, M. (2008) MaxQuant enables high peptide identification rates, individualized p.p.b.-range mass accuracies and proteome-wide protein quantification. *Nat. Biotechnol.*, 26, 1367–1372.

Duranti, M., Consonni, A., Magni, C., Sessa, F. and Scarafoni, A. (2008) The major proteins of lupin seed: Characterisation and molecular properties for use as functional and nutraceutical ingredients. *Trends Food Sci. Technol.*, 19, 624–633.

Eastmond, P.J., Astley, H.M., Parsley, K., Aubry, S., Williams, B.P., Menard, G.N., Craddock, C.P., Nunes-Nesi, A., Fernie, A.R. and Hibberd, J.M. (2015) *Arabidopsis* uses two gluconeogenic gateways for organic acids to fuel seedling establishment. *Nat. Commun.*, 6, 6659.

Fontanari, G.G., Batistuti, J.P., Da Cruz, R.J., Saldiva, P.H.N. and Arêas, J.A.G. (2012) Cholesterol-lowering effect of whole lupin (*Lupinus albus*) seed and its protein isolate. *Food Chem.*, 132, 1521–1526.

Galili, G., Avin-Wittenberg, T., Angelovici, R. and Fernie, A.R. (2014) The role of photosynthesis and amino acid metabolism in the energy status during seed development. *Front. Plant Sci.*, 5, 447.

Gdala, J. and Buraczewska, L. (1996) Chemical composition and carbohydrate content of seeds from several lupin species. *J. Anim. Feed Sci.*, 5, 403–416.

Graham, I.A. (2008) Seed storage oil mobilization. *Annu. Rev. Plant Biol.*, 59, 115–142.

Heinemann, B. and Hildebrandt, T.M. (2021) The role of amino acid metabolism in signaling and metabolic adaptation to stress-induced energy deficiency in plants. *J. Exp. Bot.*, 72, 4634–4645.

Henninger, M., Pedrotti, L., Krischke, M., Draken, J., Wildenhain, T., Fekete, A., Rolland, F., Müller, M.J., Fröschel, C., Weiste, C. and Dröge-Laser, W. (2022) The evolutionarily conserved kinase SnRK1 orchestrates resource mobilization during *Arabidopsis* seedling establishment. *Plant cell*, 34, 616–632.

Hildebrandt, T.M., Nunes Nesi, A., Araújo, W.L. and Braun, H.-P. (2015) Amino Acid Catabolism in Plants. *Mol. Plant*, 8, 1563–1579.

Hufnagel, B., Marques, A., Soriano, A., Marquès, L., Divol, F., Doumas, P., Sallet, E., Mancinotti, D., Carrere, S., Marande, W., Arribat, S., Keller, J., Huneau, C., Blein, T., Aimé, D., Laguerre, M., Taylor, J., Schubert, V., Nelson, M., Geu-Flores, F., Crespi, M., Gallardo, K., Delaux, P.-M., Salse, J., Bergès, H., Guyot, R., Gouzy, J. and Péret, B. (2020) High-quality genome sequence of white lupin provides insight into soil exploration and seed quality. *Nat. Commun.*, 11, 492.

Hughes, C.S., Moggridge, S., Müller, T., Sorensen, P.H., Morin, G.B. and Krijgsveld, J. (2019) Single-pot, solid-phase-enhanced sample preparation for proteomics experiments. *Nat. Protoc.*, 14, 68–85.

Klodmann, J., Sunderhaus, S., Nimtz, M., Jänsch, L. and Braun, H.-P. (2010) Internal architecture of mitochondrial complex I from *Arabidopsis thaliana*. *Plant cell*, 22, 797–810.

Kulak, N.A., Pichler, G., Paron, I., Nagaraj, N. and Mann, M. (2014) Minimal, encapsulated proteomic-sample processing applied to copy-number estimation in eukaryotic cells. *Nat. Methods*, 11, 319–324.

Laemmli, U.K. (1970) Cleavage of structural proteins during the assembly of the head of bacteriophage T4. *Nature*, 227, 680–685.

Lam, H.-M., Wong, P., Chan, H.-K., Yam, K.-M., Chen, L., Chow, C.-M. and Coruzzi, G.M. (2003) Overexpression of the ASN1 gene enhances nitrogen status in seeds of *Arabidopsis*. *Plant Physiol.*, 132, 926–935.

Lea, P.J., Sodek, L., Parry, M., Shewry, P.R. and Halford, N.G. (2007) Asparagine in plants. *Ann. Appl. Biol.*, 150, 1–26.

Lea, P.J. and Fowden, L. (1975) The purification and properties of glutamine-dependent asparagine synthetase isolated from *Lupinus albus*. *Proc. R. Soc. Lond. B Biol. Sci.*, 192, 13–26.

Lichtenthaler, H.K. (1987) Chlorophylls and carotenoids: Pigments of photosynthetic biomembranes. *Methods Enzymol.*, 148, 350–382.

Lucas, M.M., Stoddard, F.L., Annicchiarico, P., Frías, J., Martínez-Villaluenga, C., Sussmann, D., Duranti, M., Seger, A., Zander, P.M. and Pueyo, J.J. (2015) The future of lupin as a protein crop in Europe. *Front. Plant Sci.*, 6, 705.

Mair, A., Pedrotti, L., Wurzinger, B., Anrather, D., Simeunovic, A., Weiste, C., Valerio, C., Dietrich, K., Kirchler, T., Nägele, T., Vicente Carbajosa, J., Hanson, J., Baena-González, E., Chaban, C., Weckwerth, W., Dröge-Laser, W. and Teige, M. (2015) SnRK1-triggered switch of bZIP63 dimerization mediates the low-energy response in plants. *eLife*, 4.

Mikulášek, K., Konečná, H., Potěšil, D., Holánková, R., Havliš, J. and Zdráhal, Z. (2021) SP3 Protocol for Proteomic Plant Sample Preparation Prior LC-MS/MS. *Front. Plant Sci.*, 12, 635550.

Morkunas, I., Lehmann, T., Ratajczak, W., Ratajczak, L. and Tomaszewska, B. (2000) The involvement of glutamate dehydrogenase in the adaptation of mitochondria to oxidize glutamate in sucrose starved pea embryos. *Acta Physiol. Plant.*, 22, 389–394.

Nishio K. and Mizushima T. (2020). Structural and biochemical characterization of mitochondrial citrate synthase 4 from *Arabidopsis thaliana*. *Struct. Biol. Commun.* 76, 109–115.

Osorio, C.E. and Till, B.J. (2021) A Bitter-Sweet Story: Unraveling the Genes Involved in Quinolizidine Alkaloid Synthesis in *Lupinus albus*. *Front. Plant Sci.*, 12, 795091.

Park, J., Jeong, H.J., Yoon, E.Y. and Moon, S.J. (2016) Easy and rapid quantification of lipid contents of marine dinoflagellates using the sulpho-phospho-vanillin method. *ALGAE*, 31, 391–401.

Pate, J.S., Atkins, C.A., Herridge, D.F. and Layzell, D.B. (1981) Synthesis, Storage, and Utilization of Amino Compounds in White Lupin (*Lupinus albus* L.). *Plant Physiol.*, 67, 37–42.

Pedrotti, L., Weiste, C., Nägele, T., Wolf, E., Lorenzin, F., Dietrich, K., Mair, A., Weckwerth, W., Teige, M., Baena-González, E. and Dröge-Laser, W. (2018) Snf1-RELATED KINASE1-Controlled C/S1-bZIP Signaling Activates Alternative Mitochondrial Metabolic Pathways to Ensure Plant Survival in Extended Darkness. *Plant Cell*, 30, 495–509.

Perez-Riverol, Y., Bai, J., Bandla, C., García-Seisdedos, D., Hewapathirana, S., Kamatchinathan, S., Kundu, D.J., Prakash, A., Frericks-Zipper, A., Eisenacher, M., Walzer, M., Wang, S., Brazma, A. and Vizcaíno, J.A. (2022) The PRIDE database resources in 2022: a hub for mass spectrometry-based proteomics evidences. *Nucleic Acids Res.*, 50, D543-D552.

Pracharoenwattana, I., Cornah, J.E. and Smith, S.M. (2005) *Arabidopsis* peroxisomal citrate synthase is required for fatty acid respiration and seed germination. *Plant Cell*, 17, 2037–2048.

Pracharoenwattana, I. and Smith, S.M. (2008) When is a peroxisome not a peroxisome? *Trends Plant Sci.*, 13, 522–525.

Pueyo, J.J., Quiñones, M.A., La Coba de Peña, T., Fedorova, E.E. and Lucas, M.M. (2021) Nitrogen and Phosphorus Interplay in Lupin Root Nodules and Cluster Roots. *Front. Plant Sci.*, 12, 644218.

Raymond, P., Spiteri, A., Dieuaide, M., Gerhardt, B. and Pradet, A. (1992) Peroxisomal β-oxidation of fatty acids and citrate formation by a particulate fraction from early germinating sunflower seeds. *Plant Physiol. Biochem.*, 30, 153–161.

Reymond, P., Weber, H., Damond, M. and Farmer, E.E. (2000) Differential gene expression in response to mechanical wounding and insect feeding in *Arabidopsis*. *Plant Cell*, 12, 707–720.

Rybiński, W., Kroc, M., Święcicki, W., Wilczura, P., Kamel, K., Barzyk, P. and Mikulski, W. (2018) Preliminary Estimation of Variation of Alkaloids Content in White Lupin (*Lupinus albus* L.) Collection. In *Breeding grasses and protein crops in the era of genomics*, 131-136. Springer International Publishing.

Sanyal, R., Kumar, S., Pattanayak, A., Kar, A. and Bishi, S.K. (2023) Optimizing raffinose family oligosaccharides content in plants: A tightrope walk. *Front. Plant Sci.*, 14, 1134754.

Schmidtmann E, König A-C, Orwat A, Leister D, Hartl M, and Finkemeier I. (2014). Redox regulation of *Arabidopsis* mitochondrial citrate synthase. *Mol. Plant,* 7, 156–169.

Schwacke, R., Ponce-Soto, G.Y., Krause, K., Bolger, A.M., Arsova, B., Hallab, A., Gruden, K., Stitt, M., Bolger, M.E. and Usadel, B. (2019) MapMan4: A Refined Protein Classification and Annotation Framework Applicable to Multi-Omics Data Analysis. *Mol. Plant*, 12, 879–892.

Ströcker, K., Wendt, S., Kirchner, W.H. and Struck, C. (2013) Feeding preferences of the weevils *Sitona gressorius* and *Sitona griseus* on different lupin genotypes and the role of alkaloids. *Arthropod-Plant Interact.*, 7, 579–589.

Sujak, A., Kotlarz, A. and Strobel, W. (2006) Compositional and nutritional evaluation of several lupin seeds. *Food Chem.*, 98, 711–719.

Tamboli, F.A., More, H.N., Bhandugare, S.S., Patil, A.S., Jadhav, N.R. and Killedar, S.G. (2020) Estimation of Total Carbohydrate content by Phenol Sulfuric acid Method from *Eichhornia crassipes* (Mart.) Solms. *Asian J. Res. Chem.*, 13, 357–359.

Thimm, O., Bläsing, O., Gibon, Y., Nagel, A., Meyer, S., Krüger, P., Selbig, J., Müller, L.A., Rhee, S.Y. and Stitt, M. (2004) MAPMAN: a user-driven tool to display genomics data sets onto diagrams of metabolic pathways and other biological processes. *Plant J.*, 37, 914–939.

Traver, M.S. and Bartel, B. (2023) The ubiquitin-protein ligase MIEL1 localizes to peroxisomes to promote seedling oleosin degradation and lipid droplet mobilization. *Proc. Natl. Acad. Sci. U.S.A.*, 120, e2304870120.

Tyanova, S., Temu, T., Sinitcyn, P., Carlson, A., Hein, M.Y., Geiger, T., Mann, M. and Cox, J. (2016) The Perseus computational platform for comprehensive analysis of (prote)omics data. *Nat. Methods*, 13, 731–740.

Updegraff, D.M. (1969) Semimicro determination of cellulose in biological materials. *Anal. Biochem.*, 32, 420–424.

Xu, W., Zhang, Q., Yuan, W., Xu, F., Muhammad Aslam, M., Miao, R., Li, Y., Wang, Q., Li, X., Zhang, X., Zhang, K., Xia, T. and Cheng, F. (2020) The genome evolution and low-phosphorus adaptation in white lupin. *Nature Commun.*, 11, 1069.

3 Manuscript 2: Balancing nutrient remobilization and photosynthesis: proteomic insights into the dual role of lupin cotyledons after germination

Cecile Angermann[1], Björn Heinemann[1], Bianca Bueno Nogueira[2], Hans-Jörg Mai[3], Petra Bauer[3] and Tatjana M. Hildebrandt[1]

The plant journal, Volume 123, Issue 2, 21 July 2025, e70357, http://doi.org/10.1111/tpj.70357

[1]Institute for Plant Sciences, Cluster of Excellence on Plant Sciences (CEPLAS), University of Cologne, Zülpicher Straße 47a, 50674 Cologne, Germany

[2]Departamento de Biologia Vegetal, Universidade Federal de Vicosa, Vicosa, Minas Gerais 36570-900, Brazil

[3]Institute of Botany, Cluster of Excellence on Plant Sciences (CEPLAS), Heinrich-Heine-University Düsseldorf, Universitätsstrasse 1, 40225 Düsseldorf, Germany

Type of authorship:	First author
Type of article:	Research article, peer reviewed
Contribution to the publication:	I participated in designing the project. I prepared all the sample material except for mineral nutrient analysis and performed all the experiments except for mineral nutrient analysis and phosphate quantification, for which I provided support. I analysed the data with the support of TMH and BH. I contributed to constructing figures and writing the manuscript.
Journal:	The Plant Journal
Impact factor:	5.7 (2024)
Date of publication:	21. July 2025
DOI:	10.1111/tpj.70357

3.1 Abstract

Efficient nutrient mobilization from seed storage tissues is essential for seedling establishment, particularly in legumes such as *Lupinus albus* (white lupin), which thrive in nutrient-poor soils. This study investigates the role of cotyledons in nitrogen (N) and mineral remobilization after germination during their transition from storage organs to photosynthetically active tissues, including the metabolic challenges posed by the coexistence of these two functions in epigeal germination. We cultivated white lupin seedlings under nitrogen-deficient conditions, analysing cotyledon composition and function over 28 days. Our results indicate that 60 % of cotyledon-stored proteins are degraded within the first 8 days, with free amino acids transiently accumulating before being redistributed to support growth. The progressive depletion of cotyledon reserves was accompanied by structural and metabolic changes, including an increase in photosynthetic proteins. However, cotyledon photosynthetic capacity remained lower than that of true leaves, suggesting a transient role in energy metabolism. The loss of cotyledons before day 12 significantly impaired seedling development, emphasizing their critical contribution to nitrogen, phosphate, and micronutrient supply during early growth. Comparative proteomic analysis revealed dynamic shifts in nutrient transport, amino acid metabolism, and stress response pathways following cotyledon removal. These findings underscore the significance of cotyledon nutrient remobilization in legume adaptation to low-fertility soils and highlight potential targets for breeding strategies aimed at improving nutrient use efficiency. By optimizing cotyledon nutrient composition and function, future breeding efforts could enhance seedling vigor, reduce fertilizer dependency, and improve the nutritional value of lupin-based foods.

3.2 Introduction

Pulse legumes are essential to global nutritional security due to their high protein content and richness in micronutrients. They are increasingly recognized as sustainable alternatives to meat, contributing to healthier diets and environmentally friendly agricultural systems. Among them, orphan legumes, such as white lupin (*Lupinus albus*), play an important role in enhancing agrobiodiversity, as their use promotes diversification of crop systems, supports ecosystem services like nitrogen fixation, and contributes to food security in marginal environments. White lupin is among the oldest domesticated legumes in the Mediterranean region, with a cultivation history dating back over four millennia (Abraham et al., 2019). Lupins are notable for

their high seed protein content ranging from 35 to 45 % of dry matter, surpassing that of many other legumes including peas. They are also a valuable source of essential minerals, particularly iron (Fe) and zinc (Zn) (KARNPANIT ET AL., 2017; PEREIRA ET AL., 2022; SPINA ET AL., 2024). Despite these advantages, lupins currently hold a relatively modest position in global agriculture behind major grain legumes, such as soybeans, beans, peas, and lentils (FAO FAOSTAT; https://www.fao.org/faostat/en/ #data/QCL). Within the genus *Lupinus*, the white lupin is primarily cultivated in southern Europe, whereas *L. angustifolius* (narrow-leaved lupin) dominates production in Australia (ABRAHAM ET AL., 2019). Globally, only about 4 % of lupins are used for direct human consumption, with the majority utilized as animal feed (BELSKI, 2012). Nevertheless, white lupin is gaining attention as a locally sourced, sustainable plant-based protein, particularly suited to vegan and gluten-free diets and increasingly seen as a viable alternative to imported soybean.

White lupin is particularly well adapted to nutrient-poor soils due to its specialized root system and efficient nutrient remobilization strategies. As legumes, lupins are able to acquire nitrogen from the environment through symbiotic fixation (LUCAS ET AL., 2015). In addition, *Lupinus albus* can remobilize soil phosphates very efficiently by the formation of specialized cluster roots (PUEYO ET AL., 2021; XU ET AL., 2020). However, seedling establishment still presents a significant challenge in nutrient-poor soils since plants rely on internal nutrient reserves before the specialized root system becomes fully functional. This dependency places specific demands on the quantity, composition, and metabolism of seed storage compounds, which have not been fully understood.

The cotyledons represent the primary nutrient store in lupin seeds. Upon seed maturation, storage proteins and lipids are deposited in protein storage vesicles and oil bodies within the cotyledon cells (BOREK ET AL., 2009). In addition, *L. albus* seeds contain carbohydrates, mostly cellulose and oligosaccharides of the raffinose family, which are non-digestible in humans and other monogastric animals (GDALA AND BURACZEWSKA, 1996; SANYAL ET AL., 2023). During germination, raffinose is hydrolysed to sucrose and galactose, which can then serve as a source of energy and as a precursor for cellulose synthesis (ELANGO ET AL., 2022; SANYAL ET AL., 2023). The stored lipids representing 7 – 14 % of the seed dry weight (DW) are rapidly hydrolysed by lipases, and the free fatty acids are further metabolized to acetyl-CoA and NADH via β-oxidation in the peroxisomes (BAKER ET AL., 2006; BOREK ET AL., 2012; GRAHAM,

2008). The glyoxylate cycle converts acetyl-CoA to succinate for the synthesis of carbohydrates during gluconeogenesis, and citrate can be exported from the peroxisomes into the mitochondria for ATP production (Baker et al., 2006; Pracharoenwattana et al., 2005; Pracharoenwattana and Smith, 2008). White lupin seeds are remarkably rich in protein (30 – 40 %); yet, they do not primarily rely on amino acids from storage protein breakdown for energy production or anabolic processes during germination and early seedling establishment (Angermann et al., 2024). Instead, the total protein content remains relatively stable until the seedling emerges from the soil, and thus the cotyledons can serve as a nitrogen store for the developing plant after the germination process has been completed. This delayed utilization of storage proteins suggests a highly regulated nutrient allocation strategy with a strong impact on seedling development on nutrient-poor soils that warrants further investigation.

After initially serving as nutrient reserves, cotyledons undergo a dynamic transformation during seedling development. In species such as lupins, which exhibit epigeal germination, elongation of the hypocotyl lifts the cotyledons above the soil surface, where they transition into photosynthetically active organs before eventually senescing (Lovell and Moore, 1970). This transition to photosynthetic activity represents a major metabolic shift and allows cotyledons to contribute additional energy and carbon resources, reducing immediate dependence on stored metabolites. By contrast, in hypogeal germination characteristic of many other legume species, cotyledons remain underground and function solely as storage organs until fully depleted. The epigeal strategy of white lupin, therefore, presents a unique developmental context in which cotyledons must reconcile two fundamentally distinct functions: retaining large reserves of storage proteins and free amino acids while simultaneously becoming photosynthetically active. It remains to be established how lupins coordinate this functional transition without compromising the integrity of either role.

Some information can already be deduced from studies in soybean (*Glycine max*), which also performs epigeal germination. Transcriptomic analyses indicate a temporal progression of metabolic events in the cotyledons during plant development, beginning with transient activation of the glyoxylate cycle and mobilization of lipid and protein stores, followed by chloroplast development and the onset of senescence (Brown and Hudson, 2015; Gonzalez and Vodkin, 2007). While these findings provide a useful

framework, the regulatory mechanisms, developmental timing, and physiological trade-offs of such transitions in white lupin remain largely unexplored.

Additionally, the dynamics of mineral redistribution from cotyledons to the developing plant are poorly understood. Earlier work on lupin seedling nutrition (Page et al., 2006) focused primarily on root uptake of selected micronutrients and heavy metals, and did not take the internal remobilization of seed-borne mineral nutrients, such as iron, copper, zinc, and phosphorus during cotyledon transformation into account. Understanding how cotyledons contribute to spatial and temporal nutrient allocation is particularly important under nutrient-limited conditions or when root function is impaired.

Cotyledon loss experiments, involving artificial removal of the cotyledons at different timepoints during seedling establishment, can provide information on how plant development and survival are affected by the loss of stored resources. Previous studies revealed that the negative impact of cotyledon loss strongly depends on the extent and timing of tissue removal, as well as on the species and seed size (El-Amhir et al., 2017; Hanley and Fegan, 2007; Hanley and May, 2006; Nunes et al., 2024; Wang et al., 2019; Yang et al., 2021; Zhang et al., 2011). Cotyledon removal experiments mimic environmental stressors, such as herbivory and mechanical damage, both of which can severely impair seedling establishment, especially in nutrient-poor soils. Despite its ecological and agronomic relevance, little is known about the compensatory mechanisms that sustain growth following cotyledon loss in legumes like white lupin.

To address these gaps, we conducted a time-resolved analysis of white lupin seedlings using quantitative proteomics and mineral profiling to characterize the developmental transition of cotyledons from storage to photosynthesis. In parallel, we evaluated the impact of cotyledon removal on seedling growth and nutrient status under nutrient-limited conditions. Together, these approaches aim to clarify how cotyledons support early seedling vigor, not only as passive reservoirs of nutrients, but also as active and adaptable contributors to metabolism, resource redistribution, and stress resilience during early plant establishment.

3.3 Results

3.3.1 Exploring the role of the cotyledons after germination

Previous research indicates that while storage lipids play a significant role during germination, storage proteins are primarily degraded at later developmental stages (ANGERMANN ET AL., 2024). This suggests that proteins serve a different physiological purpose beyond germination. To explore this further, we cultivated *L. albus* for 28 days under nitrogen-limited conditions without rhizobia (which fix atmospheric nitrogen) and without nitrogen fertilization (M2-Fig. 1, M2-Fig. S1). This experimental set-up ensures that the plants rely entirely on their seed reserves for nutrient supply. The cotyledons were removed and analysed at five different time points (8, 12, 16, 20, 28 days after sowing, M2-Fig. 1A, B, D) and the phenotype as well as composition of the remaining plant was assessed at day 28.

The cotyledons lost half of their total biomass and 60 % of their protein content already during the first 8 days of germination and seedling establishment (M2-Fig. 1D). High levels of free amino acids transiently accumulated with a peak in the cotyledons of juvenile plants between day 8 and 12. The total nitrogen content of the cotyledons continuously decreased over the 28 days and finally reached 5 % of the original seed content. Removing the cotyledons after day 12 did not lead to any significant changes in plant biomass, total nitrogen, protein, or amino acid content compared to the control (28d) (M2-Fig. 1E). Cotyledon loss at day 8 resulted in a drastic reduction of the plant size as well as nitrogen metabolite contents at day 28 (M2-Fig. 1C, E). The total nitrogen content of the 4-week-old plant was 62 % lower than in the control (5.9 ± 0.5 vs. 15.2 ± 0.8 mg, M2-Fig. 1E) and the missing fraction corresponded almost exactly to the nitrogen content of the removed cotyledons (11.3 ± 1.4 mg, M2-Fig. 1D). The effect of cotyledon loss at day 12 was less pronounced but of a similar quality. Plants remained smaller with a lower protein and amino acid content than controls.

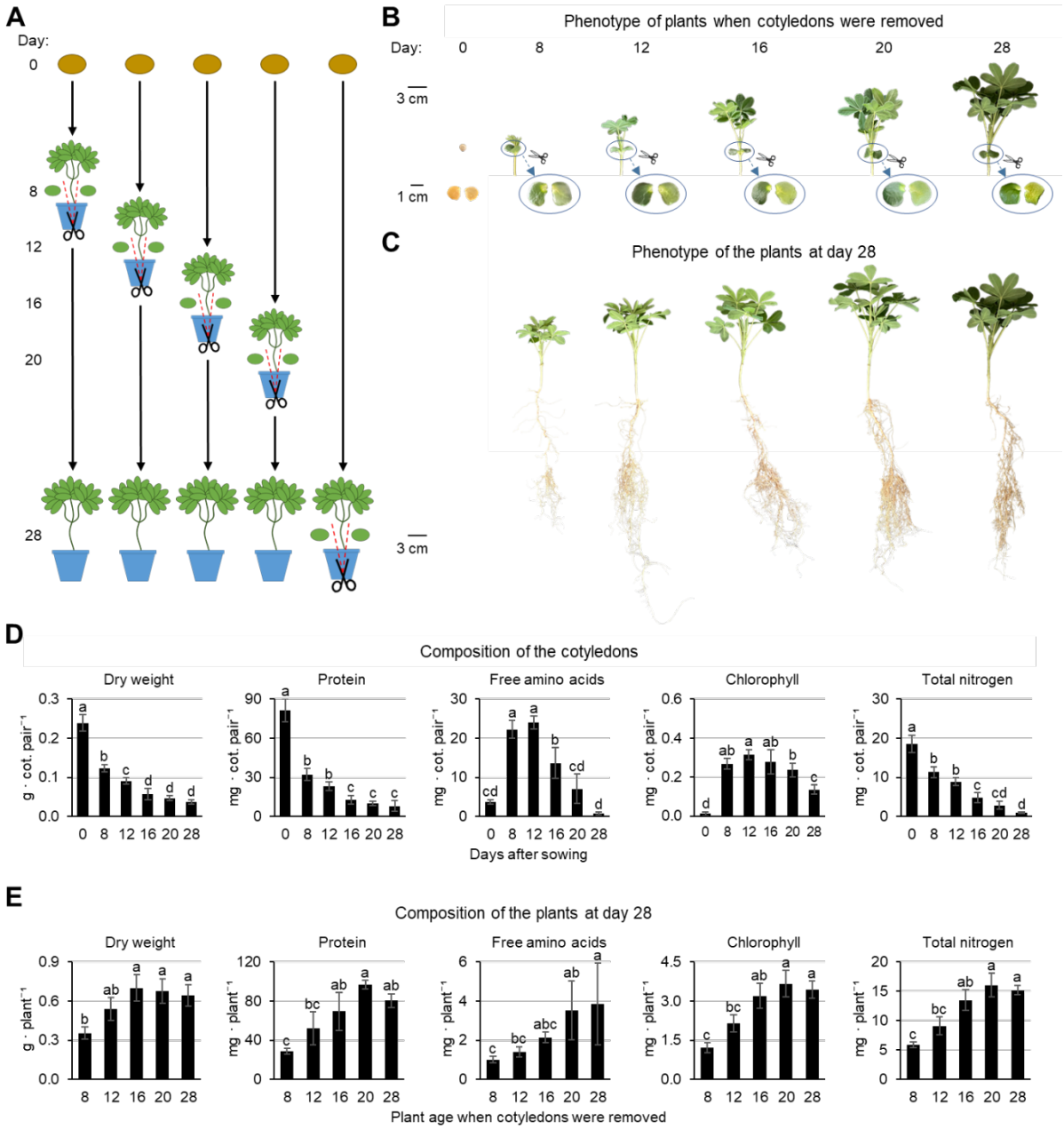

M2-Fig. 1: Exploring the role of the cotyledons after germination. (**A**) Scheme of the experimental set-up. Plants were grown for 28 days, and cotyledons were removed at day 8, 12, 16, 20, or 28 (control) after sowing. (**B**) Photos of shoots and cotyledons of representative plants at the time of cotyledon removal. Cotyledons: left: top view, right: bottom view. (**C**) Phenotype of representative plants at day 28 after sowing. (**D**) Biomass and composition of the cotyledons at day 0, 8, 12, 16, 20, and 28 after sowing. Data presented are means ± SD (n = 5). Means were compared using one-way ANOVA followed by Tukey's HSD test. Letter-based significance grouping was used at a significance level of $p < 0.05$; means sharing the same letter are not significantly different. The complete dataset is provided as Supp. Dataset S1. (**E**) Biomass and composition of the plants at day 28 after sowing. Data presented are means ± SD (n = 5). Means were compared using one-way ANOVA followed by Tukey's HSD test. Letter-based significance grouping was used at a significance level of $p < 0.05$; means sharing the same letter are not significantly different. The complete dataset is provided as Supp. Dataset S1.

3.3.2 Reorganization of the cotyledon proteome during transformation from storage organ to photosynthetic tissue

To monitor the transformation of the cotyledons from a storage organ to a photosynthetic tissue, we analysed changes in the proteome composition using our manually curated *Lupinus albus* proteome database for functional protein annotation (ANGERMANN ET AL., 2024). The cotyledons represent a large part of the seedling at early developmental stages (65 % of the DW at day 8 and 42 % at day 12) but only a minor fraction in the mature plant (M2-Fig. 2A). The seed proteome is dominated by storage proteins (28 %), LEA proteins (6 %) and proteins of the storage oil bodies (oleosins) (10 %) (M2-Fig. 2C, D). Half of these major seed protein categories are degraded within the initial 8 days of development. About 44 % of the nitrogen liberated by this proteolytic process is stored in the free amino acid pool, mainly in the form of asparagine (M2-Fig. 1D, 4A, Supp. Datasets S1, S2) and the rest is directly reinvested into new functional proteins. The most pronounced reorganization of the cotyledon proteome occurs during the first 8 days of development (M2-Fig. 2B – D). Enrichment analysis of functional annotations indicates a strong induction in primary metabolism, including amino acid metabolism, cellular respiration, lipid degradation, nucleotide synthesis, as well as photosynthesis and the production of the required cofactors (tetrapyrrole and isoprenoids, M2-Fig. 2E) during seedling establishment. Subsequently, the relative composition of the proteome does not change as drastically (M2-Fig. 2D). However, the protein fraction required for photosynthesis continuously increases during further development of the cotyledons until day 16 (M2-Fig. 2D, M2-Fig. S2). The functional category “transport” is significantly enriched in all comparisons, indicating dynamic changes in the transporter profile of the cotyledons throughout plant development. This includes an early upregulation of proteins involved in mobilization and reallocation of iron (Fe) or regulation thereof, such as orthologs of nicotianamine synthase AtNAS1, transporters for Fe, nicotianamine-Fe, and nicotianamine-Cu, as well as a transporter for Fe signals (YSL6, NRAMP3, OPT3; Supp. Dataset S2). These findings suggest that Fe and metal ion homeostasis is also a relevant feature of cotyledon transformation. During cotyledon senescence, proteins involved in nutrient signaling and transport, as well as cell wall metabolism, are increased (M2-Fig. 2D, Supp. Dataset S2).

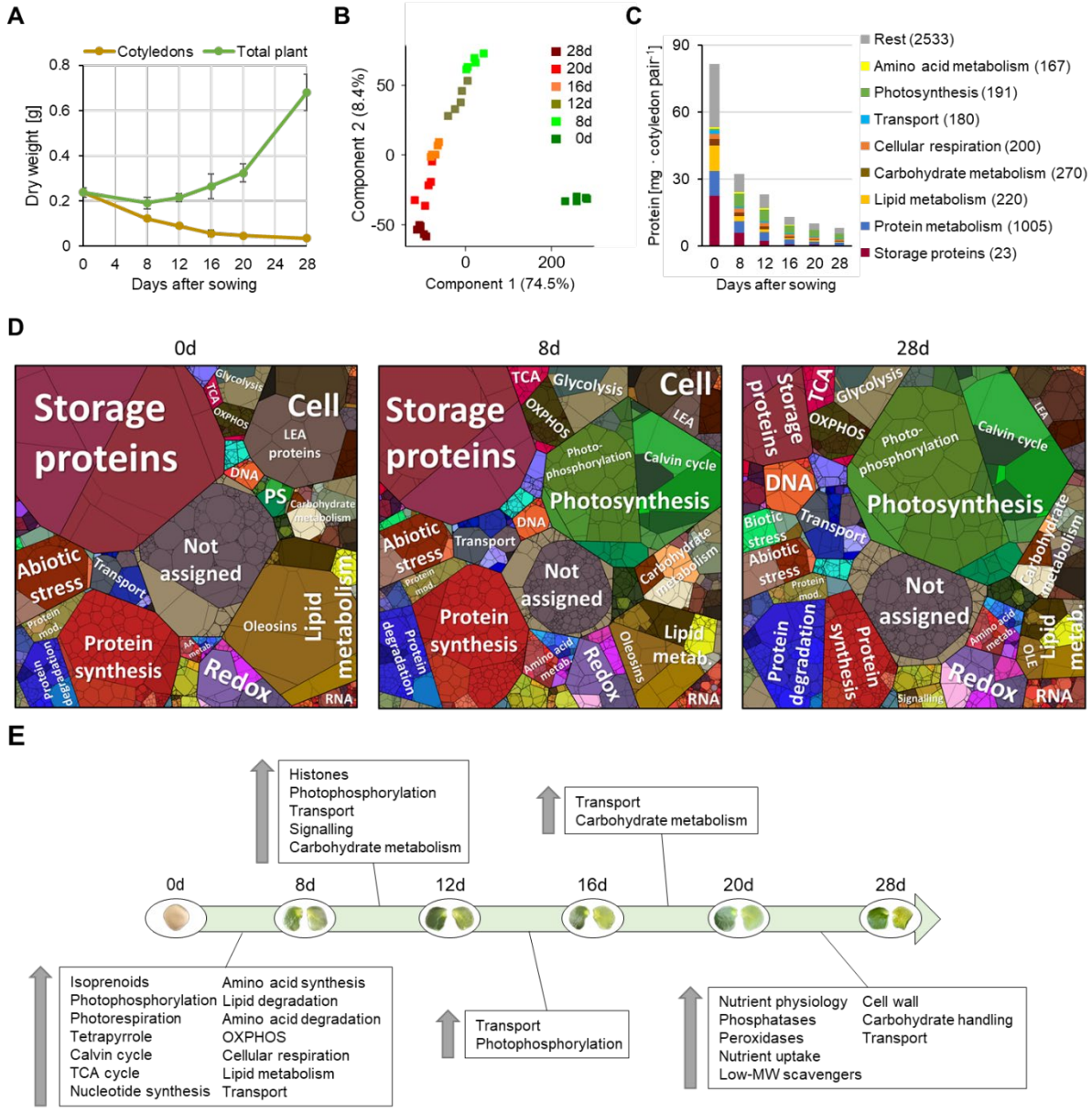

M2-Fig. 2: Reorganization of the cotyledon proteome during transformation from storage organ to photosynthetic tissue. (**A**) Biomass of lupin plants and cotyledons at 0 – 28 days after sowing. Data presented are means ± SD (n = 5). (**B**) Principal component analysis of the lupin cotyledon proteomics dataset. Data presented are means of five biological replicates. (**C**) Total protein content of the cotyledons and mass fractions covered by the major functional categories at day 0 – 28 after sowing. Numbers in parentheses indicate the number of different protein groups detected in the respective category. Mass fractions (protein abundances obtained by MS [iBAQ], multiplied with protein molecular weight) for all individual proteins are provided in Supp. Dataset S2. Data presented are means of five replicates. (**D**) Proteomaps illustrating the quantitative composition of the cotyledon proteome at day 0, 8, and 28 after sowing. LEA, LEA proteins; metab., metabolism; mod., modification; OLE, oleosins; PS, photosynthesis. Proteins are shown as polygons whose sizes represent their mass fractions (see **C**). Proteins involved in similar cellular functions are arranged in adjacent locations and visualized by colours. Proteomaps were produced using the tool provided at https://bionic-vis.biologie.uni-greifswald.de/ (LIEBERMEISTER ET AL., 2014). Data presented are means of five biological replicates. (**E**) Significant changes in the cotyledon proteome

during development from storage organ to photosynthetic tissue. Relative changes in abundance between subsequent sampling timepoints were analysed for each individual protein group. Enrichment of functional annotations in the subset of proteins with significantly increased abundance compared with the total proteome was analysed for each comparison, and significantly enriched categories are listed in the boxes in the order of descending enrichment factors. Data presented are means of five biological replicates. The complete dataset is provided as Supp. Dataset S2.

A direct comparison of the cotyledons to the true leaves at day 12 after sowing shows that while the leaves have an even higher protein content than the cotyledons at this stage, the cotyledons contain almost twice as much free amino acids (M2-Fig. 3A, M2-Fig. S3). The proteome composition is clearly different in these two tissues and shows that although photosynthetically active, the cotyledon metabolism is dominated by catabolic pathways, such as lipid, protein, and amino acid degradation, as well as mitochondrial respiration (TCA cycle and OXPHOS, M2-Fig. 3C, D). Proteins related to photosynthesis represent 22 % of the total protein mass in the cotyledons compared with 40 % in the leaves, which also contain a fourfold higher chlorophyll content combined with a larger area (8.0 ± 1.5 vs. 3.0 ± 0.3 cm^2) than the cotyledons (M2-Fig. 3A). Comparison of photosynthetic performance using the light saturation curve of photosynthesis shows much higher electron transport rates in leaves at all light intensities (M2-Fig. 3B). Comparable results were obtained by comparing the net photosynthetic rates of leaves and cotyledons. At a photon flux density of 500 µmol photons m^{-2} s^{-1}, net photosynthetic oxygen production in leaves is nine times higher than in cotyledons (23.0 ± 4.5 vs. 2.6 ± 1.8 µmol oxygen min^{-1} g^{-1} DW) (Supp. Dataset S3). Interestingly, the maximum quantum yield of photosystem II (cotyledon: 0.846 ± 0.005; leaf: 0.848 ± 0.004) is similar in both tissues at 12 days after sowing (Supp. Dataset S3). In addition to photosynthesis, the sulfur assimilation pathway, as well as protein, lipid, and amino acid synthesis reactions, are enriched in the leaves compared with the cotyledons (M2-Fig. 3C, D).

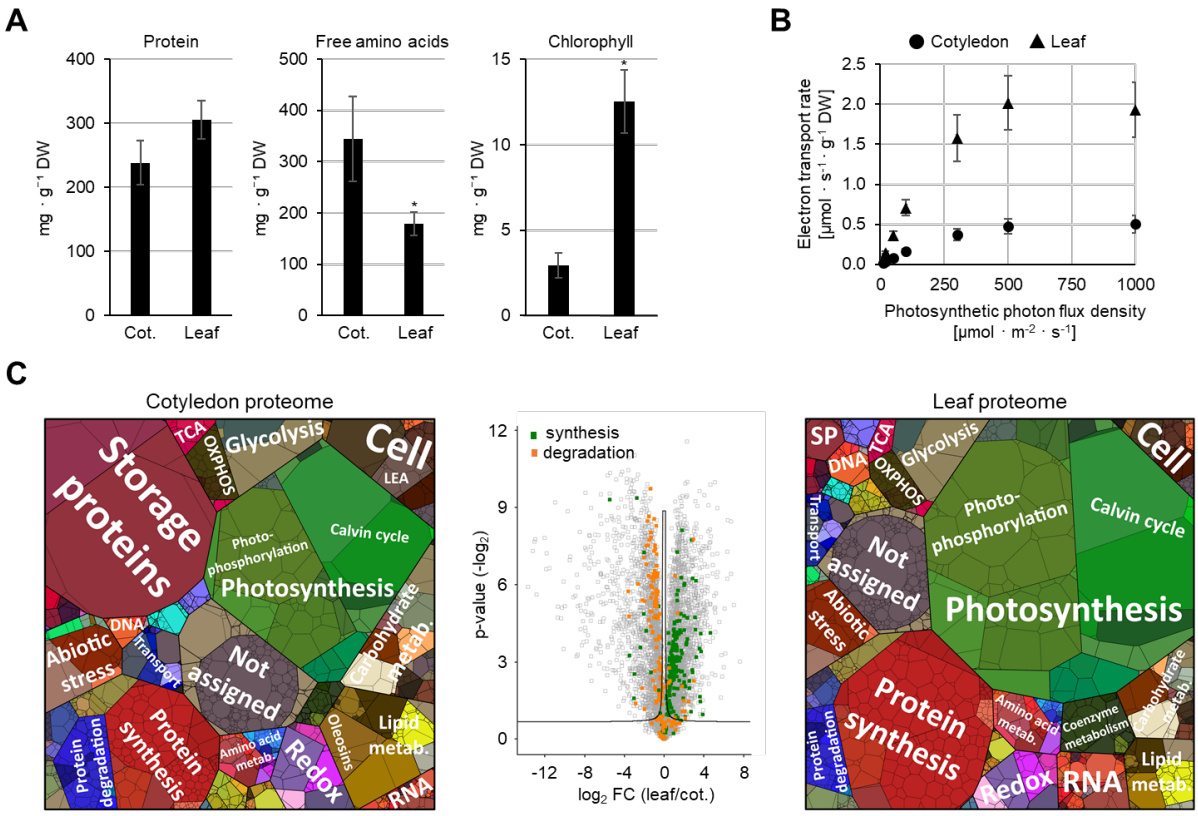

D

Enrichment in cotyledon proteome

Bins	Annotation Lvl2	Enrichment factor
4.1	conglutin	3.0
14.9	LEA protein	2.8
7.5	lipid bodies-associated activities	2.8
16.2	glutathione S transferases	2.5
15.1	14-3-3 proteins	2.4
6.2	**amino acid degradation**	2.3
3.2	**TCA cycle**	2.2
99.18	oxidoreductases	2.0
7.2	**lipid degradation**	2.0
12.2	auxin	2.0
6.3	amino acid synthesis & degradation	1.9
3.3	**OXPHOS**	1.8
2.5	minor CHO metabolism	1.8
13.2	flavonoids	1.7
2.3	carbohydrate handling	1.7
5.2	**protein degradation**	1.6

Enrichment in leaf proteome

Bins	Annotation Lvl2	Enrichment factor
11.12	S-adenosyl methionine (SAM) cycle	2.3
19.5	sulfur assimilation	2.3
1.1	photophosphorylation	2.1
11.14	tetrapyrrole	2.1
1.2	calvin cycle	1.9
9.3	DNA synthesis/chromatin structure	1.7
6.1	**amino acid synthesis**	1.4
7.1	**lipid synthesis**	1.4
5.1	**protein synthesis**	1.3
10.2	RNA processing	1.3

M2-Fig. 3: Proteome composition and photosynthetic performance of cotyledons versus true leaves in a lupin plant at 12 days after sowing. (**A**) Biomass and composition of the cotyledons and the true leaves. Data presented are means ± SD (n = 5). *Significantly different from control (cotyledon) ($p < 0.05$). (**B**) Light saturation curve of photosynthesis. Data presented are means of five biological replicates. (**C**) Comparison of the quantitative and relative composition of the cotyledon proteome and the leaf proteome. LEA, LEA proteins; metab., metabolism; SP, storage proteins. Proteomaps illustrate the quantitative proteome composition. Proteins are shown as polygons whose sizes represent their mass fractions. Proteins involved in similar cellular functions are arranged in adjacent locations and visualized by colours. Proteomaps were produced using the tool provided at https://bionic-vis.biologie.uni-greifswald.de/ (LIEBERMEISTER ET AL., 2014). The volcano plot illustrates $\log_2$ fold changes (FC) in relative protein abundances between the two tissues. The significance threshold is indicated by solid lines. Proteins of catabolic pathways enriched in the cotyledons

are highlighted in orange and proteins of synthesis pathways enriched in the true leaves are highlighted in green (see D). Data presented are means of five biological replicates. (**D**) Enrichment of functional categories in proteins that are significantly increased in the cotyledon proteome (left) or the leaf proteome (right) at day 12 after sowing. Data presented are means of five biological replicates. The complete dataset is provided as Supp. Dataset S3.

3.3.3 Remobilization of nutrients from the cotyledons

Taken together, the proteome datasets and amino acid profiles reveal that nitrogen remobilization from the cotyledons to the growing lupin plant proceeds in two stages. A large fraction of the protein store from the seed (60 %) is degraded already during germination and early seedling establishment (M2-Fig. 1D and 2C). However, high levels of free amino acids in the cotyledons of young plants (> 200 mM at day 8) indicate transient storage of nitrogen in the free amino acid pool for later utilization in the growing plant (M2-Fig. 1D and 4A). The exceptionally high share of free amino acids in the total pool persists in the cotyledons until day 20, whereas the total biomass and thus also the total amino acid content decrease drastically (M2-Fig. 1D and 4A).

In addition to nitrogen, carbon is also in high demand during germination and early seedling development and must be mobilized from seed storage reserves before photosynthesis becomes fully active. Alongside proteins, carbohydrates and lipids serve as major carbon reserves in lupin seeds, contributing approximately 23 and 12 % to seed dry mass, respectively (M2-Fig. S4, Supp. Dataset S1). Lipid stores were rapidly depleted, with total cotyledon lipid content decreasing by 75 % by day 8 after germination, accompanied by a drop in relative lipid concentration from 116 ± 20 to 54 ± 7 mg g^{-1} DW (M2-Fig. S4). In contrast, the relative carbohydrate content in the cotyledons remained stable over the same period and the total content decreased in proportion to their biomass, suggesting that any additional initial remobilization of carbohydrate reserves may have already been balanced by the onset of photosynthetic activity by day 8.

L. albus is well adapted to growing on soils with a low phosphate content due to its ability to develop specialized cluster roots (PUEYO ET AL., 2021; XU ET AL., 2020). Thus, phosphate storage and supply to the young plant might also be an important function of the cotyledons. The phosphate store of the white lupin seeds analysed in this study mainly consisted of organic compounds (M2-Fig. 4B, phosphate). The total phosphate content of the cotyledons decreased continuously during the first 4 weeks of plant growth, with the strongest drop (50 %) occurring during germination and seedling establishment until day 8. Cotyledon removal after day 12 had no significant effect on

the total phosphate content of the plants at day 28. In contrast, loss of cotyledons at day 8 or 12 resulted in a drastic reduction in the plant's phosphate content at day 28. The missing fraction corresponded to the phosphate content of the removed cotyledons (Supp. Dataset S1).

There are further important macro- and micronutrients present in the cotyledons that can serve in photosynthesis. To test whether they were utilized with a similar or different pattern from N-storage compounds and phosphate, we conducted an elemental analysis using the same approach as described above (M2-Fig. 4B). As expected, the phosphorus (P) pattern followed that of phosphate and N. There was a continuous usage of P from the cotyledons during the 28 days, while no extra P was acquired from soil (M2-Fig. 4B, phosphorus). Since phosphate is the P form in living organisms, this was expected. Surprisingly, the other tested elements showed evidence of two new nutrient usage patterns. Iron (Fe) and sulfur (S) are needed for electron transport in chloroplasts and energy production in mitochondria. Fe is also required as a cofactor for chlorophyll biosynthesis, S and N assimilation. Both Fe and S were nearly fully used from cotyledons during the first 8 days of germination prior to the onset of photosynthesis in cotyledons (M2-Fig. 4B, sulfur, iron). Already during this time frame, seedlings began acquiring residual Fe and S from the root substrate. In contrast, micronutrients like copper (Cu), zinc (Zn), and macronutrient magnesium (Mg) were used from cotyledons during the first 8 days, while only after that the increase in total plant contents must be through root uptake (M2-Fig. 4B, copper, zinc, magnesium). Hence, there are different dynamics of mineral mobilization from cotyledons and soil, with at least three different patterns for mineral utilization from cotyledons over the 28-day time span.

Premature cotyledon loss had no significant effect on the relative mineral contents of the plants at Day 28 (M2-Fig. S5). However, since early removal of the cotyledons led to a strong growth retardation, the total mineral contents of the plants at Day 28 were decreased by the same factor as the total biomass (M2-Fig. 1E, Supp. Dataset S1).

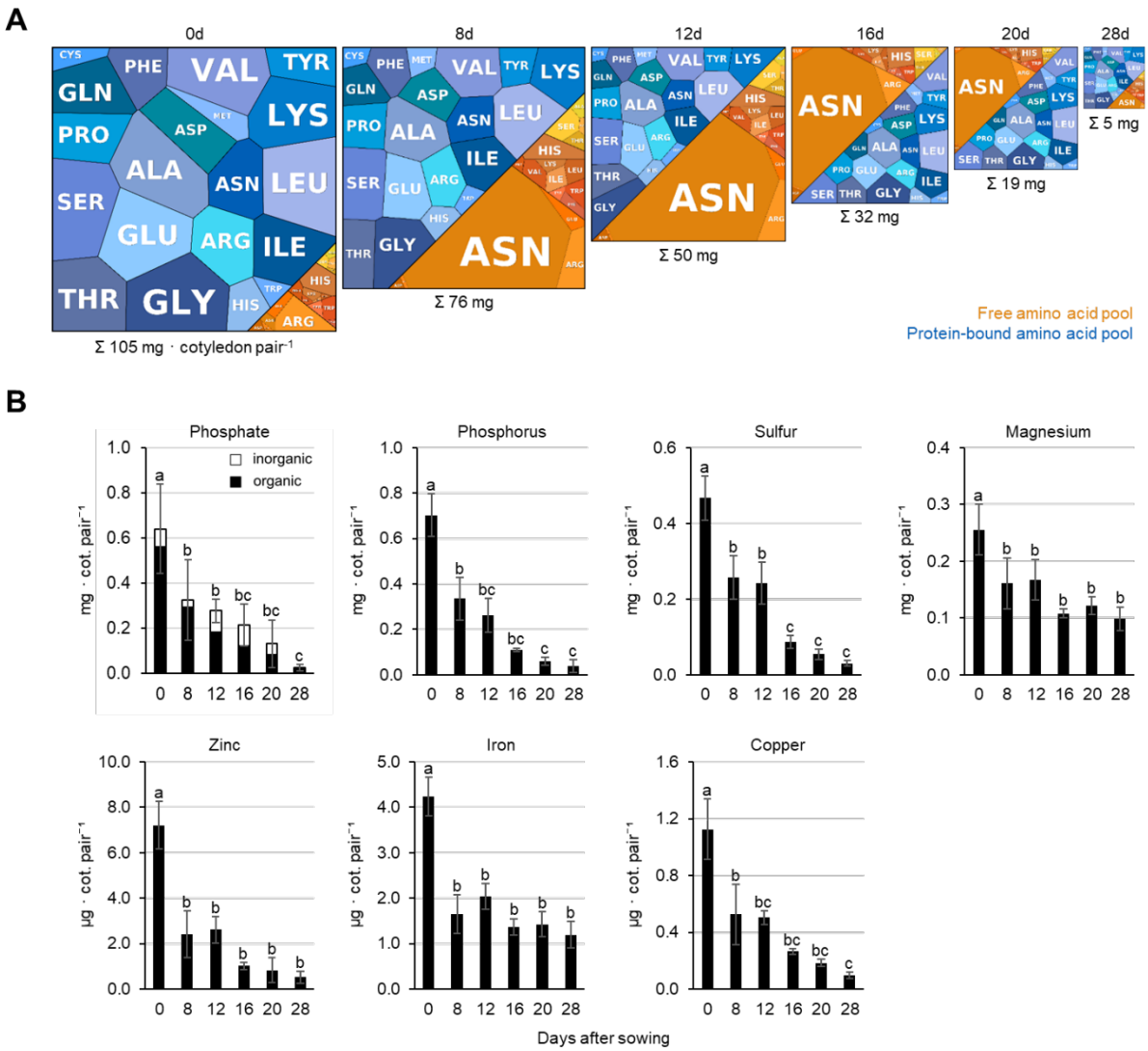

M2-Fig. 4: Remobilization of nutrients from the cotyledons. (**A**) Quantitative composition of the free (orange) and protein-bound (blue) amino acid pools in the cotyledons at day 0, 8, 12, 16, 20, and 28 after sowing. Amino acids are shown as polygons whose sizes represent the molar fractions. Free amino acid contents were quantified by HPLC, and the quantitative amino acid composition of the proteome was calculated on the basis of the molar composition of the proteome (see Supp. Datasets S1 and S2). The area of the square corresponds to the total amino acid content per cotyledon pair at a given timepoint. Aminomaps were produced using the tool provided at https://bionic-vis.biologie.uni-greifswald.de/ (LIEBERMEISTER ET AL., 2014). The complete amino acid profiles are provided in Supp. Dataset S3. Data presented are means of five biological replicates. (**B**) Mineral composition of the cotyledons at day 0, 8, 12, 16, 20, and 28 after sowing. Data presented are means ± SD (n = 3 – 9). Means were compared using one-way ANOVA followed by Tukey's HSD test. Letter-based significance grouping was used at a significance level of $p < 0.05$; means sharing the same letter are not significantly different. The complete dataset is provided as Supp. Dataset S1.

3.3.4 Responses of the *Lupinus albus* proteome to premature cotyledon loss

The results of this study indicate that the cotyledons are able to support plant growth by providing nutrients for about 2 weeks after germination in *L. albus* plants grown without external nutrient supply under control conditions. Loss of the cotyledons at day 16 or later did not lead to any significant changes in the plant phenotype (M2-Fig. 1) or the composition of the proteome (M2-Fig. 5A) at day 28. In contrast, not only the growth phenotype (M2-Fig. 1) and nutrient content (M2-Fig. 1E and 4B) but also the proteome of plants grown without cotyledons from Day 8 or 12 was clearly different from that of control plants, with 1214 and 943 proteins of significantly changed relative abundance, respectively (M2-Fig. 5A, B, Supp. Dataset S4). The profile of protein induction or repression was highly consistent, and the same trend was also visible after later cotyledon loss (red and blue squares in M2-Fig. 5A). Enrichment analysis indicates a relative increase in protein and lipid catabolism as well as nutrient signalling and transport processes in plants without cotyledons (M2-Fig. 5B, left). The strongest enrichment was detected in proteins required for phosphate assimilation, highlighting the function of the cotyledons in phosphate storage. There was also an induction of certain metal homeostasis-related proteins, which may follow the rapid early translocation of metals from the cotyledons, accompanied by adjustments to an early onset of Fe uptake from soil (Supp. Dataset S4). In addition, a biotic stress response was induced on the proteome level. Surprisingly, removing the cotyledons also led to a higher relative content of storage proteins in the remaining plant tissues at the age of 4 weeks. A significant decrease was detectable for proteins related to photosynthesis and the production of the required cofactors, amino acid and protein synthesis, as well as carbohydrate and coenzyme metabolism (M2-Fig. 5B, right). These changes in relative proteome composition provide an impression of which pathways are particularly relevant for adjusting to early loss of the cotyledons. However, taking total protein abundance into account shows that photosynthesis and protein metabolism quantitatively contribute by far the largest share to reducing the protein content of the plant after early cotyledon loss (M2-Fig. 5C). The plant is able to save 15.5 mg protein by reducing its relative protein content by 35 % from 126 ± 16 to 82 ± 13 mg g^{-1} DW after premature cotyledon loss at day 8 (M2-Fig. S6, Supp. Dataset S4). The most effective nitrogen saving strategy, however, is the reduction in plant

biomass from 644 ± 84 to 353 ± 47 mg DW that based on the mean tissue protein content of the control plant, would save 36.7 mg protein.

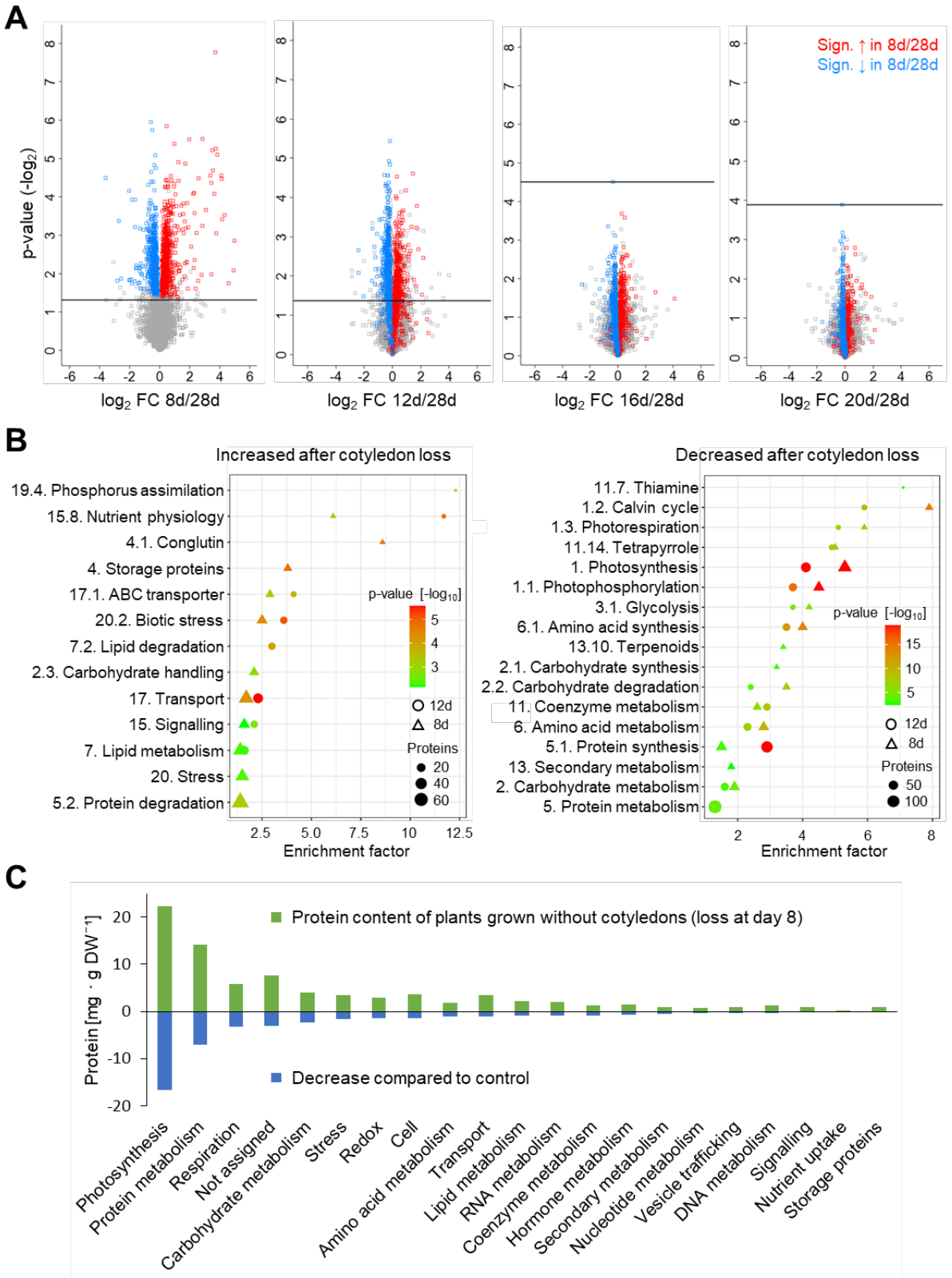

M2-Fig. 5: Response of the *Lupinus albus* proteome to premature cotyledon loss. (**A**) Volcano plots illustrating differences in the proteome of 4-week-old lupin plants grown without cotyledons from day 8, 12, 16, or 20 compared with control plants. Representative pictures of

these plants are shown in M2-Fig. 1C. To visualize the level of consistency in the effect of cotyledon loss on the plant proteome, proteins that are significantly increased or decreased after the removal of the cotyledons at day 8 compared with the control are highlighted in red and blue, respectively, in all plots. The horizontal lines mark the significance threshold ($p < 0.05$, FDR: 0.1). Data presented are based on five biological replicates. (**B**) Enrichment of functional categories in proteins that are significantly increased (left) or decreased (right) in the plant proteome at day 28 after cotyledon loss at day 8 (triangles) or day 12 (circles). Data presented are based on five biological replicates. (**C**) Protein content of lupin plants at day 28 after the removal of the cotyledons at day 8 (green bars) and difference to control plants (blue bars) for the major functional categories. All plants were harvested at day 28. Data presented are means of five biological replicates. The complete dataset is provided as Supp. Dataset S4.

3.4 Discussion

The present study focuses on the function of the cotyledons in nutrient supply of *Lupinus albus* after initial seedling establishment, including their contribution to photosynthesis as well as nitrogen and mineral nutrition (M2-Fig. 6). We investigate the timeframe of nutrient remobilization without external nutrient supply, mimicking cultivation on nutrient-poor soils, and monitor the integration of metabolic pathways with physiological requirements during cotyledon development from seed storage tissue to photosynthetic organ up to senescence. Our results reveal that *Lupinus albus* cotyledons provide essential nutrients during a critical phase of about 2 weeks after germination, with premature loss at day 8 or 12 causing significant changes in growth, nutrient content, and proteome composition, while later cotyledon removal has minimal effects on plant development.

3.4.1 Cotyledons combine nutrient storage and photosynthetic functions in the young lupin plant

The cotyledons of *Lupinus albus* serve a dual role, initially functioning as storage tissue to fuel germination before emerging from the soil and becoming photosynthetically active. During the initial germination and heterotrophic seedling development phase, white lupins use lipids as a source of energy and transiently accumulate starch (Borek et al., 2011). These carbon stores can be replenished by photosynthesis after transformation to autotrophy. While supporting photosynthetic energy production, cotyledons, however, retain substantial reserves of storage proteins and free amino acids. This transformation requires a balance of nutrient remobilization and energy generation, which we analysed through proteomics, metabolic, physiological, and functional studies over 28 days (M2-Fig. 1 - 4). Proteins related to photosynthesis are strongly induced already during the first days of seedling establishment, and the

cotyledons become photosynthetically active and thus contribute to photoautotrophic ATP production and carbon fixation. However, compared with the true leaves, they have a significantly lower photosynthetic capacity, although the efficiency of photosystem II is comparable (M2-Fig. 3). The proteome composition of cotyledons reveals a clear metabolic focus on catabolic processes and resource remobilization. Therefore, as soon as the first true leaves are fully developed, their net photosynthetic rate exceeds the contribution of the cotyledons, and the composition of their proteome is consistent with their dominant role as a source tissue for photosynthate and biosynthetic processes. Thus, white lupin cotyledons can be classified as semi-photosynthetic storage tissues with a prolonged dual function in nutrient remobilization and photosynthesis. Research on the role of soybean cotyledons in seedling establishment based on growth analysis had also indicated that cotyledon photosynthesis is not sufficient to increase plant growth, but can provide the carbohydrates needed to compensate for respiratory losses during early seedling establishment (HARRIS ET AL., 1986). A more recent study on castor bean cotyledons came to a similar conclusion, demonstrating that cotyledon photosynthesis generated sufficient carbohydrates and energy to support the emergence of the first true leaf and sustained seedling growth until the leaf had fully expanded (ZHENG ET AL., 2011). The proteome-level changes we observed in lupin cotyledons align well with transcriptomic data reported by BROWN AND HUDSON (2015) in soybean cotyledons, where early developmental stages are characterized by the transcriptional activation of genes involved in proteolysis, lipid metabolism, and nutrient remobilization, followed by a period of high expression of the photosynthetic apparatus. An additional transcriptome study focusing on earlier timepoints highlights the important transition in the role of peroxisomes from supporting lipid catabolism via the glyoxylate cycle to participating in photorespiration after the onset of photosynthetic activity (GONZALEZ AND VODKIN, 2007). This aspect is also reflected in our proteome data showing a drop in glyoxylate cycle abundance in the lupin cotyledons after day 8, while the enzymes involved in photorespiration increase in concert with the photosynthetic apparatus (Supp. Dataset S2). These examples indicate that cotyledon photosynthesis has a transient function during epigeal germination in species storing proteins as well as lipids.

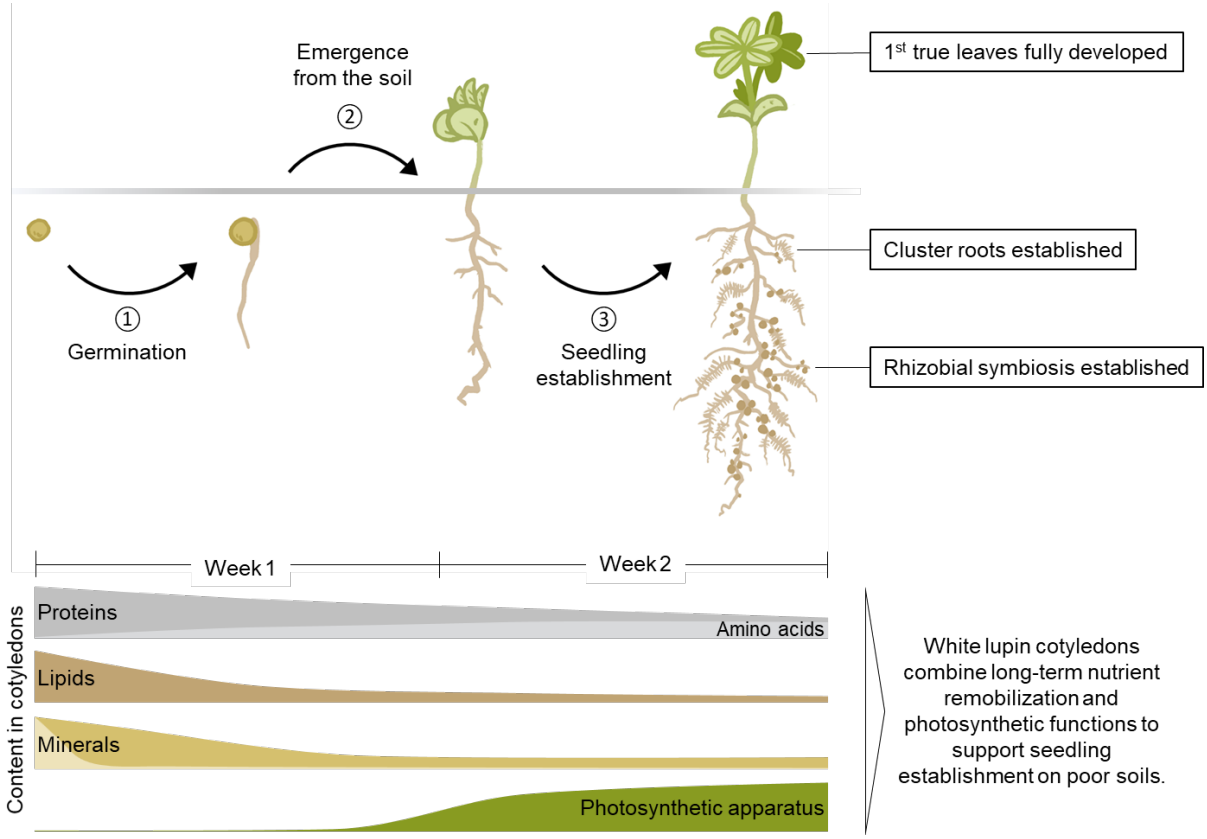

M2-Fig. 6: Combining nutrient remobilization and photosynthesis: the dual role of white lupin cotyledons during seedling establishment on nutrient-poor soils. Seed storage compounds provide energy and precursors for the synthesis of macromolecular structures during germination (1) and fully support plant growth until the seedling has emerged from the soil (2) and photosynthesis has been established. In some species including lupins, the cotyledons are transformed into photosynthetically active leaves after germination, allowing them to function as storage tissues for an extended period. The delayed remobilization of specific storage compounds, such as proteins and phosphate, is essential for successful seedling establishment (3) on nutrient-deficient soils. The internal nutrient supply supports growth until specialized root structures and symbiotic associations are developed, enabling the seedling to become fully self-sufficient. In natural environments, this is usually achieved within 2 weeks after germination (JAMES ET AL., 1997; NEUMANN ET AL., 1999). Details on remobilization patterns of the different storage compounds and reorganization of the cotyledon proteome are provided in the main text.

3.4.2 Long-term nutrient remobilization from the cotyledons to the lupin seedling supports growth on nutrient-poor soils

A major storage compound in the lupin seed is nitrogen, mainly in the form of proteins and amino acids (82 % of total N). However, *Lupinus albus* does not use amino acids as a primary substrate for energy metabolism during germination (ANGERMANN ET AL., 2024). Nitrogen remobilization from cotyledons proceeds continuously throughout the first weeks of plant development and can be divided into two steps. Within the first 8 days of germination and seedling establishment, it is clearly associated with

proteolysis and a significant transfer of amino acids from the protein-bound form to the soluble pool (M2-Fig. 1 and 4). The protein content is halved and at the same time, the amount of free amino acids strongly increases. Proteolysis releases large amounts of free amino acids, which are used as precursors for new functional proteins and nitrogenous metabolites, or accumulate in the free pool. Asparagine strongly accumulates and serves as a suitable form for storage and transport of reduced nitrogen due to its favourable C/N ratio, minimal net charge, and low reactivity under physiological conditions. The conversion of protein-bound nitrogen to the soluble form as asparagine is likely to play a key role in the remobilization and transport of nitrogen to growing tissues (LEA ET AL., 2007). The synthesis of asparagine involves the assimilation of free ammonium by the combined reactions of glutamine synthetase and asparagine synthetase (LEA AND FLOWDEN, 1975). These enzymes show a high relative increase in cotyledon protein content during seedling establishment (Supp. Dataset S2). In nitrogen-deficient substrate, the ammonium originates exclusively from internal deamination reactions and is re-assimilated into asparagine for storage and transport. Quantitative evaluation of the seed and plant composition revealed that the proteins stored in the seeds were required almost exclusively for the synthesis of new functional proteins during seedling development. Additional nitrogen-containing compounds such as chlorophyll and nucleotides quantitatively require a minor input of nitrogen resources. These results suggest that nitrogen stored in lupin cotyledons plays a crucial role in several aspects. Degradation of seed-stored proteins releases nitrogen to provide precursors for successful early germination, but also to provide storable but transportable soluble forms of nitrogen for longer periods to enable establishment on nitrogen-poor soils until the symbiosis with N_2-fixing rhizobia has been established, which is usually achieved within 2 – 3 weeks after germination (JAMES ET AL., 1997).

Another important macronutrient involved in several biological processes is phosphorus (RAGHOTHAMA, 2005). Phosphate is required for nucleic acids, membrane lipids, ATP, as well as diverse metabolic and regulatory processes. Low phosphate availability in many natural ecosystems, especially under acidic conditions promoting inorganic complexation, is a major constraint on crop production. Short-term deficiencies can be compensated by intracellular stores, but long-term phosphate starvation leads to stress responses such as an altered root architecture, an increase in the root/shoot ratio, and an induction of phosphate uptake and recycling pathways

(Raghothama, 2005). In P-limited environments, lupin seedlings rely on the phosphate stored in the cotyledons until specialized, densely packed lateral root structures called cluster roots are fully developed. This process usually requires 12 – 14 days after imbibition (Neumann et al., 1999). The cluster roots can mobilize soil phosphates very efficiently by the secretion of organic acids and acid phosphatases and an induction of a high-affinity P transport system (Pueyo et al., 2021; Xu et al., 2020). Our results show a continuous loss of phosphate from the cotyledons throughout plant development and a deficit in phosphate content in 28-day-old plants after early cotyledon loss (M2-Fig. 4, Supp. Dataset S1). Induction of phosphate assimilation, including phosphate transporters and regulatory proteins, was the process showing the strongest enrichment in the lupin proteome in response to cotyledon removal within the first 2 weeks of growth (M2-Fig. 5). These results demonstrate that continuous phosphate supply from the cotyledons is able to bridge the time gap between germination and cluster root establishment and is thus essential for successful seedling establishment on soils with a low phosphate availability.

The remobilization of micronutrients, particularly iron (Fe), copper (Cu), and zinc (Zn), from cotyledons begins before nitrogen depletion in plants. Early metal translocation from cotyledons and Fe uptake from soil coincide with the activation of metal homeostasis proteins. In *Arabidopsis thaliana*, various transporters like AtYSL6 (Conte et al., 2013), AtMfl1 (Tarantino et al., 2011), AtNRAMP3 (Lanquar et al., 2005; Li et al., 2018; Thomine et al., 2003), and AtOPT3 (Khan et al., 2018) play crucial roles in metal distribution and mobilization. Orthologs of these proteins increased in the lupin cotyledons during germination and seedling establishment (Supp. Dataset S2). An early induction of Fe uptake supports critical processes like chlorophyll biosynthesis and seedling development, as Fe-containing enzymes are essential. The process ensures Fe retention in cotyledons and supports nitrogen assimilation and metabolic functions, highlighting its importance during and after germination.

3.4.3 Premature cotyledon loss leads to nutrient deficiency and growth retardation

Premature cotyledon loss triggers profound phenotypic and molecular responses, with severity increasing the earlier the loss occurs. A major consequence is a significant reduction in plant growth, accompanied by a decrease in relative protein content in the

remaining plant tissue by Day 28 (M2-Fig. 1). Nutrient deficiencies, particularly phosphate limitation in combination with nitrogen and iron scarcity, are known to reduce biomass accumulation (PUEYO ET AL., 2021). A loss of the cotyledons before cluster roots and the symbiosis with N_2-fixing rhizobia have been established elicits severe growth retardation and specific proteomic adaptations to nitrogen and phosphate starvation (M2-Fig. 5, Supp. Dataset S4). These adaptations include a relative decline in highly abundant pathways, such as photosynthesis and protein synthesis, both of which require substantial nitrogen investment and thus bind a large share of the available nitrogen resources. Conversely, proteins involved in resource management, including signalling and transport, show a relative increase, indicating a shift toward metabolic prioritization under nutrient constraints. Our experimental approach addressed changes in the composition of the entire plant in response to premature cotyledon loss and thus made it possible to deduce quantitative information on the allocation of the nutrients stored in the cotyledons to particular functions and processes in the developing plant. However, additional experiments will be required to focus on organ-specific effects that are indistinguishable in the pooled tissues.

Previous studies have demonstrated that cotyledon loss negatively impacts early seedling establishment and can extend its effects into later developmental stages, leading to delayed flowering, reduced inflorescence production, and lower seed yield across various plant species (HANLEY AND FEGAN, 2007; HANLEY AND MAY, 2006; WANG ET AL., 2019; ZHANG ET AL., 2011). In *Arabidopsis thaliana*, some of these effects were partially mitigated by exogenous sucrose and auxin application (WANG ET AL., 2019). In the Brazilian savanna tree *Magonia pubescens*, removing one of the cotyledons led to a significant decline in growth, biomass accumulation, and mineral nutrient stocks (NUNES ET AL., 2024). Mineral nutrients as well as metabolite contents in leaf and root were also affected by cotyledon loss in the traditional Chinese herbal plant, *Astragalus membranaceus* (YANG ET AL., 2021). However, the extent of susceptibility to early cotyledon loss varies between species, suggesting that ontogenetic differences in seedling tolerance to tissue loss could significantly influence plant fitness in mature plant communities (HANLEY AND FEGAN, 2007). Seed size also plays a crucial role in tolerance; seedlings from larger seeds, such as white lupin, rely more heavily on their initial nutrient reserves and are therefore more sensitive to cotyledon loss than those from smaller seeds (HU ET AL., 2017).

Tolerance and an efficient response to premature cotyledon loss can become physiologically relevant under herbivore pressure. The lupin leaf weevils *Sitona gressorius* and *Sitona griseus* (Coleoptera: Curculionidae) cause considerable damage to lupin crops in Europe (Piedra-García and Struck, 2021). In the spring, adult weevils start feeding on newly emerged plants and can already at this stage severely weaken the young seedlings by damaging the cotyledons (Ströcker et al., 2013). Subsequently, the soil-dwelling larvae penetrate and destroy the root nodules as well as the surrounding root tissue. In addition to the negative impact on symbiotic nitrogen fixation capacity, the injuries caused by the feeding activities increase the risk of fungal infections (Piedra-García and Struck, 2021). In our study, we consistently observed an induction of pathogen response proteins following cotyledon removal (M2-Fig. 5, Supp. Dataset S4). This is consistent with studies in *Arabidopsis* showing that mechanical injury triggers innate immune responses (Savatin et al., 2014). Damage-associated molecular patterns (DAMPs) elicit local and systemic responses mediated by a combination of electrical signals, calcium spikes, reactive oxygen species, and hormones (Farmer et al., 2020). Mechanical injury activates defences that are similar to those induced by herbivores and leads to increased pathogen resistance (Chassot et al., 2007; Orlovskis and Reymond, 2020). Our dataset demonstrates a long-lasting effect of mechanic cotyledon removal on the *L. albus* proteome. Thus, cotyledon damage in white lupin may similarly prime systemic responses, which could offer some protection against subsequent biotic stressors. However, whether these responses are cotyledon-specific or represent a general wound response remains to be elucidated.

3.5 Conclusions

In this study, we observed different roles of the cotyledon at different times of plant development. Initially, cotyledons act as storage tissues for a variety of nutrients. Catabolic processes, transport, and the initialization of synthesis pathways are in the focus. Later, during epigeal germination, cotyledons act not only as nutrient stores, but depending on the species, they may also serve as photosynthetic tissues, which contribute energy and carbohydrates for plant development and growth. Once the first true leaves have emerged, the photosynthetic aspects recede into the background and cotyledon senescence, with catabolic processes and nutrient export, take priority. Seed nutrient reserves are required for adequate plant growth and development, not only during germination or until the seedling emerges from the soil and becomes

autotrophic through photosynthesis. The observed early Fe redistribution and protein analysis suggest that this transition is initiated very early after germination in the cotyledons. Internal nutrient supply is required for a prolonged period until specialized root structures and symbiotic interactions are established and the seedling becomes fully self-sufficient, even on nutrient-poor soils. Our results demonstrate the importance of the cotyledons of *Lupinus albus* during the first 2 weeks of seedling establishment. At this stage, premature cotyledon loss causes drastic phenotypic and molecular losses and responses, as well as activation of starvation and stress response pathways. The large nutrient stores in the seeds of *Lupinus albus* are thus prerequisite for thriving in nutrient-deprived environments.

Given the central role of legumes in sustainable food systems, unravelling the dynamics of cotyledon nutrient remobilization has significant implications beyond basic plant physiology. Optimizing this process could lead to the development of legume cultivars with improved seedling vigor, higher nitrogen use efficiency, and enhanced protein content, traits that are crucial for both agricultural sustainability and human nutrition. Breeding efforts focused on vigorous seeds with an optimal nutrient composition could improve not only seedling establishment but also the nutritional value of legume-based foods, addressing global challenges related to food security and dietary health. Additionally, understanding how cotyledon transformation contributes to early photosynthesis could offer novel strategies for enhancing seedling growth under suboptimal soil conditions. Beyond this, it would be thrilling to unravel the regulatory switches that determine whether a legume species uses epigeal or hypogeal germination patterns.

3.6 Materials and methods

3.6.1 Plant material and growth conditions

White lupin (*Lupinus albus* cv. “Nelly”) seeds were obtained from Revierberatung Wolmersdorf GmbH and Co. KG, Wolmersdorf, Germany (Order number: 34400) and stored in the dark at 4 °C until use. Prior to cultivation, seeds were soaked in demineralized water at 20 °C for 16 h and then transferred to water-saturated expanded clay substrate (LamstedtDan, 4–8 mm, Fibo ExClay Deutschland GmbH, Lamstedt, Germany; Information on the plant-available nutrient contents of the substrate is provided in Supp. Dataset S1). Plants were grown in a phytochamber (22–24 °C, 16 h light, 8 h dark, light: 110 µmol photons s^{-1} m^{-2}). On day 8, 12, 16, or 20 after sowing, the cotyledons were separated and harvested. The control group of plants retained their cotyledons until day 28. On day 28 after sowing, all plants were harvested, except for cotyledon versus leaf experiments, where the respective tissues were harvested at day 12 after sowing. At harvest, the remaining plant organs were frozen in liquid nitrogen. The plant material was lyophilized in an Alpha 1–2 LD+ freeze dryer (Christ, Osterode, Germany). The dried material was then ground into powder and used for the experiments. For one sample, several plants were pooled (10 seeds; 6 pairs of cotyledons at Day 8; 5 pairs of cotyledons at Days 12, 16, and 20; 4 pairs of cotyledons at Day 28; 3 plants at Day 28 with cotyledons separated at Day 8, 2 plants each at Day 28 with cotyledons separated at Days 12, 16, 20, and 28). Five different pools were analysed at each time point as biological replicates.

Plants for elemental analysis were grown as described above. Plant material was harvested at the same time points but dried at 60 °C for 2 days and ground to a fine powder.

Samples for analysis of photosynthetic parameters were grown as described above and used fresh immediately after harvest on Day 12.

3.6.2 Quantification of total carbon and nitrogen

The total carbon and nitrogen content of the samples was measured according to ANDRINO ET AL. (2019), using an Elementar vario MICRO cube C/N analyzer (Elementar GmbH, Hanau, Germany).

3.6.3 Quantification of chlorophyll

The quantification of chlorophyll was carried out according to a modified version of the method described by LICHTENTHALER (1987). About 5 mg plant powder was dissolved in 700 µl methanol (100 %) and incubated for 20 min at 80 °C with shaking. After centrifugation (10 min, 4 °C, 18 800 ×g), the chlorophyll content of the supernatant was quantified by plate reader (Multiskan Sky; Thermo Fisher Scientific, Dreieich, Germany) (wavelengths: 470, 653, and 666 nm).

3.6.4 Quantification of proteins

Proteins were extracted as described by ANGERMANN ET AL. (2024). About 4 mg of lyophilized plant powder was dissolved in 1 ml methanol (100 %) and incubated for 20 min at −20 °C. After centrifugation (14 200 ×g, 5 min, 4 °C) the pellet was dissolved in 1.4 ml of 0.1 M NaOH containing 2 % SDS (v/w) and incubated for 1 h at 60 °C, shaking. After centrifugation (7 000 ×g, 10 min, room temperature (RT)), the supernatant was diluted with demineralized water (1:10). The Pierce BCA Protein Assay Kit (Thermo Fisher Scientific, Rockford, IL, USA) was used for protein quantification with globulin as a standard.

3.6.5 Quantification of free amino acids

Free amino acids were quantified according to BATISTA-SILVA ET AL. (2019). About 10 mg of lyophilized plant powder was solubilized in 800 µl of 0.1 M HCl and incubated for 15 min at RT. After centrifugation (16 100 ×g, 5 min, RT) supernatants were mixed with an equal volume of 0.5 M potassium borate buffer (pH: 11), incubated for 15 min at RT, and centrifuged at 16 100 ×g, 5 min, RT. The supernatant was used for amino acid quantification. Beta-aminobutyrate (Sigma-Aldrich, Hamburg, Germany) was added as the internal standard for derivatizing the primary amino acids. To normalize the derivatization of secondary amino acids, 0.5 mM sarcosine (Sigma-Aldrich) was added to the dilution. The pre-column derivatization with ophthaldialdehyde (OPA) and fluorenylmethoxycarbonyl (FMOC) was based on the Agilent application note “Automated amino acids analysis using an Agilent Poroshell HPH-C18 Column.” Samples were injected onto an Agilent 100 mm, 3 mm InfinityLab Poroshell HPH-C18 column (2.7 mm) (Agilent Technologies, Waldbronn, Germany) using an Ultimate 3000 HPLC system (Thermo Fisher Scientific, Germering, Germany) for cotyledon timeline experiments and the cotyledon removal experiment. Samples for the comparison of

cotyledons with true leaves were analysed by an Agilent 1260 Infinity II HPLC system (Agilent Technologies).

3.6.6 Elemental analysis by inductively coupled plasma mass spectrometry (ICP-MS)

About 20–50 mg of dried material was digested in 1 ml of 67 % nitric acid overnight. Samples were heated to 95 °C until the solutions became clear. After cooling, the samples were centrifuged at 1 800 ×g for 30 min at 4 °C. About 600 µl of the clear supernatant were combined with 7.44 ml of ddH_2O and the solution was stored at 4 °C. ICP-MS analysis (Agilent 7700; Agilent Technologies) was conducted at the metabolomics platform, Biocentre of the University of Cologne, relating elemental contents to DW. Total plant mineral contents were calculated using a root-to-shoot ratio of 1:2 (O'Sullivan et al., 2022; Tiziani et al., 2020).

3.6.7 Quantification of phosphate

Inorganic and total phosphate were quantified according to Chiou et al. (2006). About 5 mg of lyophilized plant powder was dissolved in 250 µl extraction buffer (10 mM Tris, 1 mM EDTA, 100 mM NaCl, 1 mM 2-mercaptoethanol, pH: 8.0). A total of 100 µl of extract was mixed with 900 µl of 1 % glacial acetic acid and incubated at 42 °C for 30 min. 300 µl of this mixture was used for the quantification of inorganic phosphate. To 100 µl of this mixture, 30 µl of 10 % $Mg(NO_3)_2$ was added and then incinerated to ash. After cooling, the ash was dissolved in 300 µl of 0.5 N HCl and total phosphate was quantified. To quantify phosphate, 700 µl assay solution (0.35 % NH_4MoO_4, 0.86 N H_2SO_4, and 1.4 % ascorbic acid) was added to 300 µl of phosphate extract and incubated at 42 °C for 30 min. The phosphate content was quantified at 820 nm using a plate reader.

3.6.8 Quantification of total lipids

The total lipid content was determined using the sulfo-phospho-vanillin method, as described by Park et al. (2016). About 5 mg of plant powder were dissolved in a chloroform and methanol solution (2:1; v/v) and homogenized. Then, 0.9 % NaCl was added and homogenized again. After centrifugation (1 400 ×g, 30 sec, RT), the lower phase was evaporated. Then, 50 µl of concentrated sulfuric acid was added, mixed, and incubated at 90 °C for 10 min. After cooling on ice, 1 ml of phosphor–vanillin reagent (75 mg of vanillin in 12.5 ml of H_2O + 50 ml of 85 % orthophosphoric acid) was

added and incubated for 10 min at RT. Quantification of the lipid content was conducted at a wavelength of 530 nm using a plate reader, using commercial sunflower oil as the standard.

3.6.9 Quantification of total carbohydrates

The total carbohydrate content was determined using the phenol–sulfuric acid method described by TAMBOLI ET AL. (2020). About 5 mg of lyophilized plant powder was dissolved in 1 ml of 2.5 M HCl and incubated for 3 h at 95 °C, shaking. The extracts were diluted and 400 µl was combined with 10 µl phenol and 1 ml concentrated sulfuric acid. After incubation (10 min, 95 °C, shaking) the absorbance was measured at 490 nm using a plate reader. Glucose was used as the standard.

3.6.10 Quantification of photosynthetic parameters

FlourPen (FP110-LM/X; Photon System Instruments, Drásov, Czech Republic) protocols NPQ2 and LC3 were used for pulse amplitude modulation fluorometry. Before each measurement, cotyledons or leaves of 12-day-old plants were dark adapted by covering them with leaf clips for 15 min.

Photosynthesis and respiration rates were measured under ambient conditions using an Oxygraph+ with LeafLab2 (Hansatech Instruments Ltd, Norfolk, UK). About 200 µl of 1 M $NaHCO_3$ was added to each measurement chamber. Samples were light adapted to 200 µmol photons s^{-1} m^{-2} for 7 min and respiration rates were measured in 500 and 1000 µmol photons s^{-1} m^{-2} light were measured followed by respiration rate measurement in the dark. Leaf area and DW were measured.

3.6.11 Protein extraction, digestion, and sample preparation for proteome analysis via mass spectrometry

The procedure is based on the ’single-pot solid-phase-enhanced sample preparations (SP3)’ protocol for proteomics experiments of HUGHES ET AL. (2019) and MIKULÁŠEK ET AL. (2021). The detailed adapted protocol, which was used here, can be found in ANGERMANN ET AL. (2024). In brief, proteins were solubilized with sodium dodecyl sulfate (SDS) from lyophilized plant powder. Disulfide bridges were reduced with dithiothreitol (DTT) and subsequently alkylated with iodoacetamide (IAM). Equal shares (v/v) of hydrophobic and hydrophilic magnetic beads (No. 441521050250, No. 241521050250, Sera-Mag; Cytiva, Marlborough, MA, USA) were mixed to bind the denatured proteins. The beads were washed multiple times with 80 % ethanol to get

rid of interfering components for the digestion. Finally, the proteins were digested overnight with trypsin (Mass Spectrometry Grade; Promega Corporation, Madison, WI, USA). The peptide-containing supernatants were collected and desalted on 50 mg Sep-Pak tC18 columns (Waters, Milford, MA, USA). The purified peptides were quantified with a quantitative Peptide Assay Kit (Thermo Fisher Scientific, Rockford, IL, USA) and adjusted to 400 ng μl^{-1} in 0.1 % formic acid.

3.6.12 Quantitative shotgun proteomics by ion mobility mass spectrometry (IMS-MS/MS)

For the cotyledon timeline experiment and the cotyledon removal experiment, 400 ng peptides were injected via a nanoElute1 UHPLC (Bruker Daltonics GmbH, Bremen, Germany) and separated on an analytical reversed-phase C18 column (Aurora Ultimate 25 cm × 75 µm, 1.6 µm, 120 Å; IonOpticks, Collingwood, Vic, Australia). Using MS grade water and a multistage gradient acetonitrile containing 0.1 % formic acid (0 min, 2 %; 54 min, 25 %; 60 min, 37 %; 62 min, 95 %; 70 min, 95 %), peptides were eluted and ionized by electrospray ionization with a CaptiveSpray1 ion source and a flow rate of 300 nl min^{-1}. The ionized peptides were separated, fragmented, and analysed with a standard data-dependent acquisition parallel accumulation–serial fragmentation application method (DDA-PASEF) of the system with the following settings: Ion mobility window: 0.6 – 1.6 cm^{-2} V^{-1} s^{-1}, 10 PASEF ramps, target intensity of 20 000 (threshold 2 500), and a cycle time of ~1.1 sec. The analysis was performed on a timsTOF-Pro2 mass spectrometer (Bruker Daltonics GmbH).

For the comparison of cotyledons with true leaves (M2-Fig. 3, Supp. Dataset S3) 400 ng of peptides were injected via a nanoElute2 UHPLC (Bruker Daltonics GmbH) and separated on the same type of analytical column as described above. Using the same multistage gradient as above, but here peptides were ionized by a CaptiveSpray2 ion source and analysed on a timsTOF-HT mass spectrometer (Bruker Daltonics GmbH), which had the following DDA-PASEF settings: Ion mobility window of 0.7 –1.5 cm^{-2} V^{-1} s^{-1}, 4 PASEF ramps, target intensity 14 500 (threshold 1 200), and a cycle time of ~0.53 sec.

3.6.13 Data processing and functional annotation

The ion mobility spectrometry (IMS)–MS/MS spectra from all experiments were analysed with the MaxQuant software (Cox and Mann, 2008) using default search

parameters and the proteome database of *Lupinus albus* published by XU ET AL. (2020) on UniProt.org (UP000464885) for protein identification. The calculation of label-free quantification (LFQ) values and intensity-based absolute quantification (iBAQ) values was both enabled. Data evaluation was performed using Perseus (TYANOVA ET AL., 2016). Proteins were excluded from further analysis if they were not detected in at least four out of five biological replicates in at least one of the sample groups. Subsequently, missing values were replaced with randomly chosen low values from a normal distribution. Significant changes were calculated from the LFQ values using Student's t-tests ($p = 0.05$). Furthermore, a Fisher exact test was performed to identify significantly enriched or depleted metabolic pathways. A recently published annotation database of *Lupinus albus* was used to obtain further information such as subcellular localization and metabolic pathway involvement (ANGERMANN ET AL., 2024).

3.6.14 Statistical analysis

Statistical analysis for the cotyledon timeline experiment and the cotyledon removal experiment was performed using one-way analysis of variance (ANOVA) followed by Tukey's honest significant difference (HSD) post hoc test using R version 4.5.0. Differences between group means were considered statistically significant at $p < 0.05$. Letter-based significance grouping was used to indicate statistically homogeneous groups; means that share the same letter do not differ significantly.

Statistical analysis for the comparison of cotyledons with true leaves was performed using Student's t-tests (two-tailed test, pooled variance). Sample groups were compared with the control (cotyledons: day 0; remaining plants: day 28) at $p = 0.05$.

3.7 Data availability statement

The mass spectrometry proteomics data have been deposited to the ProteomeXchange Consortium (http://proteomecentral.proteomexchange.org) via the PRIDE partner repository (PEREZ-RIVEROL ET AL., 2022) with the dataset identifier PXD054416.

3.8 Funding

Research in TMH's lab is funded by the Deutsche Forschungsgemeinschaft (DFG, German Research Foundation) under Germany´s Excellence Strategy – EXC-2048/1 – project ID 390686111. The proteomics unit in TMH's lab (timsTOF-HT, Bruker Daltonics) is funded via DFG-INST 216/1290-1 FUGG.

3.9 Author contributions

TMH, CA, and BH designed the research; CA and BH performed and evaluated the shotgun proteomics experiments; CA and BH measured and evaluated amino acid profiles; BBN quantified phosphate; HJM conducted experiments and analysed data for mineral nutrient quantification; CA performed all the other experiments; TMH, CA, and BH analysed the data; TMH and CA wrote the paper with support from all other authors; HJM and PB wrote and corrected text; TMH agrees to serve as the author responsible for contact and ensures communication.

3.10 Acknowledgments

We thank Pascal Klein for preliminary work on this project, Christina Mack and Dagmar Lewejohann for skilful technical assistance, and Tim Hildebrandt for being curious and asking the right questions. We thank Alberto Andrino de la Fuente for support during C/N analysis. The authors thank the MS Platform and Sabine Metzger, University of Cologne, for conducting and providing support in the ICP-MS measurements. We thank Lorna Egan-Andreou for the graphic design of the lupin development scheme. Research in TMH's lab is funded by the Deutsche Forschungsgemeinschaft (DFG, German Research Foundation) under Germany's Excellence Strategy – EXC-2048/1 – project ID 390686111. The proteomics unit in TMH's lab (timsTOF-HT, Bruker Daltonics) is funded via DFG-INST 216/1290-1 FUGG. Open Access funding enabled and organized by Projekt DEAL.

3.11 Supplemental data

Supp. Dataset S1:	Metabolite profiles of cotyledons and 28-day-old plants.
Supp. Dataset S2:	Reorganization of the cotyledon proteome during transformation from storage organ to photosynthetic tissue: cotyledon proteome data.
Supp. Dataset S3:	Metabolite profiles and proteome data of true leaves vs. cotyledons at day 12.
Supp. Dataset S4:	Plant proteome at day 28 after detaching the cotyledons at different timepoints.

3.12 Supplemental figures

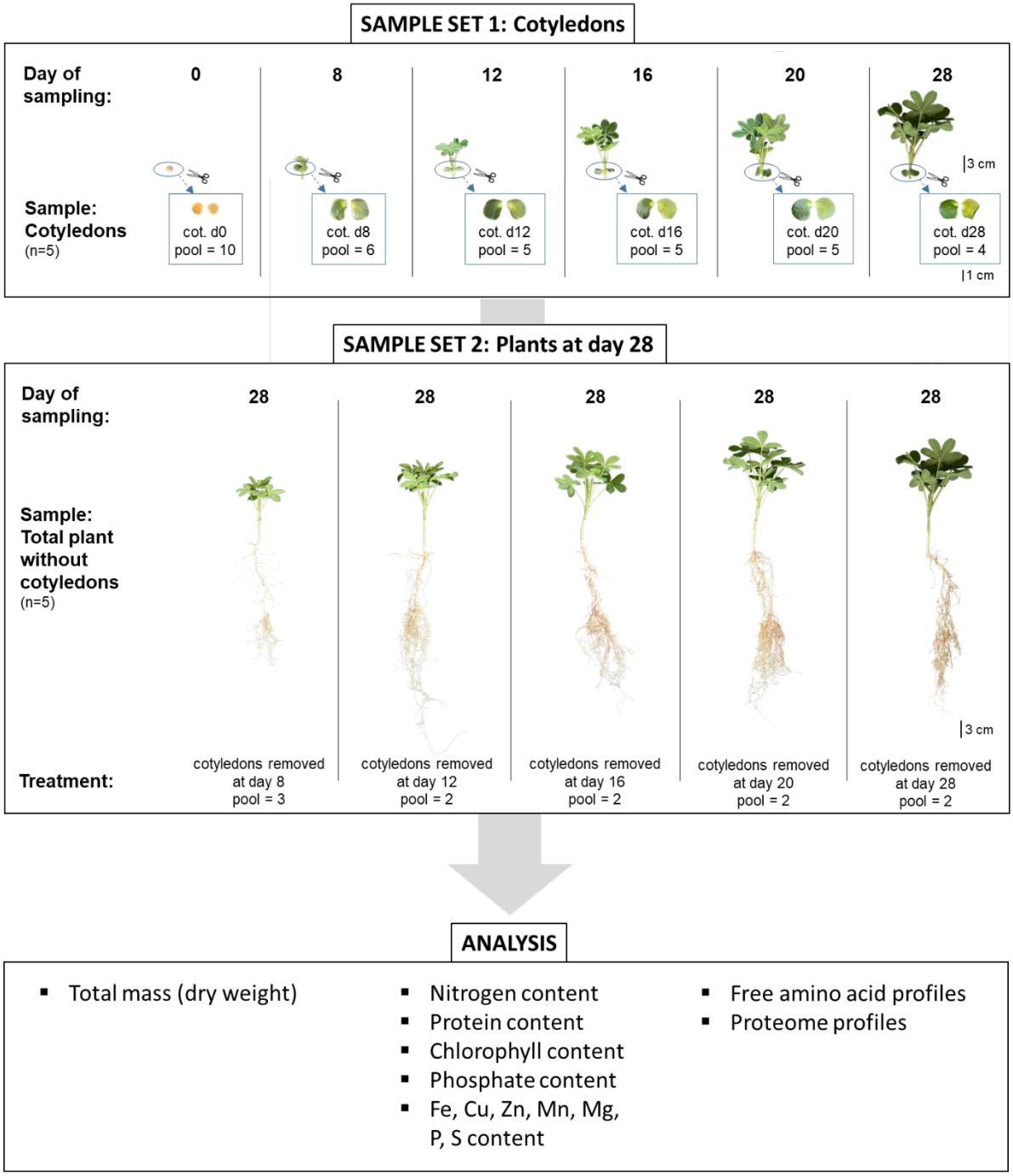

M2-Fig. S1: Scheme of the experimental set-up: *Lupinus albus* plants were grown for twenty-eight days the absence of rhizobia and without nitrogen fertilization. The cotyledons were removed from subsets of these plants at day 8, 12, 16, 20 or 28 after sowing and harvested for subsequent analysis. Cotyledons of seeds were harvested as control. The remaining plants without cotyledons were harvested for subsequent analysis at day 28. The complete dataset is provided as Supp. Datasets S1 and S2.

A

Functional protein categories	Number of proteins	Protein [mg · g DW^{-1}] 0d	8d	12d	16d	20d	28d
Storage proteins	23	93.7	45.7	25.4	12.8	9.5	11.4
Protein metabolism	1005	47.0	42.1	40.5	36.2	34.0	31.3
Lipid metabolism	220	46.9	19.5	16.4	11.8	9.7	8.9
Vesicle trafficking	134	1.6	1.2	1.4	1.3	1.1	1.2
Cell	323	33.7	12.2	11.4	9.2	8.0	8.6
Stress	169	15.5	9.3	9.1	7.7	7.9	8.9
Redox	131	11.2	8.9	9.1	8.1	7.6	7.9
Secondary metabolism	115	2.5	2.4	2.4	2.4	2.1	1.8
Amino acid metabolism	167	2.3	5.3	5.4	5.1	4.7	4.1
Carbohydrate metabolism	270	11.9	12.7	13.4	12.6	11.3	10.8
Cellular respiration	200	9.5	16.2	18.0	16.6	15.1	14.3
Coenzyme metabolism	111	1.0	2.6	2.2	2.0	1.8	1.8
Nucleotide metabolism	73	1.2	1.6	1.8	1.7	1.7	1.7
Photosynthesis	191	3.1	45.1	58.9	62.9	62.3	62.2
Signalling	79	0.9	1.2	1.5	1.5	1.5	1.8
DNA	64	2.0	2.2	2.9	3.3	3.8	4.2
RNA	313	2.8	3.1	3.3	3.2	3.3	3.2
Nutrient uptake	19	0.2	0.3	0.3	0.2	0.3	0.4
Hormone metabolism	73	1.6	1.2	1.6	1.5	1.5	2.0
Transport	180	7.0	6.7	6.8	6.7	6.6	7.1

B

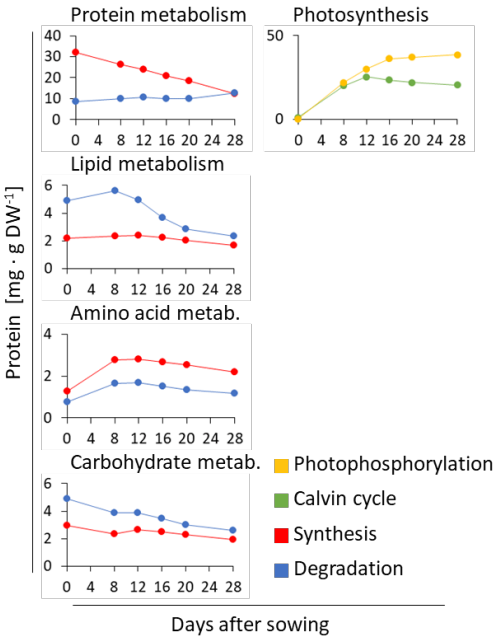

M2-Fig. S2: Protein abundance profiles of functional protein categories during *Lupinus albus* cotyledon development. (**A**) Relative protein abundance of functional protein categories and number of different proteins detected in the respective category. Categories were adapted from MapMan4. (**B**) Protein abundance profiles of selected functional categories. The complete dataset is provided as Supp. Dataset S2.

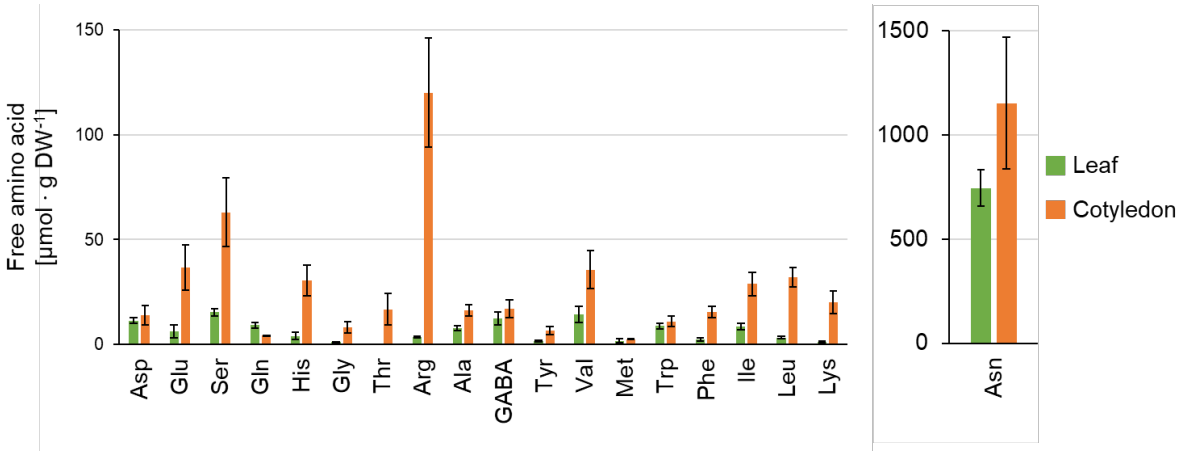

M2-Fig. S3: Free amino acid contents of cotyledons and true leaves at day 12. The complete dataset is provided as Supp. Dataset S3.

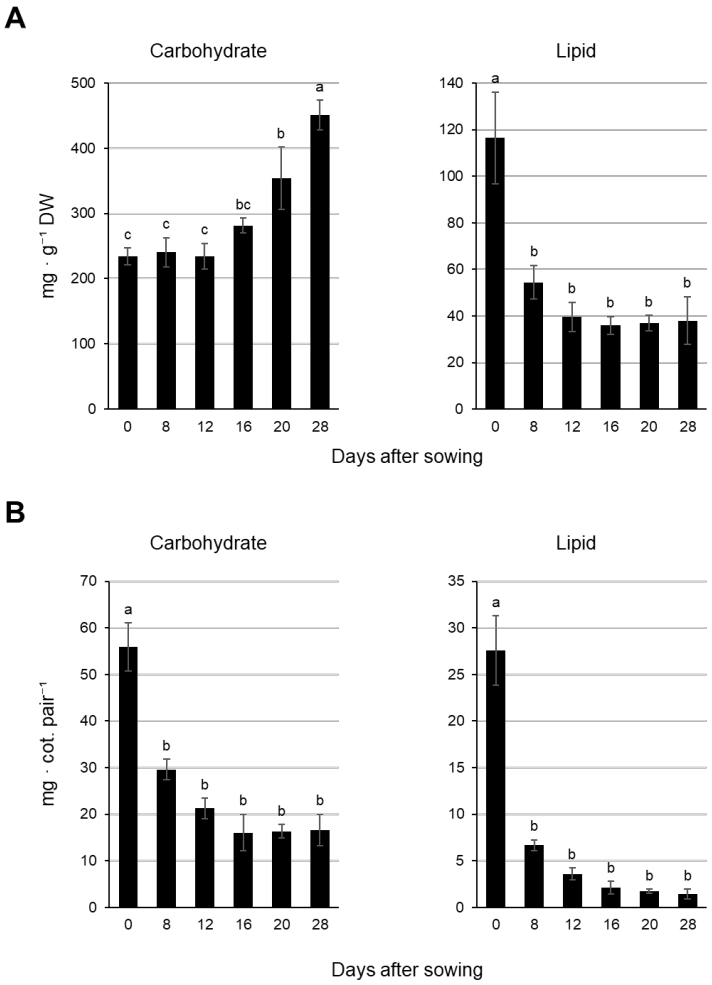

M2-Fig. S4: Carbohydrate and lipid quantities in cotyledons. (**A**) Relative amounts. (**B**) Absolute amounts. Data presented are means ± SD (n = 5). Means were compared using one-way ANOVA followed by Tukey's HSD test. Letter-based significance grouping was used at a significance level of $p < 0.05$; means sharing the same letter are not significantly different. The complete dataset is provided as Supp. Dataset S1.

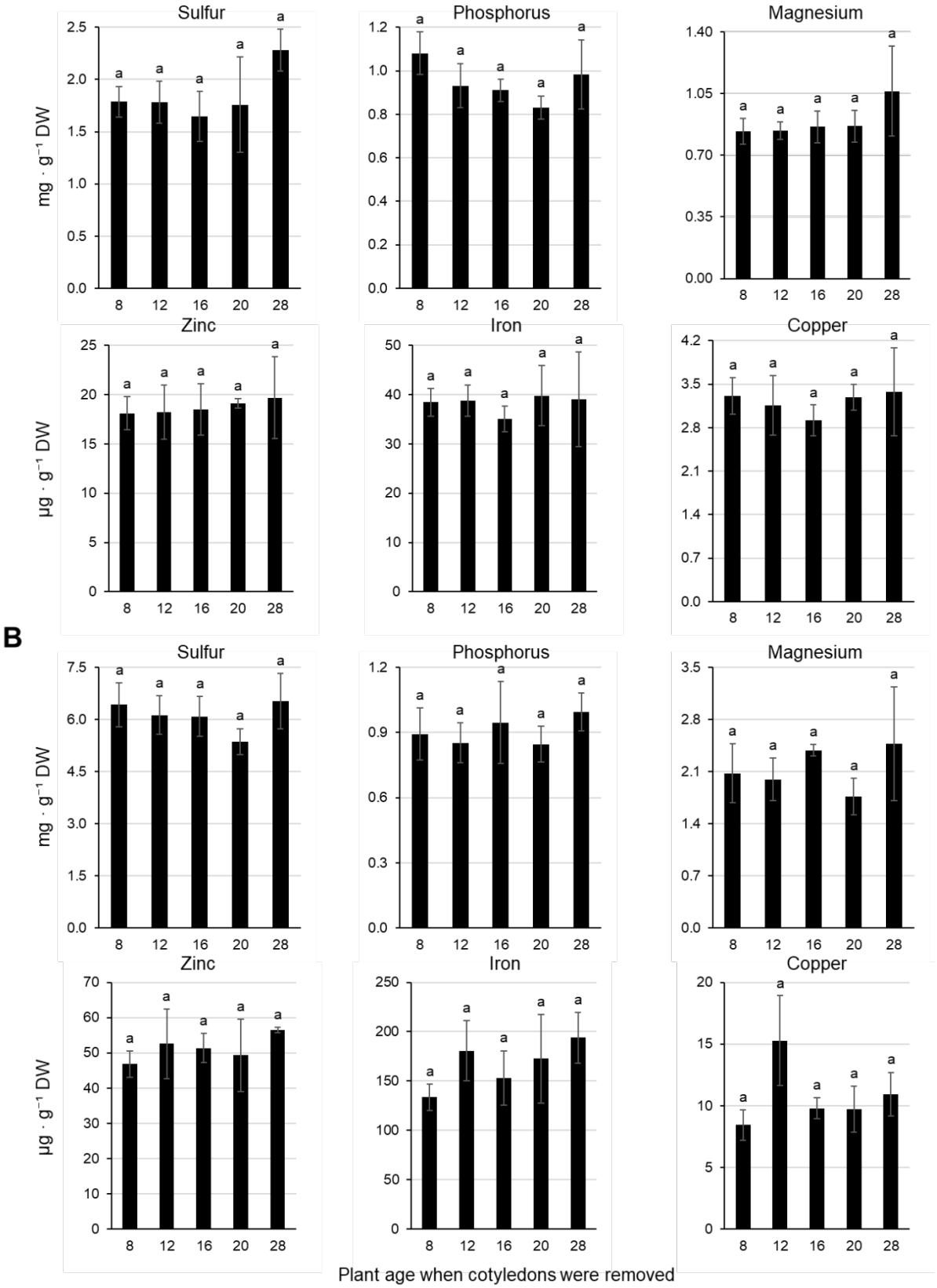

M2-Fig. S5: Mineral contents of shoots and roots at day 28. (**A**) Shoot. (**B**) Root. Data presented are means ± SD (n = 3). Means were compared using one-way ANOVA followed by Tukey's HSD test. Letter-based significance grouping was used at a significance level of $p < 0.05$; means sharing the same letter are not significantly different. Complete dataset is provided as Supp. Dataset S1.

Nitrogen saving strategies after removal of cotyledons:

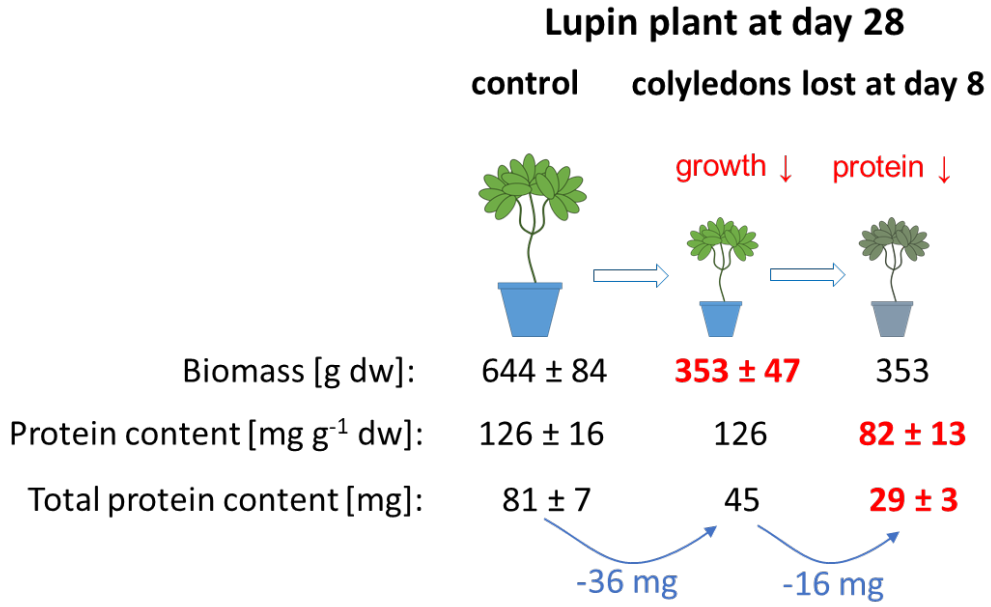

1. Reducing **plant biomass** from 644 to 353 mg dry weight

   ⇨ saves **36 mg protein**

2. Reducing **protein content** from 126 to 82 mg protein g^{-1} dry weight

   ⇨ saves **16 mg protein**

M2-Fig. S6: Nitrogen saving strategies after removal of the cotyledons: The plant is able to save 15.5 mg protein by reducing its relative protein content by 35 % from 126 ± 16 to 82 ± 13 mg g^{-1} DW after premature cotyledon loss at day 8. The most effective nitrogen saving strategy, however, is the reduction in plant biomass from 644 ± 84 to 353 ± 47 mg dry weight that, based on the mean tissue protein content of the control plant, would save 36.7 mg protein.

3.13 References

Abraham, E.M., Ganopoulos, I., Madesis, P., Mavromatis, A., Mylona, P., Nianiou-Obeidat, I., Parissi, Z., Polidoros, A., Tani, E. and Vlachostergios, D. (2019) The Use of Lupin as a Source of Protein in Animal Feeding: Genomic Tools and Breeding Approaches. *Int. J. Mol. Sci.*, 20.

Andrino, A., Boy, J., Mikutta, R., Sauheitl, L. and Guggenberger, G. (2019) Carbon Investment Required for the Mobilization of Inorganic and Organic Phosphorus Bound to Goethite by an Arbuscular Mycorrhiza (*Solanum lycopersicum* x *Rhizophagus irregularis*). *Front. Environ. Sci.*, 7.

Angermann, C., Heinemann, B., Hansen, J., Töpfer, N., Braun, H.-P. and Hildebrandt, T.M. (2024) Proteome reorganization and amino acid metabolism during germination and seedling establishment in *Lupinus albus*. *J. Exp. Bot.*, 75, 4891–4903.

Baker, A., Graham, I.A., Holdsworth, M., Smith, S.M. and Theodoulou, F.L. (2006) Chewing the fat: beta-oxidation in signalling and development. *Trends Plant Sci.*, 11, 124–132.

Batista-Silva, W., Heinemann, B., Rugen, N., Nunes-Nesi, A., Araújo, W.L., Braun, H.-P. and Hildebrandt, T.M. (2019) The role of amino acid metabolism during abiotic stress release. *Plant Cell Environ.*, 42, 1630–1644.

Belski, R. (2012) Fiber, protein, and lupin-enriched foods: role for improving cardiovascular health. *Adv. Food. Nutr. Res.*, 66, 147–215.

Borek, S., Pukacka, S., Michalski, K. and Ratajczak, L. (2009) Lipid and protein accumulation in developing seeds of three lupine species: *Lupinus luteus* L., *Lupinus albus* L., and *Lupinus mutabilis* Sweet. *J. Exp. Bot.*, 60, 3453–3466.

Borek, S., Kubala, S. and Kubala, S. (2012) Regulation by sucrose of storage compounds breakdown in germinating seeds of yellow lupine (*Lupinus luteus* L.), white lupine (*Lupinus albus* L.) and Andean lupine (*Lupinus mutabilis* Sweet): I. Mobilization of storage protein. *Acta Physiol. Plant*, 34, 701–711.

Borek, S., Kubala, S., Kubala, S. and Ratajczak, L. (2011) Comparative study of storage compound breakdown in germinating seeds of three lupine species. *Acta Physiol. Plant*, 33, 1953–1968.

Brown, A.V. and Hudson, K.A. (2015) Developmental profiling of gene expression in soybean trifoliate leaves and cotyledons. *BMC plant biol.*, 15, 169.

Chassot, C., Nawrath, C. and Métraux, J.-P. (2007) Cuticular defects lead to full immunity to a major plant pathogen. *Plant J.*, 49, 972–980.

Chiou, T.-J., Aung, K., Lin, S.-I., Wu, C.-C., Chiang, S.-F. and Su, C.-L. (2006) Regulation of phosphate homeostasis by MicroRNA in *Arabidopsis*. *Plant Cell*, 18, 412–421.

Conte, S.S., Chu, H.H., Rodriguez, D.C., Punshon, T., Vasques, K.A., Salt, D.E. and Walker, E.L. (2013) *Arabidopsis thaliana* Yellow Stripe1-Like4 and Yellow Stripe1-Like6 localize to internal cellular membranes and are involved in metal ion homeostasis. *Front. Plant Sci.*, 4, 283.

Cox, J. and Mann, M. (2008) MaxQuant enables high peptide identification rates, individualized p.p.b.-range mass accuracies and proteome-wide protein quantification. *Nat. Biotechnol*., 26, 1367–1372.

El-Amhir, S.-H., Lamont, B.B., He, T. and Yan, G. (2017) Small-seeded *Hakea* species tolerate cotyledon loss better than large-seeded congeners. *Sci. Rep.*, 7, 41520.

Elango, D., Rajendran, K., van der Laan, L., Sebastiar, S., Raigne, J., Thaiparambil, N.A., El Haddad, N., Raja, B., Wang, W., Ferela, A., Chiteri, K.O., Thudi, M., Varshney, R.K., Chopra, S., Singh, A. and Singh, A.K. (2022) Raffinose Family Oligosaccharides: Friend or Foe for Human and Plant Health? *Front. Plant Sci.*, 13, 829118.

Farmer, E.E., Gao, Y.-Q., Lenzoni, G., Wolfender, J.-L. and Wu, Q. (2020) Wound- and mechanostimulated electrical signals control hormone responses. *New Phytol.*, 227, 1037–1050.

Gdala, J. and Buraczewska, L. (1996) Chemical composition and carbohydrate content of seeds from several lupin species. *J. Anim. Feed Sci.*, 5, 403–416.

Gonzalez, D.O. and Vodkin, L.O. (2007) Specific elements of the glyoxylate pathway play a significant role in the functional transition of the soybean cotyledon during seedling development. *BMC Genomics*, 8, 468.

Graham, I.A. (2008) Seed storage oil mobilization. *Annu. Rev. Plant. Biol.*, 59, 115–142.

Hanley, M.E. and Fegan, E.L. (2007) Timing of cotyledon damage affects growth and flowering in mature plants. *Plant Cell Environ.*, 30, 812–819.

Hanley, M.E. and May, O.C. (2006) Cotyledon damage at the seedling stage affects growth and flowering potential in mature plants. *New Phytol.*, 169, 243–250.

Harris, M., Mackender, R.O. and Smith, D.L. (1986) Photosynthesis of cotyledons of soybean seedlings. *New Phytol.*, 104, 319–329.

Hu, X.W., Zhang, R., Wu, Y.P. and Baskin, C.C. (2017) Seedling tolerance to cotyledon removal varies with seed size: A case of five legume species. *Ecol. Evol.*, 7, 5948–5955.

Hughes, C.S., Moggridge, S., Müller, T., Sorensen, P.H., Morin, G.B. and Krijgsveld, J. (2019) Single-pot, solid-phase-enhanced sample preparation for proteomics experiments. *Nat. Protoc.*, 14, 68–85.

James, E.K., Minchin, F.R., Iannetta, P.P.M. and Sprent, J.I. (1997) Temporal Relationships between Nitrogenase and Intercellular Glycoprotein in Developing White Lupin Nodules. *Ann. Bot.*, 79, 493–503.

Karnpanit, W., Coorey, R., Clements, J., Benjapong, W. and Jayasena, V. (2017) Calcium, Iron, and Zinc Bioaccessibilities of Australian Sweet Lupin (*Lupinus angustifolius* L.) Cultivars. *J. Agric. Food Chem.*, 65, 4722–4727.

Khan, M.A., Castro-Guerrero, N.A., McInturf, S.A., Nguyen, N.T., Dame, A.N., Wang, J., Bindbeutel, R.K., Joshi, T., Jurisson, S.S., Nusinow, D.A. and Mendoza-Cozatl, D.G. (2018) Changes in iron availability in *Arabidopsis* are rapidly sensed in the leaf vasculature and impaired sensing leads to opposite transcriptional programs in leaves and roots. *Plant Cell Environ.*, 41, 2263–2276.

Lanquar, V., Lelièvre, F., Bolte, S., Hamès, C., Alcon, C., Neumann, D., Vansuyt, G., Curie, C., Schröder, A., Krämer, U., Barbier-Brygoo, H. and Thomine, S. (2005) Mobilization of vacuolar iron by AtNRAMP3 and AtNRAMP4 is essential for seed germination on low iron. *EMBO J.*, 24, 4041–4051.

Lea, P.J. and Flowden, L. (1975) The purification and properties of glutamine-dependent asparagine synthetase isolated from *Lupinus albus*. *Proc. R. Soc. B. Biol. Sci.*, 192, 13–26.

Lea, P.J., Sodek, L., Parry, M., Shewry, P.R. and Halford, N.G. (2007) Asparagine in plants. *Ann. Appl. Biol.*, 150, 1–26.

Li, J., Wang, L., Zheng, L., Wang, Y., Chen, X. and Zhang, W. (2018) A Functional Study Identifying Critical Residues Involving Metal Transport Activity and Selectivity in Natural Resistance-Associated Macrophage Protein 3 in *Arabidopsis thaliana*. *Int. J. Mol. Sci.*, 19, 1430.

Lichtenthaler, H.K. (1987) Chlorophylls and carotenoids: Pigments of photosynthetic biomembranes. *Methods Enzymol.*, 148, 350–382.

Liebermeister, W., Noor, E., Flamholz, A., Davidi, D., Bernhardt, J. and Milo, R. (2014) Visual account of protein investment in cellular functions. *Proc. Natl. Acad. Sci. U.S.A*, 111, 8488–8493.

Lovell, P.H. and Moore, K.G. (1970) A Comparative Study of Cotyledons as Assimilatory Organs. *J. Exp. Bot.*, 21, 1017–1030.

Lucas, M.M., Stoddard, F.L., Annicchiarico, P., Frías, J., Martínez-Villaluenga, C., Sussmann, D., Duranti, M., Seger, A., Zander, P.M. and Pueyo, J.J. (2015) The future of lupin as a protein crop in Europe. *Front. Plant Sci.*, 6, 705.

Mikulášek, K., Konečná, H., Potěšil, D., Holánková, R., Havliš, J. and Zdráhal, Z. (2021) SP3 Protocol for Proteomic Plant Sample Preparation Prior LC-MS/MS. *Front. Plant Sci.*, 12, 635550.

Neumann, G., Massonneau, A., Martinoia, E. and Römheld, V. (1999) Physiological adaptations to phosphorus deficiency during proteoid root development in white lupin. *Planta*, 208, 373–382.

Nunes, T.C., Ferreira, C.S., Williams, T.C.R. and Franco, A.C. (2024) Cotyledons as the primary source of carbon and mineral nutrients during early growth of a savanna tree. *Theor. Exp. Plant Physiol.*, 36, 265–282.

O'Sullivan, J.B., Jin, J. and Tang, C. (2022) White lupin (*Lupinus albus* L.) exposed to elevated atmospheric CO_2 requires additional phosphorus for N_2 fixation. *Plant Soil.*, 476, 477–490.

Orlovskis, Z. and Reymond, P. (2020) Pieris brassicae eggs trigger interplant systemic acquired resistance against a foliar pathogen in *Arabidopsis*. *New Phytol.*, 228, 1652–1661.

Page, V., Le Bayon, R.-C. and Feller, U. (2006) Partitioning of zinc, cadmium, manganese and cobalt in wheat (*Triticum aestivum*) and lupin (*Lupinus albus*) and further release into the soil. *Environ. Exp. Bot.*, 58, 269–278.

Park, J., Jeong, H.J., Yoon, E.Y. and Moon, S.J. (2016) Easy and rapid quantification of lipid contents of marine dinoflagellates using the sulpho-phospho-vanillin method. *ALGAE*, 31, 391–401.

Pereira, A., Ramos, F. and Sanches Silva, A. (2022) Lupin (*Lupinus albus* L.) Seeds: Balancing the Good and the Bad and Addressing Future Challenges. *Molecules*, 27, 8557.

Perez-Riverol, Y., Bai, J., Bandla, C., García-Seisdedos, D., Hewapathirana, S., Kamatchinathan, S., Kundu, D.J., Prakash, A., Frericks-Zipper, A., Eisenacher, M., Walzer, M., Wang, S., Brazma, A. and Vizcaíno, J.A. (2022) The PRIDE database resources in 2022: a hub for mass spectrometry-based proteomics evidences. *Nucleic Acids Res.*, 50, D543-D552.

Piedra-García, D. and Struck, C. (2021) Lupin Root Weevils (*Charagmus* spp., Curculionidae: Sitonini), a Lupin Pest: A Review of Their Distribution, Biology, and Challenges in Integrated Pest Management. *Insects*, 12, 950.

Pracharoenwattana, I., Cornah, J.E. and Smith, S.M. (2005) *Arabidopsis* peroxisomal citrate synthase is required for fatty acid respiration and seed germination. *Plant Cell*, 17, 2037–2048.

Pracharoenwattana, I. and Smith, S.M. (2008) When is a peroxisome not a peroxisome? *Trends Plant Sci.*, 13, 522–525.

Pueyo, J.J., Quiñones, M.A., La Coba de Peña, T., Fedorova, E.E. and Lucas, M.M. (2021) Nitrogen and Phosphorus Interplay in Lupin Root Nodules and Cluster Roots. *Front. Plant Sci.*, 12, 644218.

Raghothama, K.G. (2005) Phosphorus and Plant Nutrition: An Overview. In Phosphorus. Agriculture and the environment (Sims, J.T. and Sharpley, A.N., eds). Madison, Wisconsin: American Society of Agronomy, pp. 353–378.

Sanyal, R., Kumar, S., Pattanayak, A., Kar, A. and Bishi, S.K. (2023) Optimizing raffinose family oligosaccharides content in plants: A tightrope walk. *Front. Plant Sci.*, 14, 1134754.

Savatin, D.V., Gramegna, G., Modesti, V. and Cervone, F. (2014) Wounding in the plant tissue: the defense of a dangerous passage. *Front. Plant Sci.*, 5, 470.

Spina, A., Benedetti, S. de, Heinzl, G.C., Ceravolo, G., Magni, C., Emide, D., Castorina, G., Consonni, G., Canale, M. and Scarafoni, A. (2024) Biochemical Characterization of the Seed Quality of a Collection of White Lupin Landraces from Southern Italy. *Plants*, 13, 785.

Ströcker, K., Wendt, S., Kirchner, W.H. and Struck, C. (2013) Feeding preferences of the weevils Sitona gressorius and Sitona griseus on different lupin genotypes and the role of alkaloids. *Arthropod-Plant Interact.*, 7, 579–589.

Tamboli, F.A., More, H.N., Bhandugare, S.S., Patil, A.S., Jadhav, N.R. and Killedar, S.G. (2020) Estimation of Total Carbohydrate content by Phenol Sulfuric acid Method from *Eichhornia crassipes* (Mart.) Solms. *AJRC*, 13, 357–359.

Tarantino, D., Morandini, P., Ramirez, L., Soave, C. and Murgia, I. (2011) Identification of an *Arabidopsis* mitoferrinlike carrier protein involved in Fe metabolism. *Plant Physiol. Biochem.*, 49, 520–529.

Thomine, S., Lelièvre, F., Debarbieux, E., Schroeder, J.I. and Barbier-Brygoo, H. (2003) AtNRAMP3, a multispecific vacuolar metal transporter involved in plant responses to iron deficiency. *Plant J*., 34, 685–695.

Tiziani, R., Mimmo, T., Valentinuzzi, F., Pii, Y., Celletti, S. and Cesco, S. (2020) Root Handling Affects Carboxylates Exudation and Phosphate Uptake of White Lupin Roots. *Front. Plant Sci*., 11, 584568.

Tyanova, S., Temu, T., Sinitcyn, P., Carlson, A., Hein, M.Y., Geiger, T., Mann, M. and Cox, J. (2016) The Perseus computational platform for comprehensive analysis of (prote)omics data. *Nat. Methods*, 13, 731–740.

Wang, L., Liu, P.-C., Wu, L.M., Tan, J., Peacock, W.J. and Dennis, E.S. (2019) Cotyledons contribute to plant growth and hybrid vigor in *Arabidopsis*. *Planta*, 249, 1107–1118.

Xu, W., Zhang, Q., Yuan, W., Xu, F., Muhammad Aslam, M., Miao, R., Li, Y., Wang, Q., Li, X., Zhang, X., Zhang, K., Xia, T. and Cheng, F. (2020) The genome evolution and low-phosphorus adaptation in white lupin. *Nat. Commun.*, 11, 1069.

Yang, N., Jiang, W., Jiang, B., Liu, J., Liu, Y., Wang, H., Guo, X. and Tang, Z. (2021) Cotyledon loss of *Astragalus membranaceus* hindered seedling establishment through mineral element reallocation and carbohydrate depletion. *Plant Physiol. Biochem.*, 167, 481–491.

Zhang, S., Zhao, C. and Lamb, E.G. (2011) Cotyledon damage affects seed number through final plant size in the annual grassland species *Medicago lupulina*. *Ann. Bot*., 107, 437–442.

Zheng, W., Wang, P., Zhang, H. and Zhou, D. (2011) Photosynthetic Characteristics of the Cotyledon and First True Leaf of Castor ('*Ricinus communis*' L.). *Aust. J. Crop Sci.*, 5, 702–708.

4 Manuscript 3: The seed mitochondrial proteome of *Lupinus albus* provides insight into energy metabolism during germination

Cecile Angermann[1], Hans-Peter Braun[2], Tatjana M. Hildebrandt[1]

bioRxiv 2025.09.19.677279; https://doi.org/10.1101/2025.09.19.677279

[1]Institute for Plant Sciences, Cluster of Excellence on Plant Sciences (CEPLAS), University of Cologne, Zülpicher Straße 47a, 50674 Cologne, Germany

[2]Institute of Plant Genetics, Leibniz Universität Hannover, Herrenhäuser Str. 2, 30419 Hannover, Germany.

Type of authorship:	First author
Type of article:	Research article, preprint
Contribution to the publication:	I participated in the design of the project. I performed all the experiments, analysed the data with TMH's support and prepared all the figures. I contributed to the writing of the manuscript.
Journal:	bioRxiv
Date of publication:	21. September 2025
DOI:	10.1101/2025.09.19.677279

4.1 Abstract

Despite their essential role in fuelling the onset of metabolism, the composition and functional state of seed mitochondria are still a matter of debate. Using white lupin (*Lupinus albus*) as a model, we provide a comprehensive proteomic characterization of seed mitochondria in a legume with protein-rich reserves. Highly enriched mitochondrial fractions isolated from quiescent seeds revealed fully assembled oxidative phosphorylation (OXPHOS) complexes and supercomplexes, demonstrating that mitochondria are preconfigured for immediate energy production upon imbibition. Quantitative proteomics identified 1,162 mitochondrial proteins and highlighted marked tissue-specific differences compared to leaves, including distinct transporter profiles and a dehydrogenase complement supporting amino acid and fatty acid catabolism. Early germination was accompanied by remodelling of coenzyme metabolism and transport capacity, while core respiratory complexes remained stable. Notably, ~12 % of the proteome consisted of uncharacterized proteins, many of which displayed dynamic changes during early germination, suggesting yet undiscovered, potentially legume-specific mitochondrial functions.

4.2 Introduction

Mitochondria are central integrators of energy metabolism in plants. They generate ATP through the combined action of the tricarboxylic acid (TCA) cycle, other catabolic pathways and the respiratory chain, providing an essential complement to photosynthesis, especially in darkness or in non-green tissues. Beyond energy supply, mitochondria are also key players in redox balance, signal transduction, programmed cell death, and the coordination of metabolic networks (MØLLER ET AL., 2021). The complexity of mitochondrial function is reflected in their molecular and structural organization. Plant mitochondria are small (1–3 µm) double-membrane organelles with cristae and a protein-rich matrix (LOGAN, 2006; TAIZ ET AL., 2023). They are highly dynamic, moving along the cytoskeleton and undergoing fusion and fission (LOGAN, 2006; 2010). Their endosymbiotic origin is evident from the presence of their own genome (BRENNICKE AND LEAVER, 2007). Compared with animals, plant mitochondrial genomes are strikingly larger (10–40-fold), but gene-sparse and dominated by repeats (GUALBERTO AND NEWTON, 2017; ALVERSON ET AL., 2011). Only 1–2 % of the proteome is mitochondrially encoded, while the vast majority of the ~2,000–3,000 proteins are nuclear-encoded and imported via N-terminal targeting sequences (WHITE

AND SCANDALIOS, 1989; RAO ET AL., 2017). The dense protein environment of the matrix promotes the formation of metabolons, which are functional enzyme complexes that enable the direct channelling of metabolites (SWEETLOVE AND FERNIE, 2013). This increases the efficiency of metabolic processes. They also contribute to a high buffer capacity, stabilising the mitochondrial redox balance and preventing toxic increases in coenzyme concentrations (KASIMOVA ET AL., 2006).

Technological advances in isolation and analysis methods such as tag-based pull-down techniques now allow mitochondria to be isolated rapidly and specifically, even from individual tissues and developmental stages (BOUSSARDON ET AL., 2020; KUHNERT ET AL., 2020; NIEHAUS ET AL., 2020). However, mitochondrial preparations from low abundant material remains a challenge (DITZ ET AL., 2025; BOUSSARDON ET AL., 2025). Current studies suggest that mitochondria can be considered plastic in terms of their number, shape and function. These properties vary depending not only on the cell type (LOGAN AND LEAVER, 2000), but also on the developmental stage of the plant (PASZKIEWICZ ET AL., 2017; RODRÍGUEZ ET AL., 2015).

Seeds provide a particularly striking example of a tissue requiring high metabolic plasticity. They tolerate extreme desiccation, remaining viable at water contents as low as 5 - 15 % for years or even decades and thus enable long-term survival and dispersal of plants, even under harsh or fluctuating environments (BEWLEY ET AL., 2013 LINKIES ET AL., 2010). This remarkable resilience depends on a suite of protective mechanisms, including accumulation of osmolytes, non-reducing sugars, antioxidant systems, and specialized proteins such as LEA (Late Embryogenesis Abundant) proteins and heat shock proteins that stabilize cellular structures during drying (SANO ET AL., 2016). Upon rehydration under favourable environmental conditions, metabolic activity resumes within minutes (PASZKIEWICZ ET AL., 2017; NIETZEL ET AL., 2020). Stored carbon and nitrogen reserves are remobilized to provide precursors and energy for repair of storage-induced cellular damage, the resumption of transcription and translation, and the synthesis of metabolites and cellular structures to support cell expansion and growth (WEITBRECHT ET AL., 2011; PASZKIEWICZ ET AL., 2017; LAW ET AL., 2012). Mitochondria provide ATP efficiently through respiration and are thus particularly important for seed vigor with impaired mitochondrial function frequently leading to germination defects (FERGUSON ET AL., 1990; KÜHN ET AL., 2015; RACCA ET AL., 2022).

Despite their central role, the nature of mitochondria in dry seeds remains debated. Early electron microscopy studies described poorly differentiated “pro-mitochondria” lacking cristae and respiratory chain complexes in different plant species (ATTUCCI ET AL., 1991; LOGAN ET AL., 2001; HOWELL ET AL., 2006). In this model, mitochondria would only achieve full functionality after imbibition through rapid synthesis and assembly of oxidative phosphorylation (OXPHOS) complexes (LAW ET AL., 2012; PASZKIEWICZ ET AL., 2017). More recent proteomic and functional studies in *Arabidopsis thaliana*, however, argue that seed mitochondria are already competent, containing pre-assembled respiratory complexes and unique protein adaptations for desiccation tolerance (NIETZEL ET AL., 2020; DITZ ET AL., 2025). This unresolved discrepancy highlights the need for in-depth characterization of mitochondrial proteomes across diverse seed types.

In this study, we characterize the mitochondrial proteome of white lupin (*Lupinus albus*), a legume of agronomic and ecological importance. Lupin seeds are notable for storing a large fraction of their reserves as protein (~40 %), making them an ideal system to study seed-specific adaptations in amino acid and energy metabolism (ANGERMANN ET AL., 2024). Their large size facilitates experimental handling and yields sufficient material for high-purity organelle preparations. Leveraging our curated *L. albus* proteome annotation database, we present a comprehensive analysis of seed mitochondria, revealing distinct compositional features that reflect their specialized role in seed physiology.

4.3 Results

Highly enriched mitochondrial preparations from stratified white lupin seeds provide insight into the seed mitochondrial proteome composition

Upon imbibition under favourable conditions, white lupin seeds rapidly initiate respiration and complete germination with radicle emergence after approximately 30 h (M3-Fig. 1, ANGERMANN ET AL., 2024). This instant metabolic activation suggests that mitochondria are preconfigured to support the transition from quiescence to active growth. Yet, the mechanisms by which mitochondria are primed for this role, and the molecular features that enable them to drive seed metabolism in the context of protein-rich reserves, remain poorly understood. To address these questions, we aimed to isolate highly enriched mitochondrial fractions from seeds in a quiescent state prior to germination. Direct isolation from dry seeds proved technically challenging, prompting

us to apply a cold stratification step. Lupin seeds soaked in demineralized water for 24 h at 4 °C underwent water uptake and swelling while maintaining minimal metabolic activity (M3-Fig. 1). Following transfer to room temperature, they remained viable and proceeded to germination, confirming that the treatment preserved seed physiology.

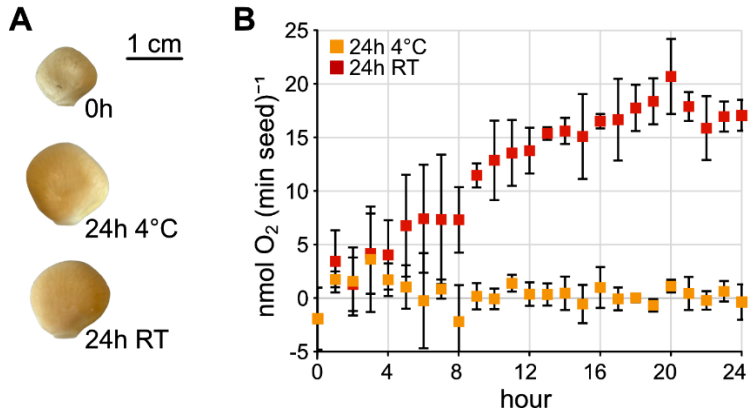

M3-Fig. 1: Imbibed *Lupinus albus* seeds rapidly start respiring at room temperature but not in the cold. (**A**) Pictures of representative *Lupinus albus* seeds in the dry state (0 h) as well as after 24 h imbibition at 4 °C (24 h 4 °C) or room temperature (24 h RT). (**B**) Respiration rates of *Lupinus albus* seeds during imbibition at 4 °C and at room temperature (RT). Data presented are means ± SD (n = 3).

Proteome analysis by two-dimensional (2D) blue-native/SDS polyacrylamide gel electrophoresis (BN/SDS-PAGE) revealed that mitochondria from lupin seeds contain fully assembled OXPHOS complexes and supercomplexes (M3-Fig. 2A). Although the amount of seed tissue was equal for all mitochondrial isolations, the preparations from dry seeds showed only faint bands and spots, most likely reflecting inefficient recovery of the organelles from this starting material. In contrast, 2D gels from imbibed seeds clearly showed the characteristic spot pattern of the respiratory chain complexes I-IV, the ATP synthase (complex V), the supercomplex composed of complex I and dimeric complex III and further complexes like the HSP60 complex, all well-known from work with *Arabidopsis thaliana* (KLODMANN ET AL., 2011).

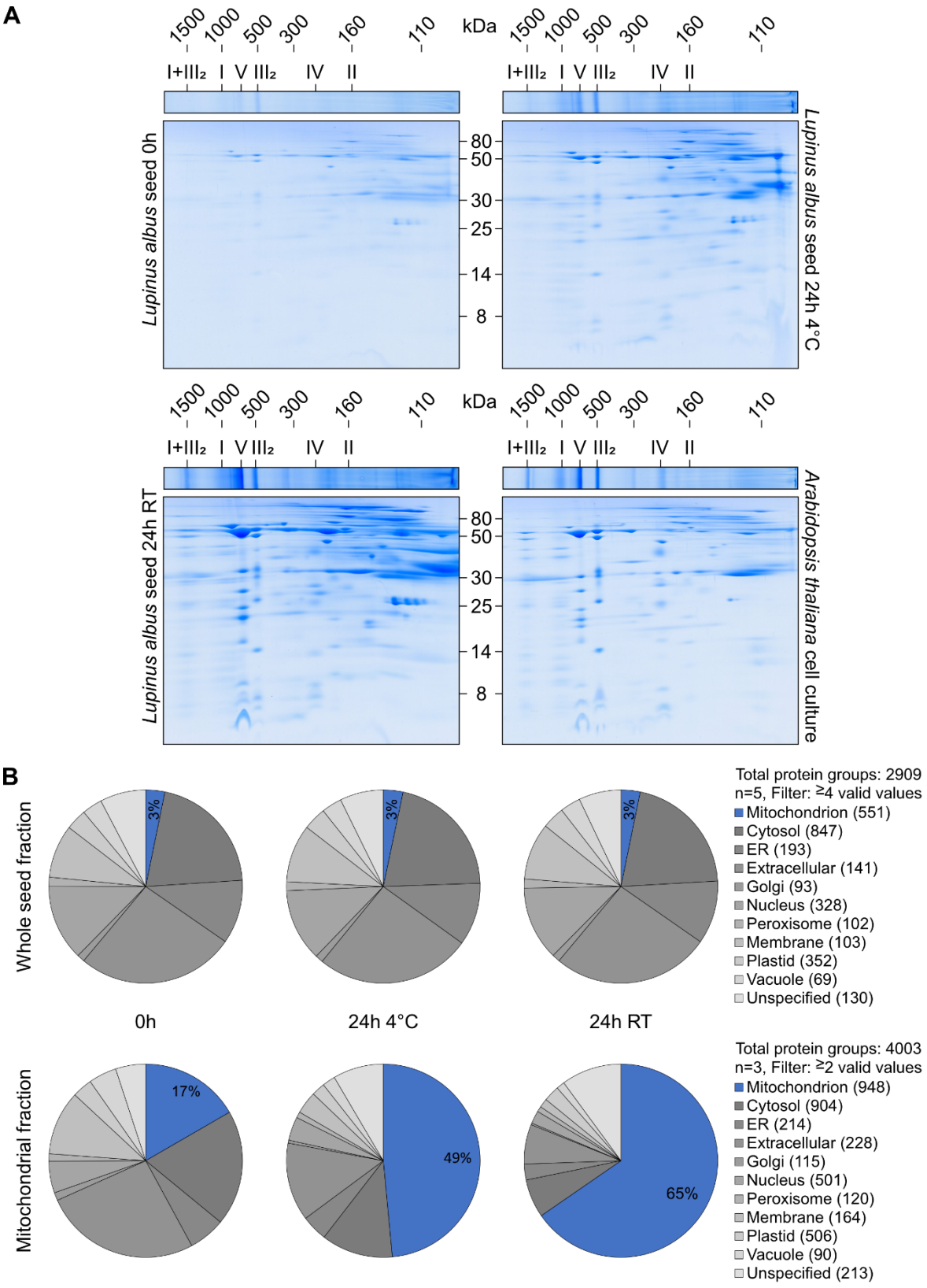

M3-Fig. 2: *Lupinus albus* seed mitochondrial proteomics. (**A**) Analyses of mitochondrial protein complexes from *Lupinus albus* (0 h: top left; 24 h 4 °C: top right; 24 h RT: bottom left) and *Arabidopsis thaliana* (cell culture: bottom right) by 2D BN/SDS-PAGE. Lanes of 1D BN gels were transferred horizontally onto SDS gels for electrophoresis in orthogonal direction (see “Materials and methods” section for details). The identities of the protein complexes as well as molecular masses [kDa] are indicated above the gels (identifications based on *A.*

thaliana reference gels, see KLODMANN ET AL., 2011). Molecular masses of monomeric standard proteins [kDa] are indicated between the gels. (**B**) Quantitative proteome composition of total seed extracts (top) and isolated mitochondrial fractions (bottom). Proteins were assigned to subcellular compartments based on SUBA5 (HOOPER ET AL., 2014) and mass fractions [%] were calculated from cumulated iBAQ values for all compartments. Numbers in parentheses indicate the number of different distinct proteins detected in the respective category. Data presented are means of five replicates for whole seed samples and means of three replicates for mitochondrial fractions. The complete dataset is provided as Supp. Dataset S1.

We analysed the proteome composition of the enriched mitochondrial fractions and the original protein extracts from seeds by LC-MS/MS (Supp. Dataset S1). For protein annotation we used our manually curated extended *Lupinus albus* annotation database (ANGERMANN ET AL., 2024), which based on sequence alignments also provides a link to the extensive resources available for *Arabidopsis thaliana* such as functional annotation of pathways according to the MapMan system (https://mapman.gabipd.org; THIMM ET AL., 2004) and assignments to subcellular compartments using the SUBA5 database (HOOPER ET AL., 2014; HOOPER ET AL., 2017; HOOPER ET AL., 2022). Based on SUBA5, 551 distinct proteins were assigned to mitochondria in total seed extracts and 948 distinct proteins in the mitochondrial fractions (Supp. Dataset S1). We calculated the quantitative composition of the individual proteome samples based on normalized iBAQ values to estimate the purity of the mitochondrial preparations (M3-Fig. 2B, Supp. Dataset S1). Mitochondrial proteins accounted for 3 % of the total seed protein content. Their proportion increased to 17 % in the mitochondrial fractions prepared from dry seeds (6-fold enrichment), and to 49 % and 65 % in mitochondrial fractions obtained from seeds imbibed at 4 °C and room temperature (16- and 20-fold enrichment, M3-Fig. 2B). Thus, cold stratification proved effective in facilitating mitochondrial isolation from metabolically inactive seeds, enabling the preparation of enriched mitochondrial fractions suitable for proteomic analysis prior to the onset of germination.

4.3.1 Identification of new mitochondrial proteins in white lupin seeds

Proteins with a mitochondrial annotation according to SUBA5 were highly enriched in the mitochondrial fractions prepared from *L. albus* seeds imbibed for 24 h at 4 °C or RT compared to the total seed extract reflected by their strongly and significantly increased relative abundance in the mitochondrial preparations (M3-Fig. 3A, dark blue

dots, Supp. Dataset S2). To identify previously unknown bona fide mitochondrial proteins, we defined thresholds for log_2-fold change (mitochondrial fraction/total protein fraction) and -log_{10} p-value above which 70 % of all proteins were annotated as "mitochondrial" (M3-Fig. 3A, dotted lines, Supp. Dataset S2, Supp. M3-Fig. S1). From the 175 proteins above this threshold without a mitochondrial SUBA annotation, 29 could be assigned to mitochondria based on complementary evidence (light blue), 84 proteins could not be confidently linked to an *Arabidopsis* homolog and were thus lacking a localization annotation (orange), while 62 proteins remained as strong candidates for novel mitochondrial components (red).

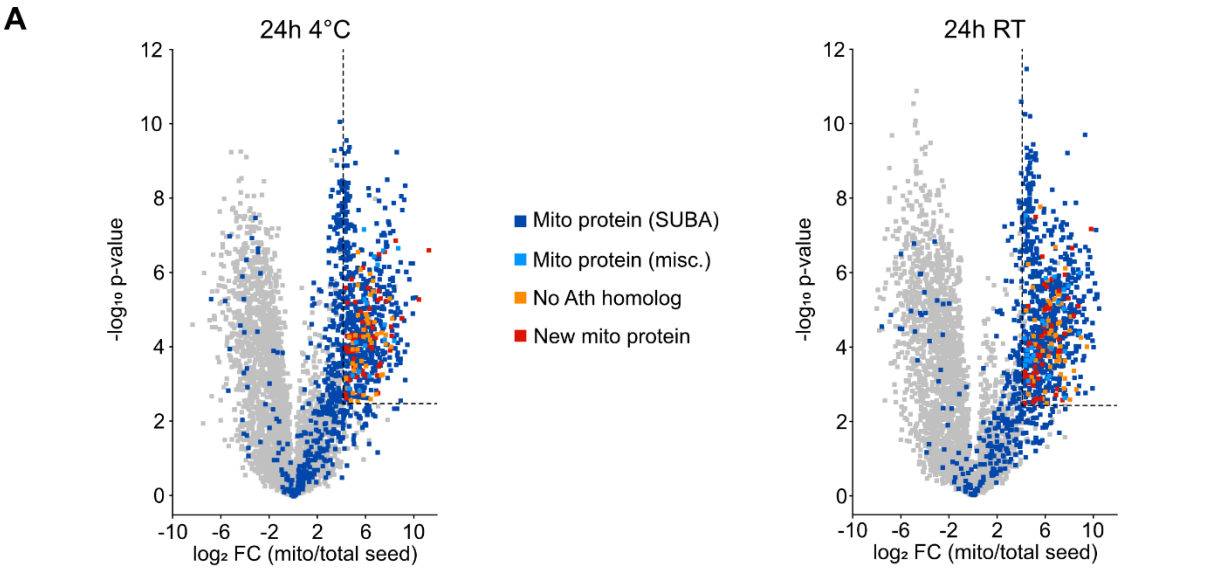

B

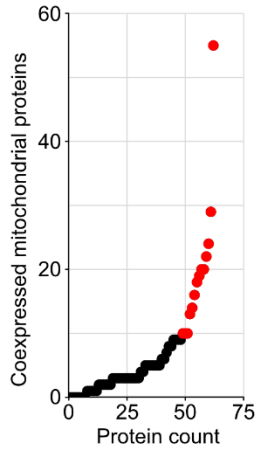

Protein ID	Name	Coexpression profile Mito	Coexpression profile Pathway
A0A6A4QPV7	Methenyltetrahydrofolate cyclohydrolase	55	Purine metabolism
A0A6A5L820	Ribosomal L5P family protein	29	OXPHOS & ribosome
A0A6A5NXG9	DNA topoisomerase (ATP-hydrolyzing)	24	DNA/RNA metabolism
A0A6A5NFX5	D-aminoacyl-tRNA deacylase	22	mitochondrial carriers
A0A6A5LZ00	UDP-glucose pyrophosphorylase 1	20	MDH, AspAT, STR1, SHMT2
A0A6A5MF95	tRNA/rRNA methyltransferase	20	PPR proteins
A0A6A4QKE8	DEAD-box ATP-dependent RNA helicase	19	DNA/RNA metabolism
A0A6A5N3C5	RCC1 family protein	18	PPR proteins
A0A6A5ND17	L-ascorbate peroxidase	16	no clear pattern
A0A6A5MW10	Translation initiation factor IF-2	14	FeS synthesis
A0A6A4NIG3	NAD/NADH kinase family protein	13	RNA, lipid & protein synthesis
A0A6A4QBR9	Glycine-tRNA ligase	10	DNA/protein synthesis
A0A6A5PB83	Tyrosine-tRNA ligase	10	protein synthesis
A0A6A5M4Z5	ADP,ATP carrier protein	10	mitochondrial carriers

M3-Fig. 3: Identification of new seed mitochondrial proteins. (**A**) Volcano plots illustrating differences in relative protein abundances in mitochondrial fractions compared to total seed extracts. Dark blue: proteins annotated as mitochondrial in SUBA5, light blue: proteins annotated as mitochondrial based on other sources (MULocDeep, JIANG ET AL., 2021, JIANG ET AL., 2023), orange: no prediction possible due to missing *Arabidopsis* homolog, red: new mitochondrial protein candidate predicted as non-mitochondrially localized in *Arabidopsis*

thaliana, but according to our enrichment analysis located in mitochondria in *Lupinus albus*. The dotted line indicates the threshold for new mitochondrial protein candidates. (**B**) Coexpression analysis for new mitochondrial protein candidates: The graph illustrates the fraction of genes encoding mitochondrially localized proteins in the 100 most strongly coexpressed genes for each candidate (ATTED-II; OBAYASHI ET AL., 2018). Additional information is given in the table for the candidates with the highest mitochondrial association (red dots). The complete dataset is provided as Supp. Datasets S2 and S3.

To gain further insight into the functional context of these candidates, we performed coexpression analyses of their *A. thaliana* homologs using ATTED-II (OBAYASHI ET AL., 2018, Supp. Dataset S3). Fourteen candidates displayed coexpression patterns in which at least 10 % of the top 100 co-expressed genes were mitochondrially localized (M3-Fig. 3B). These coexpression profiles suggest links to processes such as mitochondrial translation, RNA editing, and transcription, as well as metabolite transport, energy metabolism, and amino acid metabolism. Such associations highlight these proteins as promising targets for further investigation into mitochondrial function in seeds.

4.3.2 The quantitative proteome composition of white lupin seed mitochondria

Including the newly identified candidates our *L. albus* seed mitochondrial proteome dataset comprises 1 162 distinct proteins (Supp. Dataset S4). For functional annotation, we used a modified and manually curated version of the MapMan system (THIMM ET AL., 2004), which divides the *L. albus* proteome into 20 major categories with two levels of sub-categories (ANGERMANN ET AL., 2024). The quantitative distribution of protein abundances across functional categories is illustrated by Proteomaps (LIEBMEISTER ET AL., 2014, M3-Fig. 4A, Supp. Dataset S4). As expected, oxidative phosphorylation (OXPHOS) dominated the seed mitochondrial proteome, with respiratory chain complexes representing ~40 % of the total protein mass. ATP synthase subunits α and β were the most abundant individual proteins (2.5 % each), and complex V as a whole accounted for 17 % of mitochondrial protein mass. Voltage-dependent anion channel (VDAC) isoforms were also highly abundant, collectively comprising 7 % of the proteome and dominating the functional category “transport” (11 %). The top 10 most abundant seed mitochondrial proteins also include an NAD-dependent formate dehydrogenase, a cystathionine beta-synthase family protein, an adenine nucleotide translocator, malate dehydrogenase, and a homolog of *A. thaliana*

early nodulin 93 (Supp. Dataset. S4A, sorted by rank: column BH). A striking feature of the *L. albus* seed mitochondrial proteome is the large fraction of uncharacterized proteins consisting of 238 distinct proteins covering ~12 % of the mitochondrial protein mass (Supp. Dataset. S4B “Not assigned”). For 102 of these, reliable functional annotation based on *A. thaliana* was not possible due to only weak homology, suggesting they may represent lupin- or legume-specific mitochondrial proteins.

4.3.3 Seed mitochondrial proteome remodelling during the transition to metabolic activity

To capture initial changes associated with germination, we compared mitochondrial fractions from seeds imbibed for 24 h at 4 °C (hydrated but metabolically inactive) with those from seeds imbibed for 24 h at room temperature (actively germinating). The proteomaps indicate substantial stability of the core proteome (M3-Fig. 4A), consistent with the presence of fully assembled respiratory complexes already in dry seeds as revealed by 2D BN/SDS-PAGE (M3-Fig. 2A). Statistical analyses identified 158 proteins that increased and 108 that decreased significantly during the first 24h of germination (M3-Fig. 4B, Supp. Dataset S4A, filter column G). The strongest responses were detected in upstream supply and support pathways of oxidative phosphorylation (M3-Fig. 4C, Supp. Dataset S4A, filter column BC). Enzymes of the TCA cycle and amino acid catabolism as well as malic enzyme increased in abundance. Several metabolite and protein transporters, including the dicarboxylate carrier and TIM subunits, were strongly induced. Coenzyme metabolism was also upregulated, with elevated levels of enzymes involved in lipoic acid and thiamine biosynthesis and Fe-S cluster assembly (M3-Fig. 4C, Supp. Dataset S4A, filter column BC).

Notably, several of the seed mitochondrial proteins strongly induced during the transition to metabolic activity remain uncharacterized (M3-Fig. 4B blue dots, Supp. Dataset S4A, filter column BD). 17 of the 31 uncharacterized germination induced proteins had only weak homology to *Arabidopsis* genes, suggesting lupin- or legume-specific functions. Coexpression analysis of the remaining candidates indicated potential roles in ribosome biogenesis and cofactor biosynthesis (Supp. Dataset S5). Among the new mitochondrial proteins identified in this study, six increased during germination whereas 29 decreased, suggesting that they may play specific roles in dry seed mitochondria that are lost as metabolism is reactivated.

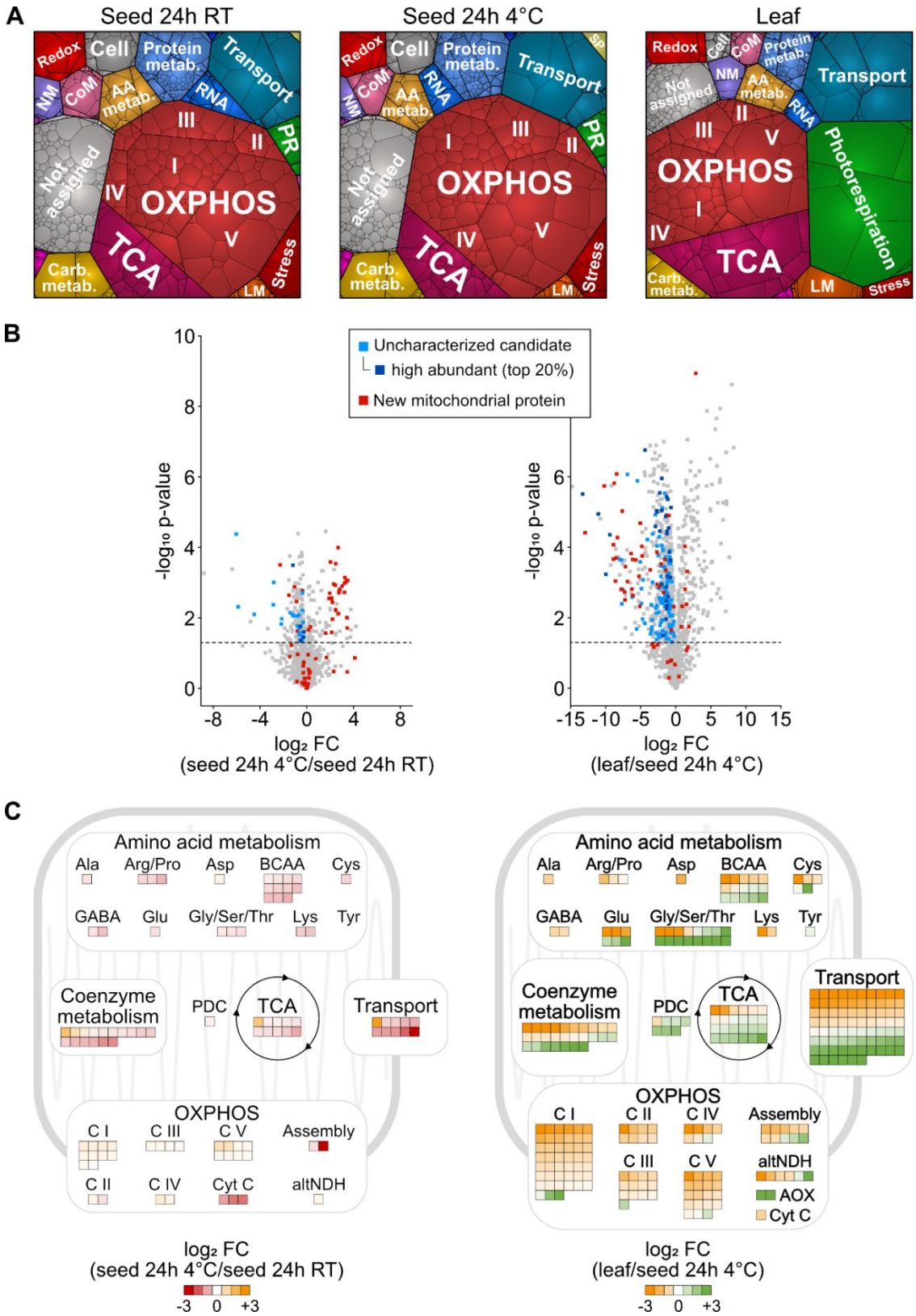

M3-Fig. 4: Comparative analysis of mitochondrial proteomes in seeds and leaves. To ensure comparability across datasets with different enrichment levels, all proteomes were filtered for mitochondrial proteins (SUBA5 annotations plus the new seed mitochondrial proteins identified in this study) before normalization and statistical analysis (Supp. Dataset S4A). (**A**) Proteomaps illustrating the quantitative composition of the mitochondrial proteome of seeds imbibed for 24 h at 4 °C or at RT and of leaves. Proteins involved in similar cellular

functions are arranged in adjacent locations and visualized by colours. Proteins are shown as polygons whose sizes represent their relative abundance (%iBAQ). Proteomaps were produced using the tool provided at https://bionic-vis.biologie.uni-greifswald.de/ (LIEBERMEISTER ET AL., 2014). Data presented are means of three biological replicates. (**B**) Volcano plots illustrating log_2-fold changes (FC) in relative protein abundances between the mitochondrial proteome of seeds imbibed for 24 h at 4 °C and seeds imbibed for 24 h at RT (left) or leaves and seeds imbibed for 24 h at 4 °C (right). Dashed lines mark the significance threshold. The new mitochondrial proteins identified in this study are highlighted in red. Uncharacterized proteins significantly induced during germination (left) or in seeds vs. leaves (right) are highlighted in blue with dark blue representing high abundant proteins (top 20 %). Data presented are means of three biological replicates. (**C**) Relative abundance of proteins involved in major mitochondrial pathways in the mitochondrial proteome of seeds imbibed for 24 h at 4 °C vs. seeds imbibed for 24 h at RT (left) or leaves vs. seeds imbibed for 24 h at 4 °C (right). The coloured squares represent significant log2-fold changes in the abundance of individual enzymes and their subunits (n = 3) with orange indicating increased abundance in quiescent seeds (24 h at 4 °C) in both comparisons. AA metab.: amino acid metabolism; altNDH: alternative NADH dehydrogenase; BCAA: branched chain amino acid; C I: Complex I; C II: complex II; C III: complex III; C IV: complex IV; C V: complex V; CoM: coenzyme metabolism; Cyt C: cytochrome C; LM: lipid metabolism; NM: nucleotide metabolism; PDH: pyruvate dehydrogenase; PR: photorespiration; SP: storage protein.

4.3.4 Distinct features of the seed mitochondrial proteome

To assess tissue specificity of the mitochondrial proteome, we compared seed mitochondria with those from *L. albus* leaves. Leaf mitochondria were less challenging to isolate and yielded highly enriched fractions, with 89 % of protein mass annotated as mitochondrial (Supp. Dataset S1). Visualization of the quantitative proteome compositions using proteomaps immediately highlights clear tissue-specific differences, both in highly abundant mitochondrial proteins and in the representation of major pathways (M3-Fig. 4A). Statistical analyses further resolved the pronounced compositional differences reflecting distinct metabolic requirements of the two tissues (M3-Fig. 4B, C, Supp. Dataset S4A). A total of 566 mitochondrial proteins were significantly more abundant in seeds than in leaves (Supp. Dataset S4A filter column H). Pathway enrichment analysis revealed a strong overrepresentation of OXPHOS proteins, particularly subunits of complex I, within this group (Supp. Dataset S4C). In the 227 proteins with a significantly higher abundance in leaves, TCA cycle enzymes were enriched as well as enzymes involved in photorespiration and transport. Transporter profiles differed strikingly between the two tissues. Of the 101 identified transporters and protein translocators, 76 showed significant changes in abundance, indicating contrasting requirements for respiratory substrates, metabolite exchange, and protein import (M3-Fig. 4C, Supp. Dataset. S4A, filter column BE “Transport”). In

seeds, VDAC isoforms and several protein translocators were significantly elevated, whereas a range of substrate carriers predominated in leaves.

To pin down the major differences in mitochondrial energy metabolism between the two tissues we focused on the quantitative distribution of dehydrogenases since these enzymes directly provide the electrons to fuel oxidative phosphorylation (M3-Fig. 5, Supp. Dataset S4A, filter column BI, Supp. Dataset S4D). Formate dehydrogenase was dominant in seed mitochondria contributing ~3 % of total mitochondrial protein mass compared to only ~0.3 % in leaves. The pyruvate dehydrogenase complex and malate dehydrogenase and the glycine cleavage system were also high abundant but not as prominent in seeds as in leaves. The oxoglutarate dehydrogenase complex, several dehydrogenases involved in amino acid catabolism as well as an uncharacterized alcohol dehydrogenase were increased in seed mitochondria whereas isocitrate dehydrogenase was more abundant in the leaves.

Seed mitochondria were further distinguished by a larger fraction of uncharacterized proteins, accounting for 12 % of total mitochondrial protein mass compared with 5 % in leaves (M3-Fig. 4A). Approximately one quarter of the proteins with significantly higher abundance in seeds remain functionally uncharacterized (M3-Fig. 4B, blue dots, Supp. Dataset S4A, filter column BF). Among them, 32 belonged to the 20 % most abundant proteins in seed mitochondria (M3-Fig. 4B, dark blue dots) and 64 proteins showed only week homology to *A. thaliana* and might thus have lupin- or legume-specific functions. Coexpression analysis suggests some of these uncharacterized proteins might be involved in RNA processing, OXPHOS, or transport processes (Supp. Dataset S5). Moreover, 43 of the newly identified mitochondrial protein candidates were significantly more abundant in seeds than leaves and thus might have seed-specific functions.

4.4 Discussion

Successful germination critically depends on the rapid re-establishment of energy metabolism in seeds, with mitochondria playing a central role as the primary source of ATP supply. In this study, we provide the first comprehensive proteomic characterization of mitochondria isolated from *Lupinus albus* seeds, thereby expanding the understanding of mitochondrial function during the onset of germination. Our findings reveal both conserved features and novel aspects of mitochondrial metabolism in a legume with protein-rich reserves.

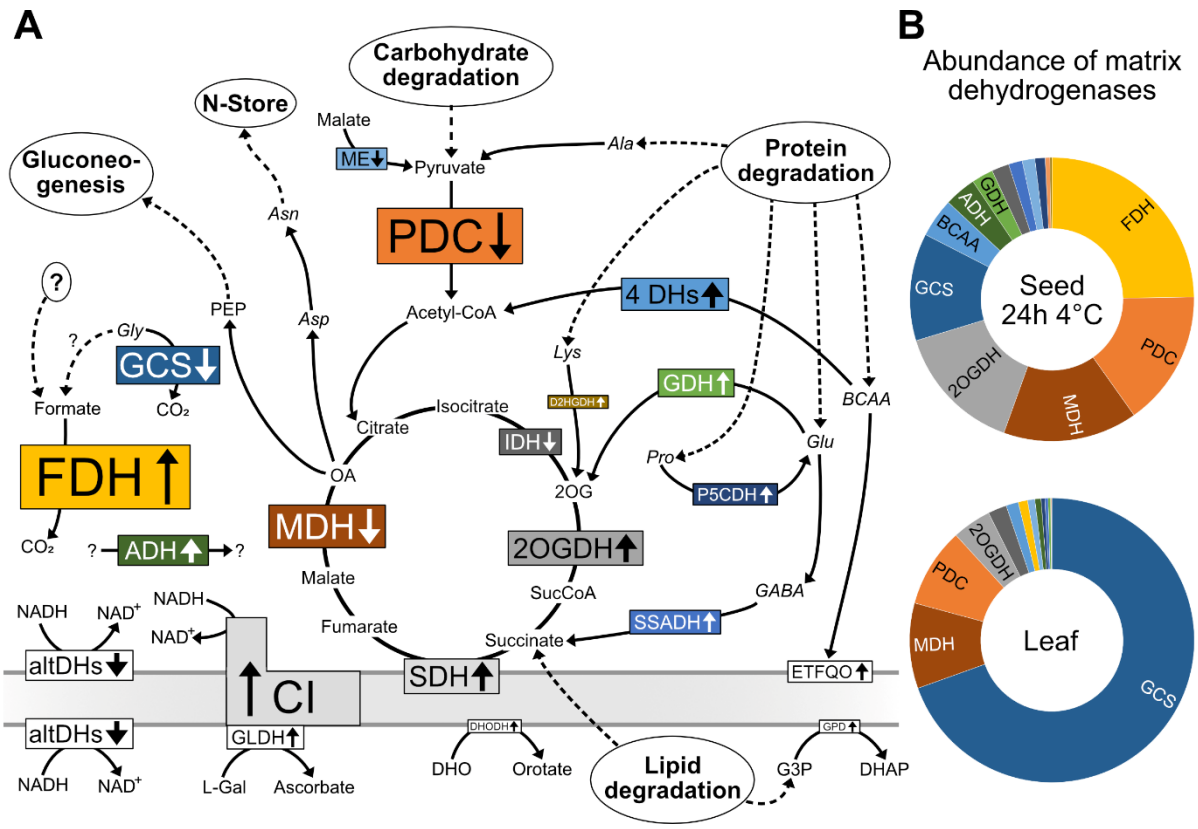

M3-Fig. 5: Dehydrogenases in seed mitochondrial energy metabolism. Schematic representation of mitochondrial metabolic pathways, highlighting the roles of dehydrogenases and their associated pathways in seeds. (**A**) The text size corresponds to the total abundance of the individual dehydrogenases or dehydrogenase complexes in quiescent seed mitochondria (%iBAQ), which is also illustrated in the respective diagram on the right. Arrows indicate relative protein abundance in seed vs. leaf mitochondria. Remobilization of seed storage compounds provides substrates for mitochondrial energy metabolism and gluconeogenesis (dashed lines). Dehydrogenases: ADH: alcohol dehydrogenase; altDH: alternative NADH dehydrogenases; BCAA/4 DHs include the four dehydrogenases involved in branched-chain amino acid catabolism (branched-chain alpha-keto acid dehydrogenase complex, isovaleryl-CoA-dehydrogenase, 3-hydroxyisobutyrate dehydrogenase, methylmalonate-semialdehyde dehydrogenase); D2HGDH: D-2-hydroxyglutarate dehydrogenase; DHODH: dihydroorotate dehydrogenase; ETFQO: electron-transfer flavoprotein:ubiquinone oxidoreductase; FDH: formate dehydrogenase; GCS: glycine cleavage system; GDH: glutamate dehydrogenase; GLDH: L-galactono-1,4-lactone dehydrogenase; GPD: glycerol-3-phosphate dehydrogenase; IDH: isocitrate dehydrogenase; MDH: malate dehydrogenase; ME: malic enzyme; P5CDH: delta-1-pyrroline-5-carboxylate dehydrogenase; PDC: pyruvate dehydrogenase complex; SDH: respiratory chain complex II (succinate dehydrogenase); SSADH: succinic semialdehyde dehydrogenase; 2OGDH: 2-oxoglutarate dehydrogenase complex. Proline dehydrogenase and D-Lactate dehydrogenase were not detected in our samples. DHAP: dihydroxyacetone phosphate; DHO: dihydroorotate; G3P: glycerol-3-phosphate; L-Gal: L-galactono-1,4-lactone; OA: Oxaloacetate; PEP: Phosphoenolpyruvate; SucCoA: Succinyl-CoA; 2OG: 2-Oxoglutarate. (**B**) Abundance of matrix dehydrogenases in mitochondria of seeds imbibed for 24 h at 4 °C and leaf based on their mass fraction (%iBAQ). The complete dataset is provided as Supp. Dataset S4.

4.4.1 Seed mitochondria are preconfigured for metabolic activation

Our shotgun proteomic and BN/SDS-PAGE analyses demonstrate that seed mitochondria contain fully assembled OXPHOS complexes and supercomplexes even in the quiescent state. This is consistent with recent findings in *Arabidopsis thaliana*, where cristae structures and intact electron transport chain complexes were observed in dry seeds, indicating that mitochondria are primed to support energy production immediately upon imbibition (DITZ ET AL., 2025). The ability to rapidly resume respiration ensures efficient ATP production during the early germination process, which is tightly linked to seed vigor (FERGUSON ET AL., 1990; KÜHN ET AL., 2015; RACCA ET AL., 2022). Our quantitative proteome confirms this preconfiguration, with ~40 % of protein mass dedicated to OXPHOS, highlighting the centrality of respiration for energy supply in seeds during early germination.

4.4.2 Diversification of respiratory substrates in seed mitochondria

Comparison of the lupin seed mitochondrial proteome with that of leaf mitochondria reveals striking differences that reflect the contrasting metabolic demands of these tissues. Whereas leaf mitochondria integrate into photorespiration and cooperate with chloroplast metabolism, seed mitochondria operate in a photosynthetically inactive environment, where their primary function is to support the mobilization of storage reserves and to generate ATP for biosynthetic processes. This is consistent with the observation that respiratory chain (MRC) components are highly abundant and fully assembled in dry seeds, whereas TCA cycle proteins are less prominent. Such a profile indicates reliance on alternative sources of reducing equivalents rather than a canonical TCA cycle.

The quantitative profile of dehydrogenases provides insights into how seed mitochondria sustain respiration independently of a full TCA cycle. A remarkable feature of lupin seed mitochondria is the exceptionally high abundance of NAD-dependent formate dehydrogenase (FDH), which ranks third among all identified mitochondrial proteins. FDH catalyses the oxidation of formate to CO_2 with concomitant production of NADH, thereby directly linking detoxification with energy supply. Previous studies demonstrated that FDH is highly abundant in mitochondria of non-photosynthetic tissues such as potato tubers, dark-grown shoots, storage roots,

and cell suspensions, but much less present in leaf mitochondria (Des Francs-Small et al., 1992). Its abundance can reach up to 9 % of mitochondrial protein in tubers, with activities 5–8 times higher than in leaves, suggesting a key metabolic role in non-green tissues (Des Francs-Small et al., 1993). High activities have also been observed in mature seeds (Davison, 1949). Our findings confirm that FDH is a key metabolic enzyme in seed mitochondria and suggest that formate detoxification may be particularly important during early germination. The metabolic sources of formate in seeds remain incompletely understood. Potential pathways include pectin demethylation, glyoxylate metabolism, and amino acid degradation, all of which are active during reserve mobilization in seeds (Igamberdiev et al.,1999). In this context, the high activity of FDH may serve as an adaptive mechanism to prevent formate accumulation while simultaneously fuelling respiration during the metabolic transition.
The observed differences in quantitative dehydrogenase composition between mitochondria from lupin seeds and leaves as well as proteome dynamics during seed transition from a dormant to a metabolically active state reflect adaptations to remobilization of the seed storage compounds and are well in line with a combined metabolism of fatty acids and amino acids postulated based on previous findings (Angermann et al., 2024). The dehydrogenases involved in mitochondrial amino acid catabolic pathways are of higher abundance in seed compared to leaf mitochondria and thus potentially contribute more to ATP production. In addition, amino acid degradation pathways are induced during early germination. Ample availability of glycine would promote transamination to glyoxylate and support a linear flux mode through parts of the glyoxylate cycle being combined with acetyl-CoA from fatty acid β-oxidation at the level of malate synthase to produce oxaloacetate for gluconeogenesis (Angermann et al., 2024). Malate dehydrogenase, catalysing the oxidation step of malate to oxaloacetate in this pathway, is much more abundant in lupin compared to *Arabidopsis* seed mitochondria (1.7 % vs. 0.15 % of the mitochondrial proteome, *A. thaliana* data from Ditz et al. (2025)) and it increases during germination.

4.4.3 Coenzyme metabolism and mitochondrial activation during early germination

Our quantitative proteome data also reveal that coenzyme metabolism is upregulated in *Lupinus albus* seed mitochondria during the early stages of germination, with

elevated levels of enzymes involved in lipoic acid and thiamine biosynthesis as well as Fe–S cluster assembly. These cofactors are essential for the activity of mitochondrial dehydrogenase complexes, including pyruvate dehydrogenase, 2-oxoglutarate dehydrogenase, and glycine decarboxylase. Disruption of lipoic acid biosynthesis causes embryo lethality in *Arabidopsis* (EWALD ET AL., 2014), while thiamine deficiency severely impairs seedling establishment (RASCHKE ET AL., 2007). Fe–S clusters are indispensable for respiratory chain function and mitochondrial metabolism more broadly (LILL AND FREIBERT, 2020), and defects in their assembly compromise embryo development as well as seedling establishment and root growth (BERNARD ET AL., 2009; MOSELER ET AL., 2015). The simultaneous induction of these pathways suggests that the activation of mitochondrial metabolism during germination requires coordinated cofactor provisioning to ensure that enzyme complexes are fully functional.

4.4.4 Transporter complement reflects energetic and metabolic priorities of seed mitochondria

In addition to metabolic enzymes, the distinct profile of mitochondrial transporters highlights functional specialization in seeds. The high abundance of the ADP/ATP carrier (ANT) underscores the central role of mitochondria in ATP provision to the cytosol during germination, in contrast to the more balanced role of ANT in leaf mitochondria, where photorespiratory metabolism predominates. Similarly, the very high levels of VDAC in seed mitochondria suggest a strong demand for metabolite exchange across the outer membrane during the initiation of metabolism. Such elevated transport capacity is consistent with the requirement for efficient coordination between storage compound degradation, respiratory activity, and biosynthesis in germinating seeds. VDAC has also been identified as the protein with the highest copy number in mitochondria isolated from a heterotrophic *Arabidopsis thaliana* cell suspension culture (FUCHS ET AL. 2020). A large fraction of the high abundant seed mitochondrial metabolite transporters has not been characterized yet and might include functional adaptations to storage compound metabolism.

4.4.5 Lupin seed mitochondria reveal potential legume-specific functions

Beyond the conserved features shared with *Arabidopsis*, the lupin seed mitochondrial proteome exhibits specific signatures that may reflect legume-specific adaptations. Two regulatory proteins, the cystathionine beta-synthase family protein CBSX3 (A0A6A5NX76/AT5G10860) and EARLY NODULIN 93 (ENOD93, A0A6A5MA33/ AT5G25940), are among the most abundant proteins in lupin seed mitochondria but are much less prominent in *Arabidopsis*. CBSX3, a regulator of thioredoxin-o, is implicated in redox homeostasis and may be critical in balancing ROS production during the early burst of respiratory activity (YOO ET AL., 2011; SHIN ET AL., 2020; OK ET AL., 2012). ENOD93, originally described in the context of legume nodulation, has recently been identified as a regulator of cytochrome c oxidase activity (LEE ET AL., 2024). By modulating respiratory ATP production, ENOD93 maintains mitochondrial energy balance, and its loss leads to reduced ADP-dependent respiration and altered membrane potential. Its high abundance in lupin seed compared to leaf mitochondria indicates that additional layers of respiratory regulation fine-tune energy balance during germination.

Our study also revealed a high proportion of uncharacterized proteins in lupin seed mitochondria, accounting for ~12 % of total protein mass. Many of these proteins lack close homologs in *Arabidopsis*, raising the possibility of legume-specific mitochondrial adaptations. Some uncharacterized proteins were among the most abundant components of the seed mitochondrial proteome and showed dynamic changes during germination, suggesting important but as yet undefined roles. Coexpression analyses linked subsets of these proteins to mitochondrial translation, ribosome biogenesis, and cofactor biosynthesis, highlighting them as promising candidates for functional studies.

4.4.6 Lupin as a model system for seed mitochondrial biology

Our study demonstrates the high potential of lupin seeds as a model to study the role of mitochondria during germination. Their large size allows for efficient organelle purification and high protein yields without the need for elaborate tag-based enrichment procedures. Our curated annotation database provides the opportunity to use the established tools and extensive resources available for *Arabidopsis thaliana*. In total, we identified 1 162 seed mitochondrial proteins in *L. albus*, closely comparable to a recent *Arabidopsis* seed mitochondrial proteome dataset comprising 1 148 distinct

proteins derived from an in-depth analysis of the total seed proteome (DITZ ET AL., 2025). The overlap of 749 distinct proteins between the two datasets underscores a strong conservation of mitochondrial function across species, while the observed differences open perspectives to investigate species-specific adaptations.

4.5 Conclusion

Our study provides a comprehensive analysis of the lupin seed mitochondrial proteome, revealing both conserved features shared with *Arabidopsis* and unique aspects likely reflecting legume-specific adaptations. Seed mitochondria are primed with fully assembled OXPHOS complexes, enriched in specialized dehydrogenases and transporters, and undergo targeted remodelling of coenzyme metabolism and substrate utilization pathways during germination. The large fraction of abundant, uncharacterized proteins highlights the potential for discovering new mitochondrial functions specific to seed biology and legumes. Together, these findings establish white lupin as a valuable model for studying the mitochondrial basis of seed vigor and germination.

4.6 Materials and Methods

4.6.1 Plant material

White lupin (*Lupinus albus* cv. "Nelly") seeds were obtained from Revierberatung Wolmersdorf GmbH and Co. KG, Wolmersdorf, Germany (Order number: 34400) and stored in the dark at 4 °C until use. Seed samples were cultivated as follow: 0 h seeds were used for protein extraction or mitochondrial isolation directly without any treatment. For imbibition seeds were soaked for 24 h in demineralized water at 4 °C or 22 °C (RT). Fresh plant material was used to isolate mitochondria (five pools of 100 g (fresh weight)) or measure respiration rates (single seeds).

For total protein extraction five pools of 10 seeds were used. The seed coats were removed and the remaining plant organs were deep-frozen in liquid nitrogen. The plant material was lyophilized in an Alpha 1-2 LD+ freeze dryer (Christ, Osterode, Germany). The dried material was ground into powder.

Leaf mitochondria were isolated from 28-day old plants. For plant cultivation, seeds were soaked in demineralized water at 22 °C for 16 h and then transferred to water-saturated expanded clay substrate (LamstedtDan, 4 – 8 mm, Fibo ExClay Deutschland GmbH, Lamstedt, Germany). Plants were cultivated in a phytochamber (22 – 24 °C,

16 h light, 8 h dark, 110 µmol m^{-2} s^{-1} light). At day 28 leaves of several plants were collected and pooled to 5 batches of 100 g (fresh weight) and used for isolation of mitochondria.

The germination capacity of seeds that had been soaked for 24 hours at either 4 °C or RT was tested. This was achieved by placing 100 seeds from each group on a wet paper towel in the dark at room temperature and allowing them to germinate. 99 of the RT-soaked seeds germinated within 6 hours. Germination of the seeds that had been imbibed at 4 °C for 24 h was delayed. Three days after placing them on the paper towel, a total of 98 seeds had germinated.

4.6.2 Mitochondrial preparation

Mitochondria were isolated from *Lupinus albus* seeds following the protocol described in WERHAHN ET AL. (2001). All steps are prepared in a cold room or on ice. In short, 100 g (fresh weight) of each sample were homogenized in pre-cooled extraction buffer (450 mM sucrose, 15 mM 3-(N-morpholino)-propanesulfonic acid (MOPS), 1.5 mM EGTA, 0.6 % (w/v) polyvinylpyrrolidone 40, 0.2 % (w/v) bovine serum albumin, 10 mM sodium ascorbate, 10 mM cysteine, 0.2 mM phenylmethylsulfonyl fluoride (PMSF), pH: 7.4) by a blender and filtered through two layers of muslin. Filtrate was centrifuged for 5 minutes at 4 °C and 2 700 ×g. The supernatant was centrifuged for 5 minutes at 4 °C and 8 300 ×g. Mitochondria were pelletized by centrifugation (10 minutes at 4 °C and 17 000 ×g). The mitochondrial pellet was resuspended in wash buffer (300 mM sucrose, 10 mM MOPS, 1 mM EGTA, 0.2 mM PMSF, pH: 7.2) and layered on a three-step Percoll gradient (18 % [v/v], 23 % [v/v], and 40 % [v/v] Percoll in 300 mM sucrose and 10 mM MOPS, pH: 7.2). After centrifugation for 90 minutes at 4 °C at 70 000 ×g the mitochondria can be isolated from the 23 % / 40 % interphase. The purified mitochondria were washed twice in resuspension buffer (400 mM mannitol, 1 mM EGTA, 0.2 mM PMSF, 10 mM Tricine, pH: 7.2) and centrifuged for 10 minutes at 4 °C at 14 500 ×g. Isolated mitochondria were snap-frozen in liquid nitrogen and stored at -80 °C.

Mitochondria from 28-day old leaves were purified by differential centrifugation and Percoll density gradient centrifugation following the protocol by KEECH ET AL. (2005). All steps were performed in a cold room or on ice. In short, Percoll gradients were prepared as follows: 50 % (v/v) Percoll and 50 % (v/v) buffer (600 mM sucrose, 20 mM N-tris [hydroxymethyl]-methyl-2-aminoethanesulphonic acid (TES), 2 mM EDTA,

20 mM KH_2PO_4, 2 mM glycine, pH: 7.5), centrifuged for 40 minutes at 4 °C at 69 400 ×g and stored at 4 °C until use. 100 g (fresh weight) of each sample were homogenized in pre-cooled extraction buffer (300 mM sucrose, 60 mM TES, 25 mM sodium pyrophosphate decahydrate, 10 mM KH_2PO_4, 2 mM EDTA, 1 mM glycine, 1 % polyvinylpyrrolidone 40, 1 % (w/v) bovine serum albumin, 50 mM sodium ascorbate, 20 mM cysteine, pH: 8) in a blender and filtered through two layers of muslin. The filtrate was centrifuged for 5 minutes at 4 °C and 2 500 ×g. The supernatant was centrifuged for 15 minutes at 4 °C and 15 100 ×g. The mitochondrial pellet was resuspended in wash buffer (300 mM sucrose, 10 mM TES, 10 mM KH_2PO_4, pH: 7.5) and layered on a prepared Percoll gradient. After centrifugation for 20 minutes at 4 °C at 17 400 ×g the mitochondria formed a whitish band close to the bottom of the tube. This band was aspirated, washed twice in wash buffer and centrifuged for 20 minutes at 4 °C at 17 200 ×g. Isolated mitochondria were snap-frozen in liquid nitrogen and stored at -80 °C.

4.6.3 Respiration measurements

Respiration rates were measured using two seeds per replicate in 6 ml demineralized water under ambient conditions (22 °C) or at 4 °C (in a fridge) using an Oxygraph+ with DW3 electrode chamber (Hansatech Instruments Ltd, Norfolk, UK).

4.6.4 2D Blue native (BN)/SDS polyacrylamide gel electrophoresis (PAGE)

The protein content of the isolated mitochondrial samples was quantified according to ANGERMANN ET AL. (2024). In short, ice-cold methanol (100 %) was added to the isolated mitochondria and incubated for 20 minutes at -20 °C. After centrifugation (5 minutes, 4 °C, 14 200 ×g) the pellet was dissolved in 200 ml of 10 mM NaOH containing 0.2 % SDS (v/w) and incubated for 5 minutes at 60 °C, shaking. After centrifugation (10 minutes, RT, 7 000 ×g), the protein content was quantified by the Pierce BCA Protein Assay Kit (Thermo Fisher Scientific, Rockford, Illinois, USA). Globulin was used as a standard.

2D BN/SDS PAGE was performed according to WITTIG ET AL. (2006). In summary, 1D BN PAGE was used to analyse mitochondrial protein complexes. A gradient gel (16 × 16 × 0.15 cm) was created using a MX40 gradient mixer, with two chambers filled with the following solutions: Front chamber: Gel buffer BN (250 mM acrylamide, 25 mM Bis-

Tris, pH: 7.0) containing 4.5 % (v/v) acrylamide. Back chamber: Gel buffer BN containing 16 % (v/v) acrylamide and 19 % (v/v) glycerol. Once the gradient gel had polymerised, a sample gel (gel buffer BN, 4 % acrylamide) was added on top. The wash buffer was removed from the mitochondrial samples by centrifugation and the proteins were extracted from the organelles using a solubilisation buffer (30 mM HEPES, 150 mM potassium acetate, 10 % glycerol and 5 % digitonin, pH: 7.4) at a ratio of 100 µl per 10 µg of mitochondrial protein. Following a 10-minute incubation on ice, the membrane aggregates and other insoluble materials were removed by centrifugation at 18 300 ×g for 10 minutes. Subsequently, Coomassie Blue was added to the sample to achieve a final concentration of 1 % (w/v). Blue native PAGE was conducted using the following buffers: Anode buffer: 50 mM Bis-Tris, pH: 7.0. Cathode buffer: 50 mM tricine, 15 mM Bis-Tris and 0.02 % Coomassie, pH: 7.0. Two steps were involved in performing the electrophoresis: i) max. 100 V (current set to 15 mA) for 45 minutes; and ii) max. 15 mA with a voltage of 500 V for 11 hours. The gel was then fixed and subjected to Coomassie colloidal staining (NEUHOFF ET AL., 1988) (fixation: 15 % ethanol and 10 % acetic acid with a 2-hour incubation, followed by staining with 5 % (w/v) Coomassie in 2 % (w/v) ortho phosphoric acid and 10 % (w/v) ammonia sulfate with an overnight incubation) or utilised for a second dimension SDS-PAGE.

SDS-PAGE (second gel dimension after BN PAGE): A lane was removed from the blue native gel and treated with a solution of 1 % SDS and 1 % beta-mercaptoethanol for half an hour. Then, the lane was submerged in water for 30 seconds. The gel lane was then placed between two glass plates. A separation gel containing 16 % (v/v) acrylamide and 12 % (v/v) glycerol in SDS gel buffer (1 M Tris, 0.1 % SDS, pH: 8.5) and a spacer gel containing 10 % (v/v) acrylamide in SDS gel buffer were poured directly on top of each other between the plates. After polymerisation, a sample gel containing 10 % (v/v) acrylamide, 10 % (v/v) glycerol and 0.1 % (w/v) SDS in BN gel buffer was poured between the SDS gel and the blue native gel strip. Finally, the gel (19 × 16 × 0.1 cm) was placed in the chamber and anode buffer (0.2 M Tris, pH: 8.9) and cathode buffer (0.1 M Tris, 0.1 M Tricine and 0.1 % SDS, pH: 8.5) were added. Gel electrophoresis was then performed for approximately eighteen hours at 30 mA (maximum voltage: 500 V) and stopped when the blue running front entered the anode buffer. The gel was then fixed and stained using the Coomassie colloidal method, as previously described.

4.6.5 Protein extraction, digestion and sample preparation for shotgun proteome analysis via mass spectrometry

The solvent precipitation, single-pot, solid-phase-enhanced sample preparation (SP4) protocol was used for mass spectrometry sample preparation as described in HEINEMANN ET AL. (2025). In brief, the proteins were solubilised and denatured by incubation at 60 °C for 30 minutes in SDT buffer (4 % SDS, 0.1 M DTT, 0.1 M Tris, pH: 7.6) (MIKULÁŠEK ET AL., 2021). The samples were then sonicated and centrifuged at 20 000 ×g for 10 minutes. Then, 30 µl of the extract was transferred to a new tube and mixed with 7.5 µl of iodoacetamide (IAM, 0.1 M). The mixture was incubated for 30 minutes in the dark to alkylate the reduced disulfide bridges. Then, 2 µl of DTT (0.1 M) was added to neutralise any excess IAM.

The preparation of the glass beads/ACN suspension, the protein precipitation and the washing steps were performed as described by JOHNSTON ET AL. (2022). Approximately 400 µg of glass beads were used per sample (approximately 30 µg of protein). The purified proteins were digested with 0.5 µg of mass spectrometry-grade trypsin (Promega) for 16 hours at 37 °C with shaking. The peptide-containing supernatant was collected in a low-binding tube and acidified with 1 µl of formic acid. The peptides were desalted using 50 mg Sep-Pak C18 columns (WAT054960, Waters, Milford, MA, USA) and quantified with the Pierce Quantitative Colorimetric Peptide Assay Kit (Thermo Fisher Scientific, Rockford, IL, USA). The samples were finally diluted to a concentration of 400 ng µl-1 in 0.1 % FA.

4.6.6 Quantitative shotgun proteomics by ion Mobility Mass Spectrometry (IMS-MS/MS)

Four hundred nanograms of peptides were injected via a nanoElute2 UHPLC (Bruker Daltonics GmbH, Bremen, Germany) and separated on an analytical reversed-phase C18 column (Aurora Ultimate 25 cm x 75 µm, 1.6 µm, 120 Å; IonOpticks). Using MS grade water and a multi-staged acetonitrile gradient containing 0.1 % formic acid (0 min, 2 %; 54 min, 25 %; 60 min, 37 %; 62 min, 95 %; 70 min, 95 %), peptides were eluted and ionized by electrospray ionization with a CaptiveSpray2 ion source and analysed on a timsTOF-HT mass spectrometer (Bruker Daltonics GmbH, Bremen, Germany), with the following DDA-PASEF settings: Ion mobility window of 0.7 – 1.5 cm^{-2} V^{-1} s^{-1}, 4 PASEF ramps, target intensity 14 500 (threshold 1 200), and a cycle time of ~0.53 s.

4.6.7 Data processing and functional annotation

The ion mobility spectrometry (IMS)–MS/MS spectra from all experiments were analysed with the MaxQuant software (Cox and Mann, 2008) using default search parameters and the proteome database of *Lupinus albus* published by Xu et al. (2020) on UniProt.org (UP000464885) for protein identification. The calculation of label-free quantification (LFQ) values and intensity-based absolute quantification (iBAQ) values were both enabled. Data evaluation was performed using Perseus (Tyanova et al., 2016). Proteins were excluded from further analysis if they were not detected in at least two out of three or four out of five biological replicates in at least one of the sample groups. Subsequently, missing values were replaced with randomly chosen low values from a normal distribution. Significant changes were calculated using Student's t-tests ($p = 0.05$). For comparisons between mitochondrial proteomes datasets were filtered for mitochondrial localization to remove contaminations from other compartments and iBAQ values were normalized prior to statistical evaluation. A recently published annotation database of *Lupinus albus* was used to obtain further information such as subcellular localization and metabolic pathway involvement (Angermann et al., 2024). Fisher's exact tests were performed in Perseus to identify significantly enriched or depleted metabolic pathways within the mitochondrial-localised proteins.

4.7 Data availability

The mass spectrometry proteomics data have been deposited to the ProteomeXchange Consortium (http://proteomecentral.proteomexchange.org) via the PRIDE partner repository (Perez-Riverol et al. 2022) with the dataset identifier PXD068370.

4.8 Funding

Research in TMH's lab is funded by the Deutsche Forschungsgemeinschaft (DFG, German Research Foundation) under Germany´s Excellence Strategy – EXC-2048/1 – project ID 390686111. The proteomics unit in TMH's lab (timsTOF-HT, Bruker Daltonics) is funded via DFG-INST 216/1290-1 FUGG.

4.9 Author contributions

CA and TMH designed the research; CA performed and evaluated all experiments; CA, HPB, and TMH analysed the data; CA and TMH wrote the manuscript with support

from HPB; TMH agrees to serve as the author responsible for contact and ensures communication.

4.10 Acknowledgments

We would like to thank Björn Heinemann for his invaluable help with organizing, conducting and evaluating the experiments. We thank Dagmar Lewejohann for cultivation of leaf material, isolation of leaf mitochondrial fractions and skilful preparation of the gels. We thank Christina Mack for skilful technical assistance.

4.11 Supplemental data

Supp. Dataset S1: Complete proteomics datasets of total seed and mitochondrial preparations.

Supp. Dataset S2: Identification of new mitochondrial proteins.

Supp. Dataset S3: Coexpression analysis of new mitochondrial proteins.

Supp. Dataset S4: *Lupinus albus* seed and leaf mitochondrial proteomes.

Supp. Dataset S5: Coexpression analysis of uncharacterized seed mitochondrial proteins.

4.12 Supplemental figures

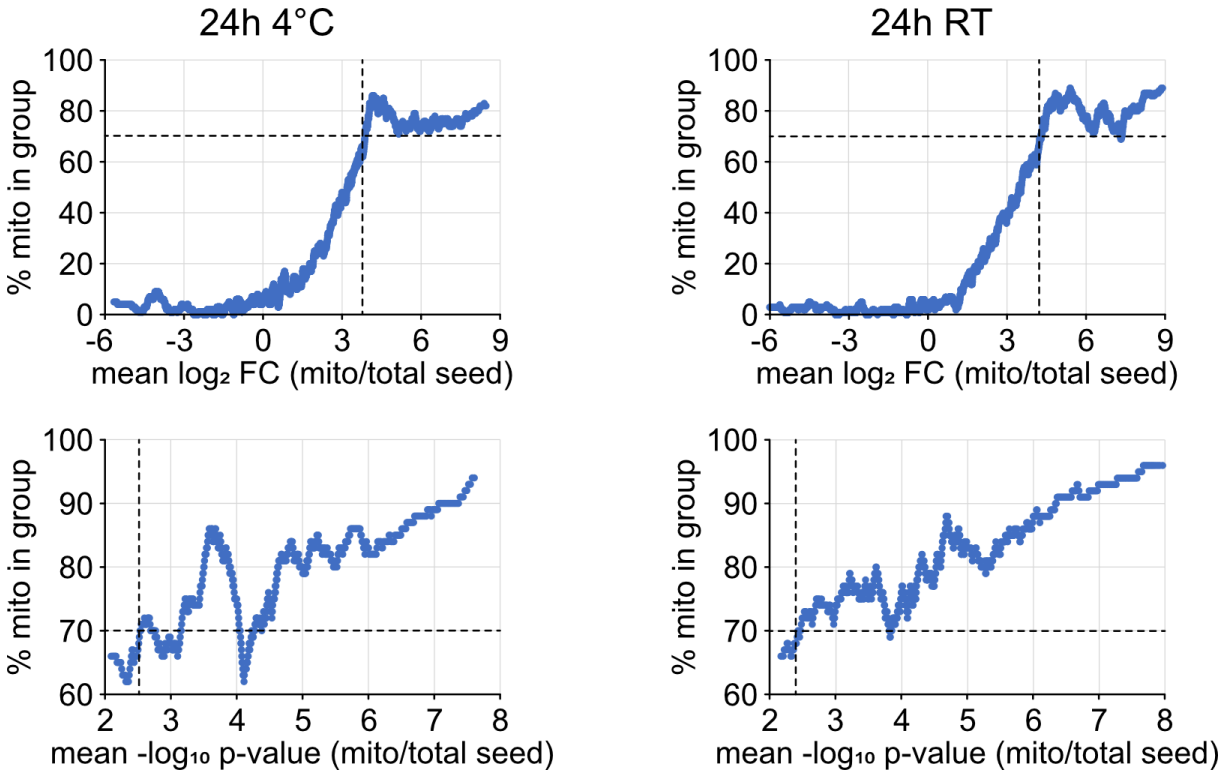

M3-Fig. S1: Specification of thresholds for identifying new mitochondrial proteins. The moving average of the enrichment factor (mean log_2-ratio of protein abundances in mitochondrial fractions and whole seed proteomes) and the respective $-log_{10}$ p-values was calculated for a window size of 100 proteins and plotted against the percentage of proteins in the same group with a mitochondrial annotation in SUBA5. The threshold for identifying new mitochondrial protein candidates was set at 70 % mitochondrial annotations (dotted lines).

4.13 References

Alverson, A.J., Rice, D.W., Dickinson, S., Barry, K. and Palmer, J.D. (2011) Origins and recombination of the bacterial-sized multichromosomal mitochondrial genome of cucumber. *Plant Cell*, 23, 2499–2513.

Angermann, C., Heinemann, B., Hansen, J., Töpfer, N., Braun, H.-P. and Hildebrandt, T.M. (2024) Proteome reorganization and amino acid metabolism during germination and seedling establishment in *Lupinus albus*. *J. Exp. Bot*., 75, 4891–4903.

Attucci, S., Carde, J.P., Raymond, P., Saint-Gès, V., Spiteri, A. and Pradet, A. (1991) Oxidative phosphorylation by mitochondria extracted from dry sunflower seeds. *Plant Physiol*., 95, 390–398.

Bernard, D.G., Cheng, Y., Zhao, Y. and Balk, J. (2009) An allelic mutant series of ATM3 reveals its key role in the biogenesis of cytosolic iron-sulfur proteins in *Arabidopsis*. *Plant Physiol*., 151, 590–602.

Bewley, J.D., Bradford, K., Hilhorst, H. and Nonogaki, H. (2013) Seeds. Physiology of development, germination and dormancy. 3rd edn. New York, Heidelberg: Springer.

Boussardon, C., Hussain, S. and Keech, O. (2025) Comparative Study of the Mitochondrial Proteome From Mesophyll, Vascular, and Guard Cells in Response to Carbon Starvation. *Physiol. Plant*, 177, e70465.

Boussardon, C., Przybyla-Toscano, J., Carrie, C. and Keech, O. (2020) Tissue-specific isolation of *Arabidopsis*/plant mitochondria - IMTACT (isolation of mitochondria tagged in specific cell types). *Plant J*., 103, 459–473.

Brennicke, A. and Leaver, C.J. (2007) Mitochondrial Genome Organization and Expression in Plants. *eLS*.

Colombini, M. (2004) VDAC: the channel at the interface between mitochondria and the cytosol. *Mol. Cell. Biochem*., 256-257, 107–115.

Cox, J. and Mann, M. (2008) MaxQuant enables high peptide identification rates, individualized p.p.b.-range mass accuracies and proteome-wide protein quantification. *Nat. Biotechnol*., 26, 1367–1372.

Davison, D.C. (1949) The distribution of formic and alcohol dehydrogenases in the higher plants, with particular reference to their variation in the pea plant during its life cycle. *Proc. Linn. Soc. N. S. W*., 26–36.

Des Francs-Small, C.C., Ambard-Bretteville, F., Darpas, A., Sallantin, M., Huet, J.C., Pernollet, J.C. and Rémy, R. (1992) Variation of the polypeptide composition of mitochondria isolated from different potato tissues. *Plant Physiol.*, 98, 273–278.

Des Francs-Small, C.C., Ambard-Bretteville, F., Small, I.D. and Rémy, R. (1993) Identification of a major soluble protein in mitochondria from nonphotosynthetic tissues as NAD-dependent formate dehydrogenase. *Plant Physiol*., 102, 1171–1177.

Ditz, N., Gasper, M., Brandt, D., Röhricht, H., Wallbott, A., Eirich, J., Rugen, N., Hegermann, J., Niehaus, M., Del Martinez, M.P., Heinemann, B., Kühn, K., Maurino, V., Müller-Schüssele, S., Hildebrandt, T., Schwarzländer, M., Braun, H.-P., Meyer, E., Herde, M., Eubel, H. and Finkemeier, I. (2025) Seed Mitochondria are Equipped with Cristae and a Full Proteome to Kickstart Germination, *Curr. Biol [preprint].*

Ewald, R., Hoffmann, C., Florian, A., Neuhaus, E., Fernie, A.R. and Bauwe, H. (2014) Lipoate-Protein Ligase and Octanoyltransferase Are Essential for Protein Lipoylation in Mitochondria of *Arabidopsis*. *Plant Physiol*., 165, 978–990.

Ferguson, J.M., TeKrony, D.M. and Egli, D.B. (1990) Changes During Early Soybean Seed and Axes Deterioration: I. Seed Quality and Mitochondrial Respiration. *Crop Sci.*, 30, 175–179.

Fuchs, P., Rugen, N., Carrie, C., Elsässer, M., Finkemeier, I., Giese, J., Hildebrandt, T.M., Kühn, K., Maurino, V.G., Ruberti, C., Schallenberg-Rüdinger, M., Steinbeck, J., Braun, H.-P., Eubel, H., Meyer, E.H., Müller-Schüssele, S.J. and Schwarzländer, M. (2020) Single organelle function and organization as estimated from *Arabidopsis* mitochondrial proteomics. *Plant J*., 101, 420–441.

Gualberto, J.M. and Newton, K.J. (2017) Plant Mitochondrial Genomes: Dynamics and Mechanisms of Mutation. *Annu. Rev. Plant Biol*., 68, 225–252.

Heinemann, B., Moormann, J., Bady, S., Angermann, C., Schrader, A. and Hildebrandt, T. M. (2025) Thermal proteome profiling identifies mitochondrial aminotransferases involved in cysteine catabolism via persulfides in plants. *bioRxiv*, 2025-05.

Hooper, C.M., Tanz, S.K., Castleden, I.R., Vacher, M.A., Small, I.D. and Millar, A.H. (2014) SUBAcon: a consensus algorithm for unifying the subcellular localization data of the *Arabidopsis* proteome. *Bioinformatics*, 30, 3356–3364.

Hooper, C. M., Castleden, I. R., Tanz, S. K., Aryamanesh, N. and Millar, A. H. (2017) SUBA4: the interactive data analysis centre for *Arabidopsis* subcellular protein locations. *Nucleic Acids Res.*, 45(D1), D1064-D1074.

Hooper, C. M., Castleden, I. R., Tanz, S. K., Grasso, S. V., Aryamanesh, N. and Millar, A. H. (2022) Subcellular Localisation database for *Arabidopsis* proteins version 5 [Dataset]. The University of Western Australia. https://doi.org/10.26182/8dht-4017

Howell, K.A., Millar, A.H. and Whelan, J. (2006) Ordered assembly of mitochondria during rice germination begins with pro-mitochondrial structures rich in components of the protein import apparatus. *Plant Mol. Biol*., 60, 201–223.

Igamberdiev, A.U., Bykova, N.V. and Kleczkowski, L.A. (1999) Origins and metabolism of formate in higher plants. *Plant Physiol. Biochem*., 37, 503–513.

Jiang, Y., Jiang, L., Akhil, C.S., Wang, D., Zhang, Z., Zhang, W. and Xu, D. (2023) MULocDeep web service for protein localization prediction and visualization at subcellular and suborganellar levels. *Nucleic Acids Res*., 51, W343-W349.

Jiang, Y., Wang, D., Yao, Y., Eubel, H., Künzler, P., Møller, I.M. and Xu, D. (2021) MULocDeep: A deep-learning framework for protein subcellular and suborganellar localization prediction with residue-level interpretation. *Comput. Struct. Biotechnol. J.*, 19, 4825–4839.

Johnston, H.E., Yadav, K., Kirkpatrick, J.M., Biggs, G.S., Oxley, D., Kramer, H.B. and Samant, R.S. (2022) Solvent Precipitation SP3 (SP4) Enhances Recovery for Proteomics Sample Preparation without Magnetic Beads. *Anal. Chem.*, 94, 10320–10328.

Kasimova, M.R., Grigiene, J., Krab, K., Hagedorn, P.H., Flyvbjerg, H., Andersen, P.E. and Møller, I.M. (2006) The free NADH concentration is kept constant in plant mitochondria under different metabolic conditions. *Plant Cell*, 18, 688–698.

Keech, O., Dizengremel, P. and Gardeström, P. (2005) Preparation of leaf mitochondria from *Arabidopsis thaliana*. *Physiol. Plant*, 124, 403–409.

Klodmann, J., Senkler, M., Rode, C. and Braun, H.-P. (2011) Defining the protein complex proteome of plant mitochondria. *Plant Physiol.*, 157, 587–598.

Kühn, K., Obata, T., Feher, K., Bock, R., Fernie, A.R. and Meyer, E.H. (2015) Complete Mitochondrial Complex I Deficiency Induces an Up-Regulation of Respiratory Fluxes That Is Abolished by Traces of Functional Complex I. *Plant Physiol.*, 168, 1537–1549.

Kuhnert, F., Stefanski, A., Overbeck, N., Drews, L., Reichert, A.S., Stühler, K. and Weber, A.P.M. (2020) Rapid Single-Step Affinity Purification of HA-Tagged Plant Mitochondria. *Plant Physiol.*, 182, 692–706.

Law, S.R., Narsai, R., Taylor, N.L., Delannoy, E., Carrie, C., Giraud, E., Millar, A.H., Small, I. and Whelan, J. (2012) Nucleotide and RNA metabolism prime translational initiation in the earliest events of mitochondrial biogenesis during *Arabidopsis* germination. *Plant Physiol.*, 158, 1610–1627.

Lee, C.P., Le, X.H., Gawryluk, R.M.R., Casaretto, J.A., Rothstein, S.J. and Millar, A.H. (2024) EARLY NODULIN93 acts via cytochrome c oxidase to alter respiratory ATP production and root growth in plants. *Plant Cell*, 36, 4716–4731.

Liebermeister, W., Noor, E., Flamholz, A., Davidi, D., Bernhardt, J. and Milo, R. (2014) Visual account of protein investment in cellular functions. *Proc. Natl. Acad. Sci. U.S.A.*, 111, 8488–8493.

Lill, R. and Freibert, S.-A. (2020) Mechanisms of Mitochondrial Iron-Sulfur Protein Biogenesis. *Annu. Rev. Biochem.*, 89, 471–499.

Linkies, A., Graeber, K., Knight, C. and Leubner-Metzger, G. (2010) The evolution of seeds. *New Phytol.*, 186, 817–831.

Logan, D.C., Millar, A.H., Sweetlove, L.J., Hill, S.A. and Leaver, C.J. (2001) Mitochondrial biogenesis during germination in maize embryos. *Plant Physiol.*, 125, 662–672.

Logan, D.C. (2006) The mitochondrial compartment. *J. Exp. Bot.*, 57, 1225–1243.

Logan, D.C. (2010) Mitochondrial fusion, division and positioning in plants. *Biochem. Soc. Trans.*, 38, 789–795.

Logan, D.C. and Leaver, C.J. (2000) Mitochondria-targeted GFP highlights the heterogeneity of mitochondrial shape, size and movement within living plant cells. *J. Exp. Bot*., 51, 865–871.

Mikulášek, K., Konečná, H., Potěšil, D., Holánková, R., Havliš, J. and Zdráhal, Z. (2021) SP3 protocol for proteomic plant sample preparation prior LC-MS/MS. *Front. Plant Sci*., 12, 635550.

Møller, I.M., Rasmusson, A.G. and van Aken, O. (2021) Plant mitochondria - past, present and future. *Plant J*., 108, 912–959.

Moseler, A., Aller, I., Wagner, S., Nietzel, T., Przybyla-Toscano, J., Mühlenhoff, U., Lill, R., Berndt, C., Rouhier, N., Schwarzländer, M. and Meyer, A.J. (2015) The mitochondrial monothiol glutaredoxin S15 is essential for iron-sulfur protein maturation in *Arabidopsis thaliana*. *Proc. Natl. Acad. Sci. U.S.A.*, 112, 13735–13740.

Neuhoff, V., Arold, N., Taube, D. and Ehrhardt, W. (1988) Improved staining of proteins in polyacrylamide gels including isoelectric focusing gels with clear background at nanogram sensitivity using Coomassie Brilliant Blue G-250 and R-250. *Electrophoresis*, 9(6), 255-262.

Niehaus, M., Straube, H., Künzler, P., Rugen, N., Hegermann, J., Giavalisco, P., Eubel, H., Witte, C.-P. and Herde, M. (2020) Rapid Affinity Purification of Tagged Plant Mitochondria (Mito-AP) for Metabolome and Proteome Analyses. *Plant Physiol*., 182, 1194–1210.

Nietzel, T., Mostertz, J., Ruberti, C., Née, G., Fuchs, P., Wagner, S., Moseler, A., Müller-Schüssele, S.J., Benamar, A., Poschet, G., Büttner, M., Møller, I.M., Lillig, C.H., Macherel, D., Wirtz, M., Hell, R., Finkemeier, I., Meyer, A.J., Hochgräfe, F. and Schwarzländer, M. (2020) Redox-mediated kick-start of mitochondrial energy metabolism drives resource-efficient seed germination. *Proc. Natl. Acad. Sci. U.S.A*., 117, 741–751.

Obayashi, T., Hibara, H., Kagaya, Y., Aoki, Y. and Kinoshita, K. (2022) ATTED-II v11: A Plant Gene Coexpression Database Using a Sample Balancing Technique by Subagging of Principal Components. *Plant Cell Physiol*., 63, 869–881.

Ok, S.H., Yoo, K.S. and Shin, J.S. (2012) CBSXs are sensor relay proteins sensing adenosine-containing ligands in *Arabidopsis*. *Plant Signal. Behav*., 7, 664–667.

Paszkiewicz, G., Gualberto, J.M., Benamar, A., Macherel, D. and Logan, D.C. (2017) *Arabidopsis* Seed Mitochondria Are Bioenergetically Active Immediately upon Imbibition and Specialize via Biogenesis in Preparation for Autotrophic Growth. *Plant Cell*, 29, 109–128.

Perez-Riverol, Y., Bai, J., Bandla, C., García-Seisdedos, D., Hewapathirana, S., Kamatchinathan, S., Kundu, D.J., Prakash, A., Frericks-Zipper, A., Eisenacher, M., Walzer, M., Wang, S., Brazma, A. and Vizcaíno, J.A. (2022) The PRIDE database resources in 2022: a hub for mass spectrometry-based proteomics evidences. *Nucleic Acids Res*., 50, D543-D552.

Racca, S., Gras, D.E., Canal, M.V., Ferrero, L.V., Rojas, B.E., Figueroa, C.M., Ariel, F.D., Welchen, E. and Gonzalez, D.H. (2022) Cytochrome c and the transcription factor ABI4 establish a molecular link between mitochondria and ABA-dependent seed germination. *New Phytol*., 235, 1780–1795.

Rao, R.S.P., Salvato, F., Thal, B., Eubel, H., Thelen, J.J. and Møller, I.M. (2017) The proteome of higher plant mitochondria. *Mitochondrion*, 33, 22–37.

Raschke, M., Bürkle, L., Müller, N., Nunes-Nesi, A., Fernie, A.R., Arigoni, D., Amrhein, N. and Fitzpatrick, T.B. (2007) Vitamin B1 biosynthesis in plants requires the essential iron sulfur cluster protein, THIC. *Proc. Natl. Acad. Sci. U.S.A*., 104, 19637–19642.

Rodríguez, J.L., Diego, J.G. de, Rodríguez, F.D. and Cervantes, E. (2015) Mitochondrial structures during seed germination and early seedling development in *Arabidopsis thaliana*. *Biologia*, 70, 1019–1025.

Sano, N., Rajjou, L., North, H.M., Debeaujon, I., Marion-Poll, A. and Seo, M. (2016) Staying Alive: Molecular Aspects of Seed Longevity. *Plant Cell Physiol*., 57, 660–674.

Shin, J.S., So, W.M., Kim, S.Y., Noh, M., Hyoung, S., Yoo, K.S. and Shin, J.S. (2020) CBSX3-Trxo-2 regulates ROS generation of mitochondrial complex II (succinate dehydrogenase) in *Arabidopsis*. *Plant Sci*., 294, 110458.

Sweetlove, L.J. and Fernie, A.R. (2013) The spatial organization of metabolism within the plant cell. *Annu. Rev. Plant Biol*., 64, 723–746.

Taiz, L., Møller, I.M., Murphy, A. and Zeiger, E. (2023) Plant physiology and development. *Sinauer Associates*.

Thimm, O., Bläsing, O., Gibon, Y., Nagel, A., Meyer, S., Krüger, P., Selbig, J., Müller, L.A., Rhee, S.Y. and Stitt, M. (2004) MAPMAN: a user-driven tool to display genomics data sets onto diagrams of metabolic pathways and other biological processes. *Plant J*., 37, 914–939.

Tyanova, S., Temu, T., Sinitcyn, P., Carlson, A., Hein, M.Y., Geiger, T., Mann, M. and Cox, J. (2016) The Perseus computational platform for comprehensive analysis of (prote)omics data. *Nat Methods*, 13, 731–740.

Weitbrecht, K., Müller, K. and Leubner-Metzger, G. (2011) First off the mark: early seed germination. *J. Exp. Bot*., 62, 3289–3309.

Werhahn, W., Niemeyer, A., Jänsch, L., Kruft, V., Schmitz, U.K. and Braun, H. (2001) Purification and characterization of the preprotein translocase of the outer mitochondrial membrane from *Arabidopsis*. Identification of multiple forms of TOM20. *Plant Physiol*., 125, 943–954.

White, J.A. and Scandalios, J.G. (1989) Deletion analysis of the maize mitochondrial superoxide dismutase transit peptide. *Proc. Natl. Acad. Sci. U.S.A*., 86, 3534–3538.

Wittig, I., Braun, H. P. and Schägger, H. (2006) Blue native PAGE. *Nat. Protoc*., 1(1), 418-428.

Xu, W., Zhang, Q., Yuan, W., Xu, F., Muhammad Aslam, M., Miao, R., Li, Y., Wang, Q., Li, X., Zhang, X., Zhang, K., Xia, T. and Cheng, F. (2020) The genome evolution and low-phosphorus adaptation in white lupin. *Nat. Commun*., 11, 1069.

Yoo, K.S., Ok, S.H., Jeong, B.-C., Jung, K.W., Cui, M.H., Hyoung, S., Lee, M.-R., Song, H.K. and Shin, J.S. (2011) Single cystathionine β-synthase domain-containing proteins modulate development by regulating the thioredoxin system in *Arabidopsis*. *Plant Cell*, 23, 3577–3594.

Publications

- **Cecile Angermann***, Björn Heinemann*, Jule Hansen, Nadine Töpfer, Hans-Peter Braun, Tatjana M. Hildebrandt (2024) Proteome reorganization and amino acid metabolism during germination and seedling establishment in *Lupinus albus*, *Journal of Experimental Botany*, Volume 75, Issue 16, Pages 4891-4903 https://doi.org/10.1093/jxb/erae197

- Jannis Moormann, Björn Heinemann, **Cecile Angermann**, Anna Koprivova, Ute Armbruster, Stanislav Kopriva, Tatjana M. Hildebrandt (2025) Cysteine Signalling in Plant Pathogen Response, *Plant, Cell & Environment*, Volume 48, Issue 10, Pages 7101-7122
https://doi.org/10.1111/pce.70017

- **Cecile Angermann**, Björn Heinemann, Bianca Bueno Nogueira, Hans-Jörg Mai, Petra Bauer, Tatjana M. Hildebrandt (2025) Balancing nutrient remobilization and photosynthesis: proteomic insights into the dual role of lupin cotyledons after germination, *the plant journal*, Volume 123, Issue 2, e70357 http://doi.org/10.1111/tpj.70357

- Björn Heinemann*, Jannis Moormann*, Shivsam Bady, **Cecile Angermann**, Andrea Schrader, Tatjana M. Hildebrandt (2025) Thermal proteome profiling identifies mitochondrial aminotransferases involved in cysteine catabolism via persulfides in plants, *bioRxiv*
https://doi.org/10.1101/2025.05.23.655777 [Preprint]

- **Cecile Angermann**, Hans-Peter Braun, Tatjana M. Hildebrandt (2025) The seed mitochondrial proteome of *Lupinus albus* provides insight into energy metabolism during germination, *bioRxiv*
https://doi.org/10.1101/2025.09.19.677279 [Preprint]

* Equally contributing first authors

Conference contributions

12th International Conference for Plant Mitochondrial Biology (ICPMB)
22.-27. May 2022, Malmö (Sweden)
Poster:
Mitochondrial respiration and the composition of the respiratory chain in germinating white lupins; **Cecile Angermann**, Björn Heinemann, Hans-Peter Braun, Tatjana M. Hildebrandt
Changes of the mitochondrial proteome of Lupinus albus during Germination; Björn Heinemann, **Cecile Angermann**, Hans-Peter Braun, Tatjana M. Hildebrandt

2. Meeting of the Molecular Bioscience
22. March 2023, Hannover (Germany)
Talk:
The biochemistry of germination in Lupinus albus

16th International Lupin Conference
19.-23. June 2023, Rostock (Germany)
Poster:
A quantitative view on metabolic changes during seedling establishment of Lupinus albus; **Cecile Angermann**, Björn Heinemann, Hans-Peter Braun, Tatjana M. Hildebrandt
A quantitative view of proteomic changes during seedling establishment in Lupinus albus; Björn Heinemann, **Cecile Angermann**, Hans-Peter Braun, Tatjana M. Hildebrandt

28th Cologne Minisymposium on Plant Biology
29. February 2024, Köln (Germany)
Poster:
Proteome remodelling and amino acid metabolism during germination and seedling establishment in Lupinus albus; **Cecile Angermann**, Björn Heinemann, Jule Hansen, Nadine Töpfer, Hans-Peter Braun, Tatjana M. Hildebrandt

13th International Conference for Plant Mitochondrial Biology (ICPMB)
26.-30. May 2024, Saint Malo (France)
Poster:
Analysis of mitochondria from white lupin seeds; **Cecile Angermann**, Björn Heinemann, Hans-Peter Braun, Tatjana M. Hildebrandt

12th Meeting of the German Plant Mito Group
26.-27. September 2024, Bonn (Germany)
Talk:
Analysis of mitochondria from white lupin seeds

38th Molecular Biology of Plants Conference
10.-13. February 2025, Hennef (Germany)
Poster:
Proteome-focused features of white lupine germination and seedling establishment; **Cecile Angermann**, Björn Heinemann, Tatjana M. Hildebrandt

13th Meeting of the German Plant Mito Group
18.-19. February 2025, Köln (Germany)

29th Cologne Minisymposium on Plant Biology
20. February 2025, Köln (Germany)
Poster:
Analysis of mitochondria from white lupin seeds; **Cecile Angermann**, Björn Heinemann, Hans-Peter Braun, Tatjana M. Hildebrandt

14th Meeting of the German Plant Mito Group
6.-8. October 2025, Wettringen (Germany)